JULY 1975

MICROWAVES

laser technology

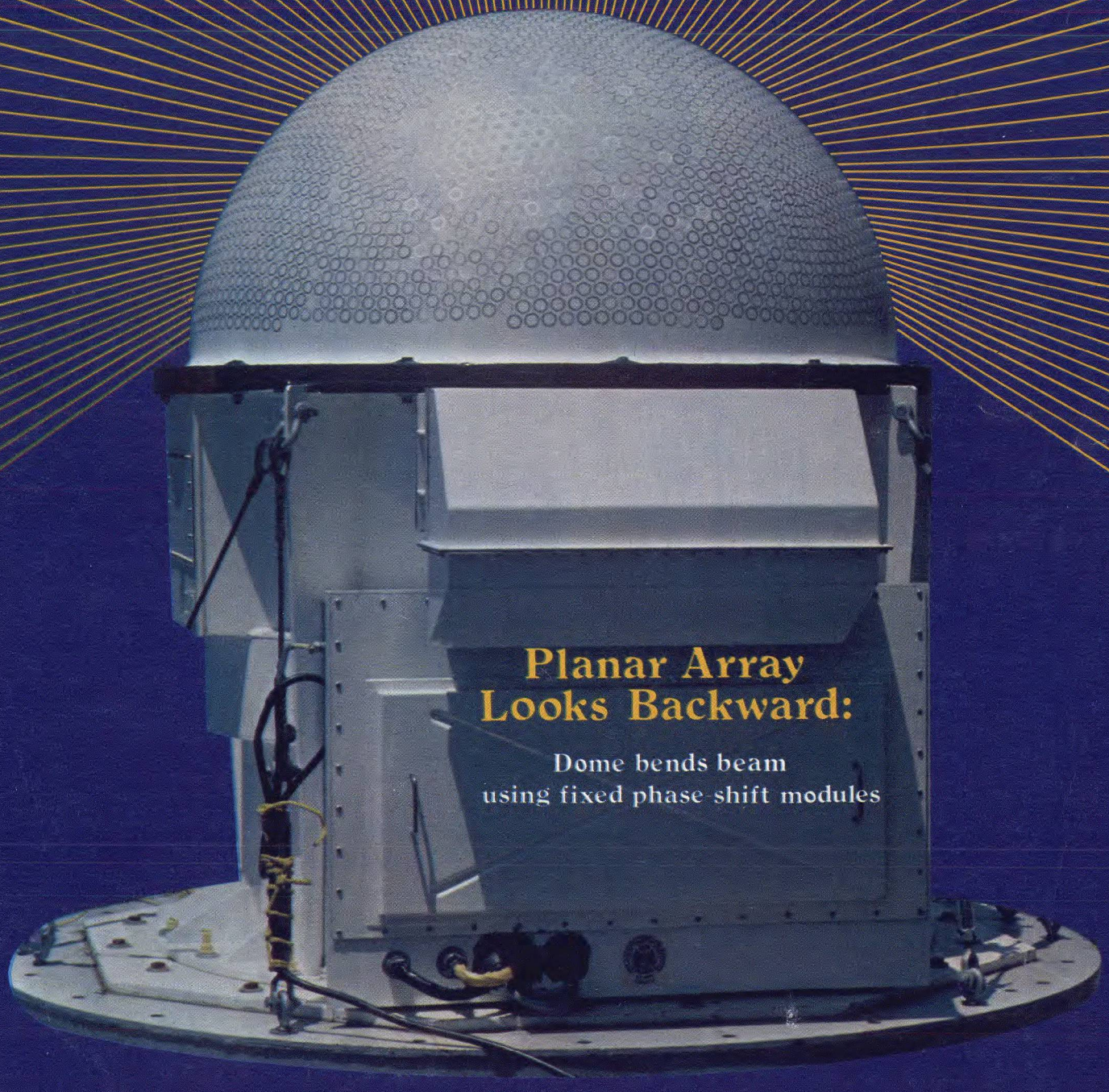

Planar Array Looks Backward:

Dome bends beam using fixed phase-shift modules

Also: Measure that field ■ Simplify corner reflector design ■ Determine polarization loss the easy way

MICROWAVES

July 1975
Vol. 14, No. 7

news

editorial

technical section

products and departments

About the cover: The dome radar, a new design concept by Sperry, Great Neck, NY, offers hemispheric coverage from a single-planar array. Cover design by Robert Meehan.

coming next month: Passive Components

Build A Better Bias Insertion Unit. Gerald W. Renken of Honeywell's Government and Aeronautical Products Division, shows how to build your own wideband bias insertion units. Two designs are detailed, one using discrete circuit elements, and a second employing a ferrite core. In addition to dc, each circuit is designed to inject video pulses with risetimes as short as 80 ns into a 200 MHz to 10 GHz system. Both units are easily, and inexpensively, assembled from converted UG-28 Tees.

Packaging Can Influence Coupled-Line Filters. Marcus Staloff of The ARO Corporation, examines the effect of packaging coupled-line bandpass filters. Enclosing the component in an MIC-type package capped with a conducting cover can lead to bandwidth shrinkage as well as an increase in the design's center frequency. Even at practical cover heights, such as 0.200 inch, this is an effect that must be reckoned with.

Nomograms Speed Design of $\lambda/4$ Transformers. Samuel Guccione, Department Chairman at Delaware Technical and Community College, eases the design of multiple section binominal quarter-wave transformers through a series of easy-to-use nomograms. Filters with up to five sections can be quickly analyzed.

Publisher/Editor
Howard Bierman

Managing Editor
Richard T. Davis

Associate Editor
Stacy V. Bearse

Contributing Editor
Harvey J. Hindin

Washington Editor
Paul Harris
Snyder Associates
1050 Potomac St., NW
Washington, DC 20007
(202) 965-3700

Editorial Assistant
Gail Murphy

Production Editor
Sherry Lynne Bogen

Art
Robert Meehan, Dir.

Production
Dollie S. Viebig, Mgr.
Dan Coakley

Circulation
Trish Edelmann, Mgr.
Peggy Long, Reader Service

Promotion Manager
Albert B. Stempel

Directory Coordinator
Janice Tapp

Editorial Office
50 Essex St.,
Rochelle Park, N.J. 07662
Phone (201) 843-0550
TWX 710-990-5071

A Hayden Publication
James S. Mulholland, Jr., President

MICROWAVES is sent free to individuals actively engaged in microwave work at companies located in the U.S., Canada and Western Europe. Subscription price for non-qualified copies is $10.00 for U.S., $15.00 a year elsewhere. Additional single copies $1.50 ea. (U.S.); $2.00 ea. (foreign); except additional Product Data Directory reference issue, $10.00 ea. (U.S.); $18.00 (foreign). POSTMASTER, please send Form 3579 to Fulfillment Manager, MICROWAVES, P.O. Box 13801, Philadelphia, PA 19101.

Back Issues of MicroWaves are available on microfilm, microfiche, 16mm or 35mm roll film. They can be ordered from Xerox University Microfilms, 300 North Zeeb Road, Ann Arbor, MI 48106. For immediate information, call (313) 761-4700.

Hayden Publishing Co., Inc., James S. Mulholland, President, printed at Brown Printing Co., Inc., Waseca, MN.

Planar array looks through lens to provide hemispherical coverage

Stacy V. Bearse
Associate Editor

The limited scan angle of traditional phased-arrays has generally made them overly expensive for applications where hemispherical coverage is required. But a new concept involving a dielectrically-loaded passive lens, or "dome" as it is referred to, promises to slash the cost of wide coverage phased-array designs by achieving hemispherical coverage with a single planar array—coverage that previously required three or four planar array faces.

"In a cost analysis of a ballistic missile defense phased-array application, a dome antenna replacing four conventional planar arrays reduced antenna costs by about 50%," notes Leon Schwartzman, program manager at Sperry Gyroscope in Great Neck, NY, where the novel antenna concept was developed. "The 50% cost savings associated with the antenna and cost savings associated with a smaller structure yields an overall system cost savings of 30%," he continues.

The dome antenna consists of a conventional planar phased-array (Fig. 1) covered by a radome studded with fixed, passive phase shifters (Fig. 2). When selected portions of the interior of the dome are illuminated by a "search light" beam, the collective phase shift of the illuminated elements changes the direction of the propagation of the energy from the feed array, acting as an rf analog to an optical prism. Thus, the planar feed array need not scan to as large an angle as is ultimately required.

"You essentially take a planar array, which is normally limited in its scan range to ±60 degrees or less and by making changes in the beam steering function and adding the dome lens, you can greatly increase the scanning ability of the array," Schwartzman explains. "In addition," he adds, "the planar array may have been signal bandwidth limited, it's a phased array not a real time array, but by adding that dome lens, you can also increase the signal bandwidth capability of the feed."

±120° scans possible

Sperry's dome concept can provide greater than hemispherical coverage—in fact up to ±120 degrees from zenith—as demonstrated by a C-band demonstration model. The prototype uses a four-foot diameter, space-fed planar array consisting of 805, digitally controllable, three-bit ferrite prase shifters to illuminate the inside of a hemispherical lens. This lens is studded with 3,636 dielectrically loaded circular waveguide sections, each designed to introduce a fixed amount of phase shift (Fig. 2). Mismatch plus insertion loss of the dome is approximately 0.8 dB.

"For the feasibility model, we designed a circular waveguide pipe with titanium styrene loading. There are two different slugs inside the waveguide, one, of dielectric constant, $\epsilon_r = 12.2$ and a second material with an ϵ_r of 7.2. By changing from element to element the relative lengths of the slugs, you basically change the insertion phase of the component," describes Schwartzman.

Eighteen combinations are used to introduce phase shift in 20-degree increments, thus covering a 0 to 360 degree range. In the feasibility model, each waveguide phase shifter is fitted into a predrilled hole in a hemispherical radome.

The dome on the feasibility model weighs "lots of pounds," according to Schwartzman, but was built without regard for weight or cost. "I would never build a dome lens like that again," exclaims the Sperry researcher. "It's pure witchcraft when you mix up those dielectric constants!"

Instead, future production versions might incorporate lightweight printed-circuit phase delays which would be glued to the inside

(continued on p. 10)

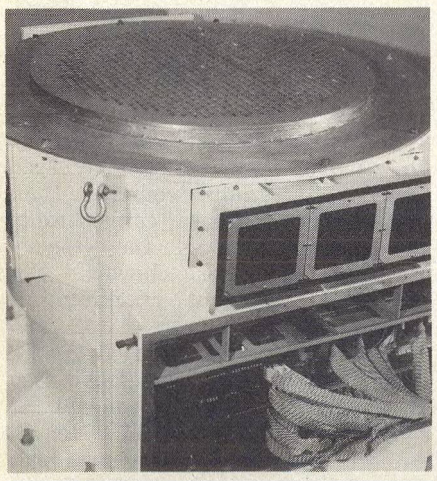

1. A simple, planar array can provide greater than hemispherical coverage when capped with a dielectrically-loaded lens.

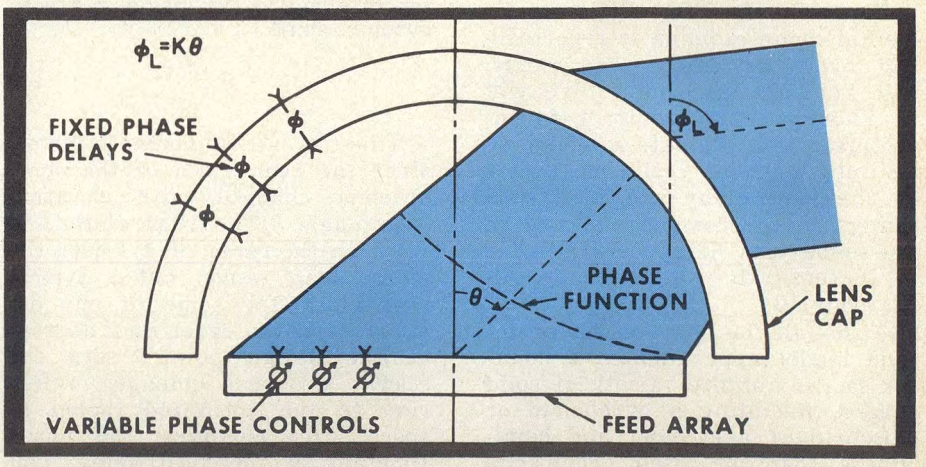

2. A passive lens bends the beam from a planar array to greatly increase its effective scan angle. The planar array's scan angle, Θ, is related to the antenna's scan angle, ϕ_L, by a constant, k, which may vary between one and two.

Efficiency gains reported for microwave power transmission

Researchers at the Jet Propulsion Laboratory in Pasadena, CA, and at Raytheon in Waltham, MA, have reported that, for the first time, a microwave power transmission system has achieved an overall efficiency of better than 50%.

"These are significant results," claims Richard M. Dickinson, who monitored the Raytheon measurements for JPL's office of Research and Advanced Development. "Overall efficiency for microwave power transmission has increased by a factor of three in the past decade."

The terrestrial tests were conducted by converting dc, rated at 914 watts, to rf. The rf was transmitted to a receiving antenna over a relatively short distance, and rectified back to dc. Usable electric power at the output end was measured at 495 watts, for a dc to dc efficiency of 54%.

A team headed by Dickinson of JPL and Owen Maynard and William C. Brown of Raytheon plans to continue the tests this summer at the NASA-JPL complex at Goldstone, CA. According to Dickinson, in future experiments the delivered power will be increased to tens of kilowatts and will be received over a distance of one mile using an 85-foot transmitting dish and a rectenna receiving array.

These experiments are attempting to investigate the feasibility of a solar power satellite system. In such a system, a satellite carrying a large solar-cell array, would be placed in a geosynchronous orbit around the earth. Solar energy would be converted to dc, then to rf for transmission back to earth. A large, six mile square antenna array on earth would intercept the high-power beam, and a rectification system would convert the energy to dc for distribution.

The present work at JPL and Raytheon is under contract to the NASA Office of Applications. ••

SVB

Planar array looks through lens to provide hemispherical coverage (cont'd)

of a radome. "The present element that we are looking at is a printed-circuit crossed dipole, with printed meanderlines," Schwartzman notes. These elements resemble the letter "H" and consist of two crossed diodes connected by a pair of transmission lines, packaged in a rectangular box. The complete element is approximately 1.5 inches long, weighs about 0.3 ounce and might be made in quantity for about $10 apiece, according to Sperry. The total antenna weight of a planar array capped by a dome using these lightweight phase shifters would be in the neighborhood of 6,500 to 7,000 lbs, including the beam steering unit and drivers used for steering the array.

Signal bandwidth of the experimental dome antenna is reportedly 2% over the entire scan range. But Schwartzman notes: We will be shortly under contract to investigate and evaluate a technique whereby without real time delays in the feed array and just by a change in the components used in the dome lens, it appears possible to increase the signal bandwidth to about 10%."

Although the dome on the prototype model approximates a hemisphere, an infinite variety of solid shapes, including a paraboloid or a hybrid of a cylinder and hemisphere, can be used. Schwartzman indicates that the precise shape of the dome can be tailored to favor particular regions in the sky.

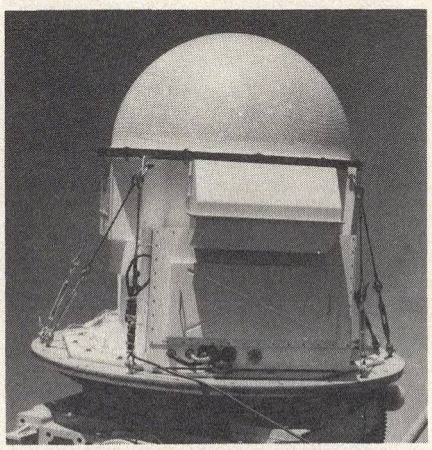

3. Passive phase shifters are visible in the hemispherical dome of this C-band feasibility model. Production models may use printed-circuit elements glued to the inside of a honeycomb dome.

This is an important factor, since the beamwidth of the dome antenna changes with elevation scan angle. "The beamwidth will vary, on the order of 4:1 over the entire scan range, but a typical beamwidth for some of our designs is on the order of 2 degrees at the design point," says the Sperry program manager, referring to the optimized region in space. "By changing the phase function in the feed array, you can change the beamwidth of the antenna. You can zoom," he adds.

One characteristic peculiar to the dome antenna is a rotation of the polarization plane of the radiated signal if linear polarization and dipole elements are employed in the planar feed array. In this case, the plane of the linear polarization varies with azimuth pointing angle, shifting one degree for every degree change in azimuth.

Vertical, monopole elements in the feed array, or a twist of the passive dome elements are two techniques being investigated to correct this problem.

If a circularly polarized feed array is used, azimuth beam position has no effect on the polarization of the radiated signal.

Any type of array and feed network that is capable of generating a non-linear phase excitation can be used as a feed for the dome. "We are also looking at the modernization of current equipment by retrofitting with the dome lens," Schwartzman indicates.

The computer used to steer the illumination from the planar feed array is no more complex than that required for a conventional phased array, says the Sperry program manager, however, a somewhat different tracking algorithm must be used.

Using computer simulations, Sperry has shown the feasibility of the dome antenna concept at frequencies as high as 15 GHz, although there has been no hardware development in Ku-band. At present, the researchers have found no high power limitations. ••

Trolly measures antenna surface fast and accurately

Richard T. Davis
Managing Editor

A simple, fast and inexpensive technique has been developed by the National Radio Astronomy Observatory for measuring the curvature of antenna surfaces to within 0.05 mm. Its precision and speed has significant implications for measuring large millimeter wave parabolic dishes such as those used in radio astronomy, where surface tolerances are very critical.

According to John M. Payne, Associate Head of the Electronics Division of the Kitt Peak National Observatory, Tucson, AZ, the technique is quite different from conventional microwave methods where it's necessary to measure distances from the focal point of an antenna using transponders on the antenna surface; or using a laser to measure distances to optical corner cubes on the surface. Instead, the new method is based on a double-integration process using computer analysis and a three-wheeled trolly that has a very precise depth transducer mounted at its center. The curvature of the surface is measured very accurately at numerous points along a radius of the antenna by drawing the trolly along a fine wire with a constant speed winch. These curvature values are then integrated twice with respect to the distance along the surface by an on-line computer. This process is repeated for different radii and a best fit parabola through the data points is computed. Contours of deviations from the best fit are computed and plotted such as shown in the contour map of an 11-meter antenna, Fig. 1. The measurements are made along a total of 48 radii (at 65 points per radius). "We found that a complete measurement took less than four hours," explains Payne, "with an accuracy of 0.05 mm."

Rms deviations from a best-fit parabola were found to be 0.3533 mm and 0.3469 mm in tests conducted in October, 1974 and March, 1975. The rms deviation, with a 10 dB illumination taper (corresponding to surface accuracies inferred from radiometric tests) showed deviations from the best-fit parabola of 0.2123 mm and 0.2074 mm, respectively. One important feature of this method is that it allows the contour derived to be optically projected onto the antenna measured, Fig. 2. "It's then possible to build up the low areas using layers of conductive material," explains Payne. By re-measuring and projecting the new contours onto the surface, the surface can be builtup gradually until it is almost perfect.

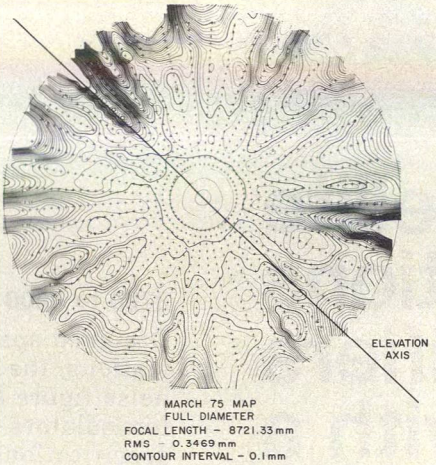

1. **Antenna surface map** for an 11-meter antenna shows up "darker" contour lines where feed legs fell onto the dish.

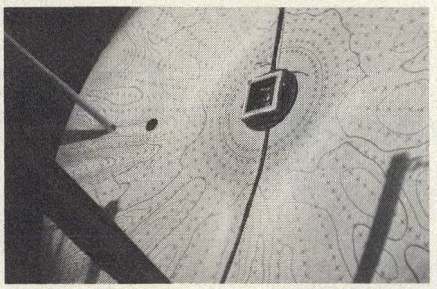

2. **By optically projecting a contour map onto the antenna** itself, it is possible to locate "low spots."

Principle of the method

The theory behind the technique is straightforward. As shown in Fig. 3, if K, the curvature at any point, P is measured nearly continuously at equal steps along surface S, then θ_p may be derived by integration. These curvature values are then integrated again with respect to the distance, along the surface resulting in "Y" as a function of S, (see Eqns. in Fig. 3).

The three-wheel trolly, Fig. 4, actually measures the values, K and S. The single front wheel has attached to its shaft an encoding transducer which gives a TTL pulse 250 times for each wheel rotation. "Each pulse represents a change of an accurately fixed amount and in the device tested, S was 0.6384 mm," says Payne. The computer measures S by counting pulses from the wheel transducer. Each wheel pulse also interrogates the depth transducer and reads it into the computer. The geometry of the 11-meter antenna is such that 6200 data points were taken on each radius. The depth below the plane on which the three wheels rest varied from 1.78 mm to 1.58 mm. The transducer has repeatability of 10^{-4} mm and a linearity of 0.01% over a range of ±0.5 mm. Because of this limited range, the transducer has to be offset by an accurately known amount. Any errors in determining this offset will result in quite severe errors in Y, because the transducer reading is integrated twice.

The effects of temperature have also been analyzed by measuring one radius repeatedly while the ambient temperature was changing. Temperature effects on the trolly were also analyzed and removed so that true change in shape of the antenna could be evaluated.

The method has to date only been applied to solid surface antennas, but it's considered applicable to most antenna surfaces. ••

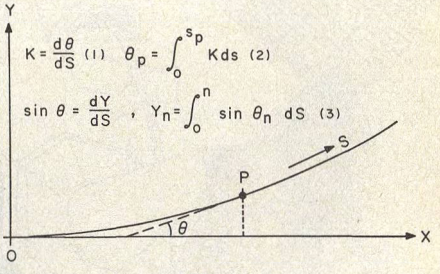

3. **Principle behind this new technique** for measuring the surface shape of reflector antennas is based on the double integration process shown in Eqns. (2) and (3).

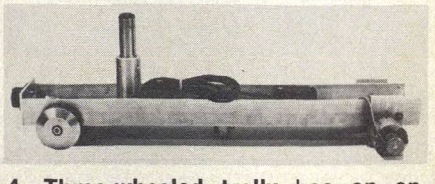

4. **Three-wheeled trolly** has an encoding transducer attached to the shaft of the front wheel.

news

Microwaves disintegrate toxic gases

Harvey J. Hindin Contributing Editor

A microwave disintegrator has been developed capable of destroying hard-to-dispose-of toxic gases, and fluids, such as nerve gases and defoliants. By injecting the contaminants into a microwave resonant cavity, where a plasma is sustained, with a Tesla coil, free electrons can collide with the molecules of the toxic gas and break them down into harmless substances, forming new hydrocarbons.

The prototype system, Fig. 1, was developed by Dr. Lionel J. Bailin and Merle E. Siebert of Lockheed Palo Alto Research Laboratory, in association with Leonard A. Jonas of Edgewood Arsenal in Maryland and Dr. Alexis T. Bell of the University of California at Berkeley.

Up until now, long term or high temperature processing was necessary to render many toxic contaminants harmless. Within recent years, both the military and chemical processing companies have been hard pressed to dispose of many unwanted chemicals and manufacturing byproducts, particularly in view of the growing concern with the environment. The idea that a microwave plasma can help in disposing of these substances and in some cases, allow reclaiming useful chemicals from previously unusable substances, brings new light to bear on a persistent problem.

Zapped with a plasma

Some substances, chemically resembling nerve gas, have already been tested and decomposed successfully. Typically, 10 cubic centimeters (cc) of gas may be processed at a time with the present system. Almost 100% decomposition is obtained at the relatively low temperature of 100-200°C. Depending on the reactants, the breakdown products may be recovered. Current plans call for detoxification of pesticides and other related materials.

The microwave disintegrator consists of an inert gas carrier supply used to transport the toxic chemicals to a quartz reaction chamber or plasma cavity and various chemical sampling systems, which allow the reaction to be monitored, Fig. 2. In the laboratory model a Varian voltage tunable magnetron is used as a power source. (Tuning is ±50 MHz). It delivers up to 2.5 kW cw of power at 2.45 GHz—depending on the type of cooling used for the cavity. Rf radiation at these levels is a concern, and as a result, an rf leakage detector is used for safety. (Levels of 1-3 mW/cm² are not detectable even near the discharge tubes with the present system). The plasma tube is made of quartz and is helium filled.

To operate the system, the pressure in the cavity and waveguide is first reduced to about 20 microns. Then, the gas to be destroyed, is introduced, where it flows into the cavity as shown in Fig. 2. After the cavity is cooled using air and water, the VTM is turned on and tuned for minimum cavity reflection. A Telsa coil is used to ignite the discharge and the plasma is thus initiated and sustained in the cavity. Constant monitoring of the chemical reaction products is performed by nuclear magnetic resonance, gas chromatography and mass spectroscopy equipment. The view port shown in Fig. 2 is for visual observations. To protect the magnetron and insure optimum power transfer to the cavity, either an H-plane double stub tuner or a coupling hole adjustment is used on the input line. Both incident and reflected waves are monitored and displayed continuously. (In the case of an extreme mismatch, the magnetron is automatically turned off). A circulator and water load may also be used on the input line to protect the tube. Additional tuning is provided by a sliding short on the back of the cavity. The microwave discharge gap length may also be adjusted from 0.75 to 1.70 inches. This is optimum for gases with an impedance in the range from 10^2 to 10^6 ohms which is the case in these experiments.

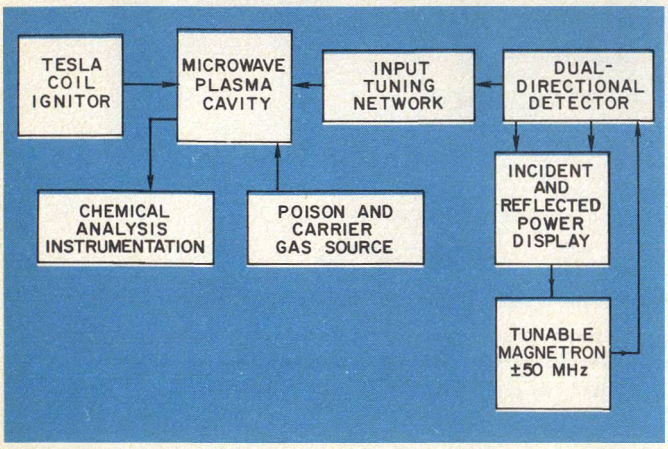

1. In the microwave disintegrator, a plasma is created in a microwave cavity using a telsa coil ignitor. The electrons that result become energetic enough to collide inelastically with air molecules resulting in additional electrons and charged ions. These charges can then react chemically with the substance to be destroyed.

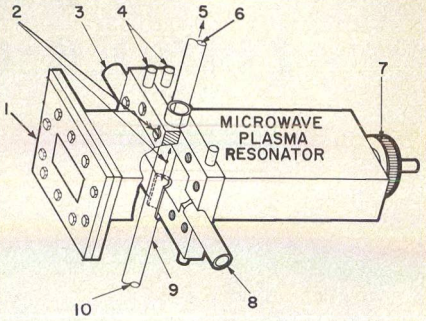

2. Cavity resonator has following ports for introducing the reactant gases and microwave power: (1) resonator flange, (2) microwave discharge gap and adjustment screw, (3) cooling air input, (4) cooling water tubes, (5) to pump, (6) reaction products output, (7) sliding short tuner, (8) aid outlet and view port, (9) gas flow systems and (10) reactant gas input.

What are the problems?

According to Dr. Bailin, the research could result in commercial equipment for handling many toxic substances that now present major disposal problems. While experiments to date have only been done on a laboratory scale, larger systems are being designed.

The present 10 cc capability is too small for commercial applications, and it is being expanded to a two-liter capacity. In addition, a newly-refined plasma system which will let the researchers maintain a more stable plasma is being developed.

The two-liter system will allow Dr. Bailin and his associates to look into the problem of reaction product accumulation and removal. System throughput, which is defined as how much of the toxic materials can be handled in a given time, is also under study. ••

Measure That Field Using Any Antenna

Here are some handy graphs for determining an antenna factor. This parameter is very useful in measuring electric-field intensities and allows practically any antenna, so characterized, to be used for this measurement.

AN antenna's main function is to act as a transducer from a conducted signal to a radiating free space electromagnetic wave and, in so doing, gives the radiated signal both polarization and directivity. Conversely, an antenna is a converter of these electromagnetic waves to a measurable conducted voltage when used as a receiver antenna. When converting quantitatively from a conducted voltage to a field intensity, a correction factor can be used called the antenna factor. This antenna factor value incorporates:

- the change in cable impedance (50, 75 or 300 ohms) to that of free space (377 ohms).
- the antenna's effective capture area to an equivalent one linear meter of space
- any losses caused by an imperfect antenna, as well as impedance mismatch losses.

The use of the antenna factor has been around ever since there were antennas and receivers. If this antenna factor is known, it is possible that most any antenna can be used as a calibrated instrument for field measurement. This capability is desirable because frequently actual field intensity measurements are required at a given location, at a specific time. Specialized antennas need not then be employed to measure field intensities.

This article provides graphs for obtaining the antenna factor of any antenna provided the antenna gain, output cable impedance are known. Example problems are presented along with some pitfalls that should be observed in using the curves.

Converting voltages to field intensities

Few antennas have published antenna factors, and those that do mostly are specialized ones used for MIL standards. However, this factor can be easily derived. Most horns, dipoles, biconicals, conical log spirals, log periodics and other common antenna types do provide gain data. This antenna gain may be converted to an equivalent factor for evaluating a field intensity for a given measured voltage.

H. Vincent Carnagan, Jr., Senior Electronic Engineer, Anaysis Branch, Frequency Management Division, USA Communications Command, White Sands Missile Range, NM.

A simple method of converting an rf conducted receive voltage to an rf field intensity for most antennas is as follows:

Antenna factor = −29.8 dB + 20 log f (MHz) − G (dBi) (for 50 ohm system)
= −31.5 dB + 20 log f (MHz) − G (dBi) (for 75 ohm system)
= −37.6 dB + 20 log f (MHz) − G (dBi) for 300 ohm system)

Alternately, Fig. 1, may be used to determine the antenna factor (AF).

When using the chart in Fig. 1, find the frequency on the abscissa, go to the 0 dBi line (50, 75 or 300 ohm) and read antenna factor off the ordinate. The gain of the individual antenna must then be subtracted from the 0 dBi antenna factor. The way to remember this is that all antennas are poor transducers (i.e., field voltages are greater than the received voltage or dBμV/m > dBμV) and the better the antenna, the closer the field density is to the conducted voltage. This perhaps is best illustrated with an example to find a field intensity. In units of dBμV (decibels above one microvolt), the field intensity (dBμV) antenna factor (dB) + receiver meter reading (dBμV) + cable loss (dB). Assume the receiver meter reads 10 dBμV on a 50-ohm system, frequency

(continued on next page)

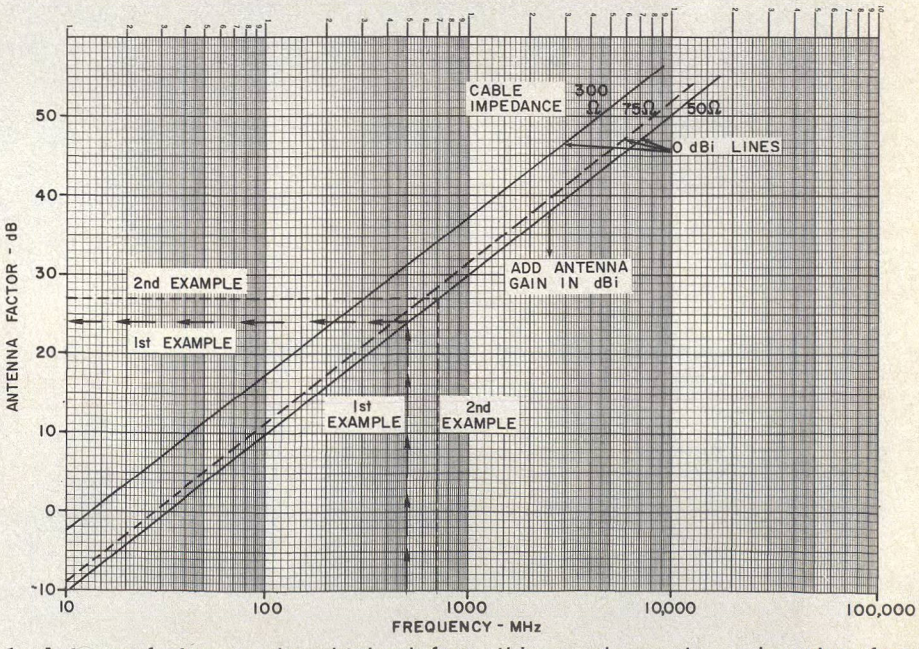

1. **Antenna factor** can be obtained from this graph as shown knowing frequency and impedance. Antenna gain must be subtracted from the antenna factor reading.

= 500 MHz and the measured antenna gain is 10 dBi. From Fig. 1, the antenna factor = 24 dB at 500 MHz for an antenna gain of 0 dBi on a 50-ohm system. Subtracting the antenna gain of 10 dBi results in a 14 dB antenna factor. Field intensity then = 14 dB + 10 dBμV/m = 24 dBμV/m = 15.8 dBVμ/m = 132 dBm/cm^2.

Another example shows how to evaluate the required gain of antenna knowing the field intensity.

Given Field Intensity = 14 μV/m at 700 MHz

The needed input to the receiver = −100 dBm on a 50 ohm system

Convert 14 μV/m to dBμV/m using dBμV = 20 log XμV (or Fig. 2) = 22.92 dBμV/m ≈ 23 dBμV/m.

Convert −100 dBm to dBμV by subtracting −107 dBm (0 dBμV for a 50-ohm system), which gives +7 dBμV for the 50-ohm receiver requirement. The next step is to find the antenna factor at 700 MHz for the 50-ohm system. For an antenna with 0 dBi gain, Fig. 2 gives an antenna factor of 27 dB. Thus 23 dBμV/m = 27 dB − G (dBi) + 7 dBμV or G = 11 dBi which is the required antenna gain.

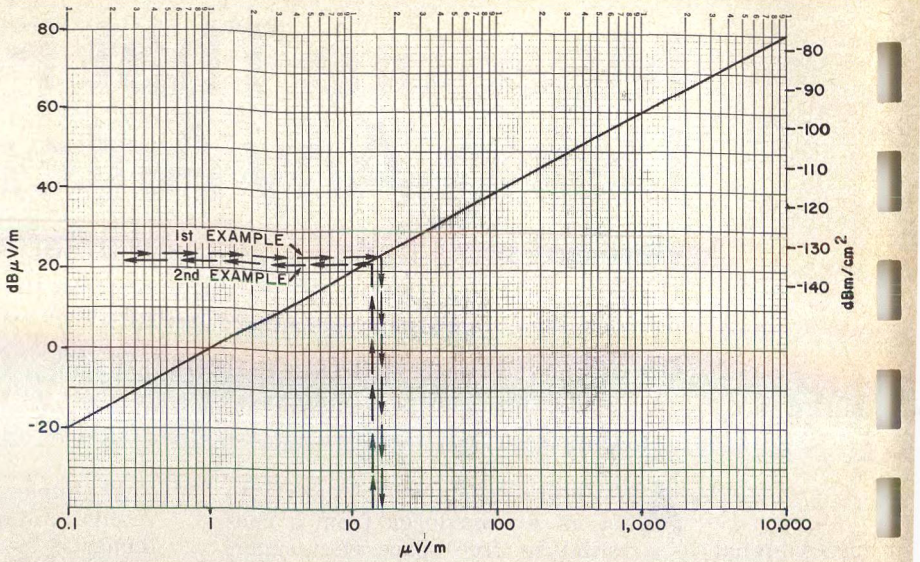

2. **Chart for converting field measurement,** dBμV/m to μV/m or dBm/cm^2, shows alignment procedure for the example problems. (Note that 0 dBμV/m = −156 dB/cm^2 = −116 dBm/m^2).

Observe these precautions

There are a few qualifications and exceptions which should be taken into consideration when applying the curves.

- Monopoles and loops: Some antennas have impedance transformers in their bases. These transformers reduce the conducted voltage up to 70 dB due to voltage transformation. This reduction must be taken into account when using the theoretical gain of these antennas.
- Circular polarized antennas: Some published gains are erroneously in terms of dBic. Use Ref. 2 for converting from linearly polarized antenna gains.

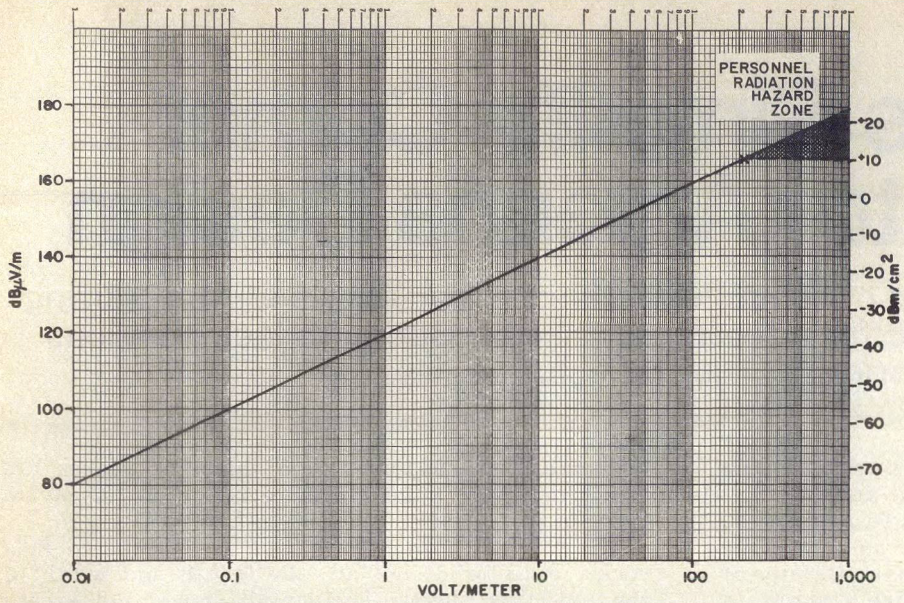

3. **For converting higher field readings,** dBμV/m to V/m or dBm/cm², this chart is useful. Note the occurrence of the personnel radiation hazard zone beginning at upper right.

- If a circular-polarized antenna is used to measure a circular-polarized wave, the procedure is the same as usual. However, if a linear antenna is used, the two rotating electromagnetic rectors must be broken into two orthogonal linear fields, E_1 and E_2. E_1 and E_2 must then be added together (V/m plus V/m, not dB plus dB) to obtain the field intensity of this wave.
- Cross polarized antennas: A vertically polarized wave is not compatible with a horizontally-polarized antenna. Neither is a righthand circular polarized wave compatible to a lefthand circular antenna.
- Low frequency antennas: Most low-frequency antennas are small compared to the wavelength. Don't be surprised with gains much less than 0 dBi.
- Re-radiation or bounce: Most reflection problems can be overcome by moving the testing antenna forward and backwards or up and down by at least a half-wave length and averaging the readings. ••

References

1. John D. Kraus, Antennas, Empire Devices, NF-105 Operators Manual, MIL-STD 461, McGraw Hill, (1950).
2. Paul J. Sroka, "Nomograph Saves Time In Converting Antenna Gain," MicroWaves, Vol. 13, No. 3, pp. 54-55, (March, 1974).

Test your retention

1. What is the antenna factor of an antenna?
2. What type of antenna can be used to measure field intensity?
3. What is the general antenna "rule of thumb" for converting field intensity levels to conducted voltage levels?

Graphs Simplify Corner Reflector Antenna Design

Here are a series of computer-derived design charts for maximizing the radiated field from a corner reflector. Optimum feed positions are shown for various corner reflector angles.

A corner reflector antenna has unique applications and interests because of its simple construction. It is formed by the intersection of two plane reflectors and usually is fed by a dipole or a collinear array. A characteristic of the corner reflector is that it will return a signal in the same direction exactly in which it was received. Because of this characteristic, a corner reflector finds some use in radar and microwave communication systems. In fact, military vehicles and ships must consider in their design the reduction of sharp corners which can form corner reflectors and thus make it easier to be seen by enemy radar. One of the greatest uses of a corner reflector is in home television reception.

Corner reflector antennas are most practical when apertures of 1 or 2 wavelengths are of a convenient size. The corner angle, Fig. 1, may vary from any angle up to 180 degrees. When the corner angle is 90 degrees, the sheets form a square-corner reflector.

David Proctor, Electronics Engineer, Naval Electronics Laboratory Center, 271 Catalina Blvd., San Diego, CA 92152.

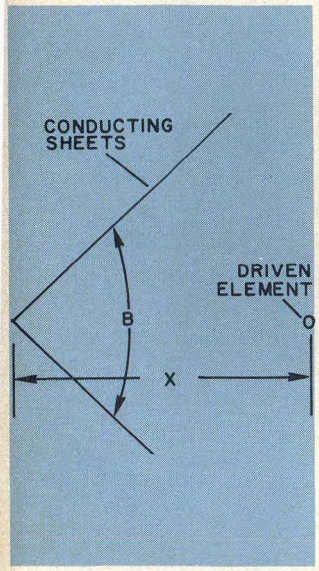

1. **Cross section of a corner reflector** reflects critical dimensions. For maximum power transfer, with a given corner angle, B, the driving placement, X, is critical.

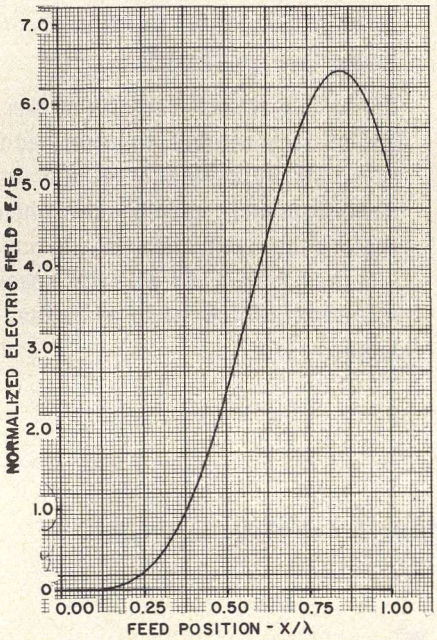

2. **A maximum field is achieved for a 45-degree corner reflector** when the driving element is located slightly over 3/4 λ from the apex.

Corner angles greater or less than 90 degrees are commonly used, although there are some disadvantages to using angles much less than 90 degrees.

The major factors which must be considered in a corner reflector design are the length and width of the reflecting sheets. The length should not exceed around three times the spacing between the driven element and apex, since further increase in size will not greatly affect the gain and beamwidth (although the bandwidth is increased somewhat).

The most critical factor in the design is the placement of the driven element relative to the corner. This article provides the information in graphic form to calculate the proper spacing for several common corner reflector angles. A thorough discussion of corner reflector design is given in Ref. 1.

Analysis by method of images

The performance of a corner reflector may be analyzed by the method of images. Moullin[2] gives an expression in the form of a series of Bessel functions from which the relative field can be calculated:

$$E/E_o = 4n(-1)^{n/2}\{J_n(k)\cos n\theta + J_{3n}(k)\cos 3n\theta + J_{5n}(k)\cos 5n\theta + \cdots\} \quad (1)$$

when n is even and

$$E/E_o = 4nj(-1)^{(n-1)/2}\{J_n(k)\cos n\theta - J_{3n}(k)\cos 3n\theta + J_{5n}(k)\cos 5n\theta - \cdots\} \quad (2)$$

where n is π/B and where the corner angle, i.e., the angle between conducting sheets is B.

θ is the angle normal to corner of the two plates and is usually zero.

k is any vector distance from the apex.

E_o = maximum value of the electric field.

However, only when n is an integer does a system of images exist and the above equations are valid. When n is a fraction, the field must be evaluated by the laborious process of adding sufficient terms of the infinite series. The following expression from Moullin[2] is valid for all values on n, integral and fractional

$$E/E_o = 4n\{e^{nj\pi/2}J_n(k)\cos n\theta + e^{3nj\pi/2}J_{3n}(k)\cos 3n\theta + \cdots\} \quad (3)$$

For all values of fractional n, there are two components of field in phase quadrature. There is no value of k which makes the forward field zero. For all values of n, the forward field fluctuates periodically as k is continuously increased.

The significance of all this is that the driving element must be placed relative to the apex of the corner reflector in such a position that the field is near a maximum for all frequencies concerned. A computer program was written to solve Eqn. (3) for maximum power transfer as a function of angle B. The curves in Figs. 2-7 show the more common angles of B equal to 45, 60, 90, 120, 150 and 180 degrees. The computer is written in Fortran IV and copies are available by writing to the author. ••

(continued on p. 52)

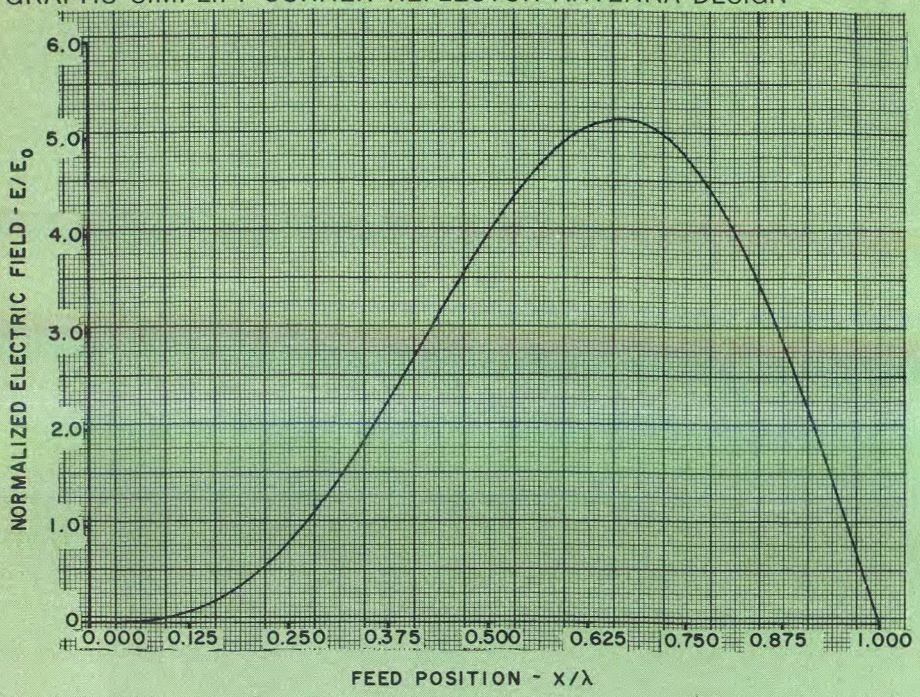

3. **A maximum field is achieved for a 60-degree corner reflector** when the driving element is located slightly less than 3/4 λ from the apex.

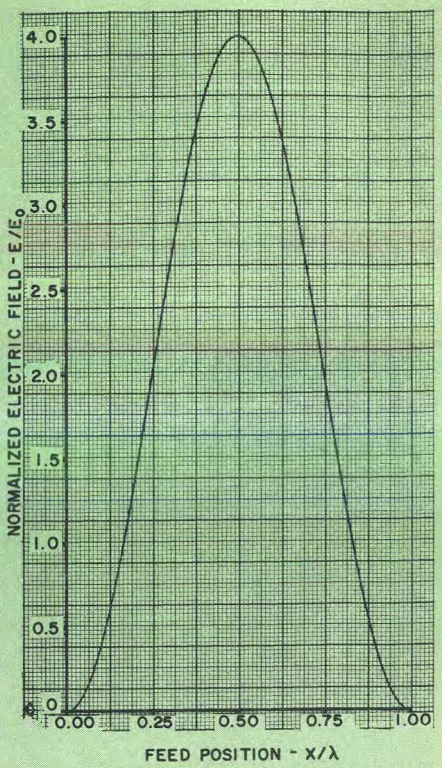

4. **A maximum field is achieved for a 90-degree corner reflector** when the driving element is located at λ/2 from the apex.

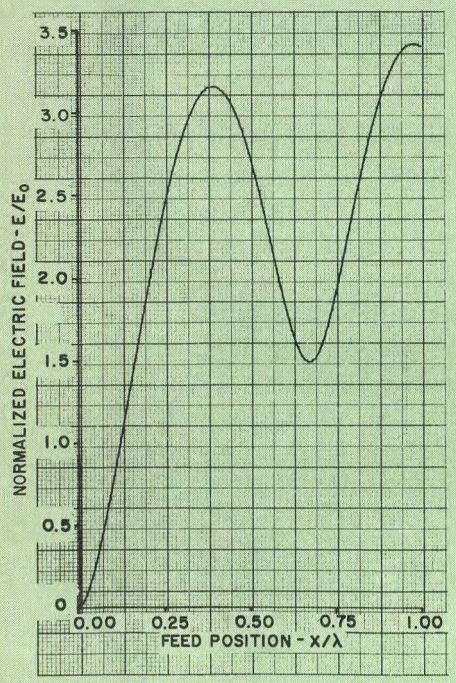

5.

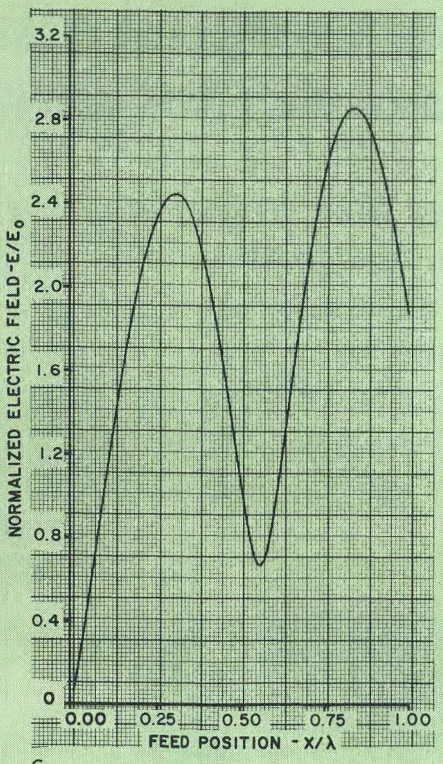

6.

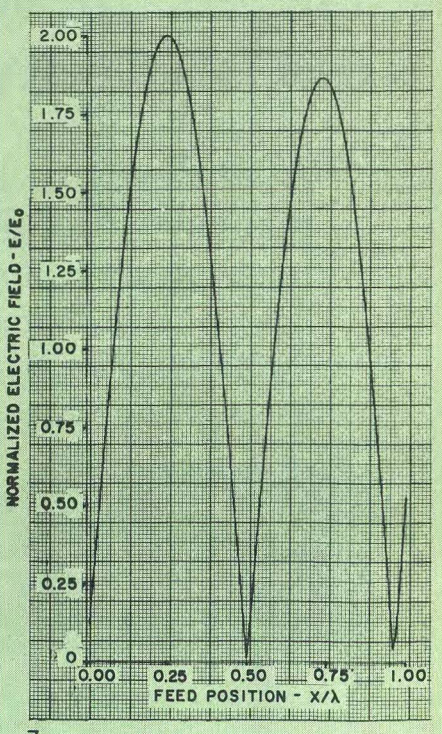

7.

5, 6, 7. **For corner angles over 100 degrees,** two peaks in the relative field occur spaced approximately λ/2 apart. Note the relative decline in field intensity for increasing angles of B: 120°, 150°, and 180° respectively.

References

1. J. D. Krause, "The Corner-Reflector Antenna," *Proc. I. R. E.*, Vol. 28, pp. 513-519, (November, 1940).
2. E. B. Moullin, *Radio Aerials*, Oxford University Press, Amen House, London E. C. 4, (1949).

Bibliography

D. Proctor, Preliminary Investigation to Expand the Capability of the AN/SPS-10 Radar Antenna, Naval Electronics Laboratory Center, TN 2713, June 19, 1974.

Test your retention

1. What principal property is associated with corner reflector antenna?
2. What mathematical method is used to analyze its performance?
3. Where must the driven element be placed relative to the apex of the corner reflector?

Determine Polarization Loss The Easy Way

Here's a graphical method to determine polarization loss that provides 0.1 dB resolution. Also included is a list of loss equations that can be solved with many pocket calculators.

THE problem of finding the loss due to polarization mismatch between two antennas is a common one and many formulas and graphs are available [1,2,3] for solving it. These formulas are, however, rather unwieldly. And, although the published graphs are easier to use, they don't provide adequate resolution.

Here's a different graphical method that can be used to solve the most common polarization problems —linear to elliptical and elliptical to elliptical—with a resolution of 0.1 dB. Since it operates like a Smith chart, the techniques for using it are familiar.

Consider the two most common polarization loss problems:

- Given a linearly polarized transmitting antenna and an elliptically polarized receiving antenna with axial ratio AR_r, what is the maximum and minimum polarization loss?
- Given an elliptically-polarized transmitter with axial ratio AR_t dB and an elliptically polarized receiving antenna with axial ratio AR_r dB, what is the maximum and minimum polarization loss?

The following examples show how each of these problems can be solved using the chart.

The first illustration involves a linearly polarized transmitting antenna and an elliptically polarized receiving antenna with an axial ratio of 2 dB. With the help of the chart, the maximum and minimum polarization loss can be found in a straightforward manner. Simply enter the chart at the lower intersection of the 2 dB semicircle with the vertical axis and project this point horizontally to the "linear to elliptical" loss scale, where the minimum loss of 2.1 dB can be read. Similarly, the upper intersection of the 2 dB circle with the vertical line, when projected horizontally to the same loss scale, will give the maximum loss of 4.1 dB.

A tougher problem involves finding the loss associated with two elliptically polarized antennas with unequal axial ratios. For example, consider an elliptically polarized transmitter with an axial ratio of 2 dB and an elliptically polarized receiving antenna with axial ratio of 5 dB, and the same polarization sense.

To find the minimum and maximum polarization loss, enter the chart at the lower intersection of the 2 dB semicircle with the vertical axis (a). Measure the distance to the lower intersection of the 5 dB semicircle (b) with a divider and transfer this distance to the "elliptical to elliptical" loss scale, reading the minimum polarization loss of 0.1 dB. To determine the maximum loss, set the dividers to the distance from the lower intersection of the 2 dB contour to the top intersection of the 5 dB contour (c). Transferring this distance to the "elliptical to elliptical" loss scale yields 0.67 dB.

Emanuel Kramer, Senior Member of the Technical Staff, ESL, Inc., 8150 Leesburg Pike, Suite 410, Vienna, VA 22180.

Use the graph, or your calculator

These polarization loss equations involve only trig, inverse trig, common log and common antilog functions and are therefore well adapted to scientific pocket calculators.

A. Linearly Polarized to Elliptically Polarized

$L_p(\max)$ = maximum polarization loss (dB) $= 20 \log_{10}(\sin(\arctan R))$ (1)

$L_p(\min)$ = minimum polarization loss (dB) $= 20 \log_{10}(\cos(\arctan R))$ (2)

$$R = \text{axial ratio} = \text{antilog}_{10}\left(\frac{R(dB)}{20}\right)$$

$1 \leq R \leq 0$, so R (dB) must be negative

L_p = polarization loss

$= 20 \log_{10}(\cos(1/2 \arccos(\cos(2 \arctan R) \cdot \cos 2\beta)))$ (3)

β = angle between linearly polarized antenna and major axis of polarization ellipse

B. Elliptically Polarized to Elliptically Polarized (some polarization sense)

$L_p(\max)$ = maximum polarization loss $= 20 \log_{10}(\sin(\arctan R) + (\arctan R'))$ (4)

$L_p(\min)$ = minimum polarization loss $= 20 \log_{10}(\cos(\arctan R) - (\arctan R'))$ (5)

R = axial ratio of 1st antenna $= \text{antilog}\left(\frac{R(dB)}{20}\right)$

R' = axial ratio of 2nd antenna $= \text{antilog}\left(\frac{R'(dB)}{20}\right)$

L_p = polarization Loss $= 10 \log_{10}[1/2 (1 + \sin(2 \arctan R) \cdot \sin(2 \arctan R') + \cos(2 \arctan R) \cdot \cos(2 \arctan R') \cdot \cos(2\beta'))]$ (6)

β' = angle between major axes of polarization ellipses ••

In other words, the minimum loss is measured by the minimum distance between any two points on the two axial ratio circles and the maximum loss is measured by the maximum distance. ••

References

1. V. H. Rumsey et al, "Techniques for Handling Elliptically Polarized Waves with Special Reference to Antennas," *Proc. IRE.*, Vol. 39, pp. 533-556, (May, 1951).

2. B. J. Lamberty, "Polarization Coupling Curves," Sylvania Electronic Defense Labs, Report EDLM-593, (1964). (Also, issued as NASA N64-18184).

3. R. Hartop, "Design Curves Speed Antenna Polarization Loss Calculations," *MicroWaves*, Vol. 3, No. 8, pp. 24-27, (August, 1964).

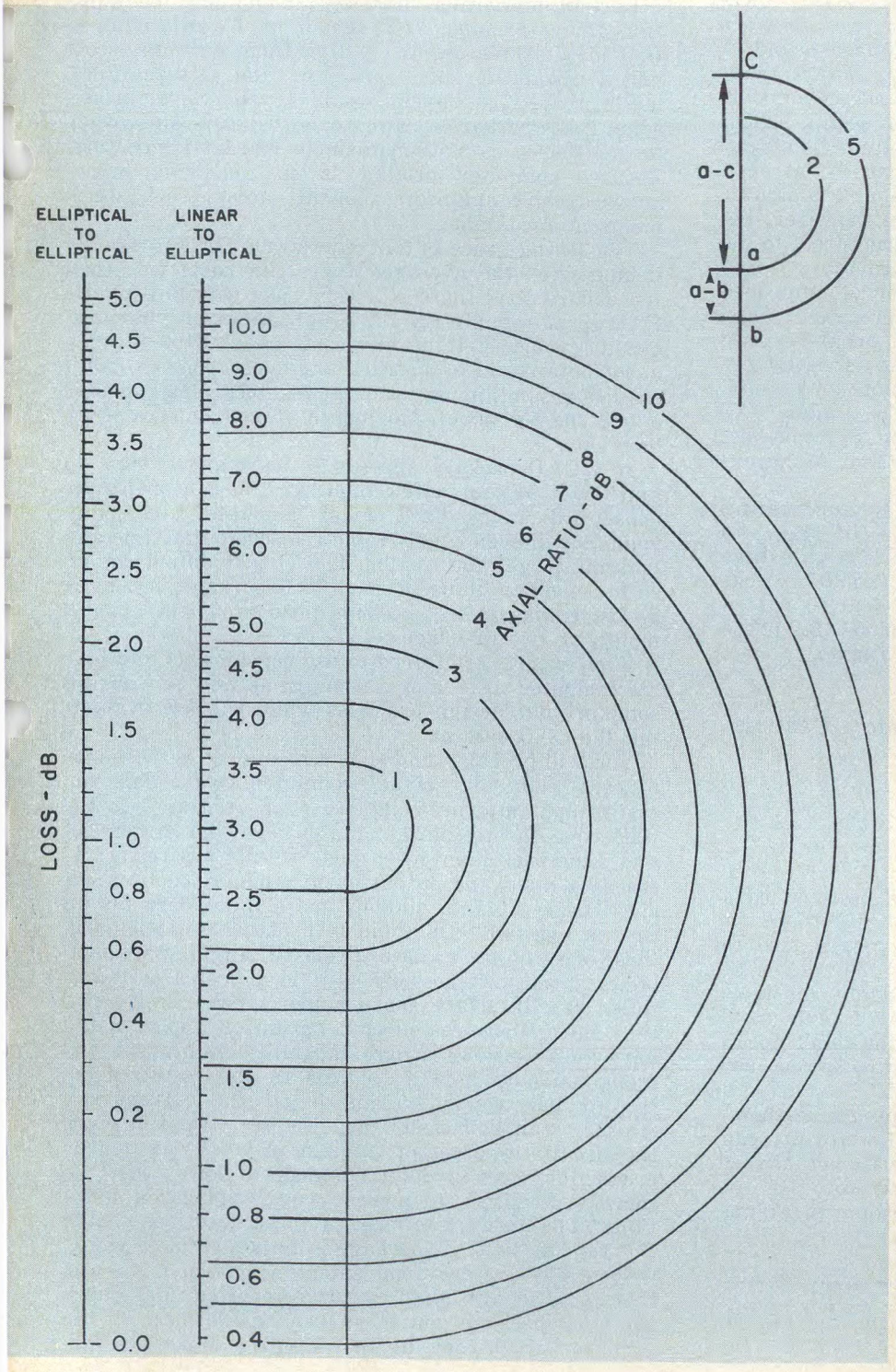

Put Some Magic Into Amplifier Design

Here are some tips on what to look for in computer-aided design software. A 2.0 to 2.5 GHz, two-stage transistor amplifier is optimized to illustrate the potential of Magic, a CAD program with versatility.

MODERN computer-based technology can greatly ease the work load and increase the efficiency of microwave and rf design engineers. The modern CAD programs available today are both convenient to use and economical; they permit significant compression of design schedules and yield considerably increased circuit performance. Most microwave engineers are usually, at best, only casually familiar with computers and computer software. This is of little consequence, however, because modern CAD programs are structured to be easily used by practical hardware designers.

Magic (Modern Analytical Generator of Improved Circuits) was one of the first of such programs. (For a complete listing of microwave CAD programs, see p. 67, June, 1974 MicroWaves.) Magic is nationally available on several computer systems on a "dial-up" basis through University Computing Co., Dallas, TX; Chi Corp., Cleveland, OH; Information Systems Design, Inc., Oakland, CA and Sci Tek, Inc., Wilmington, DE.

This article presents guidelines for engineering evaluation of CAD systems and the use of Magic to illustrate the computer-assisted design of a two-stage broadband amplifier in stripline media. You'll see that a few seconds of using Magic is sufficient to flatten a 6 dB passband "tilt" to within ±0.50 dB. These techniques are valid at any frequency range.

Evaluating a CAD system

There are five key criteria to evaluate a CAD system:

- Cost
- Convenience
- Power
- Flexibility
- Support

Cost should always be considered rather than "price" because there is a significant difference. A cheap computer program may be very expensive to use. For example, if a program costs four times as much per second and runs ten times faster, you have actually saved 250%. Computer pricing is extremely complex and quoted "per second" rates don't mean much. Frequently, the computer with the lowest per second cost is the most expensive.

The same holds true with the CAD programs themselves. A program priced with a very low royalty can be computationally inefficient and thus its actual cost very high. In addition, it is very easy to "rig" an optimization example to make a program run at unusually high efficiency.

John D. Trudel, Technical Staff, Tektronix, Inc., P. O. Box 500, Beaverton, OR 97077.

Certain marketing practices should also be questioned. For example, if a vendor of TV sets claimed that his only reasons for selling them were to establish a market for his transistors and picture tubes, most prospective buyers would laugh. Nevertheless, some CAD packages claim to be "cheap" since they are only used as a mechanism to market transistors. Because computer pricing is so confusing, many knowledgeable engineers foolishly accept such statements at face value.

The saving grace is that microwave CAD is usually inexpensive—the average Magic run costs less than ten dollars. And there is a very easy way to evaluate CAD costs—simply try the program out on your own circuit problems. It usually costs about $100 to open a computer-service contract and most vendors don't require any minimum usage guarantees. You can rent a teletype for about $50/month if you don't already have one.

If a CAD package appears to have merit, sign up and try it out for a few months. You can open purchase orders for fixed dollar amounts, and many vendors will even supply some free computer time and training to get you started. It will take only a day or so to learn how to use a good CAD package, and most design engineers will become quite proficient after a month or two of usage.

Even experts are forced to use benchmarks to evaluate computer costs, and you might as well be working some of your design problems while you are evaluating the CAD system.

You will probably find that convenience is more significant than your actual computer costs. Can you easily input measured data to your program? Is the wait time for results acceptable, can you disconnect and come back later when your results are ready? Is the data input and output easily understood by a design engineer? Is a single concise input data file all that is required? On complex problems—particularly those of a non-linear nature (class C amplifiers, multipliers, diode switches, etc.)—it is almost a certainty that you will have to make numerous short optimization runs. Does the circuit optimizer you're using have an automatic restart capability to prevent you from manually having to type in the results from the previous computer run to get the current run started? Can you easily plot, display or optimize all the circuit responses of interest to you? Can you do production runs in deferred mode at lower cost? Is someone available to answer your application questions? The answers to most of these questions should be "yes" if the CAD package is to be useful to you.

Regardless of how convenient a system is to use, there is a definite learning curve involved. Make sure the CAD package you select can handle most of the problems which come up in your firm. Make sure the

package can handle large scale (25 or more variable circuit elements) problems so that it will be efficient on circuits of normal size. You should be able to handle both active and passive circuits and optimize everything from reflection coefficients to time delay. Magic, for example, can be used for almost every type of circuit: sub-audio filters, i-f crystal filters, oscillators, broadband amplifiers, harmonic filters and antenna matching networks. It handles lumped and distributed components with equal convenience.

In addition to the power to handle a wide class of circuits, it is highly desirable that a CAD package perform a number of functions. It is quite convenient and valuable if a program can optimize, display or plot any measurable circuit response. A single run should be able to compute all circuit responses, do plots and Smith Charts and generate frequency sweeps.

Magic has certain additional features not available in some other programs: stability analysis computes stability circles, K factor, maximum available gain (MAG) and the terminations which yield MAG. Statistical (Monte Carlo) analysis computes the mean and upper and lower 1-Sigma (66% confidence) and 3-Sigma (99% confidence) limits for any element tolerances and any circuit response. Automatic restart allows the designer to continue from previous optimization runs. Sensitivity analysis allows the engineer to determine in physical terms which components are most critical for production tuning.

Finally in evaluating a program, be sure the software package you choose is proven, its results can be trusted and that someone is available to answer the technical questions which will inevitably arise in day-to-day usage. Ideally if a program such as Magic is offered by several computer-service vendors, you can feel free to "shop around" for the best service in your local area.

How to use Magic

The actual mechanics of operating Magic are quite straightforward. In an analysis mode, it is purely a matter of syntax—you have to explain your problem in terms the program understands. Magic speaks engineering English: typical commands include UNITS GHZ, NHY, PF, OPTIMIZE RHO, PLOT VSWR VSWR2 and SMITH INPUT. A parallel LC branch is called PLC, and a transmission line is called LINE. The input is conversational, free format and quite concise. Furthermore, the level of realism is high. An inductor may have an associated Q factor and dc resistance, a transmission line may be specified by impedance and either electrical or physical length and may also have associated loss. No device modeling is required. You can either input your own measured data or use built-in s-parameter data files for Hewlett-Packard and CTC transistors. (Incidentally, if vendor data is not already in Magic's library, it can be added at no cost to you or the vendor.) Magic handles up to 500 circuit elements and up to 50 may be simultaneously optimized.

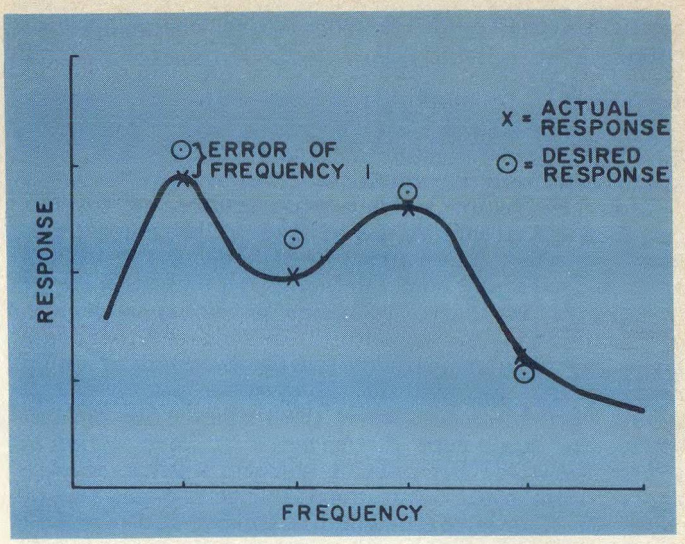

1. **The optimization process of Magic** involves minimizing a weighted error function that is the difference between the desired response and the actual response over a specified band.

With Magic, the optimization routine is more subtle than simple analysis. The user must convey his design specifications to the computer by forming an error function, and this concept must be clearly understood if useful results are to be obtained. The error function is a simple measure (Fig. 1) of the difference

(continued on next page)

between actual circuit responses and design goals or "aims":

$$\text{error} = \sum_{\text{all freq.}} (\text{actual response—"aim"})^{P} \cdot \text{weight}$$

where the power P is an arbitrary even positive integer with a default value of 2.

This "P" factor yields a least squared fit to your curves while higher values of P give Chebyshev "min-max" type fits. The "aims" are the desired responses at each frequency, and the weights merely tell Magic how important each frequency is. For example, in optimizing the insertion loss (DBINS) of a bandpass filter, the frequencies near the passband edges would normally be weighted heavily (say 10.0) so Magic would work hard to correct the tendency for the response to "sag" near the corners. As Magic tries to reduce the error function, it will run until it reaches an optimum solution or until a specified amount of computer time is consumed. The experienced user will always start his problems by making short runs while adjusting the aims, weights, frequencies and other options to impose his design judgement on the program. The restart feature of Magic is quite valuable for it allows the designer to easily continue optimization from a previous computer run.

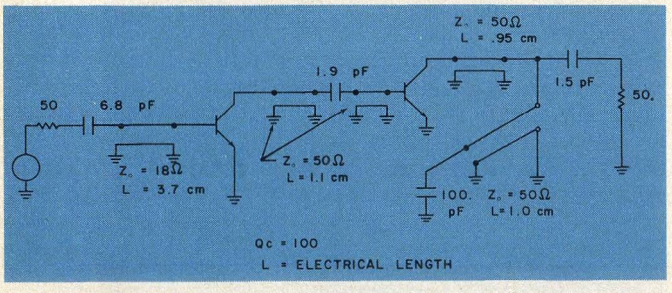

2. **Proposed two-stage transistor** amplifier design covers 2 to 2.5 GHz and is optimized for maximally flat gain (to 0.5 dB). Distributed elements are given in equivalent metric electrical lengths.

```
 10 UNITS GHZ NHY PF CM
 20 ELEMENTS
 30 SV C 6.8 100
 40 SV LINE 18. 3.7
 50  S SCAT1
 60 SV LINE 50. 1.1
 70 SV C 1.9 100
 80 SV LINE 50. 1.1
 90 S SCAT1
100 SV LINE 50. .95
110 G JUNCT 2
120 SV LINE 50. 1.
130 GV C 100. 100
140 SV C 1.5 100.
150 RESPONSE
160 2. -23. 15.
170 2.1 -23. 5.
180 2.2 -23. 5.
190 2.3 -23. 5.
200 2.4 -23. 5.
210 2.5 -23. 10.
220 SCAT1
230 .540,-175.,.068,29.,3.3,66.,.53,-64.
240 .540,-178.,.07,29.,3.21,64.6,.52,-66.
250 .54,179.5,.071,28.,3.11,63.2,.520,-67.
260 .54,178.,.073,28.,3.02,61.8,.52,-68.
270 .54,176.,.074,27.,2.92,60.4,.52,-70.
280  .540,175.,.076,27.,2.83,59.,.52,-72.
290 GENR 50.
300 LOADR 50.
310 OPTIMIZE DBTOT
320 SECONDS 60.
330 RUN
340 END
```

CIRCUIT DESCRIPTION

FREQUENCIES, AIMS, AND WEIGHTS

MEASURED DEVICE S PARAMETERS

3. **Input data lists circuit elements** of Fig. 2 from left to right from generator to the load. S-parameters characterize the transistors. Note that the Q of capacitors as well as their values are given.

```
* * * * * * * * * * * * * * * * MAGIC * * * * * * * * * * * * * * * * * * * *
                        (REVISION 5.65)


UNITS DETECTED ( GHZ  NHY  PF   CM    )
ELEMENTS DETECTED
NUMBER OF BRANCHES =       12
RESPONSE DETECTED
FREQUENCY DEPENDENT MATRIX DETECTED
NUMBER OF FREQUENCIES =     6
GEN DETECTED
LOAD DETECTED
OPTIMIZE DETECTED  ( DBTOT  )
SECONDS DETECTED. TIME =      60.0
RUN DETECTED
- - - - - - - - - - - - - - - - - - - - - - - - - - - - - - - - - - - - - - -

S MATRIX (NORMALIZED TO 50 OHMS) NUMBER  1

 MG(S11)  AN(S11)  MG(S12)  AN(S12)  MG(S21)  AN(S21)  MG(S22)  AN(S22)

 .540-00 -.175+03  .680-01  .290+02  .330+01  .660+02  .530-00 -.640+02
 .540-00 -.178+03  .700-01  .290+02  .321+01  .646+02  .520-00 -.660+02
 .540-00  .179+03  .710-01  .280+02  .311+01  .632+02  .520-00 -.670+02
 .540-00  .178+03  .730-01  .280+02  .302+01  .618+02  .520-00 -.680+02
 .540-00  .176+03  .740-01  .270+02  .292+01  .604+02  .520-00 -.700+02
 .540-00  .175+03  .760-01  .270+02  .283+01  .590+02  .520-00 -.720+02

- - - - - - - - - - - - - - - - - - - - - - - - - - - - - - - - - - - - - - -
- - - - - - - - - - - - - - - - - - - - - - - - - - - - - - - - - - - - - - -

          INPUT DATA

BRANCH   TYPE     CONNECT      VALUE1      Q1       VALUE2      Q2

   1     C        SERIES        6.800     .10+03
   2     LINE     SERIES       18.00      .00       3.700
   3     MATRX1   SERIES     SEE TABLE FOR VALUES
   4     LINE     SERIES       50.00      .00       1.100
   5     C        SERIES        1.900     .10+03
   6     LINE     SERIES       50.00      .00       1.100
   7     MATRX1   SERIES     SEE TABLE FOR VALUES
   8     LINE     SERIES       50.00      .00       .9500
   9     JUNCTN   GROUND   (NEXT  2 BRANCHES CONNECT TO JUNCTION)
  10     LINE     SERIES       50.00      .00       1.000
  11     C        GROUND      100.0      .10+03
  12     C        SERIES        1.500     .10+03


GENERATOR R =   50.00
    LOAD R =   50.00

          OPTIMIZATION REQUESTED

INITIAL LEAST SQUARE ERROR =    354.7 } IMPROVEMENT BY
  FINAL LEAST SQUARE ERROR =    5.703 } A FACTOR OF 62

INITIAL VARIABLES      FINAL VARIABLES      % CHANGE

  6.7999999              6.9360562            2.0008
 18.000000              22.568094            25.489
  3.7000000              3.3419501           -9.6770
 50.000000              55.647748            11.295
  1.1000000              1.0431429           -5.1688
  1.9000000              2.0733855            9.1256
 50.000000              49.948271            -.10346
  1.1000000              .99777582           -9.2931
 50.000000              50.730339             1.4607
  .95000000              .95552550            .58163
 50.000000              64.873655            29.747
  1.0000000              1.3102803           31.028
100.00000              101.31342             1.3134
  1.5000000              1.8113597           20.757

                                          INITIAL RESPONSE
                                          OPTIMIZED RESPONSE

 FREQ      WEIGHT     AIM      INITIAL DBTOT   FINAL DBTOT    ERROR

2.00000      15.    -23.00      -18.839        -22.642        .358
2.10000       5.0   -23.00      -21.110        -23.198       -.198
2.20000       5.0   -23.00      -23.270        -23.485       -.485
2.30000       5.0   -23.00      -24.914        -23.507       -.507
2.40000       5.0   -23.00      -25.469        -23.219       -.219
2.50000      10.    -23.00      -24.672        -22.703        .297

- - - - - - - - - - - - - - - - - - - - - - - - - - - - - - - - - - - - - - -
```

4. **Magic output adjusts circuit element values** to achieve a desired response. Optimization improves circuit by a factor of 62. Further improvements are still possible by adjusting the objectives, weights and considering additional frequencies.

The key point to remember is that optimization is iterative from both a mathematical and operational viewpoint. Magic will automatically iterate circuit element values to reduce the value of the error function, but the designer must also iterate his aims, weights and frequencies to obtain useful results. His initial choices are rarely more than educated guesses on problems of any complexity, and he should refine them as his solution converges.

Magic design example

The first thing to remember when using a computer design program is that the computer will never be a substitute for design experience. Better engineers will always get better results with Magic. Whatever design techniques you have been using are still valid, and the technique of using Magic is exactly the same at any frequency range.

Most engineers designing amplifiers at microwave frequencies now use techniques based on s-parameters. Hewlett-Packard application note No. 95 is a widely-used reference and Section V presents "quick" techniques which have proved to be quite convenient for computing rough circuit designs. The objective regardless of what technique you use is to somehow get a design which basically works—then you optimize its performance via Magic. The choice of an initial circuit is limited only by the designer's imagination.

Figure 2 shows a rough design for a two-stage amplifier which will be optimized for flat power gain over the band 2.0-2.5 GHz. Note that the distributed elements are characterized by their equivalent metric electrical lengths but lengths in electrical degrees at arbitrary reference frequencies are also allowed. A quick "analysis only" Magic run (not shown) indicated that this circuit is indeed an amplifier. Stability analysis (also not shown) indicated the circuit is unconditionally stable and that its maximum available gain range from 23.07 dB at 2 GHz to 26.86 dB at 2.5 GHz. This tells you three things: the circuit is a reasonable design, in-band stability is not a problem (better check out-of-band later) and that there is no point in asking Magic to try to get more than about 23.0 dB of gain, since it is physically impossible.

A reasonable first "crack" at the design suggests picking aims of −23.0 for DB TOT (DB TOT = $-10.0 \log P_{OUT}/P_{AVAIL}$) and weights of 15.0 and 10.0 at band edges and 5.0 elsewhere. This choice tells Magic to work harder on the band edges than the other in-band frequencies. The lower edge is weighted more heavily since this is where the least available gain occurs. Other choices of "aims" and weights will yield different optimum circuits so this is yet another area where the designer's insight can be utilized effectively.

The smart way to use Magic is to make short runs, stopping the program with SECONDS limit and using the automatic restart features to continue on from the previous run. (In this case, Magic will optimize this circuit in a single run for two reasons: to illustrate that it can operate efficiently from poor initial designs even on relatively complex circuits and to keep user interaction and computer output minimal for illustration purposes). Therefore, the program will be given a maximum time limit of 60 seconds (about $20).

Figure 3 shows the input data. The keyword, "elements," on line 20 tells Magic that it is to describe the circuit as a cascade of branches in order from the generator to the load. The first branch appears on line 30; SV ("series variable") indicates the branch is connected in series and is to be varied for optimization, C indicates the branch is a capacitor, the numbers indicate a value of 6.8 pF and a Q of 100. Line 40 indicates a series variable transmission line with a $Z\phi$ of 18 ohms and a length of 3.7 cm. Line 50 indicates that the first device to be described by a measured table of

(continued on next page)

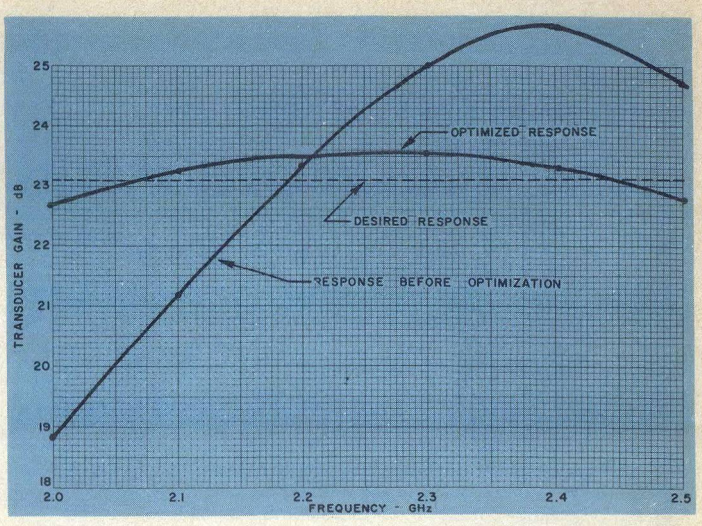

5. **Improvement in initial response** to the optimized results shown brings power ripple to within ±0.5 dB of ideal.

scattering parameters (Note on line 90 that since the second device is identical, we can share the data table. Had it not been the same the keyword SCAT2 would be used). The rest of the circuit is described in similar fashion.

Output data, Fig. 4, using optimization was fully completed in the allocated time. The error function is reduced from an initial value of 354.7 to a final value of 5.703. This represents design improvement by a factor of about 62. The circuit element values changed by an average of 11% and the passband deviation was improved from ±2.9 dB to ±0.43 dB. Figure 5 shows the circuit response before and after optimization.

Many Magic features have not been utilized. If this was an actual design rather than just an example, it would also be possible to compute circuit stability and other circuit responses, draw Smith Charts or perform statistical, worst case or sensitivity analysis. It's also possible to consider additional frequencies, adjust aims and weights and reoptimize to secure still further improvement with just a few more seconds of computer time. ••

References

1. "Magic: The Designer's Wand," *Electronics*, Vol. 46, No. 16, p. 118 (Aug. 2, 1973).
2. John D. Trudel, "Magic: A Computer Program For Optimizing Linear Circuits," *Electronics*, Vol. 47, No. 7, pp. 138-142, (Apr. 4, 1974).

Test your retention

1. Name three factors (other than cost) of critical importance when evaluating CAD services.
2. How should the design engineer interact with the optimization process?
3. How do you get a starting circuit for CAD?
4. Other than analysis and optimization, what functions are performed by modern microwave CAD programs?

technical note

Series/parallel conversion in reverse polish notation

MICROWAVE designers frequently have a need to convert a series complex impedance to its parallel equivalent circuit or vice versa. For example, one popular technique for achieving a complex conjugate match to an rf transistor requires that at the frequency of interest the shunt equivalent of the transistor's S_{11} and S_{22} be known. Such a matching solution has traditionally been computed on the Smith Chart, but with the advent of the pocket scientific calculator, many engineers are seeking algebraic, rather than graphic, solutions to their design problems.

The basic textbook formulas[1] expressing the relationship between series and parallel complex impedances are:

$$R_s = \frac{R_p X_p^2}{R_p^2 + X_p^2} \quad (1)$$

$$X_s = \frac{X_p R_p^2}{R_p^2 + X_p^2} \quad (2)$$

where R_p and X_p represent the resistive and reactive components of the parallel complex impedance, and R_s and X_s represent the components of the series equivalent circuit. It is important to note that the sign of the imaginary component does not change. That is, a complex impedance with a series capacitive component is represented by an equivalent circuit containing a shunt capacitive reactance.

Through alegebraic manipulation, the following two sets of conversion formulas can be developed:

$$R_p = R_s + \frac{X_s^2}{R_s} \quad (3)$$

$$X_p = \frac{R_s R_p}{X_s} \quad (4)$$

$$R_s = \frac{R_p}{1 + \left[\frac{R_p}{X_p}\right]^2} \quad (5)$$

$$X_s = \frac{R_s R_p}{X_p} \quad (6)$$

Applying these formulas on most calculators requires repetitive keyboard entries. But with calculators utilizing reverse Polish notation and an operational stack (notably the Hewlett-Packard 35, 45 and 65), a proper sequencing of operations can eliminate redundant keyboard entry.

Given a known series complex impedance, converting to a parallel equivalent circuit (per Eqns. 3 and 4) is accomplished as follows:

KEY in Rs	ENTER ↑	ENTER ↑	1/X		
KEY in Xs	STO	ENTER ↑	X	X	+
READ out Rp	X	RCL	÷	READ out Xp	

For the reciprocal operation, apply Eqns. 5 and 6 as follows:

KEY in Xp	ENTER ↑	ENTER ↑	X	1/X	
KEY in Rp	STO	X	RCL	1/X	+	1/X
READ out Rs	RCL	X	⇄	÷	READ out Xs

These operational sequences may appear cumbersome upon initial examination. However, experience shows that this procedure is faster by an order of magnitude than Smith Chart solutions and is capable of providing far greater resolution than any chart or nomograph of finite proportions. ••

H. P. Shuck, Chief Engineer, Micro Comm, 14908 Sandy Lane, San Jose, CA 95124.

AUGUST
1975

MICROWAVES

tuner technology

$17. Stripline Load Keeps Cool At 100 W cw

Passive Components:

- BIAS UNIT INJECTS nS SWITCHING PULSES
- OVERCOME PACKAGING EFFECTS IN FILTER DESIGN
- NOMOGRAMS SPEED λ/4 TRANSFORMER DESIGN
- SCHOTTKY DETECTORS: HOW TEMPERATURE SENSITIVE?

- Plus: HIGHLIGHTS FROM THE EUROPEAN MICROWAVE CONFERENCE

MICROWAVES

August 1975
Vol. 14, No. 8

news

editorial

technical section

products and departments

About the cover: A refreshing new tool for circuit designers, EMC Technology's stripline load keeps its cool at cw power levels up to 100 watts. Design and photo by Robert Meehan.

coming next month: Electronic Warfare

A special report on Mini-RPVs. An update of the fast-moving technology in the mini-remotely piloted vehicle field is presented. Cost cuts and performance are being stressed in the services with an eye towards exploiting advances in technology to provide low-cost systems with unique capabilities. Reconnaissance, electronic warfare and conventional ground attack are the missions now deemed most practical and economically feasible.

Noise Jamming Long Range Search Radars. Peter Dax of Westinghouse, presents graphically, the effects of noise jamming on radars and the various ECCM techniques that are available. Very low sidelobes are found to be the most effective means to defeat the noise interference.

Supercomponents Solve New DF Design Problems. Steve Lipsky of General Instrument Corporation, describes the design of two wideband microwave components, a multiplexer and rf switch, specifically designed for multioctave D/F receivers. Each component offers improved sensitivity and signal discrimination at rf, insuring better direction-finding accuracies.

Publisher/Editor
Howard Bierman

Managing Editor
Richard T. Davis

Associate Editor
Stacy V. Bearse

Contributing Editor
Harvey J. Hindin

Washington Editor
Paul Harris
Snyder Associates
1050 Potomac St., NW
Washington, DC 20007
(202) 965-3700

Editorial Assistant
Gail Murphy

Production Editor
Sherry Lynne Bogen

Art
Robert Meehan, Dir.

Production
Dollie S. Viebig, Mgr.
Dan Coakley

Circulation
Trish Edelmann, Mgr.
Peggy Long, Reader Service

Promotion Manager
Albert B. Stempel

Directory Coordinator
Janice Tapp

Editorial Office
50 Essex St.,
Rochelle Park, N.J. 07662
Phone (201) 843-0550
TWX 710-990-5071

A Hayden Publication
James S. Mulholland, Jr., President

MICROWAVES is sent free to individuals actively engaged in microwave work at companies located in the U.S., Canada and Western Europe. Subscription price for non-qualified copies is $10.00 for U.S., $15.00 a year elsewhere. Additional single copies $1.50 ea. (U.S.); $2.00 ea. (foreign); except additional Product Data Directory reference issue, $10.00 ea. (U.S.); $18.00 (foreign). POSTMASTER, please send Form 3579 to Fulfillment Manager, MICROWAVES, P.O. Box 13801, Philadelphia, PA 19101.

Back Issues of MicroWaves are available on microfilm, microfiche, 16mm or 35mm roll film. They can be ordered from Xerox University Microfilms, 300 North Zeeb Road, Ann Arbor, MI 48106. For immediate information, call (313) 761-4700.

Hayden Publishing Co., Inc., James S. Mulholland, President, printed at Brown Printing Co., Inc., Waseca, MN.

Fifth European Microwave Conference

Solid-state developments emphasized at international forum

Next month, microwave engineers from around the world will converge on Hamburg, Germany, for the Fifth European Microwave Conference. Here, at the largest annual gathering of microwave engineers and scientists in the world, conferees will meet in 24 technical seminars to discuss the ideas presented in more than 120 papers.

Indeed, if you can't make it to Hamburg in September, you will miss out on some lively, informative technical discourse. But sit back and relax; to keep you in touch with this international happening, we offer the following brief reports on some of the presentations and trends that will highlight the important conference.

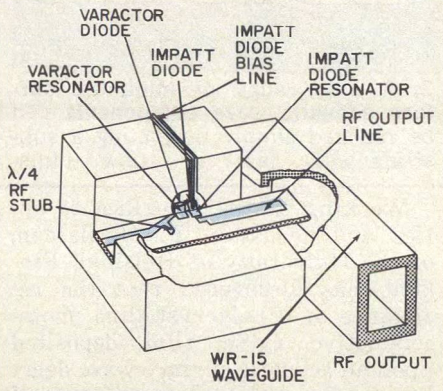

1. This varactor-tuned, microstrip Impatt oscillator circuit couples up to 115 mW at 60 GHz to the WR-15 waveguide output.

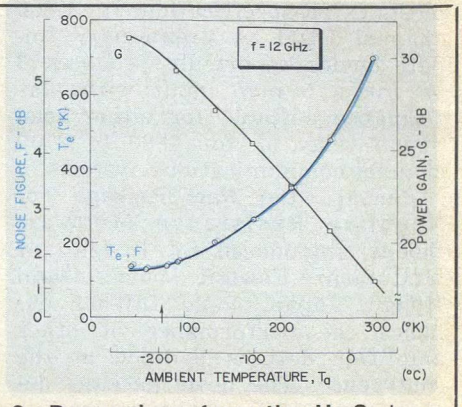

2. Researchers from the U. S. have shown that cooled GaAs MESFET amps can compete effectively with paramps in terms of noise.

Stable sources sought

Many of the papers directed toward oscillator circuits at EMC address the unique problems of Impatt oscillator design. A major challenge to millimeter-wave telecommunications centers on the design of high-power sources, which are also capable of fairly high-speed FSK modulation. Bernard Glance, representing Bell Telephone Laboratories in Holmdel, NJ, proposes one plausible solution in **"Microstrip Varactor-Tuned Millimeter-Wave Transmitter."** The 60 GHz Impatt source described by the researcher puts out 110 ±15 mW and is capable of FSK modulation rates up to 200 MB/s. Varactor (tuning) and Impatt (oscillator) circuits are both integrated on a quartz substrate (Fig. 1) using standard photolithographic fabrication techniques. The result is a very simple design, which meets telecommunication requirements with an rms fm noise level of about 400 Hz/$\sqrt{\text{kHz}}$.

The Trapatt diode, although not explored as thoroughly as Impatt devices, looks promising for pulsed transmitter application. The **Frequency Stable MIC S-Band and C-Band Pulsed Trapatt Oscillators** described by B. H. Newton of Mullard Research Laboratories, Redhill, England, operate in a fundamental mode, offering 30% efficiency at 2.6 GHz, or in a second-harmonic mode with better than 10% efficiency at 5 GHz. Operating as a locked oscillator with a stable pulsed driver, the circuit has exhibited locking gain values of up to 25 dB.

Based on recent announcements, the MESFET must certainly be viewed as a contender for high-frequency oscillator design. D. S. James of the Communications Research Centre, Ottowa, Ontario Canada, for example, uses GaAs FETS in a stabilized LO circuit for MIC mixer applications. The oscillator is stabilized using a TE_{01n} cavity coupled to microstrip by means of an aperture in the microstrip ground plane. Details are revealed in **"Stabilized 12 GHz MIC Oscillators Using GaAs FETs."**

Two other source stabilization schemes evaluated at the conference are especially noteworthy. **Temperature Stable Dielectric Microwave Resonators For High Power Applications** is the subject of a talk by H. Steyskal, Sr., of FOA, Stockholm, Sweden and Ph. Charas, of ESTEC, Nordwijk, Netherlands. By combining two dielectrics with opposite temperature coefficients, such as lithium niobate and a special ceramic, the researchers form a composite resonator which can handle cw powers up to 80 W at S-band. Both sandwhich and coaxial type resonators made in this fashion reportedly exhibit Q_o values ranging from 5,000 to 6,000 and an effective ε range of 54 to 59.

A different tack is favored by J. J. Pan, of the Harris Corp., Melbourne, FL, and Paul Sierak, of Griffiths AFB, NY. In **"High Performance, Glass Stabilized, Microwave Frequency Sources,"** they describe a low-noise, low-cost, fixed frequency S-band transistor source that features frequency and temperature stabilities of 0.9×10^{-9} parts/hour and 1.8×10^{-7} parts/°C, respectively. The researchers feel that the metalized glass-cavity stabilization techniques can be extended to tunable sources, in X-, Ku- and Ka-bands, and to fixed-frequency GaAs FET sources at frequencies up to X-band.

Impatt, FET amps stressed

Most amplifier designs discussed at the European Conference center on Impatt and FET devices. Taking advantage of the low-noise properties of the MESFET, Charles A. Liechti and colleagues of Hewlett-Packard, Palo Alto, CA, have put together a narrowband, 11.7 to 12.2 GHz, three-stage amplifier which has a 5.3 dB noise figure and 18 dB gain at room temperature. In **"A Cooled GaAs MESFET Amplifier Operating At 12 GHz With 1.6 dB Noise Figure"**, the researchers note that when the circuit is cooled at 40°K, the noise figure drops to 1.6 dB, while the gain rises to 31 dB (Fig. 2). Reverse isolation and input/output impedances are found to be nearly temperature independent.

Power Amplification of Microwave Fm Communication Signals Using A Phase-Locked Voltage-Tuned Oscil-

(continued on p. 10)

Solid-State developments emphasized (cont.)

lator, explained by M. E. Hines of Microwave Associates, Inc., Burlington, MA, relies on a varactor-tuned Gunn or Impatt source. The Gunn device produces a 250 mW output with a 2 mW input and meets CCIR specifications for 1,800 channel FDM. A preliminary Impatt device reportedly produces 3 W for a 5 mW input with performance suitable for either television relay or for 1800 to 2700 channel communications systems.

Perhaps the **New Package For Negative Resistance Microwave Diodes,** introduced by T. Ishii of Mistubishi Electric Corp. Itami Hyogo, Japan, could further enhance the performance of other amplifier designs detailed at the conference. The novel package design incorporates additional inductance and capacitance besides case and lead parasitics. The equivalent electric circuit of a diode cased in the new package is composed of the parallel resonance circuit of the ceramic case, the series resonance of lead wire, and chip admittance. Admittance levels of an Impatt diode mounted in the new package are reportedly very low, which should lead to better small signal power gain.

Acoustic devices mature

An entire session is devoted to surface-acoustic wave advancements at the 1975 EMC, and the papers serve as a testimony to the surge of world-wide interest in this field.

From the U.S. comes the announcement of a new class of **Components For Acoustic Surface Waves Based On Narrow Strip Cut Off Sections.** Power splitters, directional couplers, delay-line taps, attenuators, resonant cavities and filters of this type may be constructed on any substrate, whether piezoelectric or not, according to A. A. Oliner of the Polytechnic Institute of New York. Greater flexibility in the choice of substrate material permits optimization of vital parameters such as temperature stability and loss. Each component simply consists of a thin-film deposited on a substrate. This narrow strip of plated material acts the way a small section of below cutoff waveguide would in electromagnetic microwave devices. Simplicity is the key to this technique, as illustrated by the parallel output power splitter shown in Fig. 3.

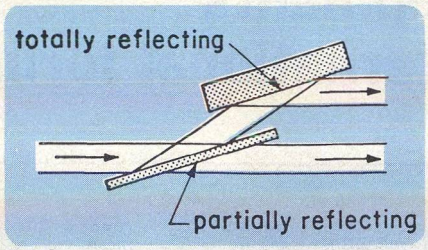

3. A wide range of miniature surface acoustic wave components can be realized simply by plating a substrate with "fast" or "slow" films.

Working at the interface of optics and acoustics, P. Merilainen, of the University of Helsinki, Finland, has discovered that the resistance of a polycrystalline photoconductive CdSe film deposited upon an acoustic surface wave delay line decreases by up to a factor of ten when an acoustic pulse is propagating down the line. According to the researcher, the **Nonlinear Effects On LiNb 0_3 Delay Line Coated With A Polycrystalline CdSe Film** may open the possibility of acoustical scanning of optical images.

SAW components operating at 1 GHz have been realized by P. Hartemann at the Laborato Central de Recherches of Thomson CSF, Orsay, France, using an electronic masker. These delay lines, filters and oscillators are based on $LiNb0_3$ substrates, and have a minimum transducer finger width of 0.3 μm. The bandwidth and delay of a typical delay line of this type has been measured at 500 MHz and 10 μsec, respectively, according to **"Microwave Acoustic Surface-Wave Components."**

A delay line with zero insertion loss is certainly a near impossibility, but T. M. Mason of the Royal Radar Establishment, Malvern, England, has designed **A Unity Gain Delay Module Operating At 3 GHz** by combining amplifiers, PIN diode switches, circulators and a Spinel bulk wave delay line. Designed for applications in chirp radar, the component provides 22 μsec of delay over an instantaneous bandwidth of 500 MHz. Peak rf input and output power is -10 dBm, giving an output signal-to-noise ratio of 40 dB. A single, unstabilized +15 Vdc bias supply is necessary.

Communications hardware detailed

Communications systems, terrestrial and satellite, receive a great deal of attention at the European conference with most papers describing new or improved hardware. As a sampling, consider the **Waveguide Multiplexer With Dual Mode Filters For Satellite Communications** designed by Gehard Pfitzenmaier of Siemens AG, Munich, Germany. The 4 GHz, four-channel multiplexer is essentially a WR229 short-circuited waveguide manifold with four bandpass filters critically spaced along the broad-wall sides. The four-pole circular waveguide filters take advantage of a dual TE_{111} mode resonance to form usable bands at 36 MHz and 72 MHz. Reflection coefficient within these bands is reportedly less than 6%

High-speed multiplexers and demultiplexers of the future may include something similar to the delay line with equidistantly placed Schottky diode switches examined in **"A New Method For Ultra-Fast Signal Processing and Pulse Regeneration in the Gbit/s Range."** Author of the paper, R. Schwarte, representing Technische Hochschule Aachen, Germany, reports that the spatial voltage distribution of a signal passing through the delay line can be stored discretely in the delay-line sections when the series switches are opened. Potential applications also include baseband repeaters for the Gbit/s range.

An interesting piece of hardware that illustrates Europe's intense interest in millimeter-wave systems is **A 30 GHz Low Noise Down Converter** developed by M. Krefft, also of Siemens, A. G. The single-ended waveguide mixer design converts a 1 GHz wide signal in the 27.5 to 31 GHz range to an i-f of about 1 to 2 GHz, with a conversion loss of about 5 dB.

On the systems level, a new method for **Reducing The Intermodulation Noise In Wideband Microwave Radio Relay Systems,** proposed by P. Lier of AEG Telefunken, Backnang, Germany, compensates for symmetrical differential gain and delay distortion by introducing fixed multi-section equalizers and appropriate slope adjustments of the delay characteristics. The technique emphasizes am-to-pm conversion effects and non-linearities of subassemblies. Equalization in the transmitter is simply a matter of adjusting the i-f voltage and oscillator level of the upconverter. Receiver equalization is achieved by a limiter arrangement with variable am/pm. •• *S.V.B.*

news
Inexpensive phased array opens up new radar applications

Richard T. Davis
Managing Editor

A low-cost phased array antenna has been developed based on a series ferrite scan principle. It offers a potential 10:1 cost reduction over conventional phased array scanning techniques which usually require a diode or ferrite phase shifter for each array element. An X-band prototype model has demonstrated ±50 degrees of scan coverage in a single plane. The simple phased array, developed by Rockwell International's Missile Systems Division, Anaheim, CA, also offers a significant reduction in weight and thus is being considered for many military and commercial applications which now could not use phased arrays because of their cost and weight.

"The series ferrite scan technique, Fig. 1(a), can be visualized as consisting of a waveguide having series connected ferrite phase shifters inserted lengthwise between each radiating element," explains Sam Wong, Manager of Antenna Systems at Rockwell.

"Electronic beam scanning is provided by controlling the propagating velocity or phase shift per unit length of the ferrite loaded waveguide. Phase shift is effected by applying current on the solenoid which induces a longitudinal magnetic field in the ferrite."

The array is presently limited to only single plane scanning, but it could be easily adapted to 2-D by using additional ferrite waveguides in the other plane," contends Wong.

"This low-cost phased array, under development for about four years, was originally designed for a missile, but other military and commercial radars which presently use dish antennas or mechanically scanned slotted arrays are being developed." Figure 2 is a 26 element planar array, consisting of two ferrite waveguides that was developed for the Naval Electronics Laboratory in San Diego. The antenna provides ±45 degree coverage and is used for an experimental battlefield surveillance radar. The beam scan control box shown has a manual and automatic scan mode selectable by a switch. The antenna provides a

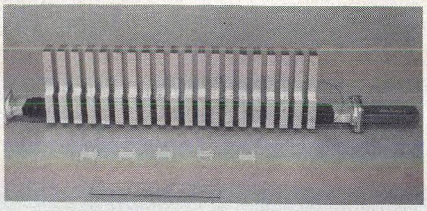

1(a). **Series ferrite scan** consists of one long series connected phase shifter to which a number of radiating linear elements may be coupled. Each phase shifter requires only one drive circuit to scan a beam in one plane.

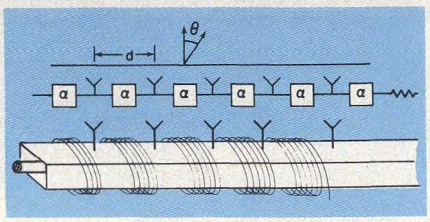

(b) **The beam scan angle,** θ, is proportional to solenoid current, I, by sin $\theta = \lambda/\lambda_g \pm m\lambda/d + \phi/2\pi$ where ϕ = phase shift/unit length $\propto$ I, λ = free space wavelength and λ_g = guide wavelength.

six × six degree beamwidth at 9 GHz with sidelobes down 18 to 20 degrees as shown in Fig. 3.

Another immediate use for the array is with small boat radars. Figure 4 shows a fan beam phased array developed for the Navy using the series ferrite scan principle. The 48 inch long X-band array provides ±45 degrees of scan coverage. "Because of its rapid scanning capability, data obtained by the radar is presented on a normal TV-type display," says Wong.

1 lb radar transceiver

The compact transceiver for this marine radar was also developed at Rockwell International. According to Art Cohn, Manager of Tactical and Electromagnetic Systems Engineering, Autonetics Group, the 6 × 5 × 0.5 in. package, Fig. 5, delivers 4 W to the antenna, including duplexer loss by means of an injection-locked double-drift Impatt diode transmitter. The 16 oz transceiver has an overall system efficiency (dc to rf) of 4.2% for a 25% duty cycle. The receiver section provides a 6 dB double sideband noise figure including the 2.5 dB noise figure of the i-f preamp. "All circuits within the package are arranged for optimum isolation," says Cohn. "The package is channelized so that each circuit fits into its prescribed area to create a waveguide operating below cutoff."

"The mixer local oscillator and transmitter output are derived from the same source with the exception of a crystal controlled 30 MHz offset oscillator to facilitate the superhet function." The fundamental transistor oscillator operates a 2.3 GHz, (tunable to 3.2 GHz). For the LO circuit, this S-band signal is multiplied by four using a shunt-mounted, step-recovery diode in microstrip, followed by a five pole bandpass filter, providing an output of 9.0 to 9.5 GHz. The balanced mixer consists of a branch line hybrid with

(continued on p. 16)

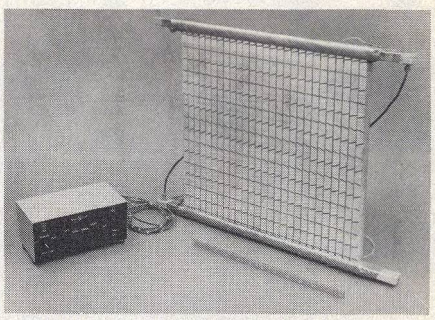

2. **Experimental battlefield surveillance radar** has 26 elements and uses two ferrite waveguides (top and bottom) to provide ±45° scan coverage.

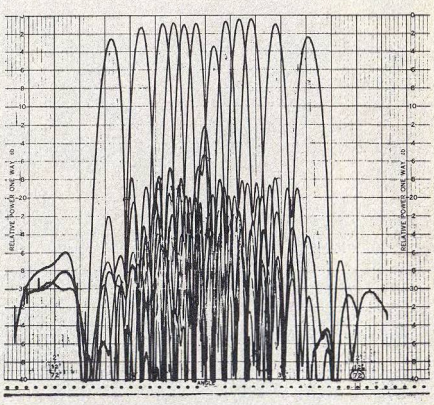

3. **Antenna pattern for the series ferrite scan array** shows slight variation in beamwidth as it scans ±45 degrees. At bore-sight, the beam is 21° and it broadens to 33° and 26° as it scans to the extreme right and left.

Horn and dish linkup with Anik, Westar satellites

In a three-day demonstration last month, AII Systems of Moorestown, NJ, showed the feasibility of quality reception of color TV and fm satellite broadcasting using small receive-only earth terminals designed for the 3.7 to 4.2 GHz band. TV signals via the Anik I Canadian satellite were received using a 4.5 meter dish antenna and a 10 ft horn antenna. Combinations of low-noise amplifier at 43°K and 130°K were used with these antennas providing a G/T ranging from 17.9 dB/°K to 24.5 dB/°K. The 3m horn manufactured by AFC, Inc., provided 39.5 dB gain at 4 GHz while the 4.5 meter dish by Andrew Corporation provided 43.7 dB gain at 4 GHz. The output from the low-noise amplifier then was fed to a downconverter and an fm/TV demodulator.

The signal received from a 40 MHz wide transponder on the Telesat Anik I satellite originated in Allen Park, Ontario. Twelve TV channels with 4 MHz sidebands can be carried per transponder.

Also on demonstration for the third time was a 4 ft diameter receive-only terminal used to receive Muzak signals via the Westar satellite. This fm signal consists of a 50 Hz to 8 kHz audio program to which a low frequency energy dispersal signal has been added. This allows the effective isotropic radiation to stay within the FCC limits. Several thousand of these 4 ft. terminals are expected to be deployed in the coming years. RCA Globcom transmitted the uplink signal for the demonstration from its Valley Forge, PA, facility. ••

FCC launches probe for INMARSAT entry

Industry comments are due at the FCC this month on the **designation of a private entry to be the U.S. participant and investor in any international maritime satellite organization that might be established.** The agency has already received word from several carriers who have indicated in a general way their interest in participating in any such organization, but is now looking for firm commitments from parties, particularly from a financial standpoint. The commission stated earlier this year that all U.S. interests would be served by designating a single U.S. entry to participate in the basic operation of any INMARSAT service.

Inexpensive phased array opens new radar applications (cont.)

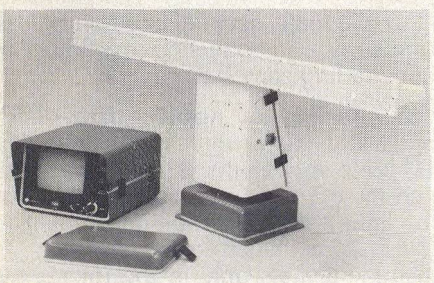

4. **Small boat radar** uses compact transceiver design and series ferrite scan array developed at Rockwell International. The fan beams has ±45° scan coverage.

two series mounted Schottky barrier diodes.

"The diodes are phased such that any reflections are directed back towards a circulator, which minimizes LO radiations," explained Cohn. "The i-f output is matched to 50 ohms at 120 MHz."

The transmit signal originating from the fundamental oscillator is modulated by a SSB diode modulator. The modulation input is derived from a 30 MHz crystal-controlled oscillator through an i-f quadrature hybrid. "The conversion is done at S-band (2.3 GHz) because high efficiency gain is available to make up for the 9 dB SSB conversion loss," notes Cohn. The rf input is split in phase and fed to two balanced mixers where the modulation input mixes with the rf at the diodes to produce upper and lower sidebands. The output from each mixer is then quadrature summed through an interdigital coupler which terminates the lower sideband and outputs the upper.

The signal is then fed to a four-stage power amplifier, three chip transistors mounted in series to provide drive power to a single PH12301 "strip pac" mounted transistor, Fig. 5. Total peak power output is 800 mW and gain is 43 dB. This power is then delivered to a times four multiplier, similar to that used in the LO channel except for a self-biasing resistor. Conversion loss is 6 dB.

The transceiver also includes an 180-degree phase shift modulator so phase coding may be implemented on the transmit signal prior to the Impatt transmitter stage. Switching time is typically 20 ns.

The Impatt is circulator coupled. Three circulators are used to provide quadrupler/Impatt,

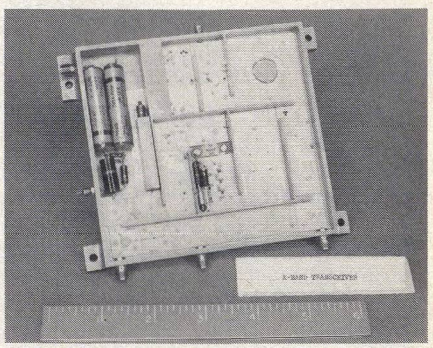

5. **One-pound transceiver** for marine radar uses injection-locked Impatt oscillator for transmitter, providing 4 W peak power to the antenna.

antenna/quadrupler and receiver/transmit diplexing. With a good load at the antenna, the Impatt-to-quadrupler isolation is over 40 dB and worst case (antenna shorted), the isolation is 20 dB. A diode limiter also provides 20 dB of receiver protection.

Cohn claims that the isolation provided between circuits, spurious mode propagation is minimal, and there is very little oscillator pulling due to modulation signals applied to the power amplifier or Impatt diode. ••

Build A Better Bias Insertion Unit

Wideband bias insertion units that can inject video signals with fast risetimes are not readily available. Here's a way to build them yourself, inexpensively, to cover a 9.8 GHz bandwidth.

ANYONE with basic transmission line theory under their belt can successfully design and build relatively cheap, yet reliable, broadband bias insertion units. This article covers the use of both ferrite and discrete circuit elements in bias insertion unit design. Both versions can be conveniently packaged in a slightly modified type N, coaxial Tee connector. Simple modifications assure an inexpensive means of assembling and mounting the bias unit while protecting it from physical abuse. Both units will pass fast switching pulses with 80 nanosecond rise times.

The video pulse passing ability of both of these bias insertion units is important. The author could not find commercially available wideband rf bias insertion units that could pass video input pulses with 100 nanosecond risetimes or less.

200 MHz to 3 GHz, the measured insertion loss and rf path isolation characteristics for the discrete element bias units are smooth and regular, as predicted from transmission line theory. However, above 3 GHz, discrete element units display wild excursions from theoretical curves.

By using wideband ferrite choke material in place of the discrete elements, the bias insertion unit can be made an ultra-wideband rf component. The rf properties of ferrite permit predictable and smooth performance all the way from 200 MHz to 10 GHz. The ferrite unit has slightly more insertion loss than the discrete element bias insertion unit, but the small additional loss is readily accepted for the gain in predictable rf bandwidth.

A bias insertion unit must be able to supply a combination of rf, dc and video voltages or signals to an active device in an rf system. Video is taken here to mean frequencies up to 100 MHz. The basic bias insertion component consists of two sections: an rf transmission path and a bias/video input section.

The rf path in the bias insertion unit is a section of low-loss, well-matched transmission line with a characteristic impedance (Z_o) equal to that of the rf system to which the bias insertion unit is connected. The type of rf path is generally chosen to best fit the physical layout of the rf system into which the bias insertion unit is to be used, and can be stripline, microstrip or coaxial in nature.

The bias/video input section at port C (see Fig. 1) is a low-pass filter formed by a series inductance (L) and a shunt capacitance (C_s). The values of L and C_s are chosen to pass the highest expected video frequencies with minimal distortion. In addition, enough shunt capacitance is provided to form an effective rf bypass to ground for any residual rf that gets past the choke, L.

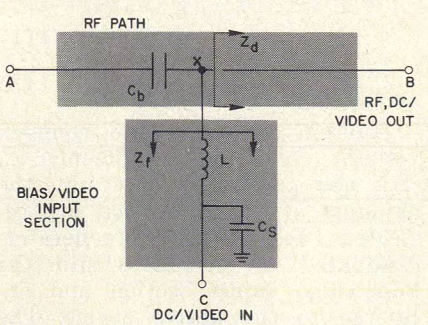

1. An analysis of a bias insertion unit hinges on defining the impedances at point x, the connection of the low-pass filter to the rf transmission line.

Injected dc bias currents and video signals must be prevented from entering the rf generator, which is connected to port A of the bias insertion unit shown in Fig. 1. Thus, the value of the blocking capacitor, C_b, must be chosen to present a large value of capacitive reactance to the video signals on the rf path, while readily passing the higher frequency rf power through it to the active device.

The active device is connected to the output of the bias insertion unit, port B in Fig. 1. Most active devices have a complex input impedance, Z_d, which must be reckoned with in the component's design. In particular, the analysis of a bias insertion unit must consider this device input impedance transformed back to point x, the connection of the low-pass filter to the rf transmission path. This transformed impedance, Z_d', can be expressed as:

$$Z_d' = \frac{Z_d + j\,Z_o \tan(\Theta)}{1 + j\,\frac{Z_d}{Z_o}\tan(\Theta)}$$

$$\Theta = \frac{2\pi\ell}{\lambda} \quad (1)$$

where Θ is the electrical length of the rf path from point x to the input of the active device, λ is the wavelength of the rf frequency and ℓ is the physical length of the rf path.

Describe the impedance perturbation

The key to designing any bias insertion unit lies in understanding the effects of connecting a low-pass filter to an rf transmission path. Assume that the low-pass filter is connected to the rf transmission line at point x, as shown in Fig. 1. The filter's out-

(continued on p. 34)

G. W. Renken, Development Engineer, Honeywell Government & Aeronautical Products Division, 1625 Zarthan Avenue, Minneapolis, MN 55416.

Work performed while at McDonnell Douglas Astronautics Corporation, Eastern Division, under contract number NOO178-73-C-0362 from the U.S. Naval Surface Weapons Center Dahlgren Laboratory.

put impedance, as seen from point x looking into the filter, is Z_f. When the low-pass filter is connected to the rf path at point x, there will be a local impedance change to the rf path there, resulting from the interaction between Z_f, Z_o and Z'_d.

Both Z_f and Z'_d are complex impedances. Depending on the relative mismatch between Z_f and Z_d, a considerable percentage of the rf power flow to the active device may be disturbed. Effects from a mismatch at point x can show up throughout the entire rf system.

In terms of L, C_s and Z_g, the impedance of a video generator connected to port C, the low-pass filter's output impedance at point x is:

$$Z_f = \frac{Z_g + j\omega(L + Z^2_g(\omega^2 L\, C^2_s - C_s))}{1 + \omega^2 Z^2_g\, C^2_s} \quad (2)$$

Z_g is assumed real here, and ω represents the rf input frequency expressed in radians per second.

Z_f can also be expressed explicitly in terms of real and imaginary parts:

$$Z_f = Z_{fr} + jZ_{fi} \quad (3)$$

Where:

$$Z_{fr} = \frac{Z_g}{1 + \omega^2 Z^2_g\, C^2_s} \quad (4)$$

$$Z_{fi} = \frac{\omega(L + Z^2_g(\omega^2 L\, C^2_s - C_s))}{1 + \omega^2 Z^2_g\, C^2_s} \quad (5)$$

The local impedance at point x is determined by the interaction of Z_f and Z'_d and by the shunt-loading effect on the rf path by the filter output impedance, Z_f. Shunt loading affects the flow of rf power to the active device even if the additional interaction at point x, caused by Z'_D combined with Z_f is not considered. The loading effect manifests itself in two ways.

First, there is a partial reflection of the incident rf power back to the generator. This reflection is caused by Z_l, the parallel combination of Z_f and Z_o, not being equal to the rf path characteristic impedance, Z_o, as shown in Fig. 2.

Second, some of the remaining, non-reflected power enters the bias/video input section at point x, and is either stored in the reactive components, L and C_s, or dissipated in the video generator source impedance, Z_g.

Both effects of shunt loading lower the efficiency with which the bias unit can deliver rf power to the active device. When the interaction of Z'_d and Z_f is also considered, an indication of this efficiency may be written in terms of insertion loss and isolation.

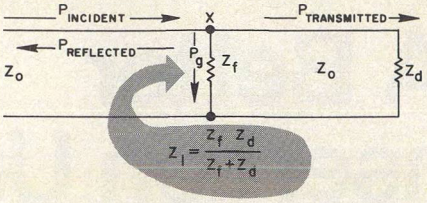

2. Reflections are caused by the parallel combination of Z_f and Z_d not being matched to Z_o.

To the right of point x in Fig. 2, the equivalent load impedance on the rf path, Z_l, is the parallel combination of Z_f and Z'_d:

$$Z_l = \frac{Z_f Z_d}{Z_f + Z_d'} \quad (6)$$

$$Z_l = \frac{(Z_{fr} + jZ_{fi})(Z_{dr}' + jZ'_{di})}{(Z_{fr} + Z'_{dr}) + j(Z_{fi} + Z_{di}')} \quad (7)$$

Or, explicity in real and imaginary parts:

$$Z_l = Z_{lr} + Z_{li}$$

$$Z_{lr} = \frac{(Z_{fr}\, Z_{dr}' - Z_{fi}\, Z_{di}')(Z_{fr} + Z_{dr}')}{(Z_{fr} + Z_{dr}')^2 + (Z_{fi} + Z_{di}')^2} + \frac{(Z_{fi}\, Z_{dr}' + Z_{fr}\, Z_{di}')(Z_{fi} + Z_{di})}{(Z_{fr} + Z_{dr}')^2 + (Z_{fi} + Z_{di}')^2} \quad (8)$$

$$Z_{li} = \frac{(Z_{fi}\, Z_{dr}' + Z_{fr}\, Z_{dr}')(Z_{fr} + Z_{dr}')}{(Z_{fr} + Z_{dr}')^2 + (Z_{fi} + Z_{di})^2} - \frac{(Z_{fi} + Z_{di}')(Z_{fr}\, Z_{dr}' - Z_{fi}\, Z_{di})}{(Z_{fr} + Z_{dr}')^2 + (Z_{fi} + Z_{di})^2} \quad (9)$$

Γ_x, the complete voltage reflection coefficient at point x, is given by:

$$\Gamma_x = \frac{Z_l - Z_o}{Z_{lr} + Z_o} = \frac{(Z_{lr} - Z_o) + j\, Z_{li}}{(Z_{lr} + Z_o) + j\, Z_{li}} \quad (10)$$

or,

$$\Gamma_x = \Gamma_{xr} + j\Gamma_{xi}$$

where

$$\Gamma_{xr} = \frac{(Z_{lr} - Z_o)(Z_{lr} + Z_o) + Z^2_{li}}{(Z_{lr} + Z_o)^2 + Z^2_{li}} \quad (11)$$

$$\Gamma_{xi} = \frac{2Z_{li} Z_o}{(Z_{lr} + Z_o)^2 + Z^2_{li}} \quad (12)$$

Having computed the complex voltage reflection coefficient, Γ_x, it is now possible to determine the amounts of rf power that are reflected back to the rf generator, dissipated or stored within the bias/video input section and delivered to the active device. The following expressions assume that all source impedances are real, and the dc blocking capacitor, C_b, has no effect on the rf passing through it.

The ratio of reflected to incident power at X is given by:

$$\frac{P_{reflected}}{P_{incident}} = |\Gamma_x|^2 \quad (13)$$

The ratio of power transmitted to the active device to the incident rf power at point x is given by:

$$\frac{P_{transmitted}}{P_{incident}} = 1.0 + |\Gamma_x|^2 + 2\Gamma_{xr} \quad (14)$$

Or, in the more familiar terms of rf insertion loss:

$$\text{Insertion loss (dB)} = -10 \log_{10} \frac{P_{transmitted}}{P_{incident}} \quad (15)$$

The ratio of power passing into the low-pass filter at point x and being either dissipated in the video generator or stored in the reactive elements to the incident rf power at point x is given by:

$$\frac{P_g}{P_{incident}} = 1.0 - \frac{P_{reflected}}{P_{incident}} - \frac{P_{transmitted}}{P_{incident}} \quad (16)$$

Or, in terms of the complex voltage reflection coefficient:

$$\frac{P_g}{P_{incident}} = -2(\Gamma_{xr} + |\Gamma_x{}^2|) \quad (17)$$

In terms of rf isolation from the rf path to the input port of the bias/video section:

$$\text{Isolation (dB)} = -10 \log_{10} \frac{P_g}{P_{incident}} \quad (18)$$

With these expressions, especially Eqns. (15) and (18), the theoretical performance of an ideal bias insertion unit can be compared to the measured performance of the two types of bias insertion units described here.

Discrete elements: A first choice

The first type, designed with discrete components, uses a sparsely wound coil for the series inductance, L, and coaxial capacitor for C_s. A commercial dc blocking capacitor functions nicely as C_b. The complete bias insertion unit, consisting of the rf path, L and C_s, can be built into a slightly modified UG-28 Type N coaxial Tee. The blocking capacitor is attached externally.

This bias insertion unit was initially designed to operate from 200 MHz to 10 GHz and pass video input signals up to 100 MHz. The resonant cutoff frequency (f_{co}) of the filter was set at 60 MHz. With this stipulation, the values of inductance and capacitance of the filter elements can be determined from:

$$f_{co} = \frac{1}{2\pi\sqrt{L\, C_s}}$$

(continued on p. 37)

BIAS INSERTION DESIGN

Using the constraint that L must be a sparsely wound coil that fits into a UG-28 Tee, the coil inductance can be computed from:

$$L = \frac{n^2 r^2}{(9r + 10\ell)} = 0.0244 \text{ microhenries}$$

where:

n (number of turns in the coil) = 6

r (coil radius) = 0.040 inches

ℓ (coil length) = 0.200 inches

The coil form is a cylinder of machined Teflon® dielectric, built to the above dimensions, that is mounted between sections of the slightly modified removable stem of the UG-28 A/U Type N coaxial Tee. A portion of the stem is cut out and replaced with the Teflon® coil form. The ends of the Teflon® coil form are pinned to the two stem sections to form an integral, new stem.

Knowing the value of the inductor, C_s can be determined from Eqn. (19):

C_s = 288 picofarads

The maximum diameter of this 288 pF coaxial capacitor is fixed by the size of the UG-28 housing. Thus, the length of the plates can be determined from:

$$C = 8.50\,\epsilon_r \frac{(b/a + 1)\ell}{(b/a - 1)\,12} \quad (21)$$

ϵ_r (relative dielectric constant of capacitor dielectric) = 2.55

b (the radius of the outer plate) = 0.160 inches

a (the radius of the inner plate) = 0.159 inches

The length of the capacitor was computed from Eqn. (21) to be:

ℓ = 0.500 inches

The inner plate of the coaxial capacitor is designed to fit slightly above the coil along the length of the stem of the UG-28 Tee. Both the inner and outer plates of the coaxial capacitor are machined out of brass. The outer plate is formed into a caplike piece with threads cut into the inside of its bottom portion so that it can be screwed to the top of the Tee. The same type and size of threads are cut into the outside top of the outer capacitor plate so that other Type N coaxial connectors mate to this modified UG-28 Tee.

When assembling the bias-insertion unit (Fig. 3), the center stem is unscrewed from the center cross piece, and the cross piece is placed into the rf path of the Tee. The stem is then screwed into the cross piece to hold both items in the Tee. The outer capacitor plate is screwed on atop the Tee and the bias insertion unit is ready for use. A Microlab/FXR, HR-50N dc block functions as C_b and protects the rf generator.

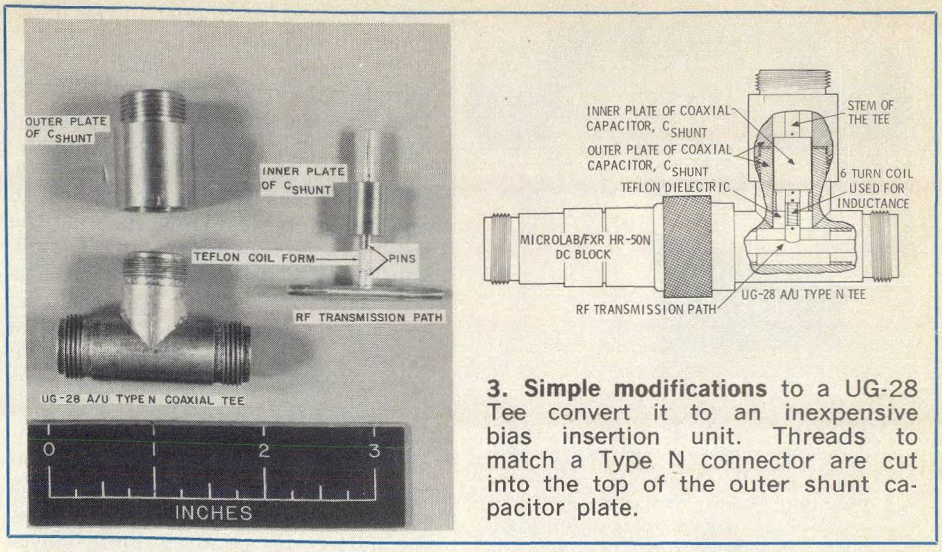

3. Simple modifications to a UG-28 Tee convert it to an inexpensive bias insertion unit. Threads to match a Type N connector are cut into the top of the outer shunt capacitor plate.

Insertion loss becomes unpredictable

Laboratory tests indicate that this discrete component bias-insertion unit exhibits predictable performance from 200 MHz to 3 GHz. Above 3 GHz, its insertion loss becomes too irregular and unpredictable for it to be used. Insertion loss and isolation data were taken on a swept frequency basis from 200 MHz to 10 GHz using an HP 8410 network analyzer. Data was taken with the network analyzer connected to two ports of the bias-insertion unit, while a 50-ohm termination was used on the third. When rf insertion-loss data was being taken, the 50-ohm load was placed on the bias/video input port to simulate a generator impedance, Z_g, of 50 ohms. The 50-ohm load was placed on the rf output port, simulating Z_d, when isolation was measured

(continued on p. 38)

from the rf input port to the bias/video input port.

Rf insertion loss data is compared with the theoretical insertion loss in Fig. 4. The rolloff of the low-pass filter shows up nicely. From 250 MHz to about 3.0 GHz, insertion loss is relatively smooth and predictable. However, at the resonant frequencies of 4.05, 7.00, 8.90 and 10.0 GHz, insertion loss increases to −17, −20, −24 and −28 dB, respectively. Very little rf power would be delivered to the active device at these resonant frequencies.

Rf path isolation data is compared with the theoretical data in Fig. 5. This theoretical curve was computed using Eqn. (18), setting the active device input impedance, Z_d, equal to (50 + j0 ohms). The rolloff of the low-pass filter is sharp, and follows the theoretical rolloff nicely until 2.60 GHz is reached. Above 2.60 GHz, there are three serious reasonances at approximately 4.05, 6.75 and 9.10 GHz. These resonances are caused, in part, by the coil's interwinding capacitance interacting with its lumped and distributed inductance as resonant frequencies are encountered. Note that these resonant frequencies nearly coincide with those in the rf insertion loss data.

Rf path isolation does not become systematically greater as frequency is increased to 10.0 GHz because of losses due to rf coupling at these frequencies. The rf fields couple energy to the low-pass filter, even though in theory the conducted energy should be hindered from leaving the rf path by the low-pass filter.

On the basis of measured isolation data, one could conclude that there is sufficient isolation over the entire 200 MHz to 10 GHz range. Even with the resonant peaks at 4.05, 6.75 and 9.10 GHz, there is a minimum of 25 dB isolation from the rf path to the input of the bias/video section.

Both data sets for the discrete component bias insertion unit prove that this type of bias insertion unit is useful for narrow or medium bandwidth applications. At the higher frequencies covering wider bandwidths, greater care must be taken to build the discrete components used in the low-pass filter.

However, when frequencies are reached for which the combined effects of the distributed circuit elements begin to dominate the desired lumped circuit values, the designer loses control over the performance of the bias insertion unit. This is the case in this bias insertion unit data at the four resonant frequencies. For frequencies above 3.0 GHz, bias insertion units using discrete circuit elements cannot be used effectively over wide bandwidths.

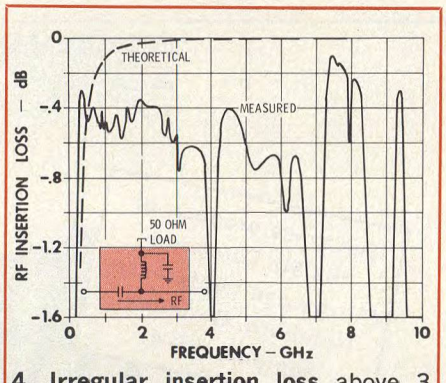

4. Irregular insertion loss above 3 GHz illustrates the erratic high-frequency behavior of discrete components.

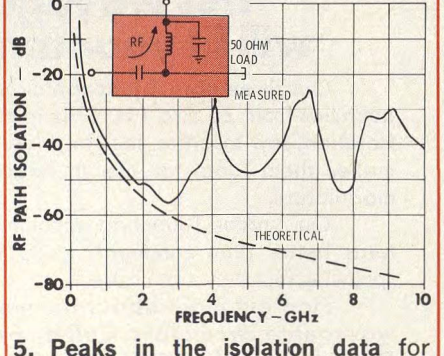

5. Peaks in the isolation data for the discrete element unit occur at nearly the same frequencies as valleys in the insertion loss curve shown in Fig. 4.

Ferrite: A better choice

Wideband performance of a discrete component bias insertion unit above 3.0 GHz has been shown to be severely hampered essentially by the unpredictable nature of Z_f, the input impedance to the low-pass filter at these frequencies. Ferrite choke cores, on the other hand, preserve their equivalent circuit qualities exceptionally well over wide bandwidths above 3.0 GHz, including the lower frequencies. The wide bandwidth results from the fact that Z_f is very large compared with Z_o.

In particular, Ferroxcube's VK 200 21/4B ferrite choke core, when wound with 2 1/2 turns of wire, initially looks inductive, below 60 MHz. Above 60 MHz, the electrical properties of this ferrite core make a sharp transition from those of a choke to those of a large value of resistance. Ferrite retains the electrical property of

appearing consistently as a large dc resistance over the entire rf bandwidth from 200 MHz to 10.0 GHz.

The ferrite is also packaged in a UG-28 type N coaxial Tee, but different modifications are necessary. In this bias insertion unit the ferrite replaces the entire shunt stem center pin inside the Tee. To accommodate the choke, the shunt stem of the UG-28 Tee must be routed with a 5/16 inch flat-end mill to a depth of 0.78 inches, as measured from the outside lip of the Tee stem. This allows the ferrite choke to be placed as close as possible to the rf line while preventing the body of the ferrite choke core from interfering with fields about the rf path passing through the Tee. Figure 6 is a top view of the UG-28 Tee showing the Tee after its shunt stem had been routed out in the manner described.

To insure a good, snug holdown of the choke to the rf line within the routed Tee, care must be taken to support the ferrite firmly. One end of the choke coil is soldered to the rf line passing through the center of the Tee. The other end of the choke coil passes through a 0.75 inch long, 9/32 inch diameter polystyrene rod through which a small hole has been drilled down its longitudinal axis. After the wire passes through the plastic rod, its end is soldered to the center pin of a UG-21 cable connector. The plastic rod supports the long end of the choke wire, and prevents the center pin of the UG-21 connector from being pushed down when the connector is tightened.

Note, in Fig. 7, how the bottom of the ferrite choke is held above the rf line in the Tee by the choke's placement atop the dielectric over the rf line. The ferrite choke is prevented from any type of movement since it is tightly held down atop this dielectric with pressure from the plastic rod.

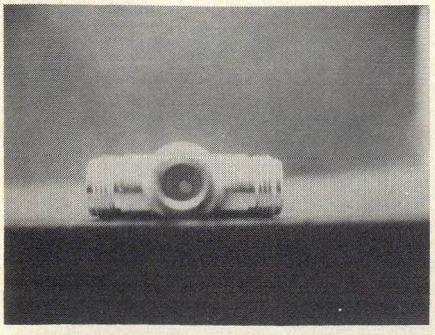

6. The interior of the UG-28 Tee must be routed to properly accommodate the ferrite choke.

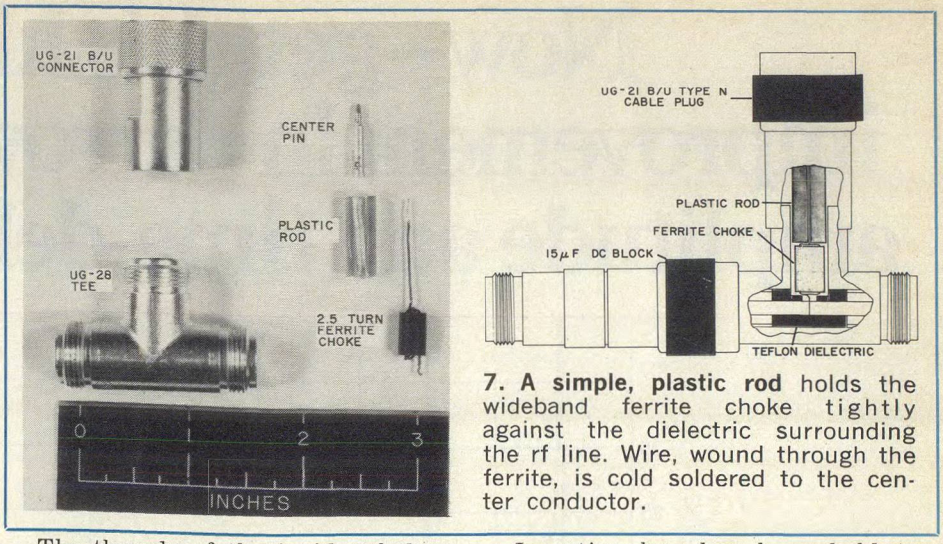

7. A simple, plastic rod holds the wideband ferrite choke tightly against the dielectric surrounding the rf line. Wire, wound through the ferrite, is cold soldered to the center conductor.

The threads of the inside of the UG-21 cable connector match the threads of the outside end of the shunt stub of the UG-28 Tee. Hence, this ferrite bias insertion unit is easily assembled.

Rf path isolation data and insertion loss data were taken using the same equipment and test setups used to measure the discrete element bias insertion unit described earlier. Both data sets for the ferrite unit are smooth and quite predictable from 200 MHz to 10 GHz.

Insertion loss has been held to 3.6 dB or less over the entire 200 MHz to 10.0 GHz band as shown in Fig. 8. Note that the insertion loss increases from 0.30 dB, at 700 MHz, to a maximum value of 3.6 dB at 5.0 GHz. The insertion loss then decreases slowly to a nominal value of 1 dB above 9.0 GHz.

Figure 9 illustrates that a nominal value of 20 dB of rf isolation exists from the rf path to the input port of the bias/video section. Again, the isolation is smooth and regular with no spikes or serious

(continued on p. 41)

resonances, as was the case for the rf path insertion loss data. While the rf path isolation data has a nominal value less than that for the discrete element bias insertion unit, 20 dB of rf path isolation is sufficient for most applications.

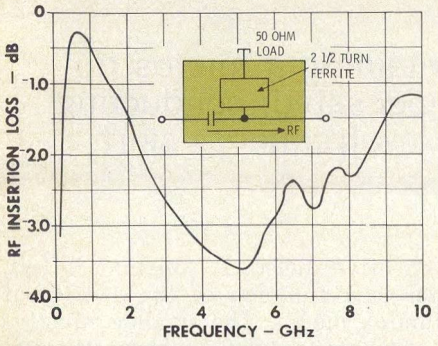

8. The insertion loss of the ferrite unit remains below 3.6 dB over the entire band.

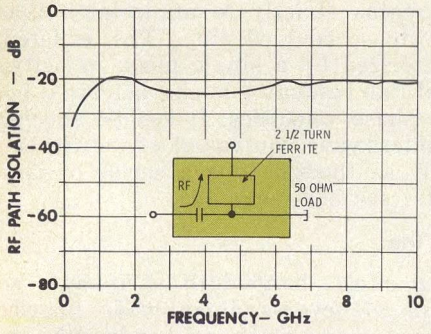

9. Although the ferrite unit offers less isolation than the discrete component unit, the rf isolation characteristic is smooth and predictable.

While basically presenting a large dc resistance as the effective input impedance to the low-pass filter, one expects the ferrite unit to deliver slightly less power to the load than the discrete component unit. But the slightly higher insertion loss is a small sacrifice for the significant increase in smooth, predictable bandwidth that the ferrite design offers. The rf path isolation of this wideband ferrite unit is also more regular than its discrete component counterpart, although the overall magnitude of the isolation is slightly less. ••

Test your retention

1. Which port, or node, should the analysis of a bias insertion unit focus on?
2. Does isolation or insertion loss preclude the use of discrete component units over wide bandwidths?
3. Briefly describe changes in the electrical properties of a ferrite choke as frequency is increased.

Packaging Can Influence Coupled-Line Filters

Use caution when covering a package containing a microstrip coupled-line bandpass filter. Unless compensated, conducting covers at normal heights can distort the low-frequency skirt.

MICROSTRIP is an unbalanced transmission medium requiring only a single ground plane. Consequently, microstrip circuits are normally designed without consideration for a conducting cover.

For circuits consisting of isolated (uncoupled) lines, there is little difference in performance. But a conducting cover in close proximity to coupled microstrip lines—such as a typical bandpass filter structure—can cause a significant performance perturbation. The cover acts to prematurely terminate the fringing flux lines above the substrate.

Even at practical cover heights, such as 0.200 inch, a conducting cover can cause an apparent upward shift of the low frequency skirt with usually little or no change in the high frequency skirt. This effect is actually a superposition of two separate circuit changes: bandwidth shrinkage and an increase in center frequency.

Center frequency shifts upward

Qualitatively, the shift in center frequency is simply a consequence of the electrical shortening of the microstrip resonators which is caused by changes in even-and odd-mode phase velocities. The electrical length of a section of transmission line is given as:

$$\theta_L = \frac{2\pi}{\lambda_g}\ell = \frac{2\pi}{\lambda_o}\ell\sqrt{K_{EFF}} \qquad (1)$$

and related to phase velocity by:

$$\lambda_g = \frac{\nu_P}{f} \qquad (2)$$

so that:

$$\theta_L = \frac{2\pi\ell}{\nu_P} f \qquad (3)$$

where:

- λ_o = free space wavelength
- λ_g = wavelength on microstrip
- K_{eff} = effective relative dielectric constant of the microstrip circuit
- ℓ = physical length of resonator
- f = operating frequency, and
- ν_P = phase velocity in an inhomogeneous microstrip medium.

The center frequency of a resonator corresponds to an electrical length of 90 degrees. More fringing flux lines are terminated via an air path in a covered microstrip circuit than in an uncovered situation. Consequently, the effective dielectric constant is less, since this parameter is a function of the density of lines in air and alumina media. The smaller effective dielectric constant implies a larger phase velocity. Thus, Eqn. (3) predicts that for a covered circuit, a higher frequency is necessary to achieve a 90-degree electrical length.

This analysis pertains strictly to an isolated line resonator and not to a coupled line. The isolated resonator is characterized by a single phase velocity, whereas the coupled line resonator is characterized by even-and odd-mode phase velocities. It can be shown, however, that the microwave equivalent structure behaves approximately as though it is a series of isolated line resonators (see box, page 44).

Bandwidth shrinks, too

The second cover effect, bandwidth shrinkage, is due to a change in the even-and odd-mode impedances. The functional dependence of bandwidth on even-and odd-mode impedances can best be demonstrated by relating the lumped element filter parameters to the microstrip circuit parameters (see box).

The circuit bandwidth is related to the microstrip parameters of the end sections as:

$$W = \frac{2\, g_o\, g_1}{\pi}\left[\frac{Z_{oe} + Z_{oo}}{2\, Z_o} - 1\right] \qquad (4)$$

Although the bandwidth is related to the internal sections by a somewhat different function, either relation taken alone, is sufficient to demonstrate the bandwidth dependency.

For a quantitative demonstration of the cover effect consider the five-pole filter shown in Fig. 1. Param-

(continued on p. 44)

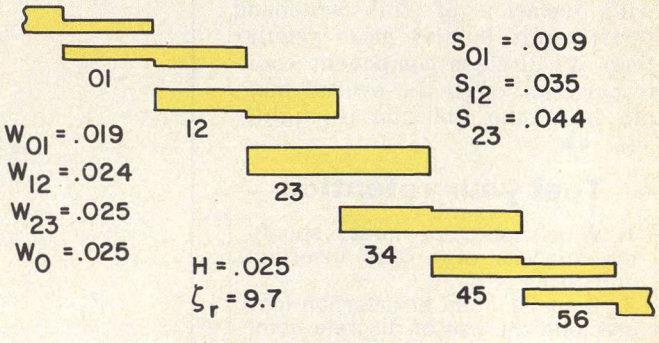

1. **This five-pole filter** was constructed and evaluated for changes in even and odd mode impedances. Correlation between measurements and calculations is very close.

Marcus Staloff*, Principal Electronics Engineer, The ARO Corporation, 3695 Broadway, Buffalo, NY 14225.
*Work performed while employed by the Raytheon Co. in Wayland, MA.

MICROSTRIP COVER

Equivalent Circuits: Lumped→ Microstrip→Transmission Line

Comparing the microstrip design to the equivalent lumped element filter parameters is the most convenient way to study the effects of a conducting cover. The simple low-pass prototype (a) is developed into the lumped element bandpass filter (d) by frequency (b) and impedance (c) scaling. The corresponding coupled line circuit is shown in (e). For simplicity, a two-pole filter is shown in this analysis, but it represents a typical case.

The notation used is fairly standard: The lower case g's are normalized element values (R, L and C), w is the percent bandwidth relative to the center frequency) and ω is the radian frequency.

The equivalent lumped element circuit (d) uses only shunt-tuned resonators and admittance inverters. The admittance inverter performs the function of branch impedance inversion and level scaling. Specifically, if a series-tuned branch is connected to an admittance inverter, the circuit appears to be shunt-tuned. The magnitude of the susceptances are also scaled according to the value of the inverter. The impedance level transforming property of the inverters allows for the adjustment of source and load resistances so that they may be different from those of the original circuit.

The salient point here, is that admittance inverters permit the realization of the original bandpass filter circuit by a simpler model containing only shunt-tuned resonators. The immediate significance is that this simpler structure is readily approximated by a transmission line structure that exhibits parallel resonance behavior.

The parallel coupled bandpass filter (e)[1] consists of cascaded, quarter-wave coupled sections. These open circuit terminated sections are equivalent to a quarter-wave long, balanced transmission line pair connected in series at each end with a quarter-wave long, open circuited pair. The balanced transmission line equivalent circuit[2] for the two-pole filter (f) is especially amenable to standard transmission line circuit analysis.

It must be noted, however, that the equivalence of the two-wire circuit is exact when the coupled lines circuit supports a pure TEM mode, such as that for shielded stripline. In that instance, the even- and odd-mode phase velocities are equal. For the microstrip case, propagation is quasi-TEM and the even- and odd mode phase velocities are unequal. The electrical line lengths of the connecting sections are then functions of both phase velocities. The justification for using this equivalent circuit as it stands in the subsequent analysis is that the filter tuning is almost entirely due to the series stubs, i.e., the loaded Q of the stubs is much higher than that of the connecting lines. ••

(continued on p. 46)

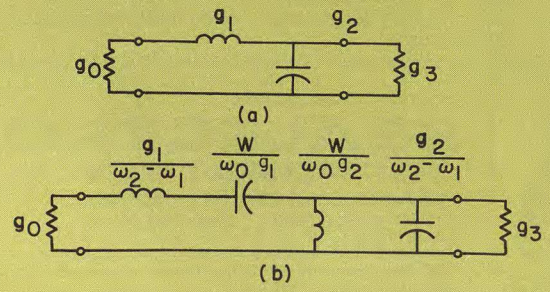

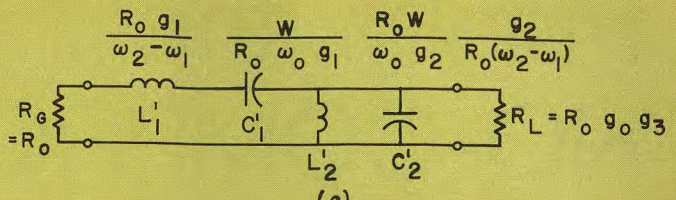

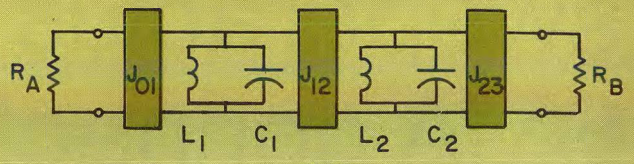

$$J_{01} = \sqrt{\frac{C_1 R_G}{L'_1 R_A}} = \sqrt{\frac{b_1 W}{g_1 R_A}}$$

$$J_{12} = \sqrt{\frac{C_1 C_2}{L'_1 C'_2}} = W\sqrt{\frac{b_1 b_2}{g_1 g_2}}$$

$$J_{23} = \sqrt{\frac{C_2 G_L}{C'_2 R_B}} = \sqrt{\frac{g_0 b_2 W}{g_2 g_3 R_B}}$$

$$C_i = \frac{b_i}{\omega_0}, \quad b_i \text{ is a susceptance slope parameter}$$

$$b_i = \frac{\omega_0}{2}\frac{dBi}{d\omega}\bigg|_{\omega=\omega_0} \qquad B_i = \omega C_i - \frac{1}{\omega L_1}$$

(d)

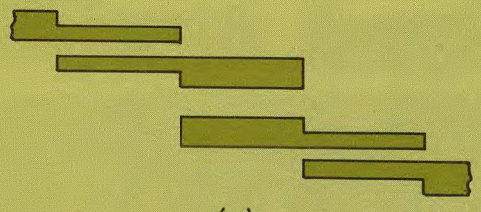

$$\frac{J_{12}}{Y_0} = \frac{\pi W}{2\sqrt{g_1 g_2}} \qquad \frac{J_{23}}{Y_0} = \sqrt{\frac{\pi W}{2 g_2 g_3}}$$

$$\frac{J_{01}}{Y_0} = \sqrt{\frac{\pi W}{2 g_0 g_1}}$$

Where: $R_A = R_B = Z_0$; $b_i = \frac{\pi}{2 Z_0}$; $Y_0 = \frac{1}{Z_0}$

$$(Z_{oe})_{01} = \frac{1}{Y_0}\left[1 + \frac{J_{01}}{Y_0} + \left(\frac{J_{01}}{Y_0}\right)^2\right]$$

$$(Z_{oo})_{01} = \frac{1}{Y_0}\left[1 - \frac{J_{01}}{Y_0} + \left(\frac{J_{01}}{Y_0}\right)^2\right]$$

(e)

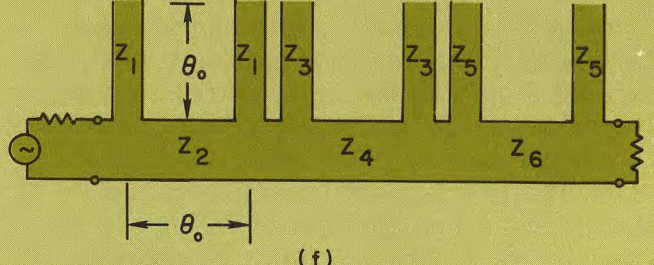

$$Z_2 = \left(\frac{Z_{oe} - Z_{oo}}{2}\right)_{01}$$

$$Z_6 = \left(\frac{Z_{oe} - Z_{oo}}{2}\right)_{23}$$

$$Z_4 = \left(\frac{Z_{oe} - Z_{oo}}{2}\right)_{12}$$

$$(Z_1 = Z_{oo})_{01};\ Z_3 = (Z_{oo})_{12};\ Z_5 = (Z_{oo})_{23}$$

(f)

eters for this circuit are listed in Table 1. These values were calculated using a modified version of the Bryant and Weiss coupled-line computer program[3,4]. Using the Bryant and Weiss notation, R = 0. 0 describes the case of no cover. When a cover is included, R is equal to the ratio of cover height above ground plane to the microstrip thickness. For the case considered here, R = 9.0 corresponds to a cover distance above the microstrip of 0.200 inch.

From this data, it is possible to compute the filter response (insertion loss function) when the cover is not present and again when the cover is in place. The theoretical performance can then be compared to the actual measured performance of the filter. In order to accurately do this, the transmission line losses must be included. To this end, the theoretical attenuation constant is determined using the theory of Pucel, Masse and Hartwig[5]:

$$\alpha_c = \frac{4.3\ R_s}{Z_o\ H} \qquad (5)$$

$R_s = 9.8\sqrt{F} \times 10^{-3}\ \Omega$ (for gold; F = GHz)
$= 16.16 \times 10^{-3}\ \Omega$ (at F = 2.716 GHz)

If Z_o is taken as the average of the even-and odd-modes (approximately 55 ohms):

$\alpha_c = 0.0058$ nepers per inch.

Using this value as a starting point, the circuit was analyzed with a microwave circuit analysis program. The mid-band loss was adjusted to be the same as the measured value; this obtained for an attenuation constant of 0.0051 nepers per inch. The adjustment for exact mid-band loss is not necessary, but facilitates the comparison of measured and calculated bandwidths and center frequency parameters.

Measurements confirm suspicions

Measured and calculated performance with and without a conducting cover is shown in Fig. 3. Figures 2(a) and 2(b) show excellent correlation between measured and calculated results, thereby validating the analytical approach. Figure 2(c) shows measured values for the bandpass filter with and without a cover. Note the upward shift in the low frequency skirt. Also, that the change in electrical length of the stubs due to the odd mode change results in a corresponding change in the center frequency of about 0.25%.

As shown in Fig. 2(c), the bandwidth change is considerably more than the coupled line impedance change. The coupled line impedance change is on the order of 1%, while the bandwidth change is about 9%. This sort of sensitivity can be seen from the following equation, which may be derived from the bandwidth expression obtained previously (Eqn. 4):

$$\frac{\Delta W}{W} = \frac{1}{1 - \left(\frac{2\,Z_o}{Z_{oe} + Z_{oo}}\right)} \left[\frac{\Delta(Z_{oe} + Z_{oo})}{Z_{oe} + Z_{oo}}\right] \qquad (6)$$

Table 1. Performance parameters with and without conducting cover

Without cover R = 0.0				
Section	Z_{oe}	Z_{oo}	K_{EFF_e}	K_{EFF_o}
01	71.01	39.33	6.881	5.540
12	55.20	45.95	6.991	5.912
23	54.03	46.77	6.924	6.014
With cover R = 9.0				
Section	Z_{oe}	Z_{oo}	K_{EFF_e}	K_{EFF_o}
01	70.51	39.33	6.799	5.540
12	54.67	45.96	6.894	5.904
23	54.40	46.87	6.850	5.983

The multiplying factor will generally be on the order of ten. Consequently, it is obvious that the presence of a conducting cover may have a marked effect.

It is apparent that accurate bandpass filter design requires the precise determination of the coupled line impedance for the particular cover height employed. The electrical parameters as a function of the physical parameters for coupled microstrip with a cover are available from numerical computer solutions of the associated boundary values problem as, for example, that due to Bryant and Weiss. If it is not practical to obtain the accurate design information, then it is recommended that uncovered coupled-

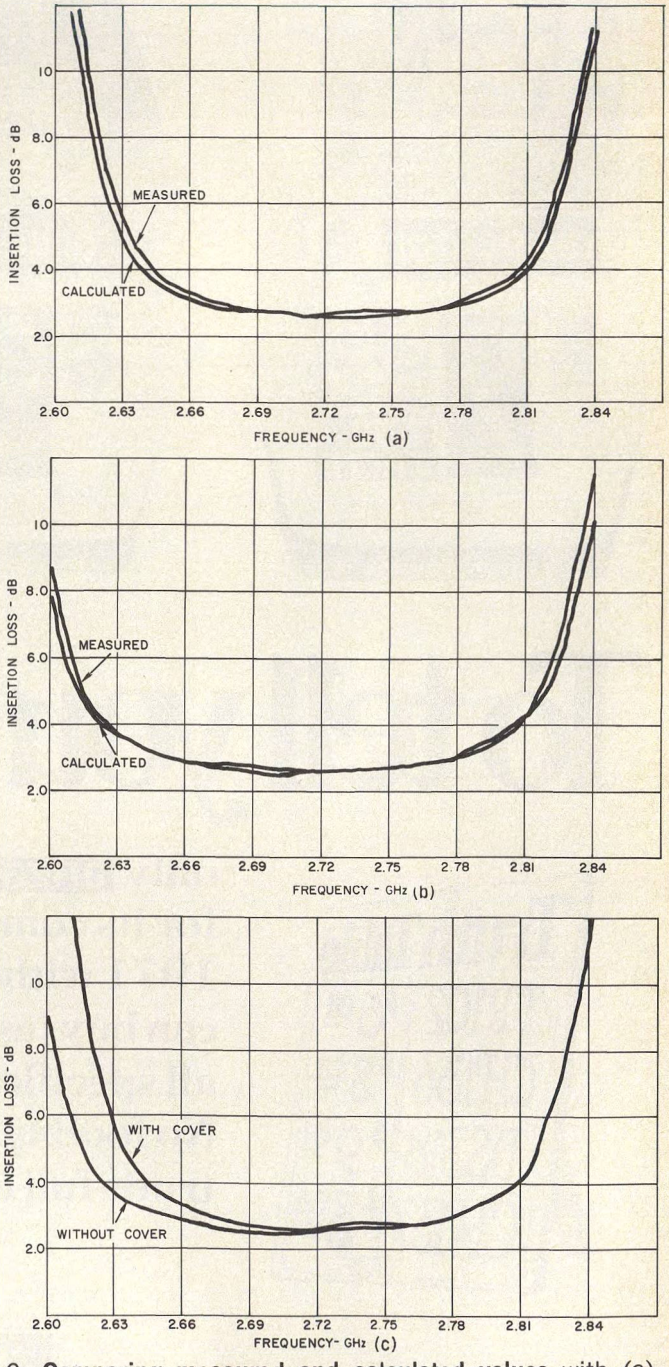

2. **Comparing measured and calculated values** with (a) and without (b) a cover proves the validity of the analysis. Measured performance (c) shows an upward shift of the low frequency skirt when a cover is introduced.

line data be employed and that the cover be placed no closer than approximately 20 substrate thicknesses to the microstrip.

A complete design, including the determination of resonator line lengths, may be accomplished by using the effective dielectric constant in the presence of the the cover and accounting for the open circuit end effect. This latter effect may be considered with the use of available design information such as that included in the papers of Farrar and Adams[6] and Rahmat-Samii, Itoh and Mittra[7]. An approximate procedure that has worked well for the author is simply calculating the resonator lengths as if they were isolated 50-ohm lines using the effective dielectric constant in the presence of the cover, then adjust for the end effect. ••

References

1. S. B. Cohn. "Parallel-Coupled Transmission-Line-Resonator filters." I.R.E. Trans. Microwave Theory and Techniques, Vol. MTT-6, (April, 1958).
2. G. L. Mathaei, L. Young and E. M. T. Jones, "Microwave Filters, Impedance-Matching Networks And Coupling Structures." McGraw-Hill Book Co., (1964).
3. T. G. Bryant and J. A. Weiss. Computer Program Descriptions, "MSTRIP (Parameters of Microstrip)," IEEE Trans. Microwave Theory and Techniques, Vol. MTT-19, (April, 1971).
4. M. Staloff. "Notes On Microstrip Coupled Lines Parameters Solutions And Computer Programs," Raytheon Co. Technical Memorandum. EM 71-0802, (Oct. 15, 1971).
5. R. A. Pucel, D. J. Masse and C. P. Hartwig. "Losses In Microstrip," IEEE Trans. Microwave Theory and Techniques, Vol. MTT-16, (June, 1968).
6. A. Farrar and A. T. Adams, "Matrix Methods For Microstrip Three Dimensional Problems," IEEE Trans. Microwave Theory and Techniques, Vol. MTT-20, (August, 1972).
7. Y. Rahmat-Samii, T. Itoh and R. Mittra. "A Spectral Domain Analysis For Solving Microstrip Discontinuity Problems," IEEE Trans. Microwave Theory and Techniques, Vol. MTT-22, (April, 1974).

Nomograms Speed Design Of λ/4 Transformers

The binomial quarter-wave transformer offers maximally flat response and wide bandwidths. It overcomes many of the undesirable features of exponential and Chebyshev transformers.

USING nomograms to design multiple quarter-wave transformers is a quick and efficient method of transformer design.[1-3] However, previous designs for the exponential and Chebyshev transformers have features which may be undesirable in some applications.

The binomial quarter-wave transformer[4] described in this article offers maximally flat performance for a two-section (N — 2) transformer and almost maximally flat for other values of N. In addition, this binomial transformer has a bandwidth which, in general, equals or exceeds the bandwidth of the exponential transformer.[1,2]. Although it does not have a bandwidth as great as the Chebyshev transformer, it does offer the advantage of lower VSWR ripple. As noted in Ref. 3, this ripple may be objectionable in some cases.

Using the nomograms

The four nomograms, shown as Figs. 1-4, can be used to determine the transformer characteristics, such as the number of sections and the impedance of each section required for a given VSWR, bandwidth and impedance ratio, Z_I/Z_L or Z_L/Z_I, where Z_L is the load impedance and Z_I is the input impedance.

Figure 1 relates the number of sections, VSWR, operating-to-design bandwidth and impedance ratio. Given any three of these values, the fourth can be determined using this nomogram. It is based on the following equation:

$S = 1 + (\cos\theta)^N \ln R$

S = VSWR

θ = electrical length of quarter-wave section

N = number of sections

R = impedance ratio Z_L/Z_I or Z_I/Z_L whichever is greater than unity

The nomograms in Figs. 2 and 3 are then used to determine the impedance required for each section for transformers having up to five sections. These nomograms are based on the equations contained in Ref. 4.

Designing λ/4 binomial transformers

Examples best illustrate the use of these nomographs.

- What is the bandwidth of a two-section transformer having a maximum VSWR of 1.1 for a load-to-input impedance ratio of 5.0?

Solution: Using Fig. 1, draw a line connecting $Z_L/Z_I = 5.0$ and S = 1.1 and intersecting the uncalibrated pivot axis. Then draw a line from the intersection through N = 2 to intersect the f/f_o axis. Read off the bandwidth on the f/f_o axis of 0.84, i.e., the bandwidth extends from 0.84 to 1.16 f_o.

- Design the two-section transformer in the previous example for a 50-ohm input.

Solution: The load, Z_L, is 250 ohms since $Z_L/Z_I = 5.0$. Draw a line connecting $Z_L = 250$ $Z_i = 50$ using Fig. 2. The intersection of the line with Z_2 and Z_4 axes gives the impedance of the transformer sections. In this example, the impedances are 74 ohms and 170 ohms, respectively.

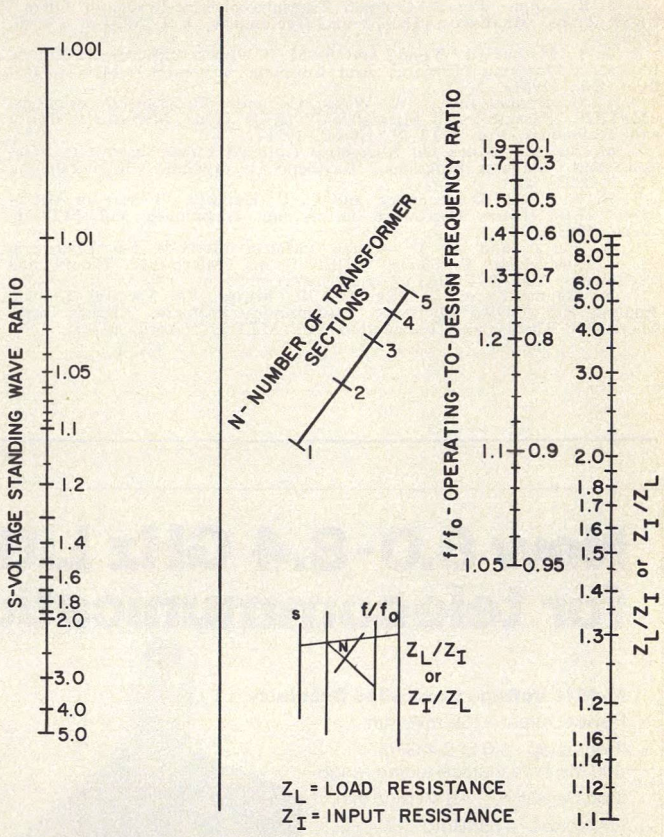

1. **Binomial transformer nomogram** relates number of sections, VSWR, bandwidth and impedance ratio by pivoting at points on bold reference line.

Samuel Guccione, Department Chairman of Engineering, Delaware Technical and Community College, Kent Campus, 1679 South State Street, Dover, DE 19901.

(continued on p. 50)

NOMOGRAMS SPEED DESIGN OF λ/4 TRANSFORMERS

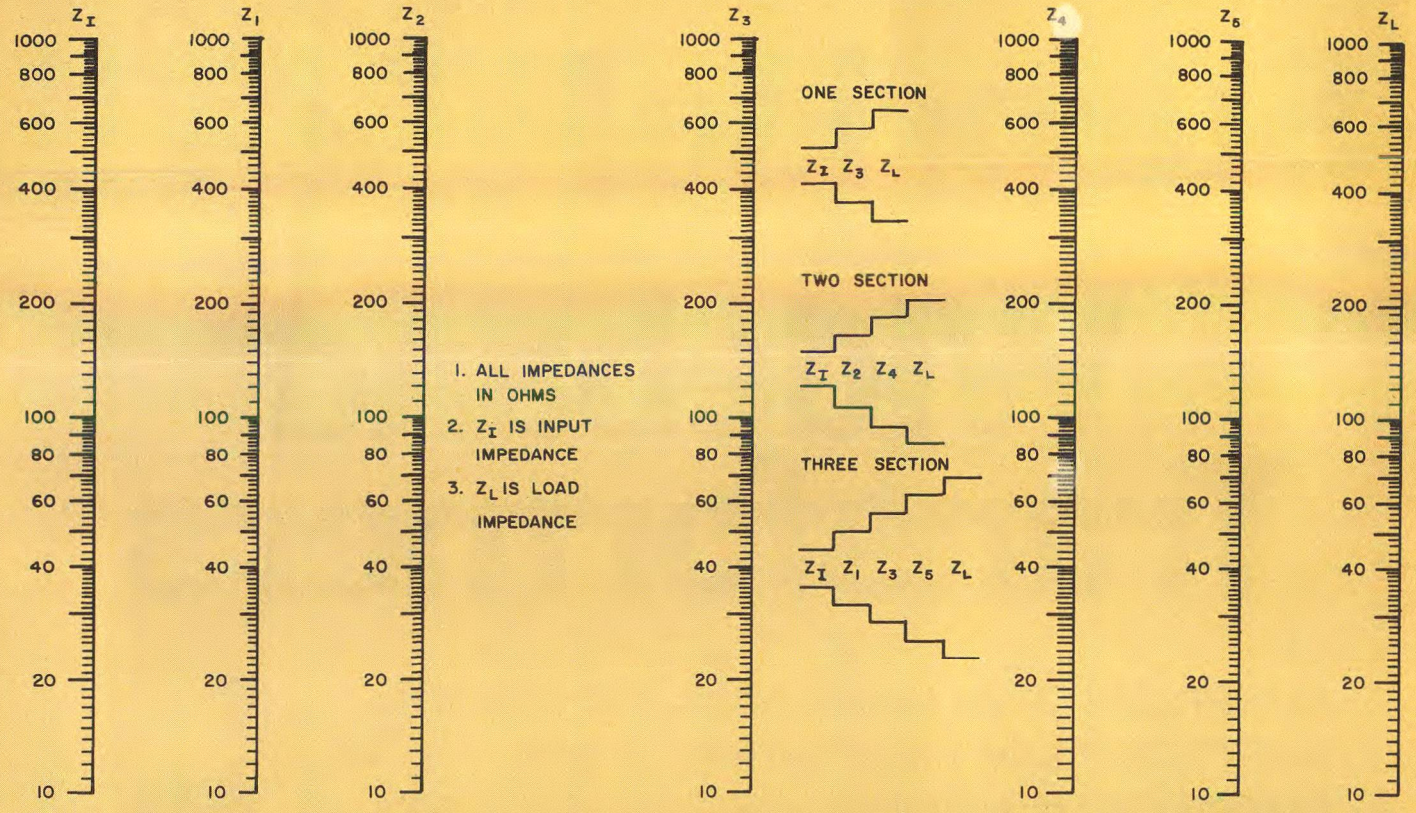

2. **Nomogram for designing one, two and three-section binomial** λ/4 transformers requires drawing a straight line between Z_I and Z_L and reading impedance values for the intermediate sections.

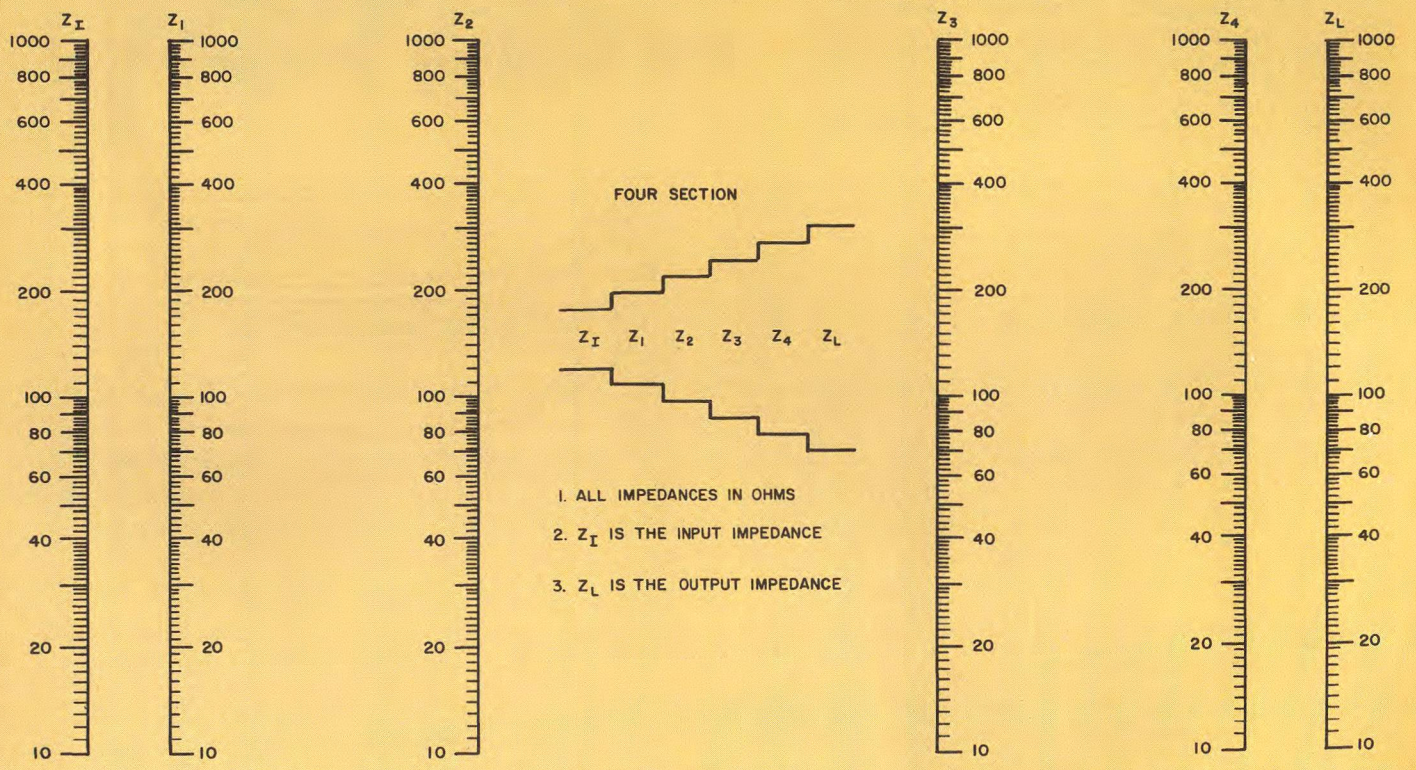

3. **Nomograms for designing four-section transformer** requires drawing a straight line between Z_I and Z_L and reading impedance value of intermediate sections.

(continued on p. 52)

NOMOGRAMS SPEED DESIGN OF λ/4 TRANSFORMERS

- Determine the number and the impedance of each section needed to match a 200-ohm load to a 50-ohm input over a bandwidth of 0.75 f_0 to 1.25 f_0 with a VSWR of 1.05 or less.

  Solution: Note that $Z_L/Z_I = 4.0$. Construct a line from $Z_L/Z_I = 4.0$ to S = 1.05 intersecting the pivot axis in Fig. 1. Next, connect the pivot axis intersection point and the $f/f_0 = 0.75$ point with a line. Note that this line intersects the N axis half way between three and four. Thus, a four-section transformer would be needed to have a VSWR less than 1.05. The impedance of the sections is determined from Fig. 3(a) by connecting $Z_L = 200$ and $Z_I = 50$ with a line. The intersections of the line and the Z_1 through Z_4 axes gives the impedance of the sections. For this example, the impedances are as follows:

  $Z_1 = 54.5$ ohm $Z_2 = 76.8$ ohms $Z_3 = 128$ ohms $Z_4 = 180$ ohms
- What will be the VSWR of a five-section transformer used to match a load if $Z_L = 10\ Z_I$ over the band of 0.5 to 1.5 f_0?

  Solution: Using Fig. 1, draw a line from $f/f_0 = 0.5$ through N = 5 intersecting the pivot axis. Extend a line from $Z_L/Z_I = 10$ through the intersection on the pivot axis to the S axis and read the VSWR as 1.4. ••

References

1. B. R. Hatcher, "Nomograms For Transmission Line Transformers," *Microwave Journal,* Vol. 5, No. 11, pp. 110-111, (November, 1962).
2. B. R. Hatcher, "Nomogram Speeds Selection of Broadband Matching Transformers," *MicroWaves,* Vol. 5, No. 11, pp. 56-57, (November, 1966).
3. F. E. Gardiol, "Chebyshev Transformer Nomograms," *MicroWaves,* Vol. 6, No. 11, pp. 56-58, (November, 1967).
4. H. Jasik, *Antenna Engineering Handbook,* McGraw-Hill, New York, pp. 31-12 through 31-14, (1961).

TEST YOUR RETENTION

1. **What is the major advantage of the binomial quarter wave transmission line transformer over the Chebyshev transformer?**
2. **The binomial transformer has a bandwidth which equals or exceeds which of the following two transformers: Exponential or Chebyshev?**

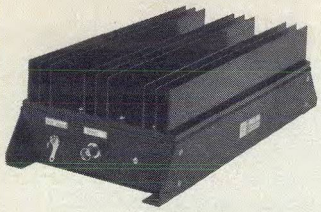

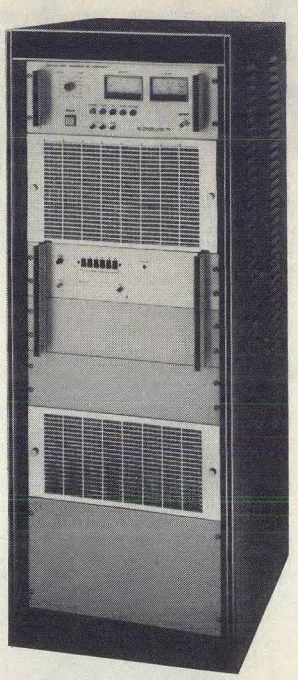

LINEAR WIDEBAND RF AMPLIFIERS

MODEL	OUTPUT	FREQUENCY RANGE	GAIN	DELIVERY
*M500	.3W	.5-500MHz	27dB	A
*M501	.5W	.5-500MHz	27dB	A
*A101	1W	1-100MHz	25dB	A
*A201	1W	2-200MHz	23dB	A
*A102	2W	1-100MHz	25dB	A
M102L	2W	16Hz-100MHz	40dB	B
*250-2M	2W	.2-250MHz	25dB	B
250-2M-C	2W	.2-250MHz	25dB	B
*300-2M	2W	5-300MHz	25dB	B
300-2M-C	2W	5-300MHz	25dB	B
*M502	2W	.5-450MHz	35dB	B
M502-C	2W	.5-450MHz	35dB	B
*M305-S	5W	.5-250MHz	40dB	B
M305	5W	.3-300MHz	40dB	B
M110	10W	.3-150MHz	40dB	B
250-10	10W	.005-250MHz	35dB	C
250-10A	10W	.25-250MHz	35dB	C
250-10C	10W	.25-250MHz	35dB	B
M310	10W	.3-300MHz	40dB	B
30-12L	12W	.01-25MHz	40dB	B
30-12LC	12W	.01-25MHz	40dB	B
M120	20W	1-150MHz	45dB	B
M320	20W	1-300MHz	45dB	B
M125L	25W	50Hz-100MHz	45dB	C
*30-25AM	25W	.1-32MHz	40dB	B
30-25-C	25W	2-32MHz	40dB	C
30-25A-C	25W	.1-32MHz	40dB	C
30-50-C	50W	2-32MHz	40dB	C
300-110	75W	.2-300MHz	9dB	C
30-100C	100W	1-32MHz	50dB	C
250-110	100W	.005-250MHz	10dB	C
260-110	100W	.25-260MHz	10dB	C
250-145	100W	.005-250MHz	45dB	C
250-145A	100W	.25-250MHz	45dB	C
250-145B	100W	2-200MHz	45dB	C
300-145	100W	.3-300MHz	47dB	C
220-250	200W	.2-220MHz	50dB	D
220-250A	200W	.2-220MHz	13dB	D
220-250B	200W	.01-250MHz	48dB	D
220-525	500W	.25-220MHz	23dB	D
220-560	500W	2-200MHz	60dB	D
220-560A	500W	.01-220MHz	60dB	D
220-1K30	1000W	.25-220MHz	30dB	E
220-1K30L	1000W	.01-220MHz	30dB	E
220-1K30M	1000W	2-200MHz	30dB	E
220-1K60	1000W	.25-220MHz	60dB	E
220-1K60L	1000W	.01-220MHz	60dB	E
220-1K60M	1000W	2-200MHz	60dB	E

*Denotes: Module without power supply

MAY 1, 1975

Delivery — A = Stock 10 days; B = 15-20 days; C = 30-40 days; D = 50-60 days; E = 90 days

rf POWER LABS

RF POWER LABS, INC.

11013-118th Place N.E. • Kirkland, Washington 98033 U.S.A. • Tel: (206) 822-1251 • TELEX No. 32-1042

READER SERVICE NUMBER 53

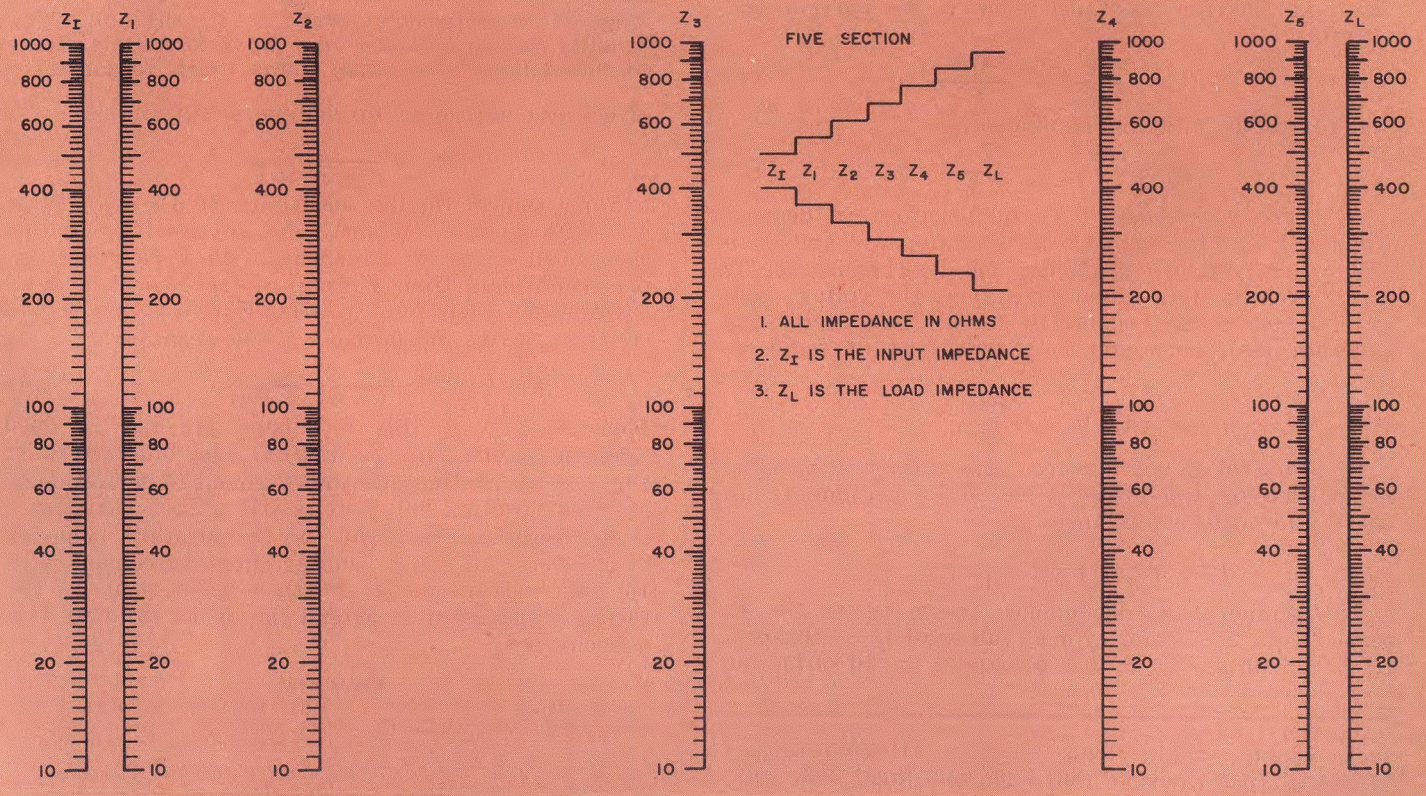

4. **Nomogram for designing five-section transformer** requires drawing straight lines between Z_I and Z_L and reading impedance value of immediate sections.

Schottky Detectors: How Sensitive To Temperature?

The change in voltage sensitivity of a Schottky barrier detector diode due to temperature variations is theoretically described for frequencies in the region of 10 GHz.

ALTHOUGH Schottky barrier diodes are less sensitive to temperature changes than are point-contact diodes[1], the effect on detector voltage sensitivity may be significant for some applications. As temperature is increased, detector sensitivity falls rather steeply, but in a predictable manner.

The diode's forward current vs. voltage characteristic also changes with temperature in a predictable manner, so that a second diode may be used in a compensating circuit to help cancel the sensitivity variations. In this scheme, which is described in detail by R. J. Turner[2], a current source feeds the compensating diode, so that the voltage drop across this diode is a function of temperature. This voltage then controls the bias to the detector diode so that the sensitivity is independent of temperature.

The temperature dependence of current sensitivity was studied by Cowley and Sorenson[3], but their analysis was not extended to voltage sensitivity. For the ideal diode with infinite cutoff frequency (zero series resistance and/or zero junction capacitance), there is no temperature effect on voltage sensitivity. The inverse temperature behavior of current sensitivity is balanced by the direct temperature variation of the diode barrier resistance. That is, for current sensitivity:

$$\beta = \frac{q}{2\,nkT} = \frac{5400}{T} \qquad (1)$$

and for diode junction resistance:

$$R_j = \frac{nkT}{qI} = \frac{T}{11\,I} \qquad (2)$$

In these equations, T is temperature in degrees Kelvin, I is bias current in milliamperes and n, q and k are constants[3]. When the load resistance is much greater than diode resistance, the voltage sensitivity, γ_o, is the product of current sensitivity and junction resistance and is independent of temperature:

$$\gamma_o = \beta R_j = \frac{490}{I} \qquad (3)$$

In practical cases, however, the voltage sensitivity is reduced by the presence of both junction capacitance and series resistance, i.e.,:

$$\gamma = \frac{\gamma_o}{1 + 4\pi^2 f^2 C_j^2 R_s R_j} \qquad (4)$$

The temperature dependence shows up in the R_j term (Eqn. 2). Using typical values of I = 0.02 mA, R_s = 25 ohms, C_j = 0.1 pF and f = 10 GHz, the effect of temperature on voltage sensitivity is:

$$\gamma = \frac{\gamma_o}{1 + .0045\,T} \qquad (5)$$

For a typical voltage sensitivity of 6.5 mV/μW at T = 293°K, γ_o = 15.1 mV/μW. Figure 1 shows this theoretical curve in agreement with a range of experimental data from a group of ten typical diodes.

However, when f = 1 GHz, Eqn. (4) predicts a response nearly independent of temperature:

$$\gamma = \frac{\gamma_o}{1 + 4.5T \times 10^{-5}} \qquad (6)$$

Measurements at this frequency are not in good agreement with this prediction. The blue curve in Fig. 1 shows considerable improvement in performance over temperature, but there is still a 25% variation.

A theoretical model of the temperature behavior of a Schottky detector is in excellent agreement with 10 GHz measurements. Further refinement of the theory is necessary to extend the model to lower frequencies. ••

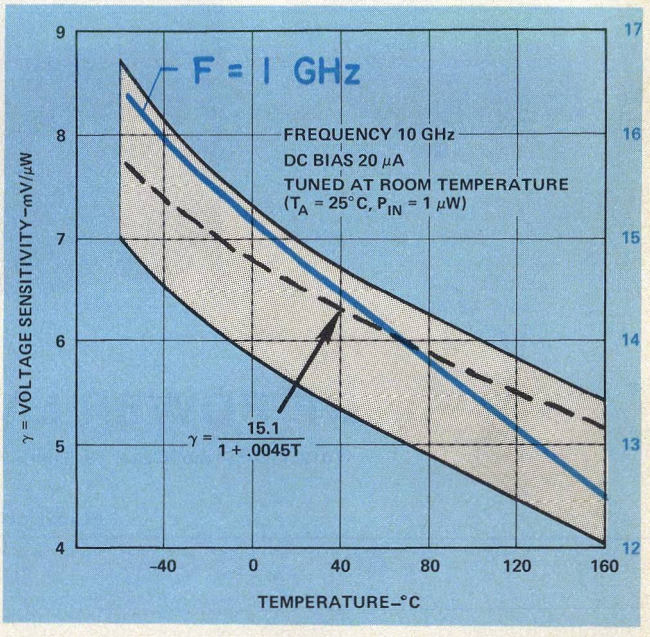

1. This theoretical (dashed) curve is based on Eqn. (5), where γ_o = 15.1 mV/μW. Note the agreement with a range of measurements taken for 10 HP 5082-2750 Schottky detectors chosen from two different lots. Colored curved (right-hand scale) shows 1 GHz response.

Jack Lepoff, Applications Engineer, Hewlett-Packard Company, HPA Division, 640 Page Mill Road, Palo Alto, CA 94304.

References

1. R. Bayliss, et al., "Why A Schottky Barrier? Why A Point Contact?", *MicroWaves*, pp. 34-45, (March, 1968).
2. R. J. Turner, "Schottky Diode Pair Makes An Rf Detector Stable." *Electronics*, pp. 94-95, (May 2, 1974).
3. A. M. Cowley and H. O. Sorenson, "Quantitative Comparison of Solid-State Microwave Detectors", *IEEE Trans. on MTT*, Vol. MTT-14, No. 12, pp. 588-602, (December, 1966).

ptember
975

laser technology

MICROWAVES

Electronic Warfare:

Mini-RPVs propelled to flight-test status

Noise jamming search radars
Supercomponents solve DF design problems
NEWS: TEO remembers threat frequencies

MICROWAVES

September 1975
Vol. 14, No. 9

news

editorial

technical section

products and departments

About the cover: Half-scale models of the Army's Aquila mini-RPV are shown here during recent flight tests. Photos courtesy of Lockheed Missile and Space Co., Inc., Sunnyvale, CA. Cover design by Robert Meehan.

coming next month: Amplifiers

Behind The Design Of An X-Band FET Amplifier. Martin Walker and colleagues from the Watkins-Johnson Company examine the strategies of X-band, multistage FET amplifier design. The particular example presented in the article covers 8.0 to 12.4 GHz with a maximum noise figure of 6.5 dB and +10 dB power output at 1 dB compression. A novel technique for self-biasing the FET is revealed which eliminates the need for a negative bias supply.

Take The Guesswork Out Of Amplifier Compression Tests. Harry F. Cooke of Avantek, Inc., outlines a simple, straight-forward approach for measuring the 1 dB compression point of amplifiers. The method requires two power meters and centers on a build-it-yourself divider network.

GaAs Impatts Boost Power and Efficiency. Steve Long and his colleagues at Varian present an overview of the various structures and heat sinking techniques being used to improve output power, efficiency and reliability of Impatt diodes.

Publisher/Editor
Howard Bierman

Managing Editor
Richard T. Davis

Associate Editor
Stacy V. Bearse

Contributing Editor
Harvey J. Hindin

Washington Editor
Paul Harris
Snyder Associates
1050 Potomac St., NW
Washington, DC 20007
(202) 965-3700

Editorial Assistant
Gail Murphy

Production Editor
Sherry Lynne Bogen

Art
Robert Meehan, Dir.

Production
Dollie S. Viebig, Mgr.
Dan Coakley

Circulation
Trish Edelmann, Mgr.
Peggy Long, Reader Service

Promotion Manager
Albert B. Stempel

Directory Coordinator
Janice Tapp

Editorial Office
50 Essex St.,
Rochelle Park, N.J. 07662
Phone (201) 843-0550
TWX 710-990-5071

A Hayden Publication
James S. Mulholland, Jr., President

MICROWAVES is sent free to individuals actively engaged in microwave work at companies located in the U.S., Canada and Western Europe. Subscription price for non-qualified copies is $10.00 for U.S., $15.00 a year elsewhere. Additional single copies $1.50 ea. (U.S.); $2.00 ea. (foreign); except additional Product Data Directory reference issue, $10.00 ea. (U.S.); $18.00 (foreign). POSTMASTER, please send Form 3579 to Fulfillment Manager, MICROWAVES, P.O. Box 13801, Philadelphia, PA 19101.

Back Issues of MicroWaves are available on microfilm, microfiche, 16mm or 35mm roll film. They can be ordered from Xerox University Microfilms, 300 North Zeeb Road, Ann Arbor, MI 48106. For immediate information, call (313) 761-4700.

Hayden Publishing Co., Inc., James S. Mulholland, President, printed at Brown Printing Co., Inc., Waseca, MN.

TED oscillator "remembers" threat frequencies

Stacy V. Bearse
Associate Editor

A microstrip Gunn oscillator that is capable of operating at any one of several closely-spaced frequencies has been developed at RCA's David Sarnoff Research Center in Princeton, NJ. Dubbed a "multiposition frequency memorizer", the oscillator can quickly jump to any of 17 different frequencies within a 2.12 GHz range in response to a short input pulse.

Normally, the compact, 2.5 × 4 inch oscillator operates at any of the stable frequency states shown in Fig. 1. But when pulsed by a different frequency within this range, the output quickly switches to the stable state nearest to the frequency of the input pulse, and locks there until changed by another input.

"The idea is to essentially identify and retain an external frequency and have it available to process at a later time," explains Walter R. Curtice, a member of the technical staff at RCA. Alluding to the device's obvious ECM application, Curtice notes that the solid-state memorizer's main advantage over present frequency identification systems, which generally use a TWT and delay line memory loop to merely store a threat signal for several microseconds, is its simplicity and low cost.

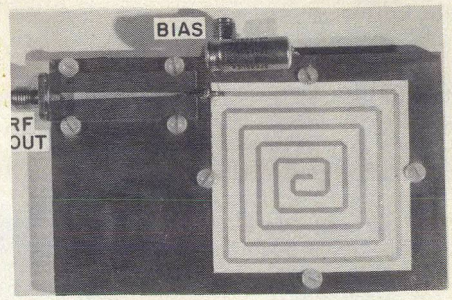

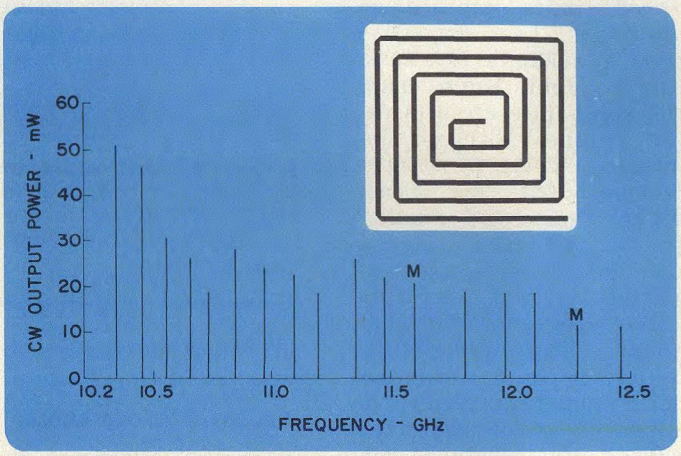

1. Stable frequency states are ideally separated by 132 MHz for this microstrip frequency memorizer. Frequencies marked M must exist simultaneously.

Output pulsed through circulator

Pulses as short as 0.1 μsec, channeled to the output of the oscillator through a circulator (Fig. 2), are sufficient to switch the X-band device, according to the RCA researcher's presentation at the 1975 MTT this past May. Rf switching power depends on how close the frequency of the input pulse is to the nearest stable frequency of the oscillator, but 200 mW is reportedly adequate if the input pulse is within several MHz of a stable state.

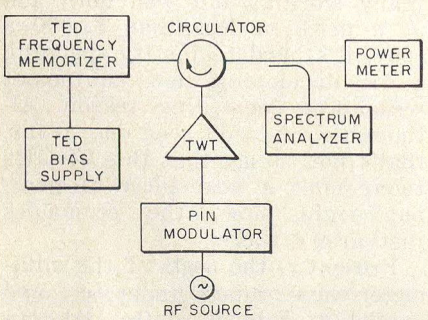

2. Short switching pulses hit the cw oscillator's output through a circulator; equipment layout for switching tests is shown above.

Curtice points out that the switching occurs due to a nonlinear mixing effect, and not by an injection-locking process. "Thus, far less rf input power is required to switch over a 1 GHz range than would be estimated from the equations for injection locking," he notes.

The miniature microstrip memorizer is designed around a conventional two-terminal Gunn diode, which is capable of a 100 mW output, and a delay line with a length equal to an integral number of half wavelengths at each mode.

"The simplest method of producing a multi-frequency resonator with a reasonably similar Q-value for each mode is to utilize a long section of transmission line with either a short or open circuit at one end," the RCA researcher explains.

A shunt-loaded, open-circuited line was chosen for this design.

The length of this long delay line governs the separation between stable modes. Ideally, the frequency spread between stable states is equal to the reciprocal of the round trip delay. For the case of this microstrip oscillator, each state is ideally separated by 132 MHz.

By using waveguide and coaxial delay lines in place of microstrip, Curtice has demonstrated other X-band frequency memorizers that exhibit much more closely spaced stable frequency states. One waveguide component, designed with a five-foot WR-90 delay line, offers 16 stable modes separated by 71 MHz. A second memorizer, designed around a 15-foot coaxial delay line, reportedly locks at 20 stable states, each separated by only 22.4 MHz.

"For long transmission lines and close frequency states, attenuation becomes the limiting factor," he cautions. ••

94 GHz radar undergoing Coast Guard evaluation

Stacy V. Bearse
Associate Editor

The United States Coast Guard is looking into the possibility of slowing down huge, ocean-going ships with tiny, millimeter waves. In collaboration with Hughes Aircraft, Torrance, CA, researchers at the Coast Guard R&D Center in Groton, CT are currently evaluating the concept of using 94 GHz portable speed detection radars to enforce speed limits imposed on inland waterways. Less expensive X-band units now handle this task.

According to John Kuno, manager of the solid-state circuits department of Hughes' Electron Dynamics Division, where prototypes were developed for the Coast Guard, higher gain and smaller beamwidth for a given antenna size are the major advantages of a speed detection radar operating at the 94 GHz atmospheric attenuation window. "The higher gain results in longer range, whereas the smaller beamwidth results in improved spatial resolution (the ability to discriminate between adjacent targets) and improved clutter rejection capability," the researcher explains.

Although Kuno claims that Hughes has not thoroughly examined the radar's highway law enforcement potential, he notes that at a range of one mile, a 94 GHz unit can clearly distinguish between two lanes of automobile traffic. Present highway radars operate in upper X-band, monitor all lanes simultaneously and rely on visual inspection to pick violators out of a group of vehicles.

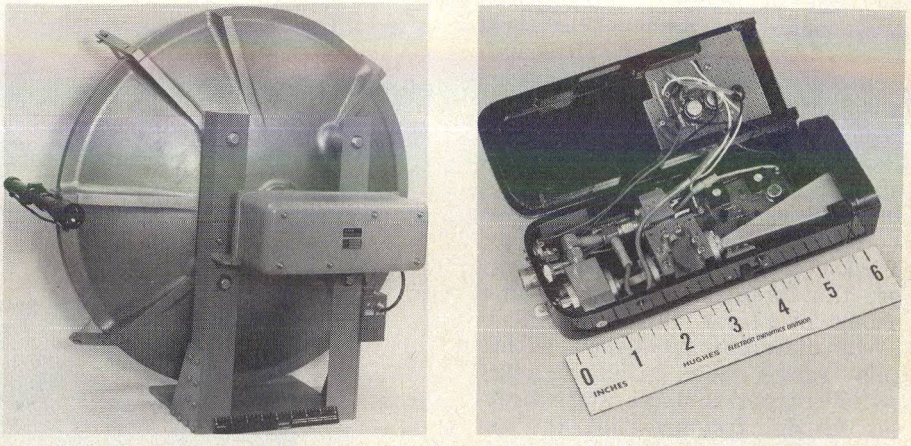

1. The 94 GHz radar developed for Coast Guard tests (a) uses a 24-inch parabolic dish with a gain of 52 dB. Circuitry is housed in the 11 × 4.5 × 4 inch box attached to the antenna's frame. Scarcely larger than a flashlight, the hand-held unit shown on the right (b) illustrates how small a 94 GHz radar can be.

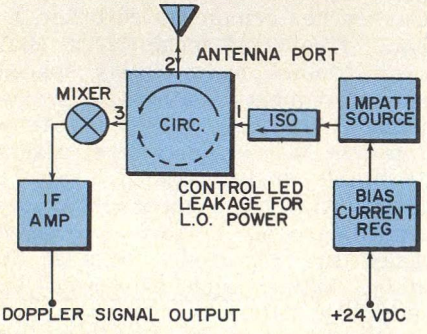

2. In this homodyne circuit, a fraction of the Impatt source's power is leaked to the single-ended mixer through a circulator.

Homodyne circuit chosen

Hughes' engineers chose a simple homodyne circuit for the Coast Guard's feasibility radar, consisting of a 100 mW Impatt source with an integral isolator feeding a circulator, single-ended mixer and an i-f preamplifier. "The circulator has the dual purpose of separating the transmit and receive signals and leaking a small fraction of the signal power to serve as local oscillator power for the mixer," Kuno describes. The mixer uses a silicon Schottky barrier diode with an extremely small, 3 μm diameter junction.

The major challenge of this design approach was minimizing noise to maintain maximum sensitivity, says the Hughes researcher. The high Doppler frequency of a 94 GHz radar—almost 10 times that of an X-band unit—helps by reducing the contribution of i/f noise, but careful design of the homodyne circuit is still necessary to fully maximize sensitivity.

"Fm noise is of no importance for target distances below two miles," Kuno explains, "but am noise could limit the sensitivity of the radar if a large amount of power is leaked through the circulator." It was discovered, however, that when this leaked LO power is reduced, the conversion loss of the mixer deteriorates. But by using a forward bias at the mixer, the Hughes designers were able to maintain a 6.5 to 8 dB conversion loss for LO powers ranging from −2 to 10 dBm.

With a transmitter power of +20 dBm and an antenna gain of 52 dB, maximum range varies between 1,000 and 3,000 meters. In field tests, cars at a distance of about 1.5 miles produced doppler signals of about 350 mV.

Cost is key question

"It's too early to draw conclusions about 94 GHz," notes Lt. Commander James McIntosh of the Coast Guard R&D Center. "Our conventional X-band radars are really working out well now, and at a price of less than $1,000 a copy, it's hard to justify spending a lot developing new equipment without a compelling reason. Although we haven't seen one so far, that's not to say that this 94 GHz radar isn't a neat piece of gear, but right now, the economics just aren't there."

Presently, the costs of the millimeter-wave radars under test and available X-band units are an "order of magnitude apart", according to the Coast Guard officer. ••

Dissatisfied with phone service, Alaska buys its own satellite earth terminals

Richard T. Davis
Managing Editor

For most individuals who are unhappy with their phone service or find it too expensive, there is little else to do but complain and hope for the best. But this is not the case for the State of Alaska. Faced with fairly primitive and unreliable phone service in many of its communities and without any service at all in about 140 bush communities, the state has made moves to become less dependent on its phone company, RCA Alaska Communications, by installing its own satellite ground stations.

According to Jack Pettit, the attorney representing Alaska before the FCC, "the state faults RCA Alascom for failure to honor their commitment to improve telephone service to 142 communities by 1973. By 1974, RCA had improved service to only 20% of them," contends Petit, "and currently has improved service to only an additional 10%." It is further alleged that Alascom has also been reluctant to make the commitment to satellite technology needed to serve the bush.

"It was not until it became clear that the state would seek satellite services from another source that RCA developed a satellite proposal," says Marvin Weatherly, Director of Alaska's Office of Telecommunications in Juneau. "Even then, the proposed earth stations were technically inferior to and more expensive than the earth stations which could be obtained by the state. Specifically, the Alascom single channel/carrier system, as proposed, was wasteful of output power by about 4 or 5 dB to achieve a given output signal-to-noise ratio, compared to the equipment selected by the state."

Louis Custrini of RCA Alascom in Anchorage, explains that from the start of their program to establish vhf phone service in 142 bush villages, "we were set back by the unanticipated need for environmental impact statements for many repeater sites, especially for mountain top repeaters located on D2 land, designated for native claims. In addition, the lengthy processing of securing land permits impeded the program even further."

Custrini also maintains, "There is no evidence to support any charge that our earth station specifications are technically inferior to any other—proposed or otherwise. The cost of RCA's earth station differed with those of the state because of different requirements. We have designed stations for message toll service, while the state has specified hardware for emergency health service."

Nonetheless, seeking a showdown, Alaska challenged Alascom's monopoly of long-distance telephone service by filing construction permit applications with the FCC in July, 1975, for 26 earth-station sites, which RCA Alascom had already filed. Last month, in an effort to expedite matters, both parties agreed to construct and own 20 small earth stations jointly. Waver permits for construction were later granted by the FCC. The agreement, worked out by Commissioner Abbot Washburn of the FCC is an interim measure. The ultimate question of ownership has been postponed pending the FCC's resolution of the matter. The agreement calls for the state to be responsible for the purchase of emergency medical equipment and RCA Alascom to provide message toll service and do the construction and installation. This agreement, however, is hardly the end to Alaska's litigation problems.

Another major concern is that widespread use of small antennas will result in poor utilization of the orbit spectrum. Comsat General Corp., Washington, DC, has filed a complaint with the FCC asking for a ban on using the 15-ft dishes planned by the state. Comsat contends that the small antennas produce relatively large interferring beamwidth with the result that synchronous satellites will have to be spaced further apart over the equator to prevent spillover onto adjacent satellites.

Single channel/carrier system

To get a handle on the technology involved with building small earth terminals, state officials, Marvin Weatherly and George Shaginaw of the Governor's Office of Telecommunications, engaged the opinion of several independent consultants as well as staff members of the University of Alaska and Stanford University. From this contact, specifications were prepared for a single carrier per channel system and bids solicited in March of 1975. "Subsystem suppliers were encouraged to bid their products as well as system suppliers," says Prof. Bruce Lusignan of Stanford's Communication Satellite Planning Center. "Vendors were also asked to quote prices for a range of quantities from 10 to 150 units." This was done to determine a system price for a smaller quantity in the event the price for the desired quantity exceeded the available budget, and to get an estimate for the learning curves used by the various manufacturers in their quantity pricing.

1. **Small dish earth stations** in Alaska can be installed without disturbing the tundra. Less than 5 W of power is required per carrier for satisfactory uplink C/kT with a 15 ft dish. The channel capacity for thin route service to small stations is between 220 and 460 simplex channels per 5W transponder, depending on location.

To serve these bush communities, a frequency modulated single channel per carrier (SCPC) system was selected due to its low cost per channel toll quality performance, and its good use of satellite power and bandwidth.

"The advantages of SCPC equipment for handling light traffic has long been recognized," says Jim Janky, Consultant at Stanford's Planning Center, "but moderate cost equipment has only recently become available. This fact, plus low-cost small aperture antennas, made these systems feasible for use in Alaska. The cost for a completed terminal with a single chan-

(continued on p. 14)

nel capability is $37,000 in 100 unit quantities. The incremental cost for the first additional channel is approximately $5,000 and for the next two, $3,300 each. The installation costs are estimated to range between $5,000 and $10,000."

Double-hop between bush terminals

In Alaska's proposed telephone system, it will be essential, at least for now, for the bush communities to link up with RCA's high-density earth-station terminal in Talkeetna, where demand access control equipment is available. Telephone communications from a bush community will initially be routed through the Talkeetna terminal on a preassigned basis. Calls will be switched either into the terrestrial network or transmitted to the destination earth station on a double-hop basis. "This will result in about a half-second pause for the transmission between bush sites," says Janky. Because of this double hop and the inefficient use of satellite capacity, Alascom, General Electric, and the Stanford group are presently working on various demand assignment multiple access designs. Once implemented, it will allow each bush station to act autonomously in getting connected to another remote community, without going through Talkeetna. "At the present time, the primary obstacle is cost," says Janky.

The equipment selected for the Alaskan thin-route station includes a 4.57 meter dish designed by Andrew Corp., Orland Park, IL. The antenna mount is on a three-point frame and the unit cost for a quantity of 100 is $7,381. Using this dish, a downlink G/T of 20 dB/°K can be achieved using a 190°K preamplifier. Janky maintains that the antenna is fully compliant with FCC specifications on antenna sidelobe performance despite what Comsat General says.

A 35 watt, 6 GHz TWTA, built by Hughes Aircraft, Torrance, CA, was selected for the ground station transmitter. It costs $6,900 each per 100 units. The low-noise preamplifier selected for the ground-station receiver is a GaAs FET amplifier built by Amplica, Westlake Village, CA. It provides a noise temperature of 190°K at 4 GHz and in 100 lot quantities will sell from $2,000 to $3,500 each. "We feel this thermoelectrically-cooled amplifier represents a real technology breakthrough for an inexpensive low-noise preamplifier," says Janky. Parametric amplifiers were proposed by four other companies. While offering lower noise temperatures in the range of 85 to 175°K, they cost anywhere from three to four times as much.

"Another main reason we were able to meet regulatory requirements with the 15 ft. dish antennas was the use of threshold extension demodulators and compandors," Janky continues, referring to the SCPC channel equipment built by California Microwave, Sunnyvale, CA.

Threshold extension demodulators can achieve a satisfactory output signal-to-noise ratio with a 3 to 4 dB lower input carrier-to-noise ratio than is required for a prescribed level of demodulated threshold noise. It thus reduces either the required station G/T or the required satellite EIRP for a given signal-to-noise ratio.

"In both cases, system cost can be reduced," explains Janky. "The system channel capacity could also be increased with these techniques but that is not nearly as important a consideration for thin-route service as the ability to reduce system costs."

The use of compandors and pre-emphasis permits a further reduction in required downlink carrier power because these techniques permit a substantial reduction in required demodulated signal-to-noise ratio. Companding is a signal-processing technique which decreases the level of large amplitude signals and increases the level of small amplitude signals at the modulator input. The converse is accomplished at the receiving end. The subjective noise improvement occurs because of the way the listener perceives noise. The expandor at the receiver end effectively turns the amplitude to almost zero when no signal is present, thereby eliminating the thermal noise from the receiver system. When a signal is present, the noise is masked, so a net subjective improvement in signal-to-noise ratio occurs, the net improvement, on the order of 23 dB is obtained.

Noise weighting provides an additional 2 dB improvement. That is, to achieve a specified weighted audio output signal-to-noise ratio, such as 50 dB, it is now possible to operate with a deviation index such that the net fm improvement amounts to 15 dB in place of what normally would be calculated as 40 dB, if neither companding or pre-emphasis were used. This assumes a 10 dB carrier-to-noise ratio, explains Janky. ••

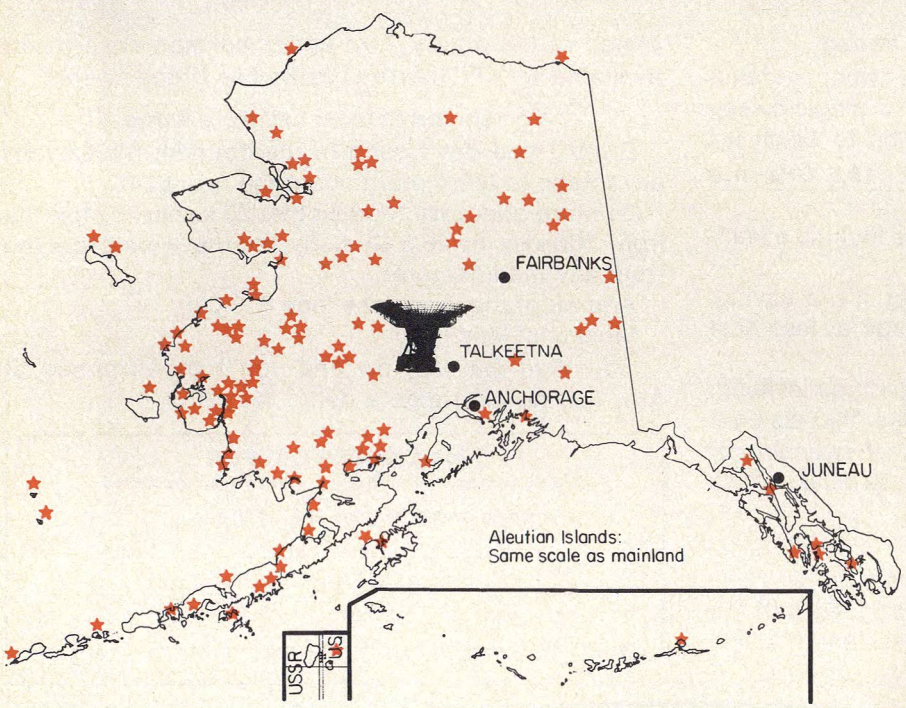

2. **Alaska's small earth station program** eventually will link up 140 remote communities scattered throughout the state and on the Aleutian chain. Early winter sites will be constructed first.

Electronic Warfare:

Military needs propel mini-RPVs into tactical flight tests

Richard T. Davis
Managing Editor

By using proven technology and readily-available equipment, the military services have thrust mini-RPVs to near operational status. Here's an update on the programs underway.

AN F-4D takes off in the first light of dawn. Under its wing, instead of its usual compliment of missiles and bombs, hang two launch pods, mounted on the two inboard pylons. No, these are not ECM pods for standoff jamming, but a miniature remotely piloted vehicle and its data link. Because the wings of the mini-RPV pivot atop the fuselage, it can be folded up and encapsulated in the pod for delivery to a target area.

As the plane heads towards a suspected enemy radar site, its route is closely followed on a console by pilots sitting in a blockhouse miles away. When within range of the target, a pilot at the console transmits a signal which frees the RPV pod from the starboard wing of the F-4. As the pod drops, a drogue chute slows its descent and soon jerks out a larger, main parachute. Reacting to the sudden deceleration, explosive bolts in the descending pod fire sequentially, splitting the pod in two to liberate the miniature aircraft. Still suspended by the main chute, the wings of the RPV rotate 90 degrees and the wing tips extend slightly before locking in place. After its piston engine is started, the main chute is separated, and the mini-RPV is soon flying under its own power towards the target area.

Now over the enemy installation, the electronically-loaded aircraft performs its vital mission—TV reconnaissance and laser target designation from an altitude of a few thousand feet. On the ground, the enemy is unaware of the RPV's encroachment, as their radars sweep right over its small, fiberglass fuselage.

Meanwhile, the F-4 that delivered the mini-RPV loiters a safe distance behind enemy defenses, relaying real-time video data to the blockhouse. Satisfied that the target is real, not merely a clever diversion, the console operators quickly plan an attack using manned aircraft. On directions from the blockhouse, the larger, armed aircraft swarm around the slowly circling mini-RPV, deliver their smart-bomb loads precisely on the designated target and get out fast. After patiently waiting for the smoke to clear, the tiny aircraft beams back its final pictures, to be used for bomb damage assessment. Mission completed, it crashes to the ground, having run out of fuel.

The above scenario is not just a concept but the goal of an actual Air Force program, called Acquare, that is presently undergoing flight tests at White Sands Missile Range, NM. It's typical of the major advances that have been made in the past few years by the military service to get mini-RPVs operational and into their inventory of weapon systems.

In fact, since the Dept. of Defense Advanced Research Projects Agency (ARPA) in Washington, DC, first started funding mini-RPV programs back in 1972-1973, mini-RPVs have progressed quite rapidly, considering the modest funding available. The main reasons for this are their low cost and the heavy reliance on using readily available components and equipments whenever possible.

"The stimulus for activities in the mini-RPV has been the opportunity to exploit advances in technology to provide lower-cost systems with unique capabilities," says Undersecretary of the Air Force, James W. Plummer. "The Air Force is minimizing the technological risk with RPVs by synthesizing the best equipment we have developed over the 10 years into a basic vehicle."

Close support to deep penetration

Defense officials believe mini-RPVs ranging in size from 60 to 120 lbs can be built in quantities of several thousand to sell for $10-20K each, including avionics payloads which represent about 70-80% of total vehicle costs.

All three services have programs under way, in the mini-RPV area, stimulated by backing by ARPA. While their missions differ, three basic areas seem most likely for the mini-RPV: reconnaissance, tar-

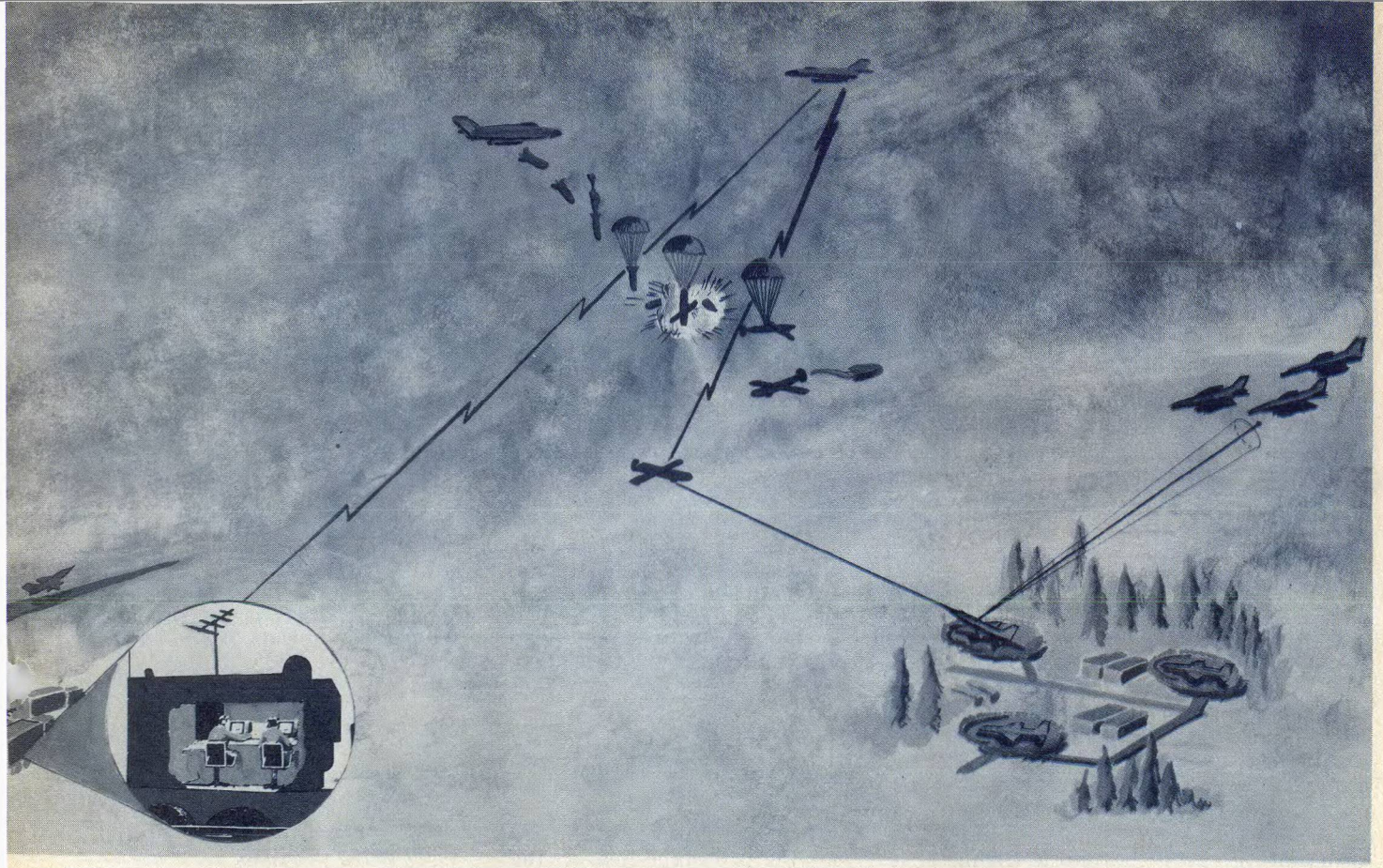

Typical scenario for the Air Force's Acquare program illustrates high-speed delivery of encapsulated mini-RPV stowed in a pod until it reaches target area. Upon command from RPV pilot at console, pod drops, releasing RPV to loiter over target area. Delivery aircraft serves to relay video data from mini-RPV to ground control up to 200 miles away. Once target is designated, attack aircraft can deliver laser-guided smart bombs into reflected laser beam or "basket."

get acquisition and designation, and to some extent, selective weapons delivery and electronic warfare. The availability of gimbaled sensor packages, weighing 10 to 20 lbs gross and all solid-state avionics now make these missions possible. Total avionics payloads can often be built weighing under 30 lbs.

The Air Force often has a need to deploy mini-RPVs well beyond FEBA as well as in short-range battlefield support roles. In deep penetration operations, it's important to get the RPV out over enemy territory promptly but once there it must be able to loiter at slow speeds for long times.

The Acquare program, under development by Lockheed Missiles and Space Corporation, Sunnyvale, CA, makes use of a high performance aircraft for delivery as well as to relay video data back to friendly lines, Fig. 1. As shown in Fig. 2, Acquare when encapsulated in a pod, can also be carried aloft and deployed from a ground-launched ballistic missile, such as the Sergeant as well as an aircraft.

The present tests at White Sands are to demonstrate target acquisition and designation at ranges of 150 to 200 n miles. For these tests, recovery of the vehicle is being made by parachute, which deploys when the engine is turned off.

Acquare's L-band airborne data link relay is, for the most part, an adaptation of solid-state

(continued on p. 36)

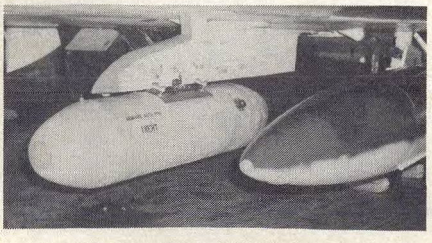

1. **Airborne data link relay pod for Acquare mini-RPV** is mounted on F-4D pylon. It is housed in fiberglass stores delivery pod. The L-band data link carries real-time video from the RPV to the ground station via the launching aircraft.

2. **Acquare mini-RPV, in stowed position** before loading in fiberglass pod, has its wings folded atop fuselage so it can fit. After it is dropped, explosive bolts release RPV from the pod and its wings pivot and lock in place for flight.

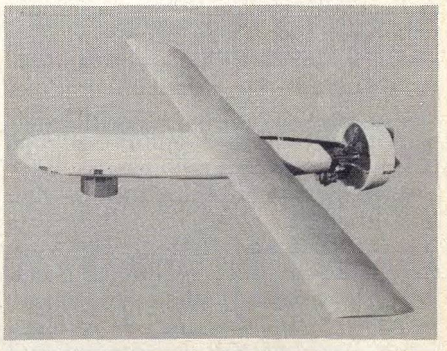

3. **Acquare mini-RPV weighs** 150 lbs and uses a 12 HP single cylinder Mc Cullough engine. Its payload includes a stabilized TV sensor plus laser designator derived from Aeronutronic Ford's Praerie II.

avionics items in current production or available from surplus inventory. To minimize jamming, only necessary commands, such as heading, altitude and airspeed are sent to the vehicle and certain mission instructions such as when to look and what mode to operate in. Command data, i.e., from the ground station to relay pod to RPV, operates at 500 MHz while the wideband video data from the mini-RPV to relay pod to ground control is at 1780 MHz. The vehicle, Fig. 3, uses separate omnidirectional stub antennas mounted on its skin for these links. It also uses the Philco-Ford (now Aeronutronic Ford) Prairie II payload, designed for laser target designation.[1]

The Navy is evaluating mini-RPVs for reconnaissance, targeting and surveillance in support of its surface fleet operations. Its current program with Teledyne-Ryan, San Diego, CA, called STAR (Ship Tactical Airborne RPV), is intended to expand the capability of its ships beyond the horizon by detecting anti-ship missiles, laser designating target beyond a firing ship's view or providing midcourse guidance signals for remotely launched vehicles. It also could support amphibious operations by handling real-time reconnaissance and target designation for guided projectiles. Other roles planned include relaying data from sonobuoy fields or even serving as a false target decoy or as a Kamikaze carrying a high-explosive warhead into radiating targets, such as radar.

Sea launch and recovery are unique problems to the Navy and are considered a major hurdle in verifying the feasibility of mini-RPVs. The Navy wants a dry recovery and not have to retrieve the RPV from the sea.

Aquila—the Army's program

The Army's mini-RPV program is basically motivated by a chronic problem that has persisted for decades; namely, a fast and accurate method for detecting and locating various targets. For this reason, operation of mini-RPVs is planned to eventually come under the artillery command rather than the aviation command. With its less demanding missions of close-in battlefield observation and target designation just "over-the-next-hill," the vehicles are relieved from many of the operational and deployment problems faced by the Air Force and Navy. As a result, the Army's major mini-RPV program, Aquila, (formerly called "Little R") is closest to an operational vehicle.

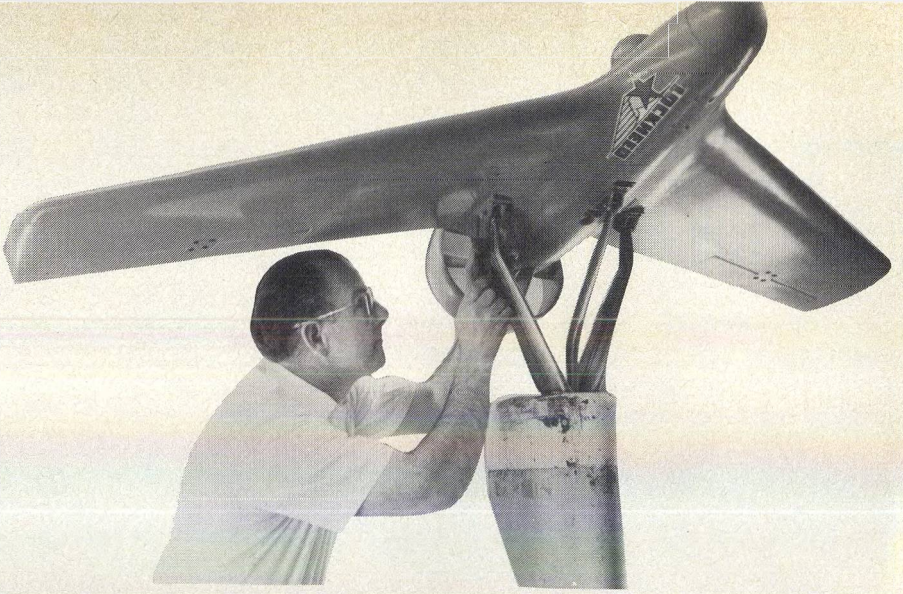

4. **Half-size model of Aquila mini-RPV** is shown here in wind-tunnel tests. The final delta wing version will be 6 ft. long with a wing span of 11.9 ft and total weight including payload will be 120 lbs. It's powered by a 14 HP Mc Cullough engine driving a ducted three-bladed propeller. It will travel at speeds of 38 to 118 kts. Ceiling is over 20,000 ft.

"The primary purpose of Aquila is to put the prototype gear in the hands of Army users and let them practice with it," says Lt. Col. Davies Powers, Army RPV Weapons System Manager at the Army's Aviation Systems Command, St. Louis, MO. Flight tests of a half-scale model have already been made, as shown by the sequence of photos on this month's cover. Testing a full-scale vehicle is expected to begin in the fall and continue into '76, first at Ft. Huachuca, AZ, and later at Fort Sill, OK, using 30 vehicles and four ground stations. From these tests, operational specifications will be derived, hopefully within 60 days of test completion.

"The Aquila program is putting together a more complete set of operational requirements than has ever been done before," claims Starr Colby, RPV-Systems Manager at Lockheed. This includes air frame, propulsion, sensors, avionics, command, control and data links, as well as launch and recovery techniques. To keep costs down and shorten the development cycle, Lockheed engineers have used available components wherever possible and conservative state-of-the-art designs when new packages such as flight control electronics were needed. Data link electronics and ground station equipments (with the exception of the receive antenna) is being built by Aacom, a subsidiary of Systron-Donner in Concord, CA. A narrowband 1 MHz uplink provides vehicle command and control while a 30 MHz downlink at approximately 4,800 MHz provides realtime video data and vehicle status.

According to Colby, the 30 vehicles will have five different interchangeable payloads providing the following mission capabilities:

- real time TV surveillance
- photo reconnaissance
- target acquisition
- target location and artillery adjustment
- laser target designation in support of terminally-guided weapons.

The mini-RPV, Fig. 4, along with its automatic pilot, flight control systems and sensors, weigh a total of 120 lbs. It is controlled by two operators situated in a port-

(continued on p. 38)

5. **Aquila program will use two operators** located in a portable shelter to control the vehicle. The RPVs progress is portayed automatically on an X-Y plotter that has a map behind it to help the operators follow the waypoint navigation.

able shelter, Fig. 5, which houses the system computer, TV displays, X-Y plotter and automatic tracking system. The vehicle is launched by a pneumatic tube launcher, Fig. 6, remotely from the ground-control station. The operators instruct the computer to send the RPV to or through specified waypoints and to have it loiter or conduct specified maneuvers and sensor activities at or between such waypoints.

"We set up the mission ahead of time with an X-Y plotter and map out its flight path," explains Colby. "We then type in digital inputs into the ground computer to set up certain marker points. The bird has enough 'smarts' in it to automatically take the waypoints in proper sequence and command itself to fly the specified sequence of legs."

"This handsoff operation eliminates a lot of potential enemy jamming problems as the vehicle flies to the target area," claims Colby.

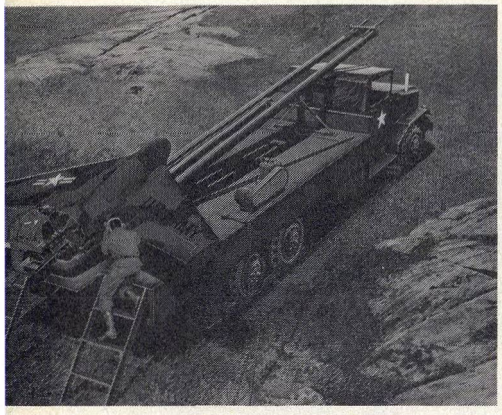

6. **Pneumatic tube launcher for Aquila mini-RPV** uses 300 psi air presser to launch vehicles at 0 to 20 degree elevation angles. The launcher is about 24 ft long and imparts a launch velocity of 44 kts.

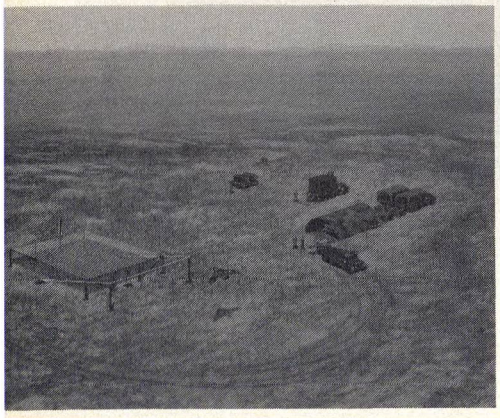

7. **Aquila is recovered by means of energy absorbers** attached to an arresting line and parallel strap retrieval net. Note hook hanging from vehicle for engaging the arrestor line.

As the RPV flies, an automatic csc² antenna tracks it, permitting the computer to display its coordinates on an X-Y plotter. "The csc² beam provides azimuth only information," explains Colby. "Range is derived from the data link and altitude, presented on an numeric display, is derived from a barometer in the vehicle itself. If there is any deviation from the planned and actual RPV positions, such as caused wind drifts, commands are sent to correct position."

The operators can command the RPV to change heading, air speed and altitude as well as to go into various search or loiter modes, to conduct specified sensor function, to measure target offsets and to laser designate targets.

The electronics in both the Aquila mini-RPV and its ground station are all solid-state, including the microwave transmitters. According to Roy Tanke, data link engineer for the program, the command data originating in the ground control station is converted to PCM, which is then put into a Barker code and further coded by phase-shift keying. The 100 MHz modulated signal is then upconverted to 1600 MHz in a mixer, put through a transistor power amplifier and then a frequency tripler, which delivers 10 W cw to the uplink antenna. The wide-beam uplink antenna is a small dish with 12 dB gain while the narrower-beam-receive-tracking-antenna provides 25 dB gain.

On the vehicle, two separate transmit/receive omni-antennas are used, providing 0 dB gain. "There is no preamplifier used in the RPV's receiver and front-end noise figure is about 8 dB." The command signal is downconverted in a double superhet which then goes to a PCM decommutator for controlling the various sensor payloads and autopilot.

"Video bandwidth from the TV camera is 4.5 MHz and the status information rides on a subcarrier of the video," explains Tanke.

The resultant bandwidth of the data downlink is about 30 MHz and output power from the RPV is 10 W. The same transmitter is used on the bird as in the ground-control station. The ground receiver does use a low-noise transistor preamplifier made by Amplica. It is mounted on the antenna pedestal and provides a 4 dB noise figure for the down-link receiver.

Range information is also extracted from the datalink because a master clock in the ground station synchronizes the command and telemetry data. The total airborne avionics package including PCM encoder and decoder is less than 6 lbs. "The present data link does not use spread-spectrum techniques, but the capability can be added," says Tanke. Video compression methods can also be eventually implemented but aren't in now. Tanke estimates a digital video compression module in Aquila would add about a pound to the vehicle's weight.

Five payloads planned

The various payloads are easily interchangeable depending on mission. The stabilized TV/laser designator package weighs about 30 lbs and it can fit in a 12-inch diameter enclosure. Alternate payloads can substitute a 35 mm panoramic camera for the laser. The simplest payload is an unstabilized TV camera which provides real time surveillance. It's capable of recognizing targets at a slant range of 0.6 miles. Another payload that is planned is real time TV surveillance plus photographic reconnaissance using a 35 mm panoramic camera. It will provide ground resolution of 1.6 ft at a 2,200 ft slant range. The target designation role uses a gyro-stabilized TV camera and laser and has an automatic tracking capability at a maximum rate of 10 degrees/second. The stabilized line-of-sight permits daytime detection of targets, such as tanks at slant ranges of 3.1 miles on roads and 1.6 miles in fields.

The payload for target location and artillery adjustment uses a stabilized TV camera and a laser rangefinder boresighted to the camera. It provides an accuracy of ±16 ft at a slant range of 1.9 miles.

The Honeywell designed optics payload includes a zoom lens on the TV camera. The laser, for range finding and designation, operates at a wavelength of 1.06 μm. It delivers 65 mjoules out of the dome and has a beam divergence of 0.5 mr. Pulse rates of 1, 10 or 20 pps can be selected. The direct-drive gimballed platform offers two degrees of freedom: 360 degrees in azimuth and 15 degrees in elevation.

Once the prescribed missions are accomplished, a semi-automatic retrieval procedure use can be implemented through the use of TV imagery. The RPV is guided down on a glide slope from its last waypoint and into a recovery window. A TV camera on the ground picks up the approaching RPV and dis-

plays it to the operator. Once on the display, a computer brings in the vehicle. As it nears the recovery area, Fig. 7, a hook on the RPV engages an arrester line and the forward energy of the vehicle is dissipated through two hydraulic energy absorbers. It then drops into the horizontal, parallel strap retrieval net where it is then removed and serviced for another flight. The system is designed for minimum damage at landing speeds of 35-40 kts.

Homing mini-RPV for attack

Although the Army is the closest to an operational vehicle, the Air Force has the biggest budget and and the most programs under way. The Air Force is examining RPVs in high and low-cost mix, compatible with modular payload changes.

The Tactical Air Command is evaluating miniature remotely-piloted vehicles to harrass hostile air defenses and draw missile and gun fire before launching manned aircraft strikes under its Harrassment Vehicle Program. In a typical scenario, a large number of vehicles would be used, either under remote or internal control. Some would be simple traffic decoys, others would have radar jammers and a few would be armed with a small explosive payload and capable of homing on defense radars or weapons. These tests, recently conducted at Eglin AFB, FL, indicate that proximity fuzed anti-aircraft shells fail to detonate because the mini-RPV doesn't return an adequate radar signal.

Melpar/Div. of E-Systems, Falls Church, VA, is actively working on an anti-radiation drone called Axillary, using their E-45 mini-RPV. This 40 lb vehicle, shown in Fig. 8, has a 75 inch wing span and carries as a payload a D/F receiver.

According to Edward Rose, Jr., Product Manager of Special Projects at Melpar, once in a target area, the vehicle goes into a loiter mode where it can stay aloft up to four hours, depending on location of the target from the launch site. When the target radar is turned on, the E-45 goes into an attack mode and rides in on a sidelobe. The monopulse radar receiver, Fig. 9, used for homing has a six arm D/F spiral antenna to provide azimuth and elevation information. Hybrid combiners are built into the antenna system to give sum and difference signals. The omni-antenna serves as a guard antenna for side-lobe blanking. It prevents the RPV from picking up the emitter on a backlobe of the six-arm spiral and homing in on a non-existent target.

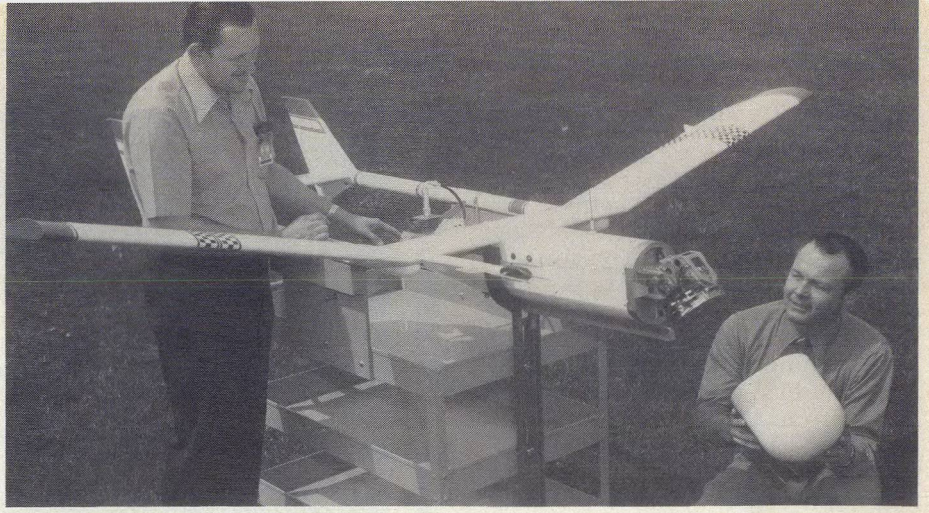

8. **Melpar's E-45 mini-RPV has a 95 inch wing span** and has a takeoff weight of 45 lbs. It uses a two HP, one cylinder engine and has an endurance of four to five hours. It's shown here with gimbaled TV reconnaissance camera in its nose but it has also been flight tested as a homing Kamakazi vehicle, with a D/F receiver as a payload.

The receiver has a dynamic range of 120 dB achieved by using switchable attenuators. A balanced mixer is used in front and the entire gimballed receiver is built on an alumina substrate. The D/F receiver is modular in design which allows its flexibility to cope with the various threat radars over a wide range of frequency. Under Axillary, Melpar ran tests for the Air Force about a year ago. The vehicle was sent out preprogrammed using its autopilot with the D/F receiver as a payload. The E-45 successfully dove at the target when it turned on, but it did not carry an explosive pay-

(continued on p. 40)

load and in these tests, a pilot pulled the vehicle out of its steep dive to avoid its destruction. Under a follow-on contract, Melpar has received an order for five additional vehicles in the E-45 class.

Melpar has also recently developed a larger, 120 lb vehicle, the E-100, using inhouse development funds. Both the E-100 and E-45 have an autopilot capability.

"It's a three-axis system," explains Rose, "and pretty simple and inexpensive." A potentiometer on the air stream serves as an angle of attack sensor which can be readily converted to air speed. Altitude is determined from an inexpensive (under $100) barometer pressure gauge originally designed to measure manifold pressure on cars. Heading is obtained from 2 rate-gyros, which read yaw and pitch and also provide short-term stability. A compass is also used as a heading sensor.

Three command signals are necessary to program the aircraft heading altitude and angle of attack (velocity). According to Rose, the autopilot which includes some on board microprocessor circuit boards, can be bought for about $2,000 or less in a packaged form.

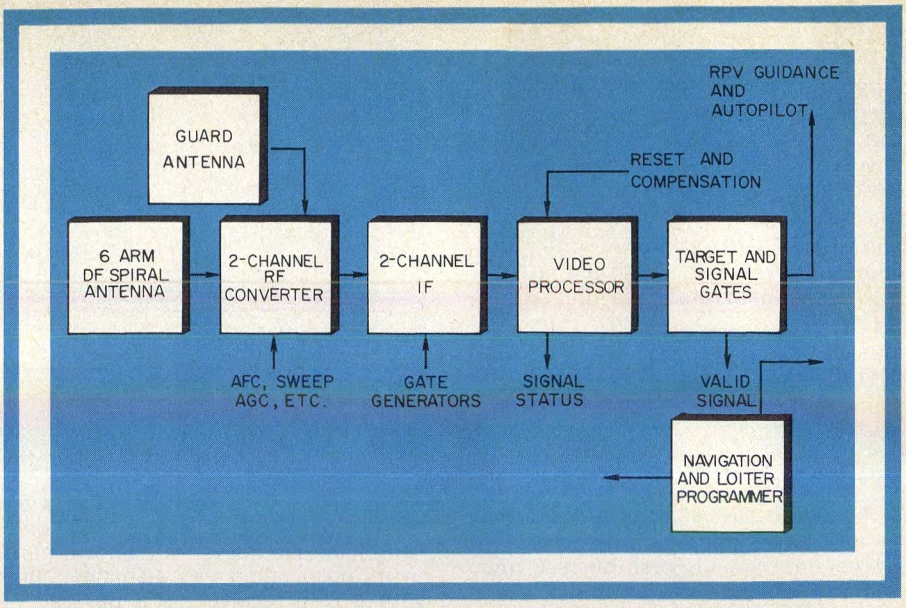

9. **Simplified diagram of Melpar's direction-finding receiver** shows A/J protection offered by guard antenna which serves as side lobe blanker. This monopulse receiver could be carried by an armed E-45 or E-100 mini-RPV, allowing than to home on defense radars. The packaged receiver weighs about seven lbs.

In volume, he predicts the autopilot will cost just a few hundred dollars each in 1,000 lot quantities.

"It's the D/F system that is the most expensive payload. That runs about $10,000," explains Rose.

The E-100 and E-45 can also be configured for a reconnaissance role using a gimballed TV camera or a modified commercial camera providing area search over ±90 degrees azimuth and 0 to 45 degrees elevation angle.

An Army version of the E-45 vehicle has also been developed and tested, Fig. 10. It has a command link as well as the autopilot commands. The Army seeks additional flexibility and wants to be able to change the error voltages from the nulling amplifiers to control the vehicle and its sensors when targets of opportunity arise. The Army version does not have the A/J protection. Vega Precision of Vienna, VA, built the C-band (5-GHz) command and control links for Melpar.

Mini-RPV's give ships better eyes

The Navy's interest with mini-RPVs is to expand the operational capability of some of its smaller surface ships, such as frigates and guided missile destroyers. The Navy considers mini-RPVs to be generally under 150 lbs, and plans to use larger remotely-piloted vehicles to support larger surface ships. The Navy is concerned with the threat of air and sea launched cruise missiles and, therefore, has interest in collecting radar and communications intelligence. By using passive ECM on RPVs it would be able to intercept, identify and locate hostile emitters while maintaining silence.

The Navy's mini-RPV program, STARS, uses a 120 lb vehicle such as shown by the model in Fig. 11. It is designed for shipboard launch and recovery and performs beyond the horizon reconnaissance and target laser designation. Although the program has been delayed by engine problems, the

delta wing mini-RPV is expected to begin initial land launch and recovery tests this fall. After the vehicle is tested at the Navy's El Centro, CA, facility, they will begin the more crucial sea tests. Here they will want to demonstrate launch into the wind and a net recovery on the deck.

New sensors development

In addition to these mini-RPV programs, there is also considerable activity, much of it sponsored by ARPA, in the development of new types of sensors. One program called HOWLES (Hostile Weapons Location Systems) is under way at Lincoln Labs in Lexington, MA, and involves looking at a wide variety of passive sensors such as radar homing, thermal imaging and spurious radiation sensing.

"Because mini-RPVs are designed to take a close-in look at a target and to stay under the cloud decks, which are so prevalent in certain theaters, it's important to make them as unobservable as possible," says Colby of Lockheed. This is one of the reasons for interest in passive sensors.

But small active radars are also being investigated. One program the Navy has with Raytheon involves adopting a low cost, X-band commercial marine radar for RPV use. These radars are presently built in large quantities for small boats and the modified version can be expected to be modest in cost.

"Millimeter radars are also being investigated for sensing although it does represent a tough design challenge," notes Colby of Lockheed. "While millimeter frequencies can afford the resolution to distinguish targets (such as an APC from a tank), the tradeoff lies in how much bandwidth you can afford to send home."

Some of the larger "midi" class of RPVs (over 150 lbs), are being looked at for carrying unattended-ground-sensors or "UGS," continues Colby. These sensors, for example, implanted by air drop from the RPV, would be capable of providing information on the number type, location, speed and heading of multiple vehicles in an enemy convoy or even the movements of infantry. Seismic or acoustic sensors are being considered and the sensor would transmit its intelligence via a low power (perhaps 1/4 W) data link using brief bursts to minimize detection and to conserve battery power. ••

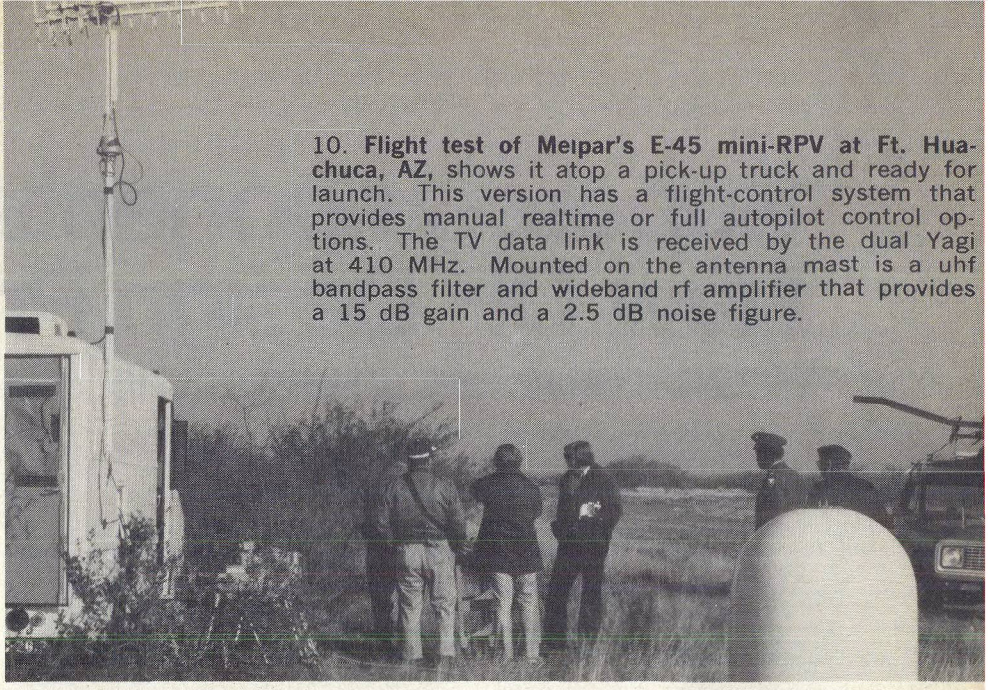

10. **Flight test of Meipar's E-45 mini-RPV at Ft. Huachuca, AZ,** shows it atop a pick-up truck and ready for launch. This version has a flight-control system that provides manual realtime or full autopilot control options. The TV data link is received by the dual Yagi at 410 MHz. Mounted on the antenna mast is a uhf bandpass filter and wideband rf amplifier that provides a 15 dB gain and a 2.5 dB noise figure.

11. **Subsonic delta wing mini-RPV developed by Teledyne-Ryan for Navy's STAR's** program weighs 120 lbs to 140 lbs depending on payload. It's wings measure 7 1/2 ft. from tip to tip. It's constructed of plastic foam for minimal radar cross section and ruggedness. It's designed to fly at altitudes from 100 ft to 10,000 ft carrying TV/laser designator payload weighing up to 50 lbs.

Supercomponents Solve New DF Design Problems

Here is the story behind two multioctave components, a multiplexer and a fast diode switch, designed to meet the need for improved rf signal discrimination and direction-finding accuracies.

MODERN electronic warfare receiving equipment has developed along certain specific lines generally due to economic as well as technical pressures. For threat-warning receivers, the simple low-cost crystal video receiver preceded by an rf multiplex filter defines a single channel of detection, capable of grouping threats into rf bands of interest.

The relatively low detection sensitivity for these receivers (usually about −40 dBm) reduces the number of signals to be handled and permits computer processing algorithms based upon pulse times of occurrances to be used to provide threat identification. As a result, a new generation of microprogrammed computer-based systems have evolved.

A problem, from a microwave view, presents itself when direction finding or DF measurements are to be made. Most systems use four broadband spiral antennas covering 2 to 18 GHz to provide an amplitude comparison monopulse capability. To permit accurate DF measurements, each of the four multiplexed channels must be balanced. The balance must also extend into the crossover region of the band separation filters. In the interest of maintaining low cost, four inexpensive front ends can be used for DF.

Microwave reconnaissance receivers generally use highly complicated and sophisticated front-end designs to provide higher sensitivities (usually about −80 dBm). These receivers are of necessity, narrow-band superheterodynes with all of the problems of achieving image and spurious signal rejection, frequency stability and accuracy. The single receive channel is costly. Where DF measurement is required, it is usually obtained by a rotating, highly directional antenna. When backlobe inhibition is required, a balanced two-channel system is often used, making total system cost prohibitive. These receivers are slow and can markedly reduce probability-of-intercept.

Recent re-evaluations of signal densities and environments, as an outgrowth of the Arab-Israeli conflict, has compounded the cost-versus-technical performance tradeoff for EW receivers. As a result, higher sensitivities and better DF accuracies are required. Essentially it is necessary to provide more and different signal discrimination at rf, pushing up single detection channel complexity and cost. Intercept probability, on the other hand, must be improved making rotating DF systems less suitable. On the whole, signal processing is more complex necessitating a greater percentage of cost to be allocated to the computer and software design.

Evolution of the supercomponent

These constraints on microwave receivers have led several ECM houses to a more fundamental re-evaluation of systems design. At the Electronic Systems Division of the General Instrument Corporation (ESD/GI), two major areas have been addressed over the past four years.

- Can the improvement of previously rejected components simplify the system's complexity?
- Can more be done by use of modern network analysis theory, improved componentry and better, more advanced design techniques?

In most of these cases, it has been found that one or more key elements or components can overcome certain limitations to achieve new system designs. Some of these new elements can best be classed as "supercomponents", or components that can, by their unusual properties, become the basis of systems that had been previously thought unattainable. For example, in the antenna area, new developments in the design of 180-degree 3 dB hybrids has resulted in units capable of tracking within ±0.5 dB over the 8 to 18 GHz band with isolation of 17 to 25 dB and with phase tracking of ±4-degrees. This work has led to the design of antenna correlation feed networks capable of significantly improving antenna accuracies.

Another example is 2 to 18 GHz slow switches (switching times greater than 100 nsec) that can be tracked to better than ±0.5 dB. These components permit new high sensitivity synchronous techniques to be applied to wide open front ends.

New designs for D/F

The requirement for direction finding in a complex system that makes use of time sharing of a single channel between four or more DF antenna inputs is an attractive possibility. Two types of sharing can be used. The first, subcommutation, simply sequences a single receive channel to each of the inputs at a slow rate. This is usually done on a pulse-by-pulse basis for radar intercepts or over a long time period for cw signals. The chief difficulty in the use of this technique is the requirement for single-signal reception. For the pulse case, it is necessary to deinterleave multiple signals in real time, to be sure that only the desired pulse of the train is being measured (time coincident pulses might come from other azimuths).

(continued on p. 44)

Stephen E. Lipsky, Director of Advanced Systems Engineering, General Instrument Corporation, Electronic Systems Division, Hicksville, NY 11802.

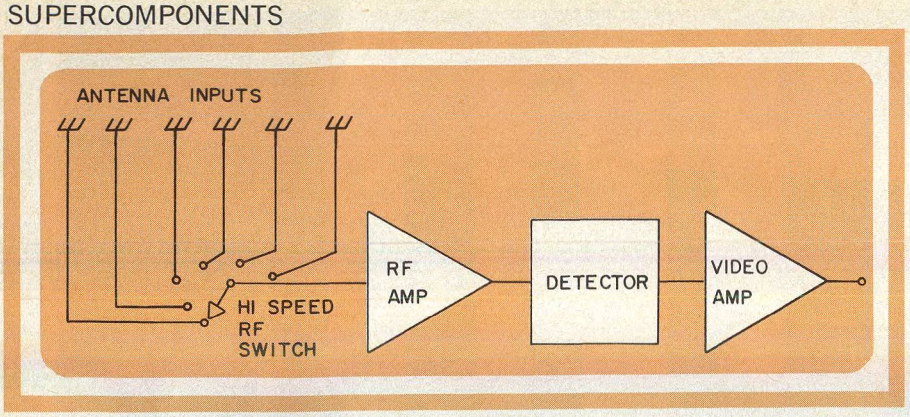

1. **Supercommutation can be achieved with this high speed multiarm rf switch** time which multiplexes the antenna inputs into a single channel. This means only a single RF amplifier is required.

For cw, only the desired signal should be used, generally requiring narrow-band of filtering. Subcommutation as a technique can make use of statistical sorting to ultimately determine signal azimuths, however, in new high density environments, overall signal intercept probability suffers drastically.

An expansion on the idea of switching leads to the concept of supercommutation or high-speed multiplexing during the analysis interval, typically a pulse width for a radar intercept signal, as shown in Fig. 1. A single high speed multiple throw switch capable of switching to each of the antenna outputs within the duration of a pulse width, effectively time multiplexes the DF information into a single channel, necessitating the use of only a single rf gain device to provide amplification.

Supercommutation provides many significant advantages; the gain is balanced for each of the DF outputs, eliminating errors that would occur for unbalanced parallel channels, the single rf channel reduces system cost dramatically, the use of high-speed switching allows the whole DF determination process to be performed on a single rf pulse.

The supercommutation technique of necessity leads to the requirement of a supercomponent, i.e., the basic rf switch. It might be more appropriate to call it "switch and driver" since it is impossible to separate these functions in any practical application. The development of this component, and the associated decommutation technology has played an important part in the development of future EW systems.

Multiplexers

The design of multiplex front-end filters represents another supercomponent. In previous years, front-end assemblies were designed as air-dielectric type coaxial filters. While these designs were often satisfactory from a performance viewpoint, they were highly expensive. In many cases, each filter would be tuned by many slugs or setscrews with the usual problem being interaction between adjustments. The advent of sweep measurement technology presented a new dimension to the problem since it was now possible to find previously undisclosed "holes" in the response and VSWR curves.

A new and fundamentally low-cost approach is to build a multiplexer using stripline and printed circuit techniques to achieve the critical balance and matching characteristics. It was important to develop the unit so that it could be placed into production without the need for any tuning screws or adjustments of any sort.

Figure 2 shows the type of multiplexer design that can be configured in accordance with the above rules. The basic 2 to 18 GHz band is divided into four outputs by a set of two modules, a high and a low-band unit. Low and high-pass filters permit the use of pseudo-complementary pairs to place signal variation responses in the stop bands of other filters and to provide a low VSWR throughout the bands of interest. These factors are important since any VSWR ripple would appear as serious unbalance between sets of multiplexers used in DF applications.

The overall objective of low cost is satisfied by the printed circuit type of construction and complete absence of any adjustments. The two module design is responsive to packaging as well as the technical requirements. The low-band module is constructed in a two-layer sandwich in which circuitry is printed over its associated ground plane with a second ground-plane-only card covering it. The high-band module uses a coplanar two-sided printed circuit mounted between two ground plane cards.

Switch development

A single-pole four throw-switch was designed to meet the general requirements of Table 1. The initial concept called for a single

(continued on p. 46)

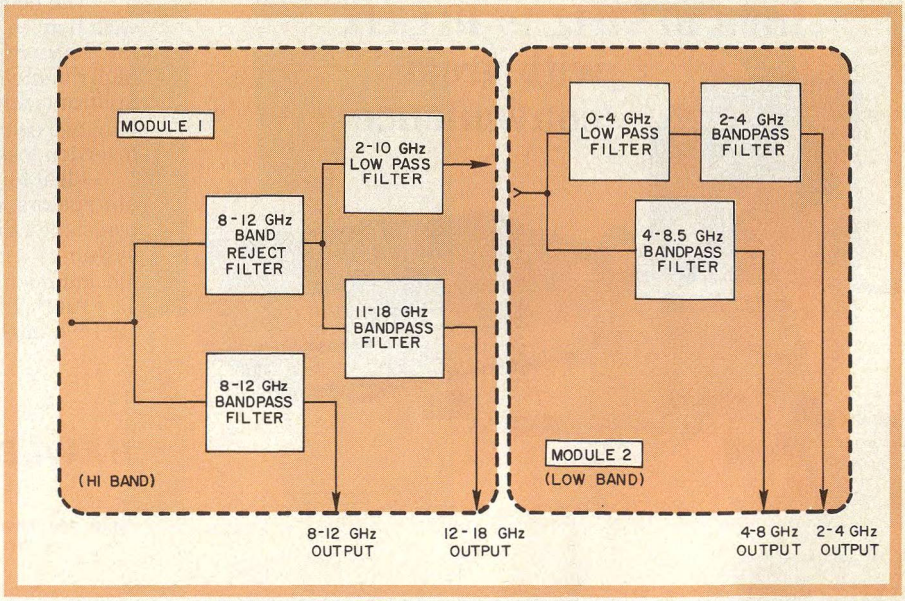

2. **A low-cost, all-stripline rf multiplexer** accepts the wide band input from switch. Module 1 is a low-band plexer, and module 2 is the highband unit.

Table 1. Rf Switch

Performance Specification	Design Objective	Minimum
1. Switching Time (nsec)	1.0	2.5
2. Frequency Range (GHz)	2-20	8-18
3. Insertion Loss (dB)	1.5	3.5
4. Isolation (dB)	30	25
5. Balance (dB)	±0.15	±0.5
6. VSWR	1.1	1.25
7. Number of Poles	8	4

series diode switch element in each of the four arms to provide high broadband isolation. This most readily permits the use of low capacitance diodes which are abundantly available. After some study and prototype modeling, it became apparent that although fast switching on-times could be achieved, storage effects prevent fast off-times. As a result, the design was recast as a shunt-diode switch.

Figure 3 shows the resulting SP4T switch design. As shown, the actual microstrip circuit is pentagonal. A center junction is constructed in 16-ohm line. Each of the four ports is fed to the junction by a 50-ohm line.

The switching action is accomplished by a single shunt diode in each of the four lines. The diode, which is mounted $\lambda/4$ away from the center junction is grounded at one end and beam-lead fed at the other. Two isolating capacitors and and a choke feed permit the drive signal to bias the diode on or off. In the on-condition, the diode appears as a short to ground, $\lambda/4$ away from the center junction. This stub makes the short appear as an open circuit effectively placing the switched arm out of the microwave path and no signal flows. The impedance transformation and parallel loading of the three stubs at the junction dictate the use of a 16-ohm transmission line at this point as shown.

When the diode is biased off, the path from any input to the center is completed and signal flows. The blocking capacitors serve to provide switch isolation and permit the drive signal to couple through the diode. A specially-designed choke isolates the rf energy from the switching signal in the band (8 to 18 GHz) of interest. The 50-ohm input line is matched to the 16-ohm center line after the choke connection as shown.

The diodes selected for the switch are Pin Mesa chip types. The cathode of the diode is conductive epoxy bonded to one side of the circuit. A 7/10 MIL wire is bonded to the 1 mil dot anode of the diode to form the series inductive portion of the transformer. In actual practice, this wire is fastened to a diode that has a greater than desired capacity and physical size. The diode is then etched to final values. This method is preferable to direct bonding which, at best, results in a 2 out of 50 yield rate. The diode is finally passivated to retain its characteristics. Following these techniques results in a diode that exhibits a shunt capacitance of less than 0.2 picofarad.

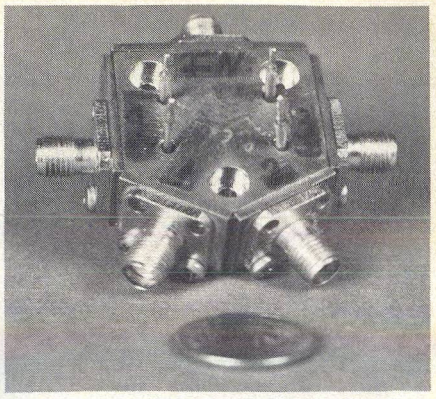

4. **Packaged microstrip rf switch** is SPT4. It uses PIN mesa chip diodes which exhibit a shunt capacitance of less than 0.2 pF.

It is necessary to consider all elements of the circuit if high switching speeds are to be achieved. Special attention to the blocking capacitances and choke feed are essential if a practical driver circuit is to be designed. It is necessary for the driver to sweep out all charge in both the diodes and the series blocking capacitors within a two nanosecond period to achieve the required transitional speeds. Considerable experimentation was necessary before a final acceptable configuration was achieved.

The finished single pole four-throw switch, Fig. 4, has a switching speed less than 2.5 nanoseconds. The switching characteristics, Fig. 5, are measured with an rf reflectometer oscilloscope at 18 GHz. The switch turns

(continued on p. 48)

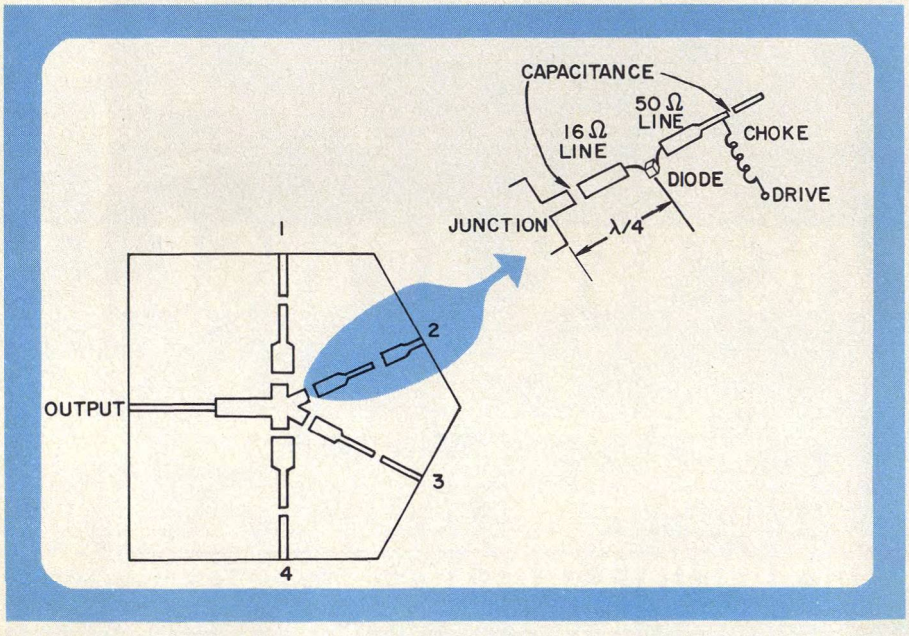

3. **Microstrip switch** operates from 8 to 18 GHz and switches in under 2.5 ns using PIN diodes in chip form. Signal and drive paths are shown.

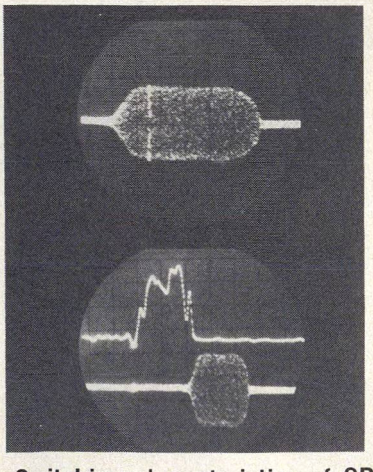

5. **Switching characteristics of SP4T switch,** at 18 GHz shows the switch turning on in 2 ns, staying on for 7 ns and turning off in 2 ns. (a) shows drive current level with scope calibrated at 5ns/cm and (b) has a 2ns/cm scale.

on in two nanoseconds, stays on for seven nanoseconds and turns off in two nanoseconds. Note the preshaped current drive pulse that actuates the switch.

The switch exhibits an insertion loss of approximately 5 dB, a balance from worst-to-best arm of ±0.5 dB to approximately 15 GHz. Isolation is approximately 25 dB over the 8 to 18 GHz range providing an on-to-off switching ratio of approximately 20 dB.

Further improvements in the switch are possible by reducing the size and by making use of better diodes as they become available. The isolation can be increased by 15 to 20 dB by use of a second shunt diode at the expense of a small increase in insertion loss.

The development of the switch has permitted the design of a full supercommutated receiver operational over a 2-18 GHz frequency range. The basic theory of the supercommutation approach has been verified at ESD/GI, permitting the design of a new generation of low-cost EW equipment.

Multiplexer development

Specifications for the stripline rf multiplexer in Fig. 2 are presented in Table 2. The resulting design, Fig. 6 consists of two modules, shown in Figs. 7 and 8.

Each module of the multiplexer follows the pseudo-complementary filter pair approach. The 8 to 18 GHz high-band unit has a bandpass filter (shown along the bottom edge of the top card of Fig. 7), constructed of half-wave resonators, quarter-wave coupled. The light (40%) coupling is obtained by overlap coupling from one side of the board to the other as shown with the bottom board.

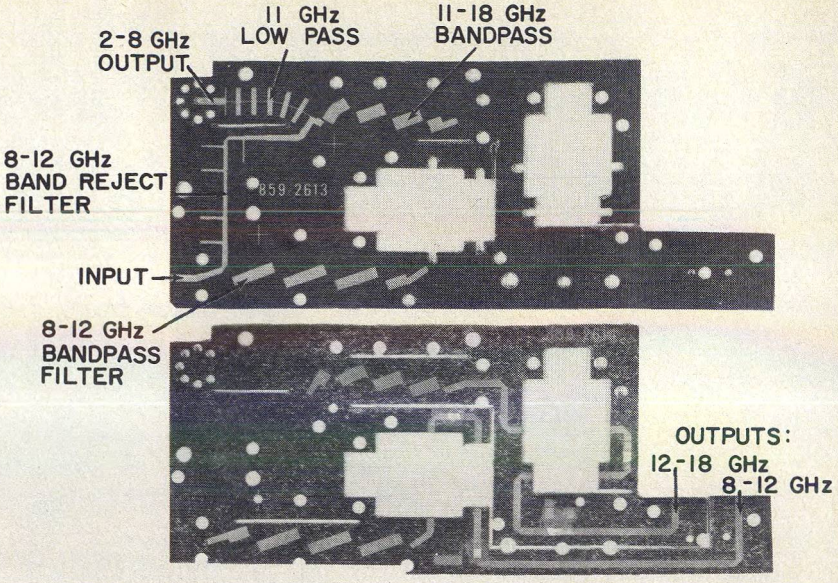

7. **High band module for stripline multiplexer** receives inputs from 8 to 18 GHz. It uses halfwave resonators for separating out the signals as shown.

The band-reject filter shown from the bottom edge to the top uses the stub spaced λ/4 apart. The output of this filter feeds a 2 to 18 GHz low-pass filter (to left corner) and an 11 to 18 bandpass filter. As shown in Fig. 2, the energy is channeled into detectors from 8 to 12 and 12 to 18 GHz and into the low-band module for band division and detection. Since overlap coupling is required, the high-band module is constructed of a double-sided PC center board sandwiched between two ground plane PC cover plate (not shown). Duroid 5880 dielectric is used throughout.

The low-band module, Fig. 9, covering 2 to 8 GHz, uses printed interdigital bandpass filters in place of the λ/4 resonators resulting in a considerable saving in size. The design of these filters posed an interesting problem. Since octave band coverage is required, the dimensional spacing between the resonators is close, negating the usual assumption that the coupling from one resonator past its neighbor to another is negligible. As a result, special computer programs had to be written to solve the more complex coupling case. The required grounding of the interdigital lines also presented a manufacturing problem since manual grounding

(continued on p. 51)

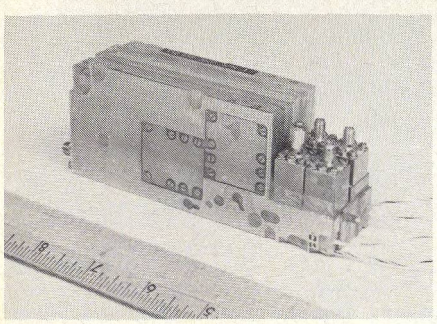

6. **Overall view of complete 2-18 GHz four band multiplexer** features detectors with field replaceable diodes.

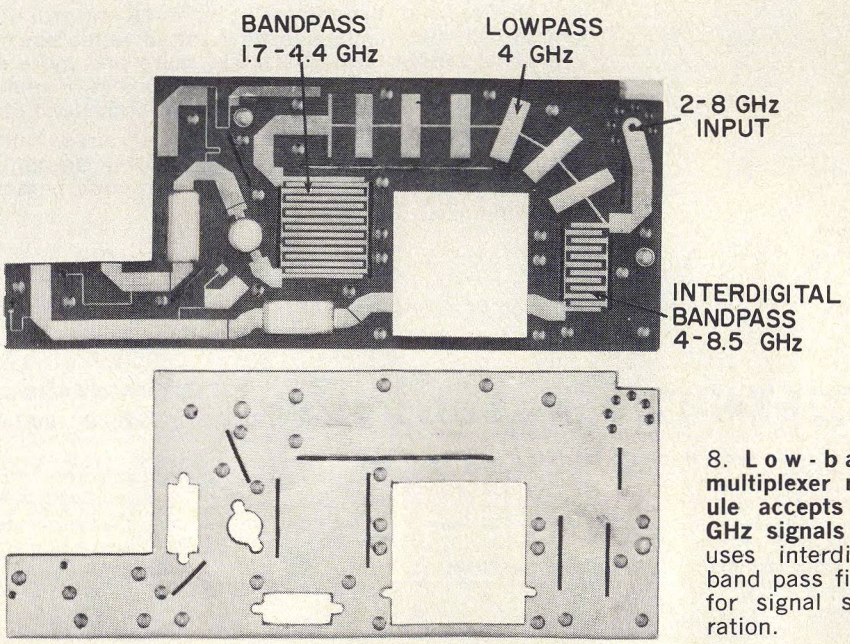

8. **Low-band multiplexer module accepts 2-8 GHz signals** and uses interdigital band pass filters for signal separation.

Table 2. Multiplexer

Performance Specification	Design Objective	Minimum
1. Frequency Coverage (GHz)	2-18 GHz in four bands: 2-4, 4-8, 8-12, 12-18	2-18 GHz in four bands: 2-4, 4-8, 8-12, 12-18
2. Crossover Accuracy (%)	2	3
3. Out-of-Band Rejection (dB)	> 55	> 51
4. Insertion Loss (passband) (dB)	4	6
5. Unit-to-Unit Track typical at 25° ±5°C (dB peak)	3	2
6. Input VSWR	2.5	3.5

by soldering a feedthrough foil from the ground plane side of the card is time consuming. This latter problem has recently been solved by identification of two vendors who have perfected the technique of "plating through" teflon glass (Duroid) PC materials. One such vendor is Soladyne in San Diego. The 0 to 4 GHz low-pass filter which is series connected with the interdigital bandpass filter provides the 2 to 4 GHz output which is purposely restricted to prevent out-of-band signals from being detected. The 4 to 8 GHz output is detected directly at the output of the 4 to 8.5 GHz bandpass filter.

Isolators are used to terminate the three high-band outputs. These are expensive but necessary devices since the relatively high VSWR of even the best Schottky diode detector can create in-band perturbations. The 2 to 4 GHz output is padded prior to detection due to the size of an isolator in this range, and the available higher sensitivity, which can be traded off. Test data shows that unit-to-unit match of better than 0.5 dB can be attained. Crossover frequency stability is better than 1% permitting the crossover slope to be used as a coarse frequency discrimination. ••

Acknowledgement

Thanks are extended to David Kraker and his group, who developed the components described in this article.

Test Your Retention

1. What is supercommutation?
2. Why are special design techniques required for octave-band printed circuit interdigital filters?
3. Why must isolators or padding be used to terminate the detected ports of the multiplexer?
4. What technique is used to ground the printed circuit interdigital filters?

Noise Jamming of Long Range Search Radars

Jammer noise usually exceeds the receiver front-end noise by many tens of dB. Of the various ECCM techniques to combat standoff noise jamming, very low sidelobes are the most effective.

THE simplest technique for an attacking aircraft to defeat enemy search radars consists in transmitting broadband noise or barrage jamming over the known radar bands.

There is a popular misconception that it should be possible to defeat noise jamming by some processing technique that "pulls the signal out of the noise." The fact is that not only is this impossible to do directly, but indirect methods are powerless when the extent of the gap between the jammer capabilities and the radar sensitivity is realized. Such ECCM techniques, as CFAR for example, are of no use in this situation. Other measures such as frequency agility, sweep-to-sweep correlation and burnthrough are not sufficiently powerful to cope with the problem.

Only spatial discrimination obtainable by using antennas with very low sidelobes is effective. A radar with very low sidelobes will at least make it possible to:

- Detect quiet targets outside the direction of the jammer.
- Obtain good azimuth data on the jammer to help locate it by triangulation.

Any form of active jamming, however, presents certain disadvantages. In particular, the presence of the jammer is revealed so that it can be engaged by passive homing missiles. Basic tactic consists, therefore, in fitting specialized aircraft with suitable jammers and "standing-off" while "quiet" strike aircraft come in under cover of the jamming. Several of these stand-off jammers can effectively wipe out all long range search radars within range.

The graphs in Figs 1-4 show the relation between skin returns and jamming levels in a typical radar receiver, for various ranges and sidelobe levels. The effects of a noise jammer (stand-off or otherwise) on long range search radars can easily be estimated. The figures show that a radar with very low sidelobes is very effective in countering standoff jamming but one with less than 20dB sidelobes can easily be rendered useless.

Jammer noise vs. front-end receiver noise

The overwhelming factor in the ECM jammer vs. radar electronic-counter-countermeasures (ECCM) game is the tremendous disparity between the energy contained in the desired radar signal reflected off the target. The received jammer power at the front end of a radar receiver is:

$$J = \frac{P_j\, G_j\, (B_r/B_j)}{4\pi\, R_j^2} \cdot A \cdot \frac{1}{L_r} \qquad (1)$$

where: P_j = Jammer transmitted power
G_j = Jammer antenna gain in the direction of the radar
B_r = Radar bandwidth
B_j = Jammer bandwidth ($B_j > B_r$)
L_r = Losses in receiving system up to front end
A = Effective antenna area = $G_r \cdot \lambda^2/4\pi$
G_r = Radar antenna receive gain
λ = Wavelength
R_j = Range of jammer

(continued on p. 54)

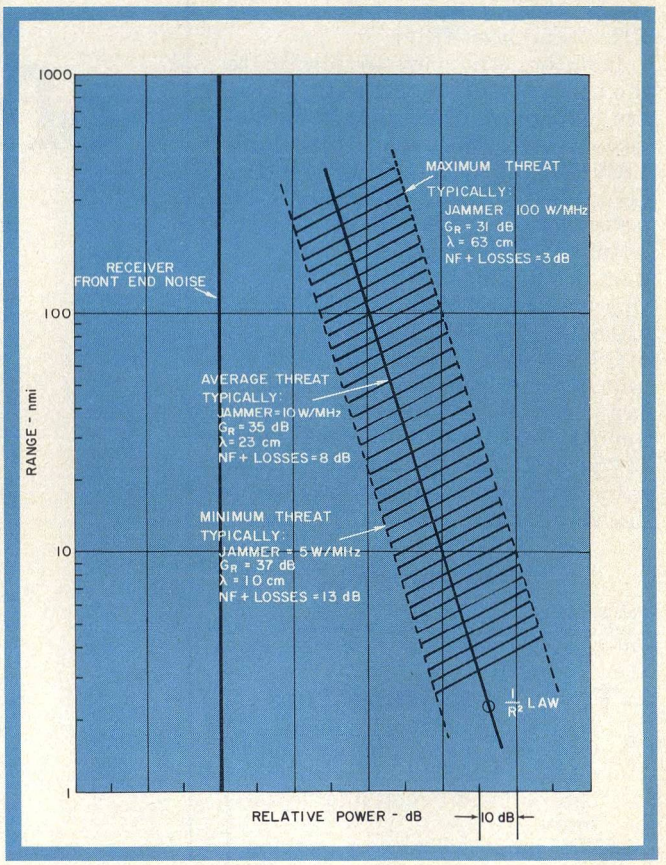

1. **The average J/N power ratios for practical search radars** show effects of various threats. In any "reasonable" situation, the jammer noise in the receiver will exceed the front-end noise by at least 20 dB and more usually by 50 dB.

Peter R. Dax, Advisory Engineer, Westinghouse Electric Corporation, P. O. Box 1897, Baltimore, MD 21203.

NOISE JAMMING

For a typical L-band radar where $\lambda = 23$ cm, G_r might be 34 dB. Hence, A = 10 dB relative to 1 m^2 = 10 m^2. For practical reasons, the effective area of 90% of all land-based search radars fall within ±5 dB of this figure. This amounts to saying that 90% of all landbased search radars have effective antenna areas between 3 m^2 and 30 m^2. (A typical S-band search radar might have $G_r = 39$ dB and $\lambda = 10$ cm, hence A = 8 dB relative to 1 m^2.)

Since the front-end receiver noise is:

$$N = KTB_r \cdot NF \qquad (2)$$

where: K = Boltzmann's constant
T = Temperature (°K)
NF = Receiver Noise Figure

Then the ratio of jammer power to receiver front-end noise power is,

$$\frac{J}{N} = \left[\frac{P_j G_j}{B_j}\right] \cdot \frac{A}{4\pi R_j^2 \cdot L_r} \cdot \frac{1}{KT \cdot NF} \qquad (3)$$

Assuming a modest 500 W of transmitted noise power over 200 MHz bandwidth with an antenna with 6 dB gain:

$$\frac{P_j G_j}{B_j} = 10 \text{ Watts/MHz}$$

If NF × L_r (in dB) = 8 dB typically and if A = 10 dB relative to 1 m^2 then, at 200 nmi range:

J/N = −50 dB (rel. to 1 W/MHz) + 10 dB (A, rel. to 1 m^2)
−11 dB (4π) − 2 × 55.7 dB (R, rel. to 1 m)
+204 dB (KT) − 8 dB (NF × L_r) = 33.5 dB

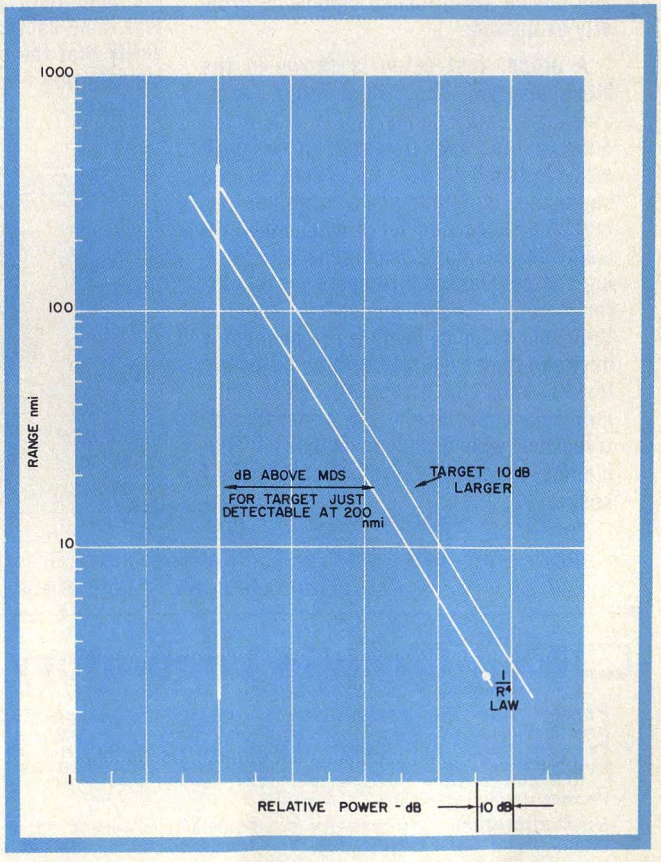

2. **Signal levels for a 200 mile radar** show $1/R^4$ relationship between actual target and mini detectable signal.

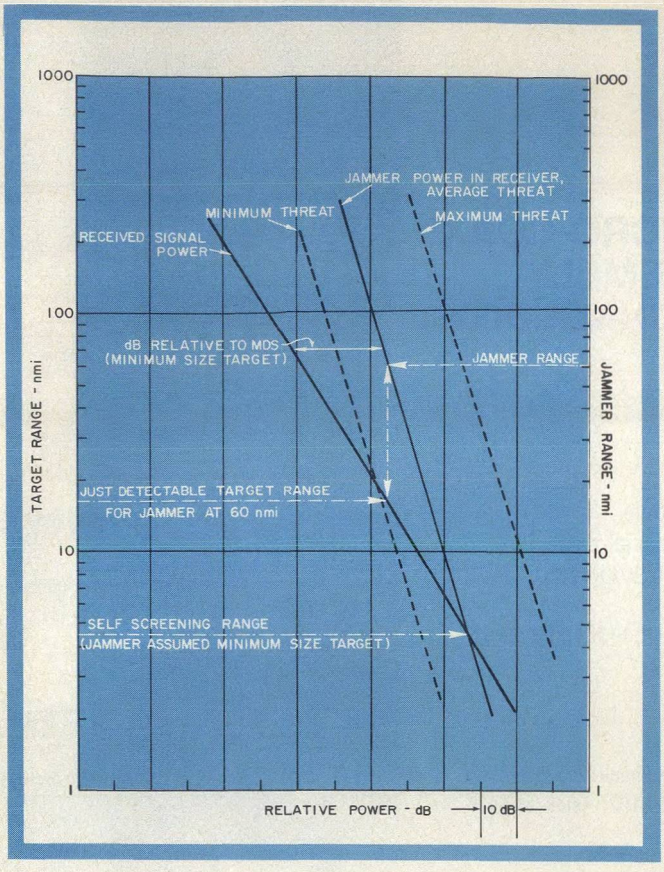

3. **Average S/N power ratio for a practical search radar** shows how it is very easy for any reasonable jammer to deny range information from any search radar on any target when the target is in the main beam simultaneously with the jammer. The self-screening range for such a jammer is only a few miles.

This relationship between J/N and range is shown in Fig. 1 with the slope of the jammer power line following a $1/R^2$ law. At 100 nmi, this ratio, J/N = 60 dB, a very high number indeed.

The numbers quoted for A and (NF × L_r) are typical. If A is at the upper limit of its practical range (5 dB higher), while (NF × L_r) is 5 dB lower and if the jammer can generate 5 kW of noise instead of 500 W over 200 MHz, then the line shown is displaced 20 dB over to the right. Conversely, a minimum threat can be represented by a line 13 dB to the left (A = 4 m^2 — 5 dB smaller than the average and P_j = 250 W). Thus almost any situation encountered in practice will result in a J/N ratio that will correspond to the distance between the receiver front end and some point in the cross hatched area of Fig. 1. Note that all the points in the cross hatched area lie many dB to the right of the receiver front-end noise line.

Signal power vs. jammer power

If the radar is designed to detect a certain size target at, say 200 nmi, the relationship between actual target signal and the minimum detectable signal (MDS) as a function of range can be represented by Fig. 2 where the sloping line follows an $1/R^4$ law. If the target is 10 dB larger, then the sloping line is displaced 10 dB over to the right as shown.

In the presence of a noise jammer covering the instantaneous bandwidth of the radar, the front-end noise can be ignored and Figs. 1 and 2 can be combined to produce Fig. 3 from which the target signal

(continued on p. 56)

NOISE JAMMING

in dB relative to MDS can be determined, given the relative ranges of jammer and targt.

Thus in the previous example, a 10 watts/MHz standoff jammer at 60 nmi will screen a minium size target into 16 nmi. It can also screen itself (assuming it has the same cross section) into 5 nmi. **Both ranges quoted are operationally useless for a search radar.**

Jammer in the sidelobes

A standoff jammer attempts to hide quiet targets by generating enough noise to swamp the skin returns from the quiet target even if the jammer is in the sidelobes of the radar Fig. 4. Fig. 5, shows various jammer power levels plotted for various sidelobe levels. Typically, in the maximum threat situation, a standoff jammer at 100 nmi will reduce the range performance of a 20 dB sidelobe radar to a tenth of its normal maximum range.

With 60 dB sidelobes, however, it is impossible for the jammer to hide a quiet target that is closer to the radar than itself. In the average threat case, a 40 dB sidelobe level is sufficient to make standoff jamming impossible.

With 29 dB sidelobes, the jammer's noise will be in evidence on virtually all azimuths. Very wide dynamic range will be necessary to detect the jammer azimuth even with only a single jammer present. With several jammers, it will be almost impossible to determine the true jammer azimuths.

Thus, without at least 40 dB sidelobe levels, a jammer will obscure quiet targets on azimuths different from its own azimuth and will prevent clear-cut bearings being obtained, hence making triangulation impossible.

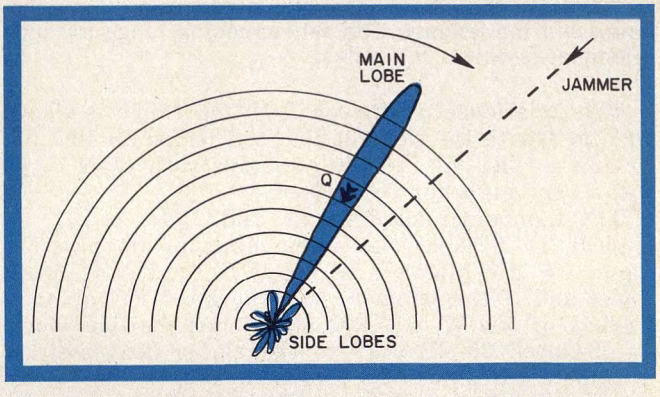

4. **Very low sidelobes** are the most effective way to combat standoff jamming. Usually sufficient noise from a jammer can enter the sidelobes to swamp the Skin returns from a quiet target, Q, in the main beam.

How effective are the ECCM techniques?

The principal electronic defenses (or ECCM) available to the radar are frequency agility and space discrimination. If the radar can change frequency on each transmitted pulse, then the jammer must dilute his effort by spreading his available power over the whole range of possible radar frequencies. Unfortunately, the total frequency range rarely exceeds 5% each side of center frequency, and the best that the radar can do is to force the jammer to dilute its power by two orders of magnitude or so. This represents a 20dB improvement over a tailored narrow band jammer. This is such common practice however that in the examples cited earlier, it is already assumed that the jammer is a broad band barrage jammer. It is possible, however, that the jammer may have holes in its coverage

(continued on p. 58)

so that "intelligent" frequency agility may yield substantial advantages by enabling the radar to utilize only those frequencies at which the jammer power is at a minimum.

Space discrimination is a matter of filtering out the jammer energy on the basis of antenna gain in the required direction vs. antenna gain in the jammer's direction. When looking for target data in the jammer's direction (i.e., on the jammer azimuth), no space discrimination can be made, of course, but it is important to prevent a jammer from denying target information over all azimuths and all altitudes.

The ability to reject jammer signals by space discrimination is limited by the sidelobe levels of the antennas. Unfortunately, the blocking of the aperture by the feed, spillage and distribution limitations in a conventional feed/reflector antenna system makes it impossible to achieve better than 20 to 30 dB sidelobe levels. This is a long way off from the 60 dB levels required to be really effective.

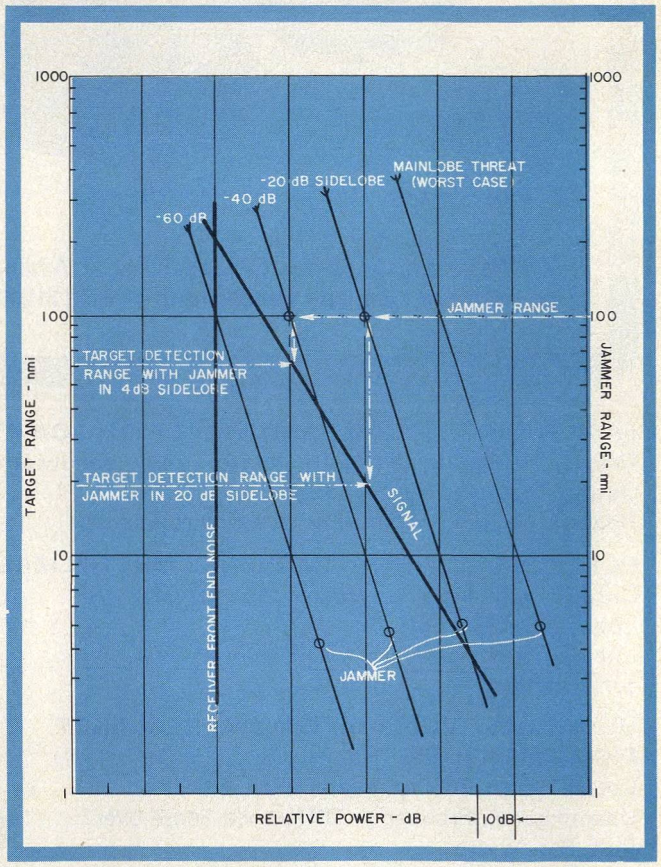

5. **Target detection ranges** with a jammer in the side lobes shows improvement in MDS with lower sidelobes.

One possible alternative is the array antenna. Even in this case, very careful design is necessary both to provide the required phase and amplitude distributions and to achieve the necessary mechanical accuracies. (In addition, a physically larger antenna is required for a given beamwidth: the penalty between theoretical 40 dB sidelobes and 60 dB sidelobes may be 30% in aperture size.) The slotted waveguide array design used in the AWACS lends itself to achieving such goals.

Possibility of further improvements

Once full advantage has been taken of space and frequency discrimination, only second order improve-

Authors: Plan ahead for '76

The themes that will appear in next year's issues of MicroWaves will cover the following topics. Prospective authors who wish to write technical articles pertaining to these subjects are urged to submit outlines at least three to four months prior to the publication date.

January

Front Ends

February

Semiconductors

March

Millimeter Waves

April

ECM I

May

Passive Components

June

Test & Measurements

July

Communications

August

Sources

September

ECM II

October

Amplifiers

November

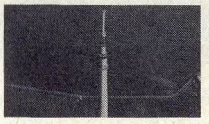

International

December

To Be Announced

ments can be achieved thereafter. As has been shown, the ultimate capability of the radar is a function of the ratio of signal energy to noise energy in the optimum passband (tailored for the radar pulse). Effective signal energy can be increased by integration over a beamwidth, i.e. by integrating the skin returns from a target as the antenna sweeps through its azimuth. If necessary, the antenna can be stopped in the suspected direction of the target and the signal energy integrated over a much longer period. This process is known as burnthrough.

Any processing of this nature (correlation, integration) cannot however achieve more than could be achieved if all the energy in the (n) pulses being integrated was concentrated in a single pulse. In theory, this would give a maximum improvement of (n). However, in practice with non-perfect integration, the improvement is closer to $\sqrt{n}$. For ten hits on target per beamwidth for instance, a gain of 5 dB would be achieved. Even if a 10 dB improvement were possible, this is still a small number when compared to the excess power that the jammer has over the receiver front-end-noise.

In dealing with noise jamming, it is equally important to avoid any form of degradation. A typical cause of degradation is saturation. If this occurs, be it in the receiver or on the display, severe losses will occur (visualize a display turned up so high that it "whites out"). As has been shown, jamming will cause the noise level to increase by many dBs. In order to avoid saturation, receivers have to have a wide dynamic range and special processing circuits known as

(continued on p. 60)

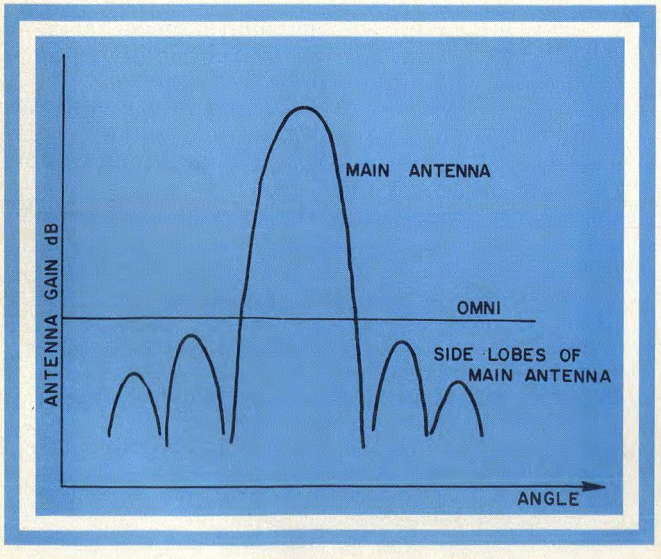

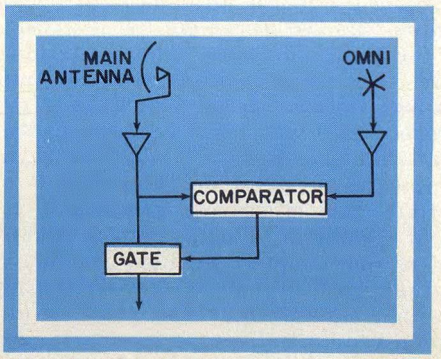

6. **With side lobe blanking** the output from the gate is inhibited if the signal in the omnichannel is greater than the signal in the main receiver channel.

NOISE JAMMING

CFAR (constant false alarm rate) receivers have to be used to effectively maintain a constant noise level. CFAR in effect, automatically varies the threshold to maintain a constant rate of threshold crossings. It prevents saturation by noise (from any source) and will enable targets that are stronger than this noise to be detected. A CFAR receiver, however, will not "extract signals out of the noise."

It is interesting to note however that some CFAR circuits are so efficient that the operator may be unaware that his radar is being jammed (the PPI has the normal appearance but there are few targets). Special circuits then have to be added to warn the operator of the presence of a noise jammer.

Sidelobe blanker and sidelobe cancellation are two other techniques that are used to combat jamming. With a sidelobe blanker, Fig. 6, the output of an omni is compared with the output of the main antenna. Any pulse that has a higher amplitude in the omni than in the main antenna must come from a sidelobe and can be removed by blanking. This is effective for pulse jamming where the duty ratio is low. In the case of high-powered noise jamming, the main channel is liable to be blanked for most of the time, severely affecting target detectability.

Sidelobe cancellation is an adaptive system where the combination of main antenna and reference antenna outputs can effectively generate a null in the direction of a jammer. This system is usually complex and requires one adaptive loop per jammer. The main problem, therefore, is how to deal with a multiplicity of jammers. In addition, a low sidelobe antenna design is required initially and an additional depth of null of 20 dB can only be achieved with difficulty.

In comparison, in the case of the radar defending itself against sidelobe noise jammers by having very low sidelobes, the noise level only increases by 3 dB everytime the number of jammers doubles. This is a small increase when compared to a jammer-power/receiver-noise-power ratio which is of the order of 30 to 40 dB. The following conclusions may, therefore, be drawn:

- It is useless to expect to see a noise jammer (or any other target in the same direction as the jammer) at any reasonable range, with any long range search radar.
- Burnthrough will not help.
- Frequency agility is mainly useful when associated with a spectrum analyzer to locate the minimums in the jammer power spectrum.
- CFAR is useful only to avoid further degradation.
- Sidelobe blanking will not defeat noise jammers and sidelobe cancellation is limited in its capability to deal with a number of jammers.
- A radar with only 20 dB sidelobes can easily be made useless over 360 degrees by a standoff noise jammer. Even its ability to obtain azimuth information on a jammer is impaired.
- Very low sidelobes are the most effective way to combat standoff jamming. ••

Test your retention

1. What is the role of a CFAR receiver in a noise jamming situation?
2. What has to be added to a frequency agility scheme to make it really effective?
3. Can jammer noise be distinguished from front-end noise?
4. What kind of an antenna is necessary to achieve really low sidelobes?

Two Techniques For Stable Signal Synthesis

Two methods of microwave frequency synthesis are examined. Direct synthesizers are fast switchers, but indirect units cost less, and offer better phase noise performance.

MICROWAVE frequency synthesizers have long been considered specialty items due to the interdependent factors of low demand, complex circuitry and high costs. Today however, a technique called indirect synthesis is being exploited to develop a new generation of off-the-shelf general-purpose synthesizers which offer frequency coverage to 18 GHz and beyond at relatively moderate prices.

There are two basic methods by which a signal may be synthesized: "direct" and "indirect". Both methods of synthesis transfer the stability of a single precision reference oscillator (usually crystal controlled) to all output frequencies. The direct method relies upon algebraic manipulation of the reference signal to produce the output frequency. The indirect method achieves the same result through the use of programmable phase-lock loops.

Each method has unique advantages and disadvantages for specific applications. Generally, microwave frequency direct synthesis is complex and expensive, but inherently gives faster switching times between frequencies. However, inexpensive direct synthesizers are becoming available at lower frequencies. Indirect synthesis is usually less complex and less expensive, but due to the length of time required for the phase-lock loop to attain lock, the method has drawbacks in applications where rapid frequency stepping is necessary.

Direct synthesis is agile

The theory of operation of a direct synthesizer is best demonstrated by the simplified block diagram shown in Fig. 1. First, multiples of the reference oscillator frequency are produced in a harmonic generator. Particular harmonics are then selected by individual bandpass filters followed by amplifiers. In the present example, a set of ten harmonics is selected from the N^{th} to the $(N + 9)^{th}$. The ten frequencies, all harmonics of the reference oscillator, are fed into a switch matrix.

The switch matrix has two output frequencies (designated as F_n and F_m), which are selected by a logic word to the switch matrix. Each output may be programmed to any of the input frequencies. The first output (F_n) is fed into a mixer, which acts as a frequency adder. The frequency of the second output (F_m) is divided by ten, filtered, then fed into the second port of the mixer. The output frequency thus is $F_n + F_m/10$, where F_n is selected by the first frequency word to the switch matrix and F_m by the second one. This output signal from the mixer is filtered and forms the output of the synthesizer. The example cited here is capable of providing 100 programmable frequencies, however, this scheme could be easily expanded to provide larger numbers of programmable frequencies.

An examination of the block diagram reveals that the long and short term stabilities of the output frequency are directly derived from the stabilities of the reference oscillator. The spurious performance of the synthesizer, however, depends on the particular frequency scheme chosen and on several other design parameters. Suppression of spurious products is, in fact, the major problem in the design of a direct synthesizer.

In the present example, the only desired output is $F_n + F_m/10$. All unwanted combinations of the two input frequencies have to be rejected by filtering. Also, since there are many different frequencies present simultaneously, the designer is faced with a potentially severe RFI problem.

As also may be seen in this example, the switching time between any two of the 100 possible frequencies is dependent upon the response time of the switch matrix. This response time can be made very short; thus the switching time of this and more practical direct synthesizer designs may also be very short, typically in the low microsecond time range.

To generate frequencies in the microwave region, X or K band, for example, the direct synthesis generally is performed first at lower frequencies and the output is then multiplied or upconverted. A single multiplication is usually the preferred method in cases where the output range is relatively narrow. In order to cover wide frequency ranges, however, upconversion by mixing against stable microwave signals is usually employed. Either of these methods, or a combination of the two, will preserve the fast switching speed of the direct synthesizer but with greater complexity, size and cost.

As suggested above, the direct synthesizer at microwave frequencies is usually a very complex instrument. This complexity and the large number of amplifiers, mixers, multipiers and filters cause the microwave direct synthesizer generally to be expensive and bulky. In addition, direct multiplication to higher frequencies causes a degradation in the short-term stability (i.e., phase noise). (For example, a frequency multiplication factor of ten results in a 20 dB increase of residual

(continued on p. 64)

Thomas Simon, Staff Scientist, and **Charles Foster,** Head, Frequency Synthesizer Section; Watkins-Johnson Company, 3333 Hillview Avenue, Palo Alto, CA 94304.

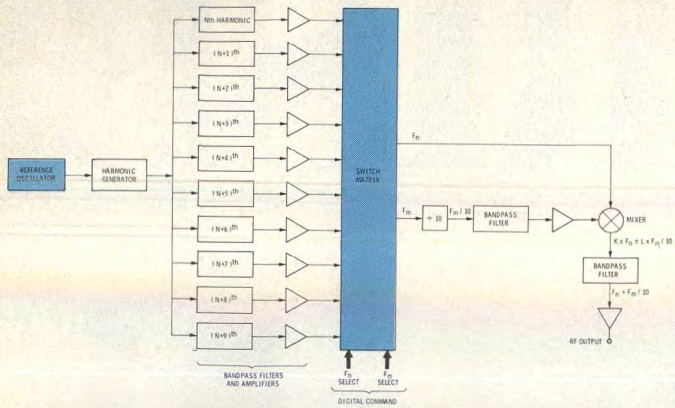

1. **Direct frequency synthesizers** rely on harmonics generated from the output of an ultra-stable reference oscillator. Advantages include fast switching, but drawbacks are cost and complexity.

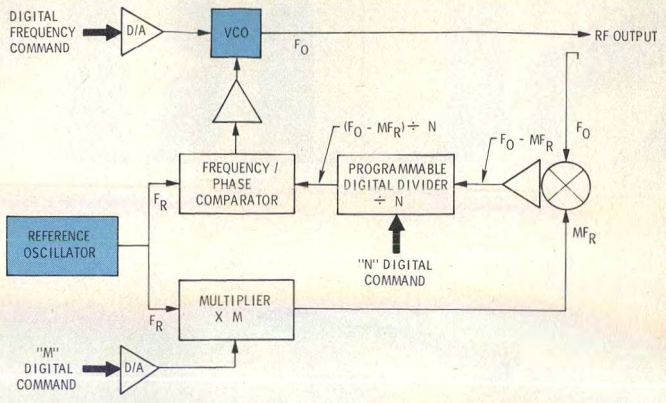

2. **Indirect frequency synthesizers** use a feedback phase-locked loop to fine-tune the output VCO. Although switching times are greater than direct units, cost and simplicity are assets.

phase noise relative to the carrier.) This will be illustrated in the discussion about indirect synthesizers.

Because of its complexity and cost, the direct synthesizer is normally employed in only those microwave applications which require switching times below 100 microseconds. As a consequence of their frequency agility requirements, ECM systems are the primary users of direct microwave synthesizers. As an example, a present day ECM system might require that a signal be switched within 25 microseconds after command, from any one frequency to any other frequency in a 2 GHz range, and to an accuracy of 1 part in 10^6. There are currently outstanding requirements for ECM systems which call for octave-band stepping speeds in the 100 nanosecond range. Communications systems of a tactical military nature may also require the frequency agility of the direct synthesizer.

Indirect Synthesis is versatile

Indirect frequency synthesizers dominate the majority of microwave applications where ultra-fast switching speed is not required. The operation of this type of synthesizer centers on the output oscillator, a voltage controlled oscillator (VCO) in the example shown in Fig. 2. The VCO is tuned initially as close to the output frequency as practically possible, usually within 1 to 0.1%. This "coarse" tuning is accomplished by converting the incoming digital frequency word into an appropriate analog voltage using a digital to analog converter (D/A).

To then enhance the instru-

(continued on p. 67)

Accuracy • Stability • Repeatability Do you know the difference?

Accuracy, long term stability and repeatability are terms which are often misunderstood and used interchangeably. However, each has a distinct definition, which should be clearly understood before attempting to specify a frequency synthesizer for your application.

Frequency accuracy is the frequency difference between the actual synthesizer output frequency and the programmed frequency. This is often expressed as the ratio of the measured frequency error to the programmed frequency. Thus an output frequency having 1530 Hz error at a programmed frequency of 15 GHz may be said to have an accuracy (or inaccuracy) of 1.02 X 10^{-7}.

Frequency accuracy of a synthesizer is a function of the reference oscillator stability over time and temperature, the elapsed time and change in temperature since the last calibration, and the accuracy of the last calibration.

Frequency stability is the drift of the synthesizer output frequency over elapsed time and changes in temperature. The rate may be expressed as Hz per second, hour, day or month or as Hz per temperature range (i.e. 30 Hz per day or ±90 Hz over 0° to +50°C). It may also be expressed as a ratio of frequency drift rate to the programmed frequency (i.e., the above rates observed with a programmed frequency of 15 GHz would be identical to 2×10^{-9} per day and $\pm 6 \times 10^{-9}$ over 0° to +50°C). Frequency stability of a frequency synthesizer (when expressed as a ratio) is identical to the frequency stability of the reference oscillator used within the synthesizer or as the external reference.

Frequency repeatability is the actual change in frequency for a single programmed frequency over a specific period of time whether the programmed frequency remains unchanged or is programmed away from and then back to the original frequency. This repeatability is a function of both the time and temperature stability of the synthesizer reference oscillator as well as the elapsed time and the temperature change during the specified time period.

The following example may serve to emphasize the differences.

Assume:
- Programmed Frequency = 18 GHz
- Measured Frequency (traceable to NBS) at time t_0 = 18.000001620 GHz
- Measured Frequency at time t_1 = 18.000001980 GHz
- $t_1 - t_0$ = 40 days
- Temperature change = 0°

Therefore:
- Frequency Accuracy at t_0 = 1620 Hz or 9×10^{-8}
- Frequency Accuracy at t_1 = 2340 Hz or 1.3×10^{-7}
- Frequency Repeatability over 40 days = 720 Hz or 4×10^{-8}
- Frequency Stability = 18 Hz per day or 1×10^{-9} per day

If after a rapid change in temperature from +0°C to +50°C the measured frequency changed 72 Hz, it could be assumed that the major portion of this frequency change was temperature dependent. The nominal frequency stability could then be identified as 72 Hz, or $\pm 4 \times 10^9$, over +0°C to +50°C. ••

ment's stability, a 'fine tune' correction is applied in the form of negative feedback. This feedback is obtained by comparing a sample of the output frequency (or a derivative thereof) to the reference oscillator frequency. Any difference in frequency or phase between the two signals results in a correction signal level which is proportional to that difference and is fed back to the VCO as an error signal. The output frequency derivative for the example shown in Fig. 2 is obtained by dividing the VCO sample frequency by 'N' in a programmable digital divider.

Since the most common frequency comparator circuit used in synthesizers is the phase detector, frequency correction feedback loops are phase-lock loops. In this phase-lock method, the open loop gain and the bandwidth of the loop determine how closely the VCO output stability reproduces the reference signal stability. The performance of an indirect synthesizer is, therefore, greatly dependent upon the phase-lock loop design.

A YIG-tuned oscillator (YTO) is normally used as the VCO in indirect synthesizers. This is a result of the YTO's high Q (on the order of 300 to 800 loaded), octave or greater frequency coverage, very good linearity (±0.1 to 0.3%) and solid-state construction. An added feature is the availability of two coils to tune the YTO—a main coil and an fm or "fine tune coil"—which eliminate the need for coarse and fine tune summing circuitry. Varactor-tuned oscillators, however, are sometimes used where a greater tuning rate is necessary and where lower Q and linearity can be tolerated.

Spurious signals from an indirect synthesizer are generally much easier to control than those from a direct synthesizer. This is because the indirect synthesizer output is derived from a single VCO and the only significant nonharmonically related spurious signals which may appear in this output are the frequency products near enough to the output signal to fall within the loop bandwidth. Because the phase-lock loop bandwidth is usually less than a few hundred kilohertz, which is much narrower than the total output signal bandwidth, design requirements to suppress spurious signals are eased for indirect units. Spurious suppression of 60dB or more below the carrier is normally expected from either synthesizer, but is more easily accomplished with the indirect synthesizer.

Harmonics of the VCO fundamental frequency are generally much larger in magnitude than any internally generated nonharmonic spurious signals. This, however, usually does not create a significant problem at microwave frequencies due to the large difference between the fundamental and harmonic frequencies and to the natural attenuation properties of associated equipment. Nevertheless, these harmonics can be relatively easily filtered out if necessary for a particular application, thus reducing harmonics from −15 to −25dB down to −50dB or lower relative to the carrier. The additional filterings, however, add costs and reduce the rf output power.

When a new frequency is programmed into the indirect synthesizer, the VCO must slew to the frequency, then lock there. The switching time, therefore, is dependent on both the slewing rate of the VCO and the response time of the loop. This switching time can be made reasonably short by using a fast-tuning VCO and a wide loop bandwidth. Yet, VCO tuning over large frequency ranges is still slower than switching between existing signals. For this reason, indirect synthesizers are generally limited to applications that require switching times greater than 100 microseconds.

Where microsecond switching speed is not a requirement, indirect synthesizers currently find more applications at microwave frequencies than direct synthesizers. This is primarily due to greater availability and usually lower cost of microwave indirect synthesizers. Little specific price comparison information can be provided, however, because of the present lack of commercial direct synthesizers above 500 MHz and of public price information about specialized units for military applications.

Another important preference for the indirect microwave synthesizer is its superior short-term stability (phase noise), a major consideration at microwave frequencies. This is of importance because short-term stability is relatively constant as a percentage of output frequency and, therefore, degrades as frequency increases. Figure 3 shows that at microwave frequencies and for offsets larger than the loop bandwidth, the short-time stability (phase noise) of a properly de-

(continued on p. 68)

signed indirect synthesizer is better than that of a direct synthesizer.

The solid line shows the phase noise of a direct synthesizer at microwave frequencies. At first,

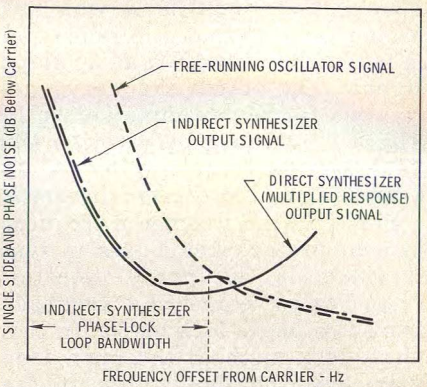

3. Short-term stability (phase noise) of the direct method is the same for low offsets, but the indirect technique gains the advantage as the offset is increased.

the phase noise decreases as the offset frequency increases. This region is characterized by the performance of the reference oscillator. As the offset frequency increases further, however, the thermal noise of the amplifiers and multipliers following the reference oscillator begins to dominate and the phase noise starts to increase with the increased offset frequency.

On the other hand, although the phase noise of a free-running VCO is appreciably higher at lower offsets, it decreases and eventually becomes lower than the direct synthesizer phase noise as the offset is increased. A properly designed phase-locked loop can act to transfer the characteristics of the multiplied reference to the VCO at low offset frequencies, while maintaining the superior performance of the VCO at higher offset frequencies. The result combines the best features of both approaches as shown by the dot-dash line in Fig. 3.

Additional but somewhat less critical advantages may also be counted on the side of the indirect synthesizer for most applications. One such advantage is the presently available minimum output power level of 10mW up to 18 GHz and 6mW up to 26.5 GHz with all solid-state construction. To achieve this power level with a direct synthesizer approach, one

(continued on p. 71)

or more traveling-wave tube amplifiers would normally be required with their attendant shorter life and increases size, weight and power requirements.

Applications are increasing

Indirect microwave synthesizer applications include automatic test system stimuli generators, receiver local oscillators, transmitter exciters and laboratory sources used for calibration and other scientific purposes. The fastest growing application is the use in automated test systems, although lab applications have also increased rapidly. In an automatic test system, the synthesizer provides the RF stimulus and sometimes a reference against which the manipulated stimulus can be down converted. This synthesized stimulus signal may be rapidly and very accurately programmed. This rapid programmability is very important for computer control, where the system under test is complex and expensive and should be tied down for testing for as short a time as possible.

Speed of testing is also important in the labor-saving areas of production testing of high volume, but less complex, products which are frequency sensitive. The accuracy and repeatability of synthesized measurements give greater depth to the test program and enable the user to test for "fine grain" characteristics which are important for the complete characterization of the unit or system under test. The stimulation of complex signals such as threat signals to test ECM equipment is also practical with the use of synthesizers.

In reconnaissance receiving systems, the accuracy, spectral purity and programmability of the synthesizer used as the local oscillator greatly increase the quality of information derived from acquired and analyzed signals. Coherence of synthesizer signals is a must in special purpose coherent receivers or in direction-finding systems. ••

Test your retention

1. What limits the switching time of an indirect synthesizer?
2. What are the major contributors to the phase noise of a direct synthesizer?
3. What is the distinction between frequency accuracy and frequency repeatability?

technical note

Check that pulse

When a transistor-power amplifier is required to amplify periodic short pulses, peak outputs are often obtained that are several times greater than the amplifier's rated cw level. Junction temperatures rise to dangerous levels when the output pulse begins to droop, and the phase shift under these stressed conditions is frequently questioned.

Normally, phase linearity may be measured using the equipment in Fig. 1 which presents a conventional polar display. A swept frequency is applied, and the "trombone" on phase shifter is adjusted for a minimum arc on the oscilloscope screen to establish equal length lines. Thus calibrated, the phase shift may be recorded at fixed frequencies.

Since the phase shift during a pulse seldom exceeds 3 degrees, this procedure is unsatisfactory under pulsed conditions because the small segment of the arc that will appear is no more than a bright dot.

This same basic setup, however, can be slightly modified to measure the phase shift resulting from a pulse. The scope is connected as before with the horizontal sweep displaying the pulse duration and the vertical deflection used to measure θ. Since sin θ and θ are essentially equal for the small phase shifts involved, it's possible to just display the sin term by getting rid of the cos term (horizontal input) via a selector switch on the scope. The cosine input pulse is then applied to the internal sync of the scope to start the horizontal sweep. Also, the trombone can be adjusted to place a horizontal reference in the center of the scope because equal line lengths are not required at a fixed frequency.

The scope is calibrated by changing the length of the trombone and recording the deflections to obtain the upper and lower traces, Fig. 2.

For example, a 1.7 ms pulse at 300 MHz with ±1 cm calibration traces results in a phase shift $\Delta\phi$ = 0.85 div × 7.2°/6.5 div. = 0.94 degrees. **Bert K. Erickson, Heavy Military Electronics Systems, General Electric Company, Syracuse, NY 13201.**

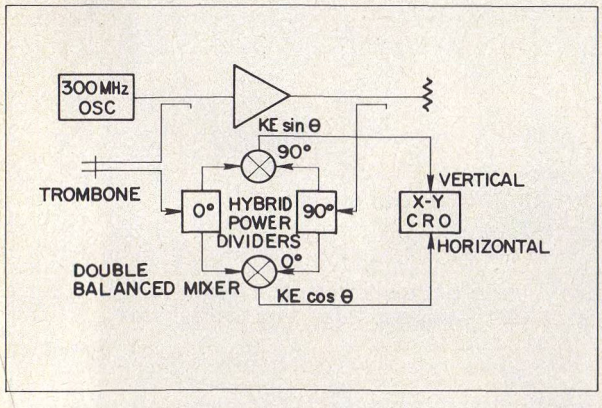

1. **The test setup for measuring swept frequency** and pulse phase shift is essentially the same except under pulse conditions the internal sync of the scope is used for the horizontal input.

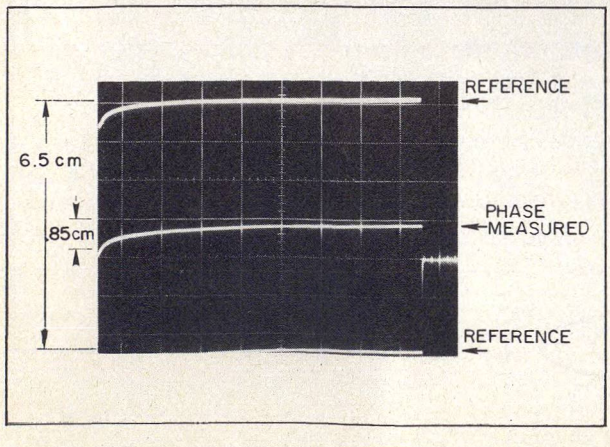

2. **Two references** are established (upper and lower traces) by measuring displacement of phase shifter (trombone) and converting to electrical degrees (7.2°). The middle trace gives the phase shift (0.85 divisions) which is converted to electrical degrees by $\Delta\phi$ = 0.85 div × 7.2°/6.5 div. = 0.94°. Horizontal scale = 0.2 msec/div.

letters

Calculator handles Z conversion

Editor, MICROWAVES:
The series/parallel conversion algorithm given in "Series/parallel conversion in reverse polish notation," MicroWaves July, 1975, p. 62 is very convenient for HP-35 calculator users. Those using HP-45's or the new and similar Corvus 500 will find the following procedure much easier to remember. It uses the familiar reciprocal sum and the 45's polar/rectangular keys. Finally, it leaves all results of interest in the stack for convenient reference. ( ) indicates data entry, (=) indicates readout of the x register display.

(X_p) 1/x (R_p) 1/x →P (=Y)
RCL Σ+ f →R $(=R_s)$ R↓
1/x (=Z) Σ+ RCL 7
$(=X_s)$ R↓ (=Z) R↓ (=0)

(X_s) ENT↑ (R_s) →P (=Z) 1/x
f →R 1/x $(=R_p)$ R↓ 1/x
(=Y) Σ+ RCL 7 RCL Σ+
$(=X_p)$ R↓ (=Y) R↓ (=0)

B. Wheeler, P O Box 131, Camden, NJ 08101

CTOBER
975

laser technology

MICROWAVES

X-BAND AMPLIFIER DESIGN:

Build an FET amplifier to cover X-Band

CAD simplifies Gunn amp design
GaAs Impatts boost power and efficiency
Take the guesswork out of compression tests

MICROWAVES
October 1975
Vol. 14, No. 10

news

editorial

technical section

Amplifiers

products and departments

About the cover: Tools of the trade for today's amplifier designers range from the ubiquitous Smith Chart to sophisticated computer optimization routines. Photo courtesy of Watkins-Johnson; design by Robert Meehan.

coming next month: International Technology

A first-hand look at the underlying currents in European microwave technology will highlight the November issue. The detailed staff-written report is based on a recent tour of major European companies and on announcements made at the European Microwave Conference.

November technical articles will include:

Don't Overlook The Package Design. Daniel Olivieri of RCA discusses a variety of manufacturing processes suitable for building MIC packages. Emphasis is placed on the importance of considering packaging early in the design stage.

Graphs Simplify Load Impedance Measurements. Keith M. Keen of the European Space Research Organization in Noordwijk, The Netherlands, presents a series of curves for converting measured phase and amplitude data to complex impedance values. Keen's technique is especially useful for spectrum analyzers not equipped with a polar display unit.

MICROWAVES is sent free to individuals actively engaged in microwave work at companies located in the U.S., Canada and Western Europe. Subscription price for non-qualified copies is $10.00 for U.S., $15.00 a year elsewhere. Additional single copies $1.50 ea. (U.S.); $2.00 ea. (foreign); except additional Product Data Directory reference issue, $10.00 ea. (U.S.); $18.00 (foreign). POSTMASTER, please send Form 3579 to Fulfillment Manager, MICROWAVES, P.O. Box 13801, Philadelphia, PA 19101.

Back Issues of MicroWaves are available on microfilm, microfiche, 16mm or 35mm roll film. They can be ordered from Xerox University Microfilms, 300 North Zeeb Road, Ann Arbor, MI 48106. For immediate information, call (313) 761-4700.

Hayden Publishing Co., Inc., James S. Mulholland, President, printed at Brown Printing Co., Inc., Waseca, MN.

news

Microwave link transports 30 kW dc over 1 mile

This 85-ft dish at Goldstone transmits 320 kW at 2.388 GHz to the rectenna array mounted on the tower in the distance, over a mile away. Intercepted rf to dc efficiency is over 80%.

Richard T. Davis
Managing Editor

The concept of beaming high-power microwave energy from orbiting solar power satellite stations to earth was nudged a small step closer to reality by the transmission and collection of over 30 kW of dc over a mile of California desert. The tests, conducted by Jet Propulsion Laboratory, Pasadena, CA, at their Goldstone Deep Space Communications Complex, represents the first large scale transportation of electric power from one point to another via a free space radiated microwave beam. The overall rf to dc efficiency, measured at 2.388 GHz, was over 80% using a 25 × 12 array of dipole receiving elements and Schottky diodes for rectification.

While JPL officials are quick to point out this is just a high power transmission technology study, there is little doubt of their ultimate objectives—to gain further insights into the feasibility of transmission of electrical energy from space. This test is only one facet of numerous technological problems that need to be looked at, not to mention the biological, legal, political and social implications that would evolve if this energy plan is ever implemented.

The concept of gathering solar energy and sending it to earth was first proposed about seven years ago by Peter Glaser of Arthur D. Little, Boston, MA. However, because of the enormous scope of the plan and expense for a single operational satellite power station, (the R&D estimate is about $57-billion) many questions remain over its feasibility.

4590 rectifying diodes in array

According to Richard Dickinson, one of the principal investigators at JPL, there are five major technological objectives of an electrical nature alone that need to be solved.

- Converting solar energy to dc via solar arrays.
- Converting the dc to rf by an array of microwave power tubes.
- Forming and pointing a beam from the solar power station to earth with properly controlled sidelobes and phase error.
- Collection and rectification on earth from rf to dc via a "rectenna" or rectifying antenna.
- Power conditioning to feed to the U. S. power grid.

The present JPL tests for NASA's Offices of Applications and Energy Programs, Wash., D.C. started in June as part of a five year cooperative study with Louis' Research Center, Cleveland, OH. The program address only the collection and rectification aspect of this tremendously complicated program. Later in the program, JPL is also going to build a modular transmitting array using beam steerable slotted waveguide arrays for maximum efficiency.

"The Goldstone facility was selected because of the availability of microwave power," says Dickinson. "We're using a 450 kW klystron amplifier and an 85 ft dish normally used for deep space communications as a power source." Actually, only 323 kW is transmitted and, of that, only about 11.4% of the tubular beam is intercepted by our rectenna, which lies about one mile from the transmitter site.

"In our initial test, we were able

(continued on p. 10)

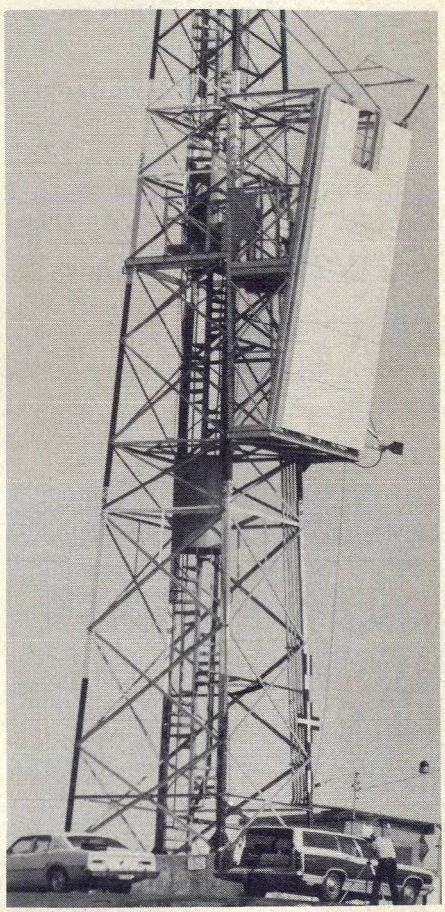

1. **Rectenna array consists of 17 subarrays** in a 3 x 6 matrix. Each subarray contains 270 dipole antennas and diode rectifiers. The standard gain horn at lower right of array is used for power calibration. The rectenna is inclined at 7 degrees so the microwave beam doesn't reflect off the ground.

 (continued from p. 9)

to recover 30.4 kW of dc power from the 36.8 kW of microwave power intercepted by the 12 ft × 25 ft array. That's an efficiency of 82.5% but our measurement error is about ±2.5% rf to dc."

The rectenna, developed by Raytheon in Waltham, MA, consists of 17 array elements, each measuring about 4 × 4 ft, stacked in a 3 × 6 matrix, (Fig. 1). Each array element consists of 270 vertically-polarized dipole elements and Schottky barrier diodes (Fig. 2). Forty-five diodes are hooked up in parallel and then grouped in six series strings to develop 170 Vdc.

"Each element delivers about 6 to 8 W depending on the quality of the diode and its location in the array," says Dickinson. "Those in the center get more power radiated on them than those at the edges because the variation in flux density across the face of the array."

The dc power first goes to a crowbar to protect the array elements in case of a load failure. Approximately two-thirds of the dc power is then dissipated by power resistors in a load box while the remaining dc power goes to a load of 36 GE spotlights.

"In case there is a diode failure, there are enough diodes remaining in parallel to provide sufficient short circuit current to fuse the faulted diode open—a sort of self-clearing function," explains Dickinson. "So far, we've had only three failures and in each case, we've been able to trace the source of the problem quickly."

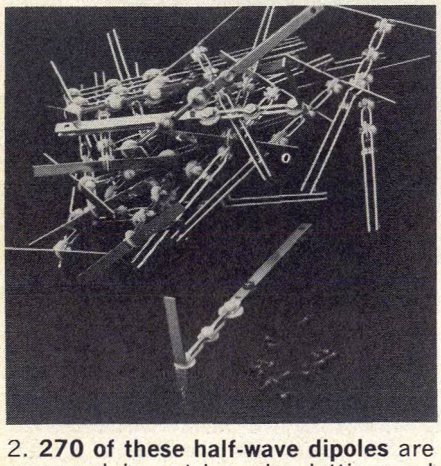

2. **270 of these half-wave dipoles** are arranged in a triangular lattice and mounted on the 4 x 4 ft sub-arrays shown in Fig. 1. Each element delivers about 6 to 8 W. The rf to dc converters behind each dipole consists of a series low-pass rf filter and a GaAs Schottky barrier diode rectifier.

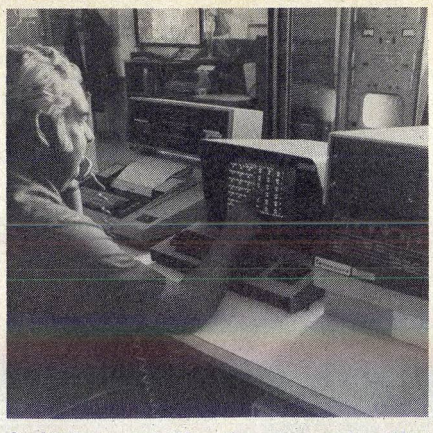

3. **Instrumentation for measuring the power transmitted and received includes this Interdata computer.** The display presents input rf power, output dc power, efficiency, voltage and temperature at the rectenna elements. Dc readings are separately calibrated to 0.5%.

Instrumentation has fault finding

Much of the effort in this test program has gone into developing suitable instrumentation so test data can be evaluated rapidly and with a high degree of accuracy. The heart of the measurement set-up is an Interdata computer, Fig. 3, with a 16 W word memory which massages and corrects the raw data before it is fed to a video display. A video tape cassette also continuously records the data while the system is operating.

"The computer is setup to store the last ten seconds just before a failure," says Dickinson, "sort of a 'Pearl Harbor file.' "

"We only started to gather data in June, and there are lots of tasks and modifications we'd like to do to improve the system. Our major limitation is obtaining access to the transmitter site," says Dickinson. "One of the first things we want to look at is varying the dc load and see if the efficiency improves. We also want to reposition the array elements and put our 'best-performer,' now at the bottom of the 3 × 6 array, right in the middle where the power density peaks."

Each rectenna element presently sees 130 ohms, but the JPL researchers would like to vary this ±20% to see if the rf impedance can be optimized. Polarization could also be varied—it's presently vertical linear to prevent birds from perching on the elements.

"While 3 GHz would probably be a better frequency to operate at, we are probably going to end up at the ISM (industrial scientific-medical) band at 2.45 GHz," explains Dickinson. "During the year, we also hope to refocus the transmitter beam so it focuses on the rectenna site."

Do we want solar power?

Whether these initial tests ultimately lead to an operational satellite power station remains to be seen. There are a tremendous number of potential problems with the proposed system that need to be worked out before an all-out effort on this program is justified. "I think most of the microwave system is feasible but the biological impact needs to be really looked at further," contends Dickinson.

The energy payback is also a question. "How much energy on earth is going to be used up to get the system in orbit and working? When would that energy be paid back? I'm in favor of keeping the concept open as an option and doing further investigation," continues Dickinson. But there is no disputing the side issues are legion. "One major problem and the major expense involved with the project, is getting the 40 million pounds required to build one system into geosynchronous orbit. To make a dent in satisfying the U. S. energy needs by the year 2000, you would need about 125 of these orbiting systems to meet just 15 to 20% of the projected U. S. power requirements," notes Dickinson. "That's equivalent to launching a large rocket everyday for several years in order to get all the parts into orbit for assembly by 'hard-hat'-astronauts." The pollutants from launching all those rockets would be enormous. "We would probably have to consider hydrogen fueled rockets, or some other alternatives."

"But that's just the beginning of the problems that need to be solved," cautions Dickinson. "We must also address how much of our vital natural resources would be used up to develop the plan." One study shows that no more than 2% of the annual production is certain critical items would be consumed.

It's the biological impacts that really need to be investigated further. The proposed power densities on the earth may vary from 20 mW/cm^2 to 70 mW/cm^2 depending on availability of real estate and cost. The rectenna-array area could be fenced off to keep people out, but there is the possibility of a helicopter flying through the beam as well as birds.

"Who knows what detrimental effects could occur with that beam focused on the earth?" We need to go through several life cycles of

(continued on p. 12)

The CATT treads softly into bipolar territory

Stacy V. Bearse
Associate Editor

A new type of solid-state microwave device, constructed with a blend of Impatt and transistor technologies, promises to offer higher power levels at higher frequencies than previous three-terminal devices. Termed a Controlled Avalanche Transit-time Triode (CATT), the new device develops additional gain over normal transistors through the use of avalanche current multiplication and transit time effects in the base-collector depletion region.

Similar in structure to an n-p-n bipolar transistor, the CATT incorporates carefully designed avalanche and drift zones between base and collector regions (Fig. 1).

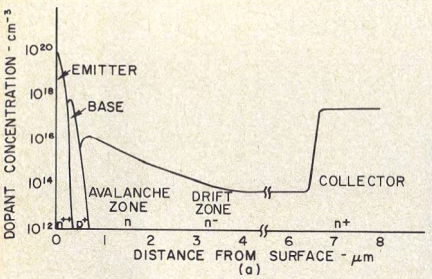

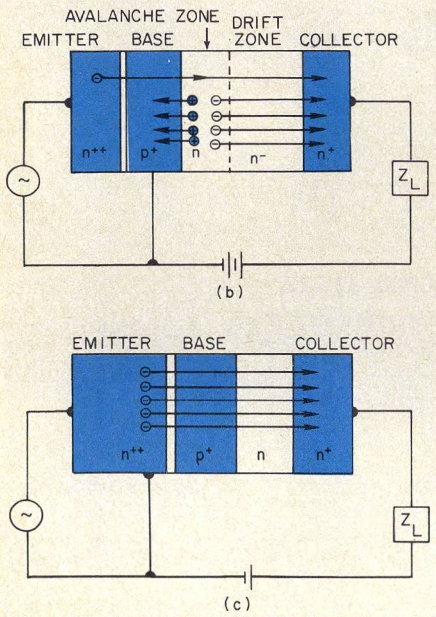

1. A CATT (b) includes avalanche and drift zones between emitter and collector. Bias arrangement is similar to the conventional n-p-n bipolar (c). Dopant profile for a typical CATT device is shown in (a).

"In a CATT, the charge giving rise to the collector current is primarily generated in the collector depletion region itself by avalanche multiplication of a relatively smaller injected signal," notes John Eshbach of the General Electric Research and Development Center in Schenectady, NY. The result of this multiplication, according to Eshbach, is that the collector current is substantially greater than the emitter current, and the E-B junction does not have to be turned on as hard to produce a given level of collector current. Most important, Eshbach stresses, the CATT therefore operates with current gain greater than unity, even in a common-base design, leading to increased power gain over a transistor with the same emitter-base geometry.

To illustrate this, GE has run several performance trials comparing CATT devices with bipolar transistors of identical structure, but having no avalanche zones. Pulsed, L-band results, shown in Fig. 2, reveal that the current multiplication phenomena of the CATT results in about 6 dB of additional gain. These measurements were taken at a bias of 140 volts, compared to a collector breakdown voltage of 240 volts.

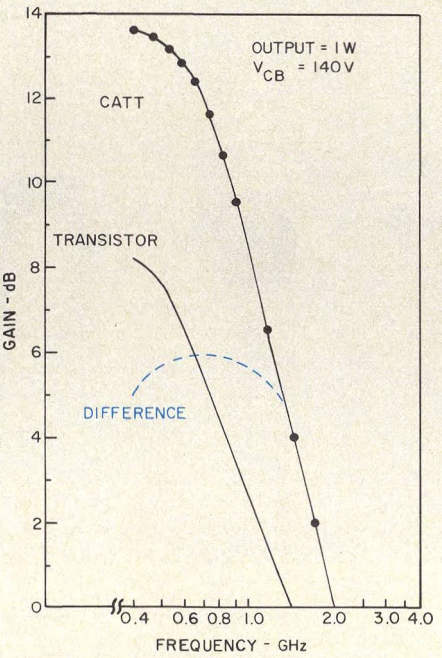

2. CATT current multiplication yields an additional 6 dB of gain compared to a traditional bipolar transistor at L-band.

A second, S-band device reportedly offers a gain improvement of 6 to 9 dB over a similar bipolar transistor at 2 GHz. Rf data for this CATT, shown in Fig. 3, demonstrates a maximum efficiency of 27% at a 13.7 watt output, and a maximum output of 17.7 watts with 11 dB gain and 24% efficiency. Rf data represents peak power output under pulsed operation, and was taken with a 70 volt bias.

"These results approach the state-of-the-art for bipolar transistors at S-band," claims Eshbach. "Note that the gain of the CATT remains high, even at low input power, in contrast to class C operated standard transistors."

Although the efficiency is somewhat less than what one would expect for a bipolar transistor at the same frequency, Eshbach points out that these CATTs are still in an early developmental stage. "Based on simple theory, it appears that the collector efficiency of CATT devices can eventually reach 35 to 50%," the GE researcher predicts.

Interdigitated structure used

Both L- and S-band CATTs are

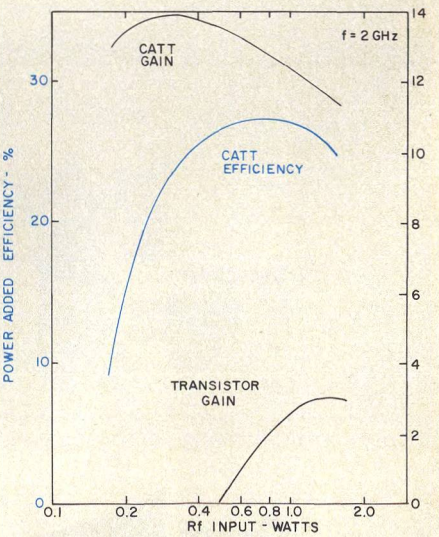

3. Although efficiency is rather low, researchers predict future levels of 35 to 50 percent. Note gain improvement over conventional transistor.

(continued on p. 18)

Quarter-watt FET amp tops 68% efficiency at 4 GHz

Results unveiled at the recent Cornell Conference on Active Semiconductor Devices for Microwaves and Integrated Optics reveal the GaAs Schottky barrier FET to be an extremely efficient medium-power Class A or B amplifier. Dr. Ira Drukier, a member of the technical staff at RCA Laboratories in Princeton, NJ, reports that power added efficiencies as high as 68.4% at 261 mW have been measured for a class B MESFET amp operating at 4 GHz (Fig. 1). "This is the highest measured efficiency ever reported for a microwave solid-state device," Dr. Drukier told the conferees.

"The small signal gain was 11 dB, and the efficiency was measured at 1.4 dB gain compression," he explains. "The corresponding drain efficiency was 77%, which is near the theoretical maximum for sinusoidal, Class B operation."

Second and third harmonic content of the amplifier was found to be 25 dB below the fundamental. Two-tone masurements indicate a third-order intermodulation ratio of −30 dB and −25 dB at efficiency levels of 30% and 40%, respectively.

The same device reportedly generated 283 mW at 8 GHz with 41% power added efficiency and 6.7 dB gain in Class B operation.

"These results show that even under Class B conditions, GaAs MESFETs have potential applications in high-efficiency, linear amplifiers," Dr. Drukier comments.

Other medium power devices developed at RCA have demonstrated useful gain and good efficiency at frequencies as high as 12 GHz. "The best results obtained to date in J-band are 520 mW at 11 GHz with a linear gain of 7.6 dB and 13.3 power added efficiency from a two-cell device, and 200 mW at 12 GHz with linear gain of 7.3 dB and 13.1% power added efficiency," Dr. Drukier reports.

All devices were fabricated using standard photolithographic techniques, allowing gate lengths as narrow as 1.2 microns. Each FET cell (Fig. 2) consists of four parallel gate stripes, each measuring 150 microns, as well as three source and two drain contacts. Devices are flip-chip mounted on a plated copper carrier to decrease thermal resistance and common lead source inductance. All bonds are made with gold ribbon, instead of wire, to further minimize parasitic reactances.

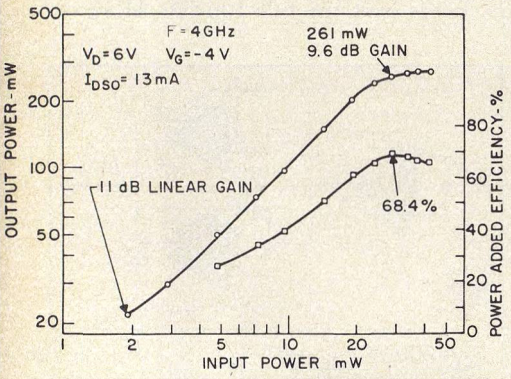

1. Peak efficiency of 68.4% corresponds to a 261 mW output.

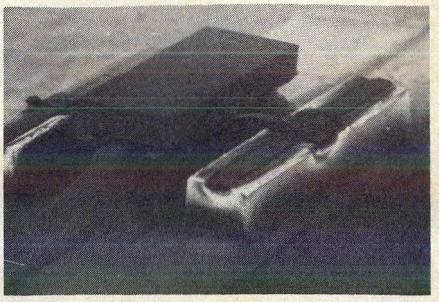

2. SEM photo of a flipped MESFET chip illustrates narrow gate length.

Sample devices available

Similar state-of-the-art power MESFETs are available from RCA on a small quantity, sampling basis. The devices are offered in unpackaged form, but fully characterized and mounted on carriers. Although efficiency depends largely on the circuit in which the FET is used, Mark Nowogrodzki, manager of division liason at RCA Laboratories says that the sample devices are capable of several hundred milliwatts between 4 and 8 GHz, and offer maximum available gains of up to 6 dB at 8 GHz.

"We feel rather strongly that the GaAs FET amplifier will be the workhorse of the future," notes Nowogrodzki, "and we want more people to become familiar with the device. •• *SVB*

The CATT treads softly into bipolar territory

(continued from p. 14)

experimental structures based on a fairly conventional metalized interdigitated emitter-base design. The L-band device has 16 emitter fingers, each measuring 5 ×1 mils, spaced on 1 mil centers. Depletion drift width is 18 microns. Although the S-band CATT has approximately the same active area dimensions, it consists of 50, 4.5-mil emitter fingers spaced on one-third mil centers. Drift width is 5.3 microns.

Eshbach, who presented the S-band CATT results at the 1975 Cornell Conference on Active Semiconductor Devices for Microwaves and Integrated Optics (August 19-21), attributes the device's high-power capability to minimization of the base widening, or Kirk effect, which limits conventional transistor peak power. According to the researcher: "Minority carrier charge density in the base is significantly reduced in a CATT for a given collector current. Further, the current at the edge of the base is primarily carried by holes returning from the avalanche zone rather than by injected electrons. These facts lead to a reduced level of minority carrier charge storage, and therefore, reduced base widening effects."

The CATT was initially developed by Dr. Se Puan Yu, William R. Cady and Dr. Wirojana Tantraporn of General Electric, and announced in the IEEE Transactions on Electron Devices of November, 1974, in a paper entitled: "A New Three-Terminal Microwave Power Amplifier." ••

news/international

MIC circuit broadens circulator's bandwidth

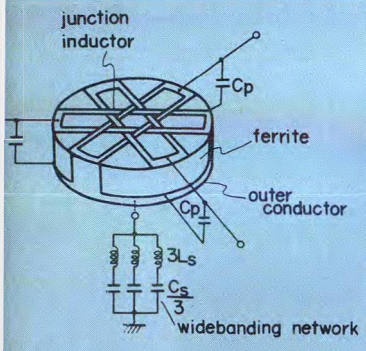

A new approach to wideband, temperature-compensated circulator design has been developed at Nippon's Central Laboratories in Kawasaki, Japan. **By bridging a circulator's outer conductor and ground with three series-resonant circuits, the Japanese researchers have demonstrated double-tuned and triple-tuned circuits that offer 20 dB isolation bandwidths of 600 MHz and 950 MHz, respectively.** According to Hidehiko Katoh of Nippon, performance is maintained over a −10°C to +60°C range.

The resonant network is realized in MIC form on the back side of a 14 mm × 14 mm garnet junction substrate (see figure). Interdigital capacitors and strip inductors are made of evaporated Cr-Au and plated Au films using air-insulated beam-lead crossovers. Typical values for L_s and C_s are 2.5 nH and 3.5 pF, respectively, at 1.7 GHz. The compact MIC circuit can be enclosed in an 18 mm × 19 mm package, exclusive of connectors.

Katoh reports that at room temperature, the best device realized in this fashion exhibits more than 20 dB isolation with an insertion loss of less than 0.85 dB (0.55 dB min) over a 700 MHz bandwidth centered at 1.67 GHz. Fractional bandwidth is about 41%.

Temperature stabilization is achieved by assigning the bias magnetic field a positive temperature coefficient to offset the thermal variation of the ferrite substrate's saturation magnetization. According to the researcher's paper published in the August *IEEE Transactions on Microwave Theory and Technique*, a magnetic field with a 0.8%/°C coefficient will result in a center frequency shift of about 0.04%/°C. The best temperature-compensated unit reported by Katoh offers 20 dB isolation over a 600 MHz bandwidth centered at 1.7 GHz. Insertion loss is less than 0.95 dB with a ripple of less than 0.15 dB. Input/output VSWRs are less than 1.22.

Open-ring waveguide holds down losses

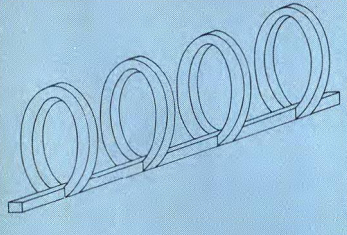

The cost of low-loss corrugated waveguide has been reduced at the University of Limoges in France by removal of the outer shielding. **The resulting open-ring line propagates the EH_{11} hybrid dipolar mode at a loss of less than 5 dB per kilometer below 1.8 GHz. The spacing of the rings determines the polarization of the hybrid mode.**

The line was constructed from aluminum alloy (AGS T_4), but researchers report that the attenuation could be reduced if the line were fabricated from copper. Although the mechanical strength depends on the thickness and width of the rings and the rod, the line's losses are essentially unaffected by these dimensions. In use, the line is supported above the ground on plastic pipes, which are set in the plane of the rod so the electromagnetic field of the dipolar mode is only slightly perturbed.

Gunn-effect logic promises high speeds

Researchers at Fujitsu Laboratories in Kawasaki, Japan have **monolithically combined logic elements based on the Gunn effect into a full-adder circuit, which reportedly operates at a speed that is one to two orders of magnitude higher than that of the fastest digital circuits available today.** The full adder consists of AND gates, exclusive OR gates and a carry generator.

According to Shinya Hasuo of Fujitsu, the most important feature of the full adder circuit is a new type of comb-shaped Gunn device which acts as a carry generator. In this device, carry propagation is achieved by taking advantage of the transverse extension of a high-field domain whose velocity is much higher than the normal domain propagation velocity. Hasuo reports carry propagation delays as short as 50 picoseconds for a four-bit generator.

Other logic elements in the adder, including AND and exclusive OR gates, were also fabricated with Gunn devices realized on a GaAs epi. AND gates are composed of a dual Schottky-barrier gate FET driving a Gunn device. An exclusive-OR function is performed by two parallel FET-driven Gunn devices connected to a common resistive load.

Cover X-Band With An FET Amplifier

GaAs FETs, now available with one-micron gate lengths, are rivaling TWTs as wideband, low-noise amplifiers. Here's an X-Band design approach that eliminates the requirement for a negative bias supply.

ONE of the most exciting solid-state devices currently available for microwave applications is the Gallium Arsenide field-effect transistor, or GaAs FET. It provides a low-noise figure in conjunction with relatively high output power, which translates into the wide dynamic range capability required for amplifier applications. As the only three-terminal device currently capable of low-noise amplification at frequencies through 15 GHz, the GaAs FET offers several inherent advantages over competitive two-terminal devices, including a high degree of isolation between input and output, which significantly reduces alignment time, a major contributor to amplifier cost.

Thus, the greatest advantage of GaAs FET amplifiers is likely to be in the area of cost. Today, GaAs FET amplifiers can be built at a cost that is competitive with amplifiers using more established technologies, in spite of the fact that GaAs FET technology is relatively new.

Currently, at least five manufacturers offer low-noise GaAs FETs, and some five amplifier manufacturers claim catalog GaAs amplifiers. Most of the commercially-available amplifiers provide broad bandwidths to 10 GHz, or narrow bandwidths to 12.4 GHz. This article will discuss the design approach to an amplifier which covers the entire X-band (8.0 to 12.4 GHz). Using available devices, it's possible to build an amp that covers this band with 6.5 dB maximum noise figure and +10 dBm power output at 1 dB compression.

Martin G. Walker, and **Fred T. Mauch,** Members of the Technical Staff; **Thomas C. Williams,** Engineer; Watkins-Johnson Company, 3333 Hillview Avenue, Palo Alto, CA 94304.

Model the device

There are many references[1,2] on the design of broadband amplifiers which can provide a basis for a viable X-band circuit. Since all these methods begin with the premise that an accurate device model is known, the first step is to characterize the active device accurately for noise and gain parameters, and thus, develop an appropriate device model. Care must be taken to perform these measurements in the actual environment that the device will eventually be operating in. Any bonding wires, ground plane discontinuities and bias components must be included. Obviously, the s-parameters of a packaged device in an air-line test fixture will be of little value to the designer of a microstrip amplifier using unpackaged devices.

At Watkins-Johnson Company, the authors use a test fixture that consists of a housing with SMA to microstrip launchers and a test carrier on which the device is mounted. The cavity is designed to be of the same width as the proposed amplifier, which is always less than a quarter-wave wide at the highest operating frequency to prevent spurious, non-TEM modes from propagating laterally and causing unwanted feedback and instabilities. SMA to microstrip launchers must be selected with care so that a reproducible, low VSWR transistion is provided. All connectors should be tested back-to-back launching onto microstrip to insure that all transitions are adequate. In general, a reflection coefficient of 0.05 or less is required to keep connector errors with test equipment error.

It is strongly recommended that the designer not rely on connector manufacturer's guarantees or specifications, but carefully measure the transition reflection magnitudes which are unique to the particular mechanical fixture design. Phelps-Dodge PDM 971 connectors were employed for the subject measurements.

Using the test fixture described above, a number of devices from different manufacturers were characterized for gain and noise parameters in the 8.0 to 12.4 GHz band. The devices were measured on an HP 8545A automatic network analyzer, then de-embedded to remove test fixture errors and provide parameters referenced to the input and output planes of the device. Of course, when de-embed-

(continued on pg. 38)

A note on noise

A two-port device can always be characterized by a generalized scattering matrix as defined by Kurakuwa. If the device is unilateral ($S_{12} = 0$ and $S_{11} < 1$) the maximum available gain can be realized by providing the positive real part generator source and load, given by S^*_{11} and S^*_{12}.

If $S_{12} \neq 0$, then the positive real source and load for maximum gain are not so easily determined. Bodway‡ defines V_{m1} and V_{m2} as the source and load that will conjugately match the device, thus, achieving the maximum available device gain. V_{m1} and V_{m2} are only less than unity if a parameter, which he defines as k, is greater than unity.

The source for optimum noise figure, Γ_{on} is defined from

$$F = F_{min} + 4r_n \frac{|\Gamma_s - \Gamma_o|^2}{(1-|\Gamma_s|^2)(1-|\Gamma_o|^2)}$$

where F_{min} = minimum device noise figure
Γ_s = generator impedance
Γ_o = source impedance for minimum noise figure
r_n = noise resistance

‡G. W. Bodway, "Two-Port Power Flow Analysis Using Generalized Scattering Parameters", Microwave Journal, (May, 1967).

(continued from p. 36)

ding the device, care must be taken to include only the parameters which are peculiar to the test fixture, and not effects of the device-mounting techniques.

Devices should not only be evaluated on such performance data as G_{max} and F_{min}, but also on the reproducibility of R_{m1} and R_{m2} and Γ_{on} (see box). In device-to-device variation, these parameters limit electrical performance of a particular design more than small differences in absolute device performance characteristics. In addition, the decrement, δ^1, at the band center, is a good indicator of the difficulty of designing a broadband amplifier gain stage. At the time the work on this design was initiated, there was only one device available in production quantities with available gain and noise figure required for X-band designs, the one-micron gate NEC V244. Today, however, the designer is free to choose from several available devices.

Upon completion of the device selection and characterization phase, several circuits were explored to provide either maximum gain or minimum noise figure, using techniques described by Matthaei[1] for matching circuit synthesis. (There are now many more recent references available for the design of broadband circuits[2,3]). The design procedure begins by using these methods to derive optimum values for the various circuit elements. Computer optimization is

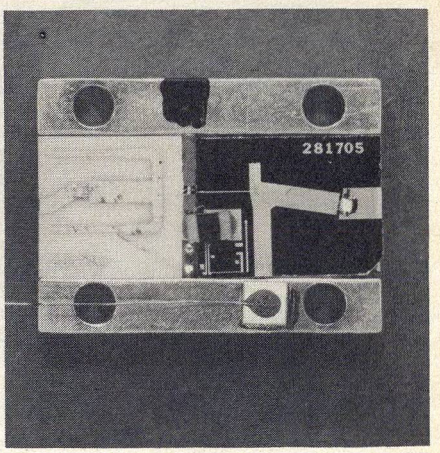

1. This single-ended gain stage illustrates the use of dual substrates. Alumina, to the left of the device, accommodates low-impedance lines while fused silica, on the right, is fine for high-impedance networks. The GaAs FET is die-attached to the carrier between the substrates.

(continued on pg. 40)

Self-biasing circuit eliminates negative supply

Early GaAs FET amplifiers had one inconvenient drawback when compared to other transistor amplifiers. Due to the nature of its N-channel structure, the FET required both positive and negative power supplies. In order to properly bias the FET, the dc gate bias, V_{GS}, must be less than zero. Thus, if the source is at dc as well as rf ground, a negative power supply is required.

It has since been learned, however, that a simple self-biasing circuit commonly used for junction field-effect transistors (JFETs) at low frequencies can be realized for X-band applications (see figure). Note that the parallel R-C circuit connecting the source to ground provides dc isolation while simultaneously providing an effective rf ground. Thus, the dc source potential can float above the gate potential, (dc ground) and only a positive bias is required. Element valves are typical for the NECV 244.

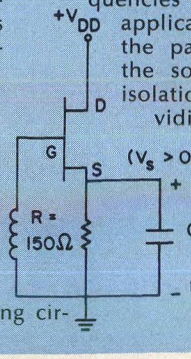

(continued from pg. 38)

then used to fine tune each element to meet the modeled device specifications. COMPACT[4], available on several timesharing services including UCS and Tymshare, will adequately serve this purpose.

Try two substrates

After computer optimization, the next task is to realize the circuit elements of the optimized values to form a gain module (Fig. 1). The main challenge of this task is to find circuit geometries which are realizable on microstrip and at the same time, do not deviate from the desired values. Simultaneously realizing the high-impedance transmission lines required at the output and first element of the input, while reproducibly achieving the low-impedance shunt stubs and series lines required at the input is a general problem in GaAs FET design.

For example, the technique outlined in Matthaei's text[1], requires a short circuited quarter-wave shunt stub of very low characteristic impedance (typically 10 ohms). This is difficult to realize, even on alumina, and must be approximated by using two half-wave open circuit stubs, as shown in Fig. 1.

A quite different problem is encountered in trying to realize the high-impedance lines required to match the GaAs FET's output. After considerable experimentation, a technique for combining two dif-

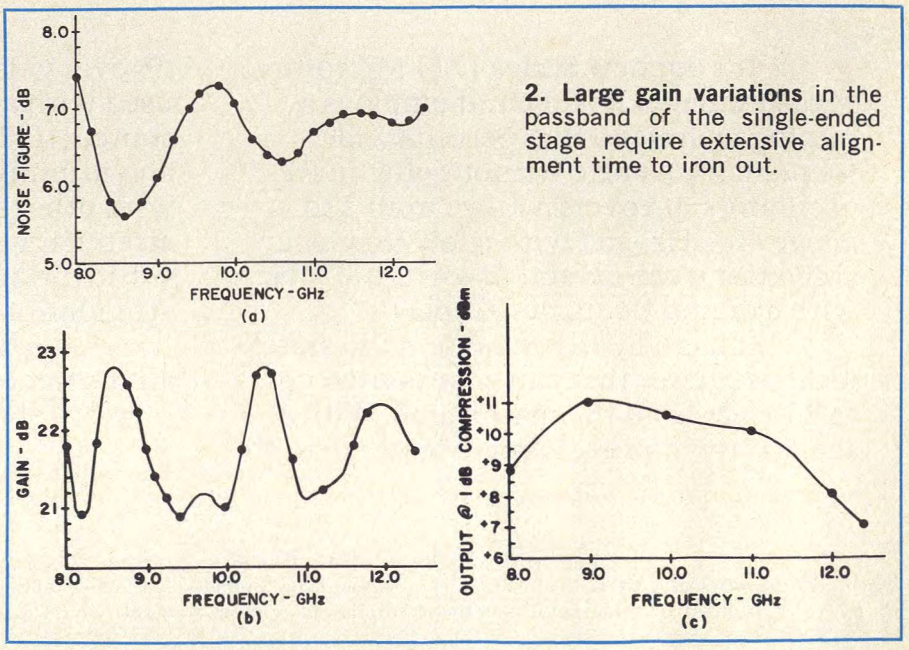

2. Large gain variations in the passband of the single-ended stage require extensive alignment time to iron out.

ferent substrates on the same carrier has been developed to ease this problem: Alumina is used at the input, and fused silica at the output. Since fused silica has a dielectric constant of 3.8 compared to the alumina dielectric constant of 9.8, a transmission line of a given width will have a characteristic impedance which is approximately 1.6 times higher on fused silica. The unpackaged device is then die attached directly to the carrier, between the substrates, as shown in Fig. 1.

A single-ended gain module, such as shown in Fig. 1, exhibits acceptable performance levels (7 dB gain, 6.5 maximum noise figure) but was found to require extensive alignment time. Thus, consideration must be given to a balanced amplifier approach.

Balanced or single-ended?

A balanced approach[5] using quadrature hybrids allows the construction of gain blocks which are easily cascadable, and, due to low VSWR, require little alignment. However, twice as many GaAs FET devices must be used to achieve a given amount of gain. This increases both material and assembly costs per module. In addition, since two parallel gain modules must be used, it becomes difficult to keep cavity width to less than a quarter of a wavelength, inviting spurious modes to propagate.

On the other hand, a single-ended module costs about half as much to fabricate as a balanced unit and the reduced width significantly simplifies packaging problems. Since half the devices are used, the critical part count decreases, reliability improves and total power dissipation decreases. In addition, slightly higher gain per stage is realized since quadrature hybrid losses are eliminated.

To investigate the attractive advantages of a single-ended approach, three amplifiers with signal-ended stages were fabricated and aligned. It was discovered, however, that due to minor variations in individual GaAs FET devices, interstage mismatches causing large gain variations were still present in the passband after normal alignment (Fig. 2). This confirmed initial suspicions that excessive alignment time is necessary. In addition, alignment time did not decrease from unit to unit; i.e., there was no significant learning curve.

Therefore, we conclude that the

(continued on pg. 44)

X-BAND FET AMPLIFIER

(continued from p. 41)

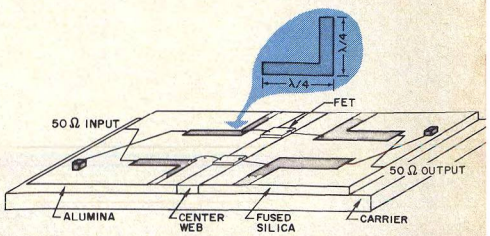

3. A balanced approach reduces alignment time, but presents packaging problems. For the NEC 244, input matching lines have a characteristic impedance of about 30 ohms, while the output series lines are approximately 150 and 70 ohms. Hybrids are formed with 50 ohm lines. Biasing elements are not shown.

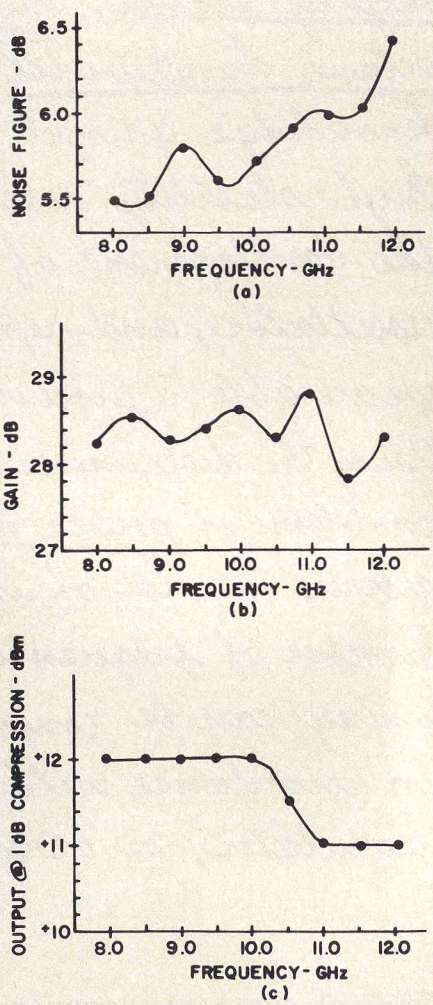

4. A cascade of five balanced modules, built with ten GaAs FETs, can provide 28.5 dB gain with a noise figure of less than 6.5 dB from 8.0 to 12.4 GHz.

most manufacturable X-band GaAs FET amplifiers with wide bandwidths are based on a balanced design, as shown in Fig. 3. The performance of five cascaded modules is shown in Fig. 4.

Performance rivals TWTs

For broadband applications, the major existing alternatives to the GaAs FET amplifier are the traveling-wave tube and tunnel-diode amplifier. The GaAs FET amplifier offers at least as low a noise figure as do these alternatives. A typical noise figure for an X-band TWT is 7 dB, degrading to 10 dB for PPM focused TWTs. The saturated output power of these units is typically 10 to 20 dB below the 1 dB compression point of a GaAs FET amplifier. Thus, the dynamic range of the GaAs FET amplifiers is superior. Although output power of TDAs can be improved by adding a Gunn effect gain stage, the input compression point is still considerably below the GaAs FET amplifier.

With at least two government sponsored R&D programs in the area, Ku-band GaAs FET amplifiers will be on the scene shortly. Already, very small quantities of the NEC V388, one-half micron GaAs FET devices, are available. This device is expected to allow fabrication of full Ku-band amplifier by late 1975 or early 1976.

Finally, because of improved performance and simpler construction, it is also likely that GaAs FET amplifiers will be found in space applications on flights scheduled after 1977, by which time GaAs FET amplifiers will have demonstrated high reliability. ••

References

1. Matthaei, Young and Jones, *Microwave Filters, Impedance Matching Networks and Structures*, McGraw-Hill, (1964).
2. W. H. Ku, W. C. Peterson and A. F. Podell, "New Results on the Design of Broadband Microwave Bipolar and FET Amplifiers," IEEE International Microwave Symposium Digest Technical Papers, p. 359, (June, 1974).
3. D. J. Mellor and J. G. Linvill, "A Complete Computer Program for the Synthesis of Matching Networks for Microwave Amplifiers," IEEE International Microwave Symposium Digest Technical Papers, p. 199, (May, 1975).
4. Les Besser, *COMPACT User Manual*, available from United Computing Systems, Version 3.3, (April, 1975).
5. J. A. Eisenberg and R. I. Disman, "Design a 4.0 to 8.0 GHz FET Amplifier with a 7 dB Noise Figure," *MicroWaves*, Vol. 12, No. 2, pp. 52-56, (February, 1973).

Acknowledgements

The authors wish to acknowledge the technical contributions of Dale Harpster, Bob DeBoo*, John Eisenberg* and Pete Jorgenson.
*Now with Ancom

CAD Simplifies Gunn Amp Design

Achieving a desired gain response can be tricky in designing broadband reflection-type amplifiers. This computer-aided approach optimizes matching circuits to overcome circulator mismatch effects.

RECENT improvements in the performance of Gunn diodes have made possible the design of negative resistance amplifiers with increased power, gain and bandwidth.[1,2] In fact, newer materials, such as Indium Phosphide, offer even higher gain and lower noise—8 dB gain and 8 dB noise figure for a 1 GHz bandwidth InP amplifier stage at 15 GHz was recently reported.[3] This potential for higher gain, however, has only aggravated the design complexity of reflection amplifiers because it now becomes more important than ever to control the gain response shape and the inherent temperature sensitivity and rf instabilities that may occur. The negative resistance of the diode that provides the desired gain, when properly biased, can also easily cause unwanted oscillations both within and outside the passband of the amplifier.

Contrary to transistor power amplifier design, where the engineer can usually refer to published tables for impedance transformations and matching, very little "handbook" help is available when dealing with negative resistance devices. One alternative for simplifying a diode amplifier design is the time-share computer which can provide both analysis and optimization. The computer can, among other things, derive a model for the diode, analyze the circuit for potential oscillation, evaluate alternative circuits without having them built and examine the gain response for "glitches" that are frequently associated with diode amplifiers (caused by the interaction between the diode and resonant circuit elements). The computer does not yet relieve the engineer from selecting the basic circuit configuration and components (although we may not be very far away from that either) but it frees him from doing lengthy complex calculations so that he can spend his time on the more critical aspects of his job.

This article centers on one of the more complicated segments of negative resistance amplifier design—achieving the desired gain response. Computer work is performed through commercial time-sharing on United Computing System's CDC-6400 computer, using a general purpose microwave optimization program, Compact.[4,5,6] The goal is to design a diode amplifier stage with at least 7.5 dB gain and less than 0.25 dB ripple between 7 and 10 GHz.

Evaluate the diode first

In a reflection amplifier, Fig. 1, the input signal is applied to port 1 of the circulator which transfers the power to the diode network connected to port 2. If the reflection coefficient of the diode network, Γ, is greater than unity, the incident power is amplified and coupled out at port 3.

The appropriate computer-aided design procedure is usually carried out in two parts. First, the reflection coefficient of the diode network is equalized for a constant magnitude. Then, the complete circuit, including the circulator, is optimized for the required overall gain response. In both optimizations, the transmission lines are assumed to be lossless striplines although the self-inductance of a 1 pF coupling capacitor (0.5 nanohenry) is included in the computation.

For this design, an STL-A230 Gunn diode, manufactured by Standard Telecommunications Laboratories, Harlow, England, was selected although other manufacturer's devices are suitable. The reflection coefficient of the diode is measured and the data is stored in the computer's data file for easy access. For this particular diode, the reflection coefficient peaks around 9.5 GHz (Fig. 2), with a 9 dB magnitude. As was expected, the rolloff at the lower frequencies result in a 7 dB slope which is not acceptable for broadband applications. The frequency response can be improved by transformations using series sections of quarter-wave transmission lines. It is important to realize, however, that

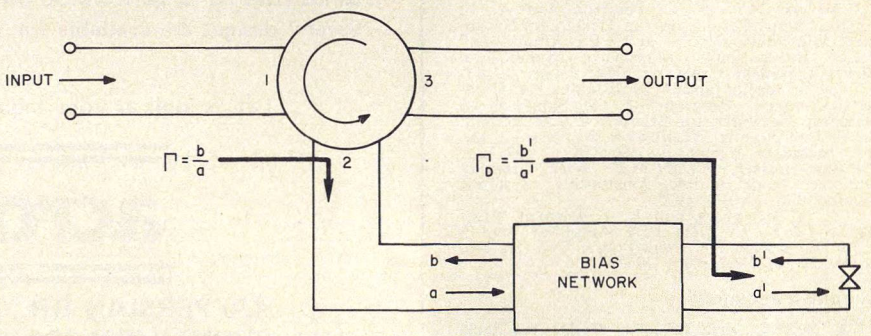

1. **Reflection amplifier** uses the negative resistance of a diode for amplification. The circulator separates the incident and reflected waves at port 2.

Les Besser, Group Head, Microcircuit Department, Farinon Electric, 935 Washington Street, San Carlos, CA 94070.

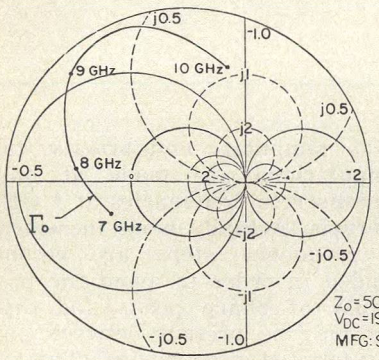

2. **Reflection coefficient of the Gunn diode** used in this design shows a strong peak of the magnitude near the center of the band.

the diode impedance is not being matched to the 50-ohm source and load. The objective of the transformation is to maintain uniform magnitude of the reflection coefficient across the desired frequency range.

The first task is to determine the required number of transmission line sections and to assign initial values to each section. Although optimization helps in finding the optimium component values, the search may fail to converge or it may converge to a "local minimum"[6] instead of the "global minimum" if the initial values are poorly chosen. Typically, the engineer is required to perform some Smith-Chart manipulation to approximate the initial component values.

Compact™ can also assist in this task. It has two different types of optimization routines; a coarse search to find the vicinity of the global optimum and a more efficient gradient type search to find the exact location of the optimum.

The details of the time-shared operation of the Compact program

(continued on pg. 48)

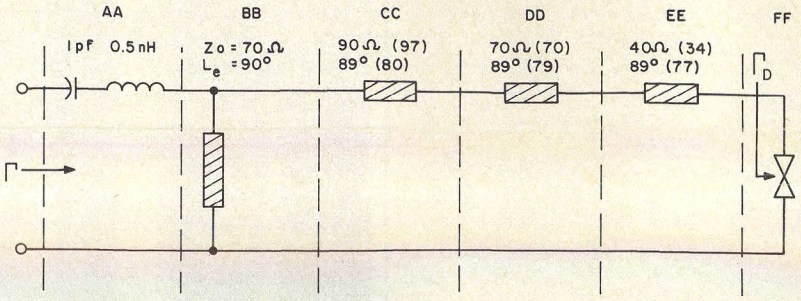

3. **Schematics of the diode network** shows component values. Those in parenthesis represent optimized values. All transmission line lengths are specified at 8500 MHz.

(continued from pg. 47)

are described in its users manual.[7] (Copies are available by circling **Reader Service No. 159).** The program accepts circuit description either by "two port" or "nodal" type interconnections. A reflection amplifier can be described either way, however, the two-port description is the more efficient one and it is used in the example.

Diode network design

The 3 GHz bandwidth and 0.25 dB maximum ripple specifications require a three-section quarter-wave transmission line network to be cascaded with the diode. The program's coarse optimization, not shown here, results in the initial circuit shown in Fig. 3. Both the impedances and the lengths of the transmission lines will be varied during the optimization. In addition the series lines, a quarter-wave (at 8.5 GHz) short-circuited stub is used to apply the dc bias to the diode. The 1 pF coupling capacitor mentioned earlier serves to block the dc voltage from the source.

Each component is defined as a two-port; the two-ports are cascaded and terminated by a one-port which represents the active device. The objective of this optimization is 8 dB gain from 7 to 10 GHz. As such, the error function to be minimized by the computer is defined as:

$$\text{ERR. F.} = \frac{1}{4}\sum_{\text{f-7,000 MHz}}^{\text{f-10,000 MHz}} 10\cdot(20\cdot\text{Log}(|s_{11}|)-8.0)^2$$

where the 1/4 factor is the frequency normalization and 10 is an arbitrary multiplier or weighing factor.

For simplicity and brevity, the computations are made at only four discrete frequencies at 1 GHz intervals. Actually more incremental frequency steps are recommended in order to avoid the possibility of sharp peaks and dips that may be present between any two selected frequencies. This is particularly true when the diode circuit must provide more than 10 dB gain.

The Compact data file corresponding to the initial diode network is given in Fig. 4. The associated computer optimization run is shown in Fig. 5. Note that the initial value of the error function

(continued on pg. 51)

```
SLC AA SE .5 1
SST BB PA 70 90 8500
TRL CC SE -90 -89 8500
TRL DD SE -70 -89 8500
TRL EE SE -40 -89 8500
ONE FF IR 50
CAX AA FF
PRI AA IR 50 0 0
END
7000 10000 1000
END
1.34 -161
1.80 175
2.82 136
2.29 74
END
.002
0 0 10 8
END
```

4. **Data file of the diode network.** The first eight lines define and interconnect the components and specify the print format. The diode reflection coefficients are given in polar form at each frequency.

```
                CIRCUIT OPTIMIZATION WITH  6 VARIABLES

 INITIAL CIRCUIT ANALYSIS:

INPUT REFL. COEF. AND VSWR IN   50 OHM SYSTEM WITH     0.  OHM LOAD

  F(MHZ)          RHO(MAGN.&ANGLE)          VSWR    RETURN LOSS/GAIN (DB)

 7000.000        1.795        118.9                        5.08
 8000.000        1.727         22.0                        4.75   BEFORE
 9000.000        4.541        -61.5                       13.14   OPTIMIZATION
10000.000        1.910         70.8                        5.62

OPTIMIZATION BEGINS WITH FOLLOWING VARIABLES AND GRADIENTS

     VARIABLES:                    GRADIENTS:

  ( 1):    90.000              ( 1):  -639.091
  ( 2):    89.000              ( 2):  1138.112
  ( 3):    70.000              ( 3):   714.895
  ( 4):    89.000              ( 4):  1613.872
  ( 5):    40.000              ( 5):  -775.531
  ( 6):    89.000              ( 6):   931.804
 ERROR FUNCT.= 128.059
      -----****-----
HOW MANY ITERATIONS BEFORE NEXT STOP?"0" WILL RESULT FINAL ANALYSIS
WANT INTERMEDIATE PRINTS?(YES="1",NO="0") TYPE 2 NUMBERS ? 10 0

  ( 1):    97.194              ( 1):     .038
  ( 2):    80.752              ( 2):    2.040
  ( 3):    70.291              ( 3):    -.028
  ( 4):    79.115              ( 4):    3.107
  ( 5):    34.005              ( 5):     .626
  ( 6):    77.527              ( 6):    1.713
 ERROR FUNCT.=    .002
      -----****-----
FUNCTION TERMINATION WITH ABOVE VALUES. FINAL ANALYSIS FOLLOWS

 7000.000        2.512        -96.3                        8.00
 8000.000        2.507         39.2                        7.98   AFTER
 9000.000        2.518        -42.4                        8.02   OPTIMIZATION
10000.000        2.512        167.2                        8.00
```

5. **Optimization printout of the diode network.** In ten iterations, the error function is reduced by a factor of 64,000. The CPU cost is about $9.

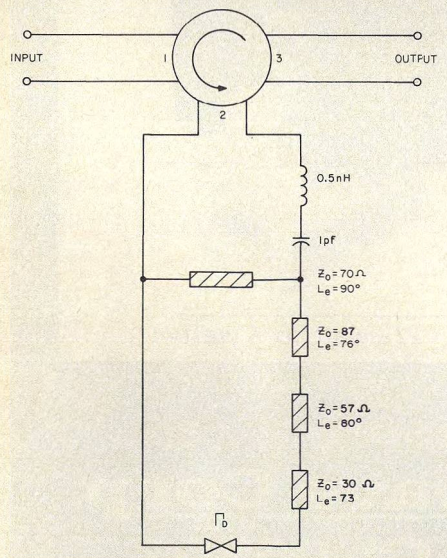

6. **Circuit diagram of the complete amplifier stage.** The final optimization has reduced the initial 2 dB slope to less than 0.25 dB.

(continued from p. 48)

(ERR. F.) has a value of 128 which corresponds to an 8.4 dB gain slope. After 12.5 seconds of optimization, the error function is reduced to 0.002, corresponding to a 0.02 dB gain ripple between 7 and 10 GHz.

Add the circulator and optimize

The next step is to add the circulator to the diode network. The circulator is first characterized by its measured three-port scattering parameters. In this case, an HP-8410 network analyzer was used to provide three separate sets of two-port measurements. In the computer analysis, the circulator is reduced to a two-port by terminating the additional port by the diode network, Fig. 6.

One may expect that adding the circulator would not change significantly the response of the diode network. However, even though the circulator has low VSWR, its interaction with the diode network causes the ripple to increase to 2 dB across the passband. Therefore, a final optimization is needed.

To allow for losses caused by the addition of the circulator, the tar-

(continued on pg. 53)

CAD DESIGN

POLAR S-PARAMETERS IN 50.0 OHM SYSTEM

F MHZ	S11 (MAGN)ANGL)	S21 (MAGN)ANGL)	S12 (MAGN)ANGL)	S22 (MAGN)ANGL)	S21 DB	K FACT.
7000.0	(.06< 22)	(2.35< 76)	(.965< 93)	(.11< 37)	7.43	1.35
8000.0	(.11<-129)	(2.34< -11)	(.958< -13)	(.11<-101)	7.37	1.35
9000.0	(.11< 116)	(2.40< 60)	(.985<-117)	(.13< 126)	7.59	1.38
10000.0	(.18< 132)	(2.37< 115)	(.978< 140)	(.18< 112)	7.50	1.33

7. **Final analysis of the complete circuit.** Note the significant magnitudes of s_{12} which may cause strong interaction between the input and output.

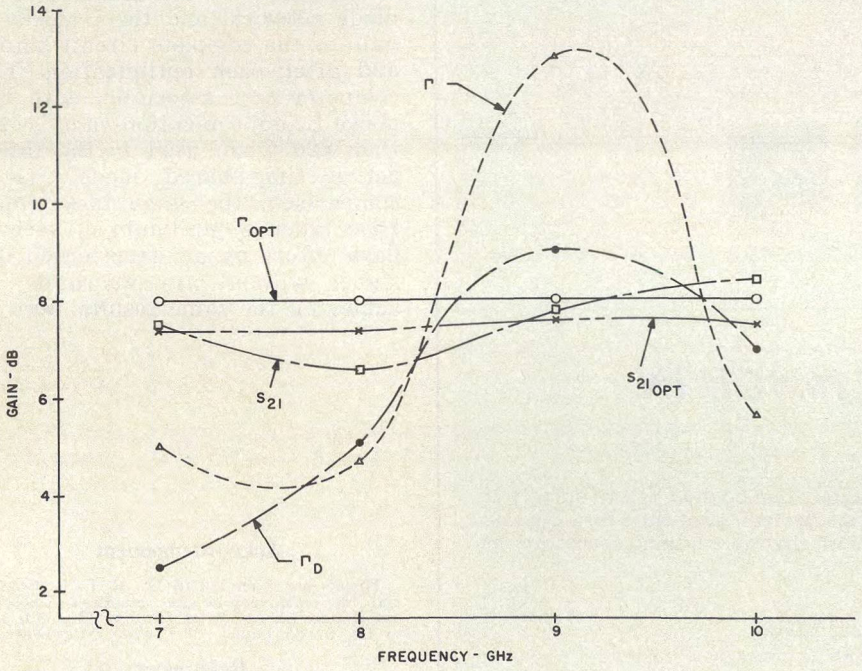

8. **Gain response of the diode** (Γ_D), the diode network (Γ and Γ_{OPT}) and the overall circuit (s_{21} and $s_{21_{OPT}}$) before and after optimization.

(continued from p. 51)

get gain between port 1 and port 3 of the complete circuit is set to 7.5 dB. The error function is the following:

$$\text{ERR. F.} = \frac{1}{4}\sum_{\text{f-7,000 MHz}}^{\text{f-10,000 MHz}} (|s_{21_{dB}}| - 7.5)^2$$

This time Compact reduces the error function from 0.411 to 0.008 (optimization not shown). A further reduction could still be obtained but the response of the amplifier is already flat within 0.25 dB, Fig. 7. The variables are changed less than 1% during the last iteration of the optimization. Therefore, for practical purposes, the optimum has been reached.

One of the points to observe is the large s_{12} term of the overall two-port, Fig. 7, due to the circulator action. The near unit magnitude should serve as warning of a strong interaction between the input and output ports. This becomes particularly important when several stages are cascaded for higher gain. In this case, another optimization may be required for the multistage circuit.

Since the stability factor, k, is greater than unity, the circuit is unconditionally stable in the passband of the amplifier. Of course, this does not assure that the circuit is unconditionally stable for all frequencies and the complete design should also include stability analysis outside of the passband.

Another recommended step is the simultaneous optimization of the circuit through several different operating temperatures—this operation can be performed with Compact by describing the diode at selected temperatures and combining the errors contibuted. The cir-

(continued on pg. 54)

CAD DESIGN

(continued from pg. 33)

cuit is then optimized until the cumulative error is minimized.

Computer optimization's power can really be appreciated by comparing the amplifier response during the various phases of the design cycle. Figure 8 shows the reflection gain of the diode and the diode network, and the transducer gain of the complete circuit before and after each optimization. The computer cost associated with the above two optimization runs is less than $20 when used in the interactive time-shared mode. As a comparison, the same task would have taken a minimum of several days' effort by an experienced designer without any guarantee of achieving the same results. ••

Acknowledgement

Thanks are extended to Dr. R. F. B. Conlon and his colleagues at the Standard Telecommunication Laboratories, Harlow, England, and to Dr. Ferdo Ivanek of Farinon Microwave.

References

1. B. S. Pearlman, "Cw Microwave Amplification from Circuit Stabilized Epitaxial GaAs Transferred Electron Devices," *IEEE ISSC Conference*, Session 11.5, pp. 136-137, (February, 1970).
2. A. S. Clorfeine, A. Rosen, J. Reynolds, "Wideband High Power Trapatt Circuits," IEEE ISSC Conference Session 9.3, pp. 96-97, (February, 1974).
3. R. M. Corlett, et al., "A Low-Noise Indium Phosphide Reflection Amplifier," *European Microwave Conference*, (September, 1975). Session C-10.3.
4. L. Besser, E. Ghoul and C. Hsieh, "Computerized Optimizational Transistor Amplifiers and Oscillators Using Compact," 1973 European Microwave Conference, Session A12.3. (September, 1973).
5. L. Besser, "Use Computer As Tool For Rf Circuit Design," *Microwave Systems News*, Vol. 4, No. 1, pp. 104-108, (February, 1974).
6. S. Ghoul, L. Besser and C. Hsieh, "Design A High Power S-Band Doubler," *Micro-Waves*, Vol. 13, No. 6, pp. 58-65, (June, 1974).
7. Compact User Manual, available from Tymshare, Inc., of Cupertino, CA; United Computing Systems of Kansas City, MO; National CSS of Stamford, MA and Computility, Inc., Boston, MA.

Test Your Retention

1. Why is the input of the diode circuit not matched to the circulator?
2. The overall single stage circuit has very low input/output VSWR. Why then would cascaded stages have possible gain ripple problem?

GaAs Impatts Boost Power and Efficiency

GaAs Impatt diode technology is maturing. Here is an overview of the various structures and heat sinking techniques being used to improve output power, efficiency, and reliability.

IMPACT Avalanche Transit Time or Impatt devices are well known for achieving high output powers. In the last two years, high efficiencies have also been obtained with certain types of Gallium Arsenide structures. For example, more than 35% cw efficiency has been reported in X-band[1,2] and efficiencies up to 46% are theoretically feasible[2]. Cw power outputs as high as 12.5 watts have also been observed[3]. Increased reliability of these high efficiency GaAs units has been achieved by improving the life times by a factor of 100 to 1,000. Median failure times of 10^7 hours at 240°C junction temperature are currently being predicted by accelerated life test studies[4]. These unique capabilities of Impatt diodes create many exciting system applications:

- Communications: High power, high efficiency solid-state injection locked oscillators using Impatt diodes are useful for high data rate fm transmitters in C, X and Ku-bands.
- Radar: Impatt oscillators and amplifiers find application in doppler radars or phased array radar transmitter modules.
- Amplifiers: Although the Impatt mechanism is inherently noisy compared to transferred electron devices or field-effect transistors, noise figures in the 30 dB range can be achieved. Impatt amplifiers or injection-locked oscillators can thus be used as rf power amplifier stages. Bandwidths, while narrower than those obtained by Gunn and FET amplifiers, are typically on the order of 20%, which is adequate for many power amplifier applications.
- High Power Transmitters: Much higher output powers can be achieved by power combining techniques. As many as 16 Si Impatt diodes have been combined for a total power output of 20 W[5]. The ultimate limitations are determined by circuit design, device impedance and thermal dissipation.

Stephen I. Long, Senior Engineer, **Robert E. Goldwasser,** Senior Engineer and **Ferenc E. Rosztoczy,** Manager, GaAs Microwave Materials and Devices, Varian Associates, 611 Hansen Way, Palo Alto, CA 94303.

Silicon or GaAs/double or single drift

Both silicon and GaAs have been widely used for Impatt devices. Operation of germanium devices has also been demonstrated but offers no advantages and several disadvantages over the other two materials.

The relative merits of Si and GaAs are contrasted in Table 1. The main advantage of silicon over GaAs is the lower production cost. If 7 to 9% efficiency and the corresponding power limitations are adequate for the circuit or system requirement, silicon Impatt diodes would be the best selection. If higher efficiencies and maximum available solid-state power are necessary, then GaAs devices are the only alternative. The reliability of GaAs Impatts is now considered comparable to that of silicon[4].

There are several different device structures which are commonly used for GaAs Impatts. These fall generally under the categories of single drift (SD) or double drift (DD) devices. Figure 1(a) shows a conventional flat profile, single drift X-band device. To complete the SD device, a barrier (either metal or p^+ epitaxial) must be added to form a junction. The electron-hole pairs, generated by the avalanche at the junction, drift with the electric field. The holes immediately recombine in the barrier region, while the electrons are swept through the drift region contributing a transit time delay required to form a negative resistance.

A flat profile double-drift device, Fig. 1(b)[6] has both its holes and electrons drift away from the junction in opposite directions. This dual drift phenomena contributes to the net negative re-

(continued on p. 60)

Characteristics of Si and GaAs Impatt devices

	Silicon	Gallium Arsenide
Technology	Well established for about 25 years	Much more complicated material technology-established for about 10 years
Efficiency	Up to 14% Typical 7%-9%	Up to 35.6% Typical 20-25%
Power Capability	Higher thermal conductivity but lower efficiency than GaAs.6.8 W reported [7]	12.5 W CW reported Powers much higher than Si are expected due to higher efficiency
Reliability	Good; $> 10^7$ hours at 200°C has been reported	Good for p-n junction devices (10^7 hours at 240°C); poor for Schottky barrier—about 10^5 hours at 175°C.
Cost	Moderate, about $25-$200/device	High, about $50-$500/device
Bias oscillations	Easily stabilized	Much more tendency toward bias oscillation than Si
Noise	Flat profile has 8 dB higher noise measure than GaAs.	Theoretical noise measure increases with efficiency

GaAs Impatts

(continued from p. 56)

sistance because the electric field extends into both the flat profile p and n regions. These devices are theoretically capable of higher power, efficiency and impedance than an SD device. Theoretically calculated and experimentally demonstrated rf performance capabilities of SD and DD flat profile devices are summarized in Table 2.

High-efficiency Impatt structures, also referred to as modified Read structures (after the original paper by Read in 1958[8]), operate with a maximum voltage drop across the drift region in order to increase dc to rf conversion efficiency. This is accomplished by dropping the electric field in a very short, heavily doped layer (0.2-0.5 μm) at the barrier interface, thus confining the avalanche region. Two structures commonly used are the n-n$^+$-n or the "lo-hi-lo" Impatt structure of Fig. 2(a) or the n$^+$-n or "hi-lo" structure in Fig. 2(b). Greater than 35% has been achieved with Schottky barrier "lo-hi-lo" structures[1,2] and 31% with Schottky "hi-lo" strucures[3] as shown in Table 2. Again either metal Schottky barriers or p$^+$ epitaxial layers must be added at the surface to create the junction.

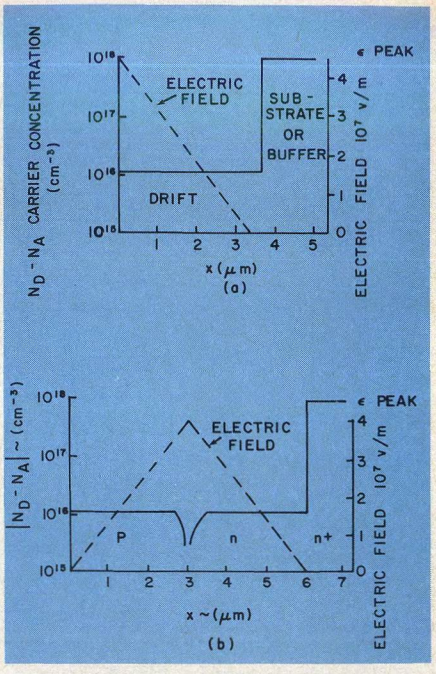

1.(a) **Doping profile and electric field profile** (dotted lines) of an X-band, flat profile, GaAs Impatt shows how electron hole pairs drift with the electric field. (b) A double drift device has both holes and electrons that drift away from the junction in opposite directions.

Efficiency and power output capabilities of GaAs Impatt structures

Structure	Calculated Efficiency*	Experimental Efficiency	Experimental RF Output (W)
Flat Profile:			
single drift	16.6%	13%	8 W [10]
double drift	23 %	16.3%	3.25 [11]
High Efficiency SB			
hi-lo	42%	31.4%	12.5 [3]
lo-hi-lo	46%	35.5%	8 [1]
Grown Junction			
double drift hi-lo p$^+$	39%	22%	4.4 (peak)
hi-lo		26.8%	8 (peak)

*Efficiencies were calculated using an Impatt device modeling program by Decker [12].

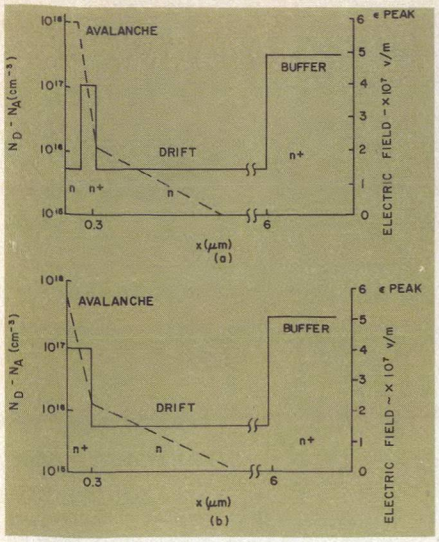

2(a). **Doping and electric field profile** (dotted lines) of an X-band, "lo-hi-lo" GaAs Impatt are designed to have a maximum voltage drop across the drift region. Efficiencies to 36% can be achieved. (b) Slightly less efficiency (31%) can be achieved with a "hi-lo" GaAs Impatt structure.

Schottky-barrier devices are capable of higher output powers and efficiencies because of their better thermal conductivity and lower series resistance. Also, minority carrier injection effects, which theoretically will limit efficiency, are not present[9].

Double-drift high efficiency structures have also been made by growing an epitaxial p-type layer on the hi-lo" or "lo-hi-lo" structures. This provides some efficiency improvement over the conventional flat profile DD device. Rf performance data for these devices and the Schottky barrier/p^+ barrier single drift high efficiency devices is given in Table 2.

From the doping profiles, it can be seen that very precise metallurgical and electrical tolerances must be maintained for high-efficiency performance. The layer thickness and carrier concentration of the avalanche region (n^+ or n-n^+) are particularly critical in the "hi-lo" and "lo-hi-lo" devices. A small change in the net charge or Q or this region has a strong effect on the electric field profile and hence, the voltage. Q control to $\pm 0.05 \times 10^{12}$ cm^2 is required.

The sensitivity of the device to small changes in the avalanche region parameters encourages potential reliability limitations due to metal migration of the Schottky barrier. The most widely used barrier material for these purposes has been platinum. Unfortunately, Pt rapidly interdiffuses with GaAs at temperatures as low as 175°C[13]. This diffusion will result in a mean lifetime of only 1,000 hours at 225°C junction temperature and 10^5 hours at 175°C for a Pt barrier "lo-hi-lo" or "hi-lo" diode. No other metal barrier material has been reported which has less reactivity than Pt yet still maintains sufficient barrier height and adherence.

Use of a germanium doped p^+ grown junction, rather than the metal Schottky barrier, eliminates the diffusion problem. The diffusivity of Ge in GaAs is very low, even at high temperatures. High efficiency GaAs Impatt devices using p^+ epitaxial on "hi-lo" or "lo-hi-lo" structures have provided a very significant improvement in reliability with only moderate reduction in efficiency. As high as 26.8% efficiency with 8 W peak output in X-band has been obtained under 25% duty cycle pulsed operation. The cw efficiency is 18.8% at an output of 2.9 W for these structures.

Results from accelerated life tests for four sample groups of diodes at four temperatures, 290°, 300°, 330° and 350°C, are summarized in Fig. 3. Premature failures due to rapid surface leakage degradation roughly 30% of the sample) were statistically removed to indicate the true capability of the grown junction device. Extrapolation to 222°C, more typical operational junction temperature, predicts a 10^6 hour median failure time—over three orders of magnitude greater than Pt devices at the same temperature.

Germanium doped p^+ junction devices have also been tested under dc bias at 7 to 10 watt power dissipation levels for extended time periods. No failures related to device degradation have been observed after 7,500 hours of testing. The comparison between Schottky barrier and grown junction GaAs high efficiency Impatts is summarized in Table 3.

Minimizing thermal resistance

Since the device reliability is always dependent on the operational junction temperature, it's important to minimize thermal resistance. For any device structure, this is best accomplished with good heat conduction away from the junction. Thermal resistance can be calculated from

(continued on p. 62)

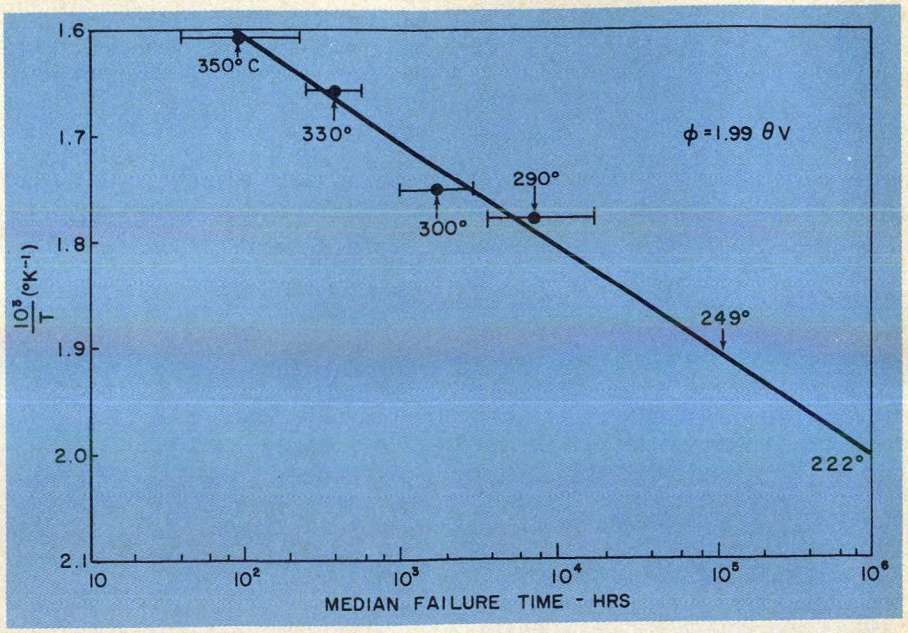

3. **Median failure time (MTTF** is shown here for P⁺-N⁺-N sample diodes measured at accelerated junction temperatures of 290°, 330° and 350°C. Extrapolation to the typical junction temperature of 256° predicts 10^6 hours of life.

Pt Schottky barrier vs. grown junction GaAs

	Pt Schottky Barrier	p-n Junction
Fabrication	Simple evaporation	More difficult, epitaxially grown junction
Efficiency	Up to 35.6% observed	26.8% observed
Power	12.5 W has been reported for a 4-mesa device	Due to higher thermal resistance and electrical series resistance, achievable efficiency and thus power may be less than Schottky barrier devices
Reliability	10^3 hours MTTF at 225°C junction temperature	10^7 hours MTTF at 200°C junction temperature

material thermal conductivities and the chip area. It consists of three components: (1) Package thermal resistance, (2) thermal spreading resistance under the chip and (3) one dimensional heat flow resistance (series thermal resistance) of the chip. For larger area devices, such as would be used below 18 GHz, the spreading resistance provides the main contribution to the total device thermal resistance.

The integral heat sink approach, Figs. 4 and 5, allows thermal resistances approaching the theoretical minimum. Here, gold is electroplated on the wafer in order to maintain optimum thermal contact with the junction. These diodes are then soldered onto gold plated copper heat sink studs in sealed ceramic packages. Other materials, such as silver or copper, have also been used as integral heat sinks to provide slightly lower resistances (75% and 85% of gold thermal resistance). In addition, type IIa diamonds have been shown to provide some improvement over silver at larger mesa diameters.

To achieve higher output powers, while constrained by a maximum safe junction temperature, larger area mesas must be fabricated in order to further reduce thermal resistance. As mesa diameters increase, spreading resistance falls off much less rapidly (r^{-1}) than thermal series resistance (r^{-2}). Multiple mesa or annular structures distribute heat generation over larger heat sink areas to reduce spreading resistance and, therefore, provide much lower total thermal resistance than an equivalent area single mesa device[14]. These effects are summarized in Table 4. Maximum device area is limited by the amount of reactance the circuit can conveniently resonate and still maintain the desired bandwidth and output power.

Another approach that's been developed for obtaining higher power outputs in Si devices (and is suitable for GaAs devices) is power combining. The rf power of several packaged diodes are combined using either separate cavities and hybrids or separate coaxial matching lines into a com-

(continued on p. 63)

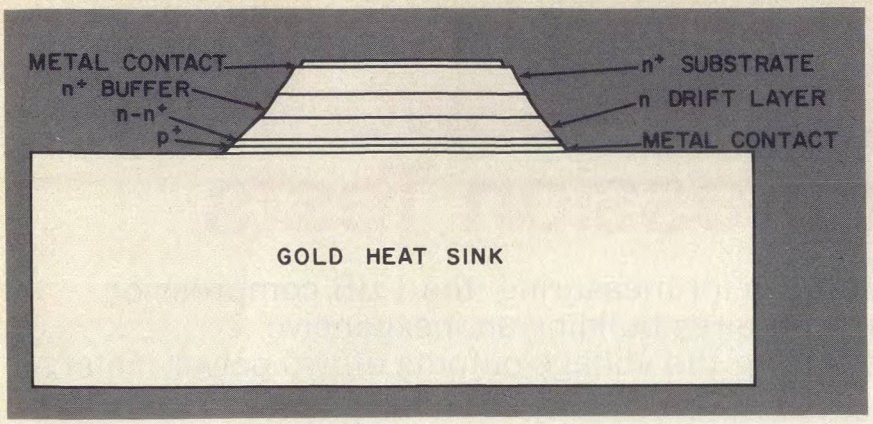

4. **A plated gold (integrated) heat sink** on an etched GaAs Impatt mesa reduces thermal resistance by allowing an optimum thermal contact with the junction.

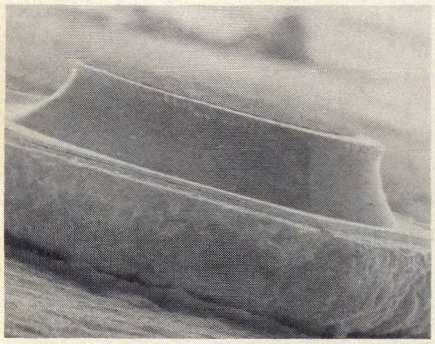

5. **Scanning electron photomicrograph** shows an Impatt mesa with plated gold heat sink. Silver and copper are also used and provides slightly lower thermal resistances.

Thermal resistance for various device structures.

Structure	Area	Rth (°C/W)	Relative P_{out}
Single mesa	10^{-3} cm²	7	1.0
Triple mesa*	10^{-3} cm²	5.25	1.33
Quadruple mesa*	10^{-3} cm²	5	1.4
Ring† ($r_i/r_o = 0.75$)	10^{-3} cm²	5.8	1.2

*On multiple mesa designs, spacing of mesas is about 3 times the radius of the mesa.
†For the ring structure, ratio of i.d. to o.d. of 0.75 is assumed (ref. 14).

mon waveguide cavity[15]. These approaches have been successful in combining as many as 16 diodes in X-band for a total of 20 W cw output[5] and eight diodes for a pulsed output of 100 W at 25% duty cycle[16].

In the future, as technological advances permit more precise control over layer thickness and carrier concentrations, efficiencies more closely approaching the theoretical limits should be achieved. Therefore, higher powers will be possible. Also, as a consequence of improved epitaxial growth capability, higher yields of useful device wafers should be obtained, thus reducing the cost of production. Finally, if the demand is sufficient, the frequency of operation of high efficiency devices could be raised above 18 GHz.

References

1. C. Kim, R. Steele and R. Bierig, "High Power, High Efficiency Operation of Read Type Impatt Diode Oscillators," *Elect. Lett. 9*, pg. 173 (1973).
2. R. E. Goldwasser and F. E. Rosztoczy, "High Efficiency GaAs Lo-Hi-Lo Impatt Devices by Liquid Phase Epitaxy for X-Band," *Appl. Phys. Lett. 25*, pp. 92-94 (1974).
3. W. C. Niehaus, L. C. Luther, J. C. Irvin and D. E. Iglesias, "Theoretical and Experimental Study of GaAs Modified Read Impatts," Device Research Conference, June 25-27, 1974, Santa Barbara, CA.
4. S. I. Long, R. E. Goldwasser, J. Kinoshita and F. E. Rosztoczy, "High Efficiency p-n Junction GaAs Impatt Devices," to be published in *Elect. Lett.*
5. R. S. Harp and K. J. Russell, "Improvements in Bandwidth and Frequency Capability of Microwave Power Combinational Techniques," 1974 IEEE International Solid State Circuits Conference, pp. 94 (1974).
6. D. L. Scharfetter, W. J. Evans and R. L. Johnston, "Double Drift Region (P^+-PN-N^+) Avalanche Diode Oscillators," *Proc. IEEE 58*, pg. 1131 (1970).
7. T. E. Seidel, W. C. Niehaus and D. E. Iglesias, "Double Drift Silicon Impatt's at X-Band," *IEEE Trans. of Elect. Dev. ED21*, pg. 523 (1974).
8. W. T. Read, Jr., "A Proposed High Frequency, Negative Resistance Diode," BSTJ *27*, pg. 401 (1958).
9. T. Misawa, "Saturation Current and Large Signal Operation of a Read Diode," Solid State Elect. *13*, pg. 1363 (1970).
10. D. J. Coleman and J. C. Irvin, "Recent Improvements of GaAs Impatt Diode Performance," Third Biennial Cornell Conference Digest, Aug. 17, 1971.
11. M. Omori, F. Rosztoczy and R. Hayashi, "X-Band GaAs Double Drift Impatt Devices," *Proc. IEEE 61*, pg. 255 (1973).
12. D. R. Decker, "Impatt Diode Quasi-Static Large Signal Model," *IEEE Trans. on Elect. Dev. ED-21*, pg. 469 (1974).
13. D. J. Coleman, Jr., W. R. Wisseman and D. W. Shaw, "Reaction Rates For Pt on GaAs," *Appl. Phys. Lett. 24*, pg. 255 (1974).
14. J. Frey, "Multimesa Versus Annular Construction for High Average Power in Semiconductor Devices," *IEEE Trans. on Elect. Dev. ED-19*, pg. 981 (1972).
15. K. Kurakawa, "The Single Cavity Multiple Device Oscillator," *IEEE Trans. on Microwave Theory and Techniques MTT-19*, pg. 793 (1971).
16. K. J. Russell and R. S. Harp, "Power Combiner Operation with Pulsed Impatts," *1975 IEEE International Solid State Circuits Conference*, pg. 136 (1975).

Test your retention

1. What are the main differences between GaAs and Si Impatt diodes?
2. What are the relative benefits and disadvantages of Schottky barrier and grown junction structures?

Take The Guesswork Out Of Compression Tests

Here is a simple approach for measuring the 1 dB compression point of amplifiers. It requires building an inexpensive divider network and using the voltage outputs of two power meters.

MEASURING the compression point of an amplifier can be a very tedious job particularly when it's done manually on a repeated basis. There are a few semiautomatic systems which can be purchased, but these are expensive and beyond the reach of many laboratories. Computer processing can also be used, but the computation cannot be done in real time which is both inconvenient and uneconomical.

The method by which most laboratories determine the 1 dB compression point requires the use of a 10 dB switchable attenuator as shown in the test setup of Fig. 1. The operator gradually increases the input power, while at the same time switching the 10 dB attenuator in and out. Under small signal conditions (no gain compression), the output signal will increase 10 dB when the attenuator is switched out. At some point, as the power input is increased, the output will rise only 9 dB when the attenuator is out. This output level is the output for 1 dB compression.

Note that in using this system it is assumed that the onset of compression occurs in less than 10 dB input signal change. While a skilled operator can develop a sense of how far to advance the input signal, the process is still one of trial and error.

The new method to be shown here is straightforward and does not involve trial and error at all. It only assumes that the power meter has a recorder output proportional to the power indicated on the meter. A simple ratio meter is used based on a divider module which allows making measurements of the 1 dB compression point on systems with an overall accuracy limited only by the drift and accuracy of the power meter used. The complexity of the setup is about the same as for the 10 dB switchable attenuator method. Cost of the ratio-meter is $200-$300 when unit quantity parts are purchased.

How it works

A typical power meter has scales which are multiples of 1.0 or 3.16 going from 0.01 to 10.0 mW. However, the recorder output on all scales is 0-1 volt. The voltage, E_{rec}, at the record terminal can be written as:

$$E_{rec} = KP$$

where P is the indicated power in milliwatts and K depends on the scale used. On the 10.0 milliwatt scale, K = 0.1; on the 3.16 mW scale, K = 0.316, etc. Note that K is simply

Harry F. Cooke, Manager, Transistor Design, Avantek, Inc., 3175 Bowers Avenue, Santa Clara, CA 95051.

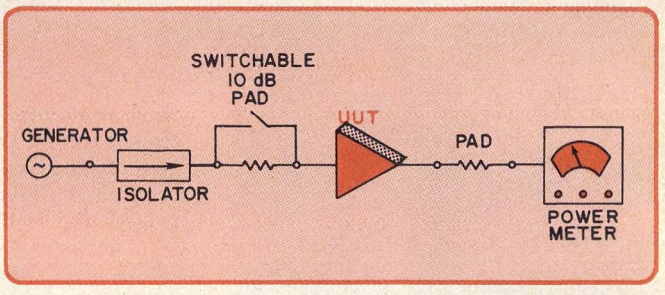

1. **Conventional compression test** procedure uses a switchable 10 dB attenuator. The operator, however, must sense how much to increase the input and some trial and error is involved.

$$K = \frac{1}{\text{max scale reading in mW}}$$

If there are two power meters each monitoring input and output power, respectively, then:

$$E_{rec_1} = K_1 P_1$$

$$E_{rec_2} = K_2 P_2$$

Therefore, power gain is simply the ratio:

$$P_1 G_1 = \frac{P_{out}}{P_{in}} = \frac{E_{rec\,2}}{E_{rec\,1}} \cdot \frac{K_1}{K_2}$$

This, in itself, is not a particularly useful result since the ratio of the recorder voltages would have to be determined continuously to measure gain.

The system to be described makes this computation on a continuous basis. It is simply an analog divider module which makes the following computation to an accuracy of 0.5%.

$$V_{out} = \frac{G_d N}{D}$$

Where N and D are voltages and G_d is the gain of an analog divider. There are several limitations to this computation. First of all, due to divider limitations, V_{out} must be less than 10 volts, which in turn, limits G_d, the system gain and the ratio of N/D. To see how this can work as a 1 dB compression indicator, assume the following:

$$N = K_i P_{in}$$

$$D = K_o P_{out}$$

G_d can be varied between 3 and 9 (set by circuit limitations)

$V_{out} = 1$, when no compression is present

The limits of gain variation also set limits on the ratio of N to D.

$$0.11 < N/D < 0.33$$

At this point, set up a test using the divider module as shown in Fig. 2. An initial reading must

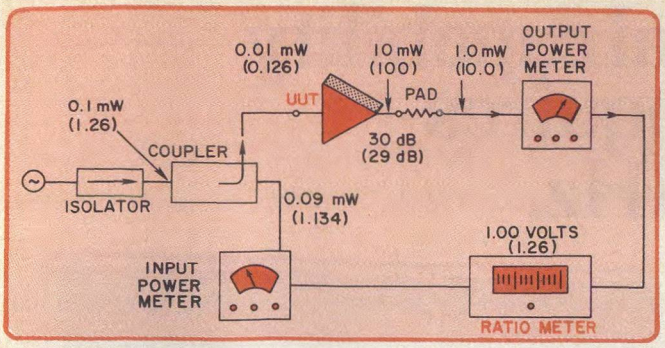

2. **The new compression test procedure** is based on the assumption that the recorder output of power meter is proportional to the power indicated on the meter. It uses a ratiometer circuit and digital panel meter. The numbers shown in mW are for the example given. Values in ( ) are when unit-under-test is in 1 dB compression.

first be made to establish the small signal or reference gain. (However, for this step, gain need not acutally be measured). Let P_{in} be low enough that small signal conditions are in effect, then:

$$V_{out} = \frac{G_d N}{D} = G_d \left(\frac{K_i}{K_o}\right)\left(\frac{P_{in}}{P_{out}}\right)$$

The output attenuator is selected to give a value of $K_i/K_o \approx 1/3$, and G_d is varied until $V_{out} = 1$. The small signal gain has been normalized to an output voltage of unity.

If P_{in} is increased until the gain drops 1 dB, this is the equivalent to saying that the ratio of P_{in}/P_{out} has increased by 1.26.

$$\text{because } \Delta P.G._{numeric} = -\log^{-1}\left(\frac{\Delta P.G._{dB}}{10}\right)$$

$$= -\log^{-1}\frac{1}{10}$$

$$= 1.26$$

$$\text{Then } V_{out} = \frac{1}{3}(P_{in}/P_{out})(1.26) = 1.26$$

and thus the output voltage from the analog divider will read 1.26 when the unit under test is in 1 dB compression. Similarly, 3 dB compression would give 2.0 volts, etc. For convenience, the output voltage from the divider module is read on a digital panel meter.

Measuring the new way

Consider the test setup shown in Fig. 2. The unit-under-test is an amplifier with a small signal power gain of 1000 or 30 dB.

It will be first necessary to determine K_i and K_o

$$K_i = 10\left[1 - \log^{-1}\left(\frac{\text{input coupling factor} \sim \text{dB}}{10}\right)\right]\left[\frac{1}{\text{max scale reading} \sim \text{mW}}\right]$$

$$K_o = \left[\log^{-1}\left(\frac{\text{output attenuation} \sim \text{dB}}{10}\right)\right]\left[\frac{1}{\text{max scale reading} \sim \text{mW}}\right]$$

Since the input coupler has a coupling factor of 10 dB, and if the amplifier input power is 0.01 mW, the

(continued on pg. 67)

(continued from p. 65)

input power meter will see 0.09 mW. It is, therefore, set to the 0.316 mW scale.

Then $N = K_i P_{in}$

$$= 10 \left[1 - \log^{-1}\left(\frac{-10}{10}\right)\right]\left[\frac{1}{0.316}\right] 0.01$$

$$= 0.285 \text{ volt}$$

Similarly if the output attenuator value is 10 dB, the output power level is 10 mW and the output power meter will see 1 mW. Using the 1 mW scale:

$$D = K_o P_{out} = \left[\log^{-1}\left(\frac{-10}{10}\right)\right]\left[\frac{1}{1}\right] 10 = 1 \text{ volt}$$

If the gain, G_d, is set to 3.52 x, then

$$V_{out} = G_d \frac{N}{D} = 3.52\left(\frac{0.285}{1}\right)$$

$$= 1 \text{ volt}$$

Next, it will be assumed that the amplifier goes into 1 dB compression at a 100 mW output level. Since a 10 dB attenuator is used, the output power meter will now see 10 mW and the meter scale must be moved two steps up from the 1 mW scale to the 10 mW scale (i.e., 1.0/3.16/10.0). The input power meter must also be advanced exactly two steps to the the 3.16 mW scale (0.316/1.00/3.16). Since the gain is now 29 dB, the input power will be 20 dB below 100 mW or 0.126 mW. The input power meter, due to the coupler, will see 1.134 mW. If the divider gain control was left untouched after the small/signal reference reading was made, G_d is still set to 3.52, thus

$$V_{out} = G_d \frac{N}{D} = G_d \frac{N_i}{N_o} \cdot \frac{P_{in}}{P_{out}}$$

$$= 3.52 \left[\frac{2.85}{0.01}\right]\left[\frac{0.126}{100}\right] = 1.26 \text{ volts}$$

Building the divider circuitry

The ratio meter circuit can be easily built based on a Burr- Brown 4290 divider module, Fig. 3. There are other dividers available at various prices which will also work well in this circuit. Note that the circuit has only three main components; the divider module, a digital panel meter and a power supply. The offset controls are recommended by the divider manufacturer for maximum accuracy, but are not actually required since the unit will not normally be operated with either meter reading less than 1/3 scale. Thus, N and D are always greater than 0.33 volts.

A 3 1/2 digit DPM was used in the example, but again for economy, a 2 1/2 digit meter would be adequate. For ease in setting G_d, the divider gain, a ten turn potentiometer is used.

To make the system practical the following points are suggested:

- Since power meters tend to drift more on the lower power scales, make your setup so as to use the highest ranges you can.
- For extremely high gain systems, the input levels may be so low, even with a 20 dB coupler, that it will be necessary to add an attenuator to the coupled arm of the input coupler (Fig. 1) or add an amplifier to the direct output.
- The particular components used in a setup are best determined by starting with the output level for 1 dB compression and working back to the input component settings.

(continued on pg. 68)

(continued from pg. 67)

3. **The ratiometer design** is based on a Burr-Brown 4290 divider module and a 3 1/2 digit DPM. It can be built for about $200 to $300. Note N/D < 1.5; N = k N/D.

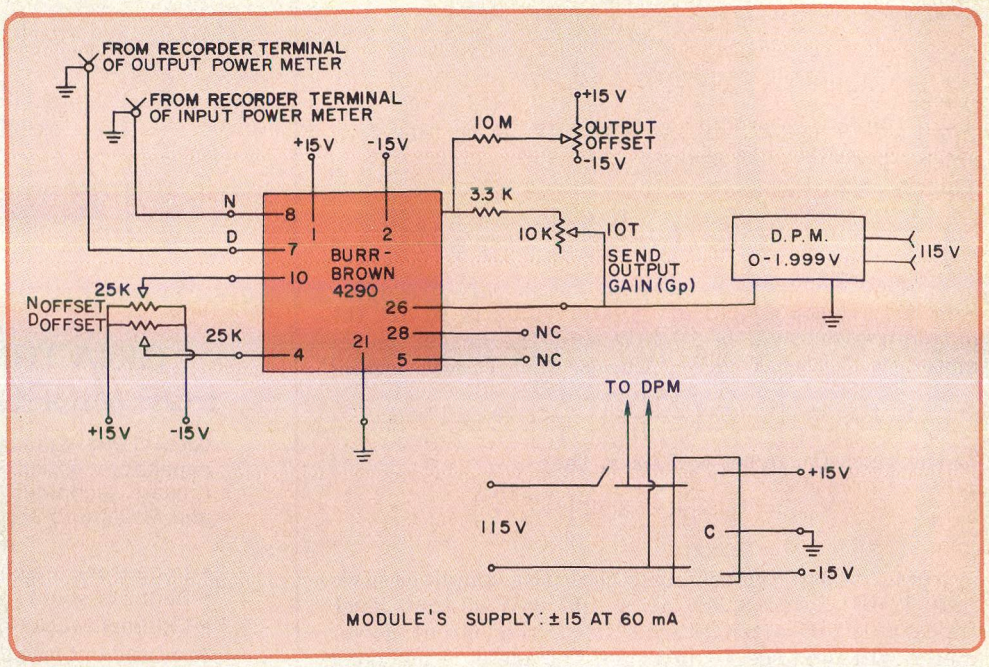

- Do not take readings or set gain when either meter is indicating much less than 1/3 scale. The analog divider is accurate for denominator voltages as low as 0.1 volts, but zero drift in the power meter's limits accuracy.
- When making final or trial test, as the input power is increased, the two power meters must be advanced the same number of ranges every time. ••

Test your retention

1. What is the fundamental difference between the system described and other methods of compression testing?
2. What factor is most important in limiting the accuracy of this new system?
3. What is the significance of the "1.26" which is displayed on the D. V. M.?

NOVEMBER
1975

MICROWAVES

laser technology

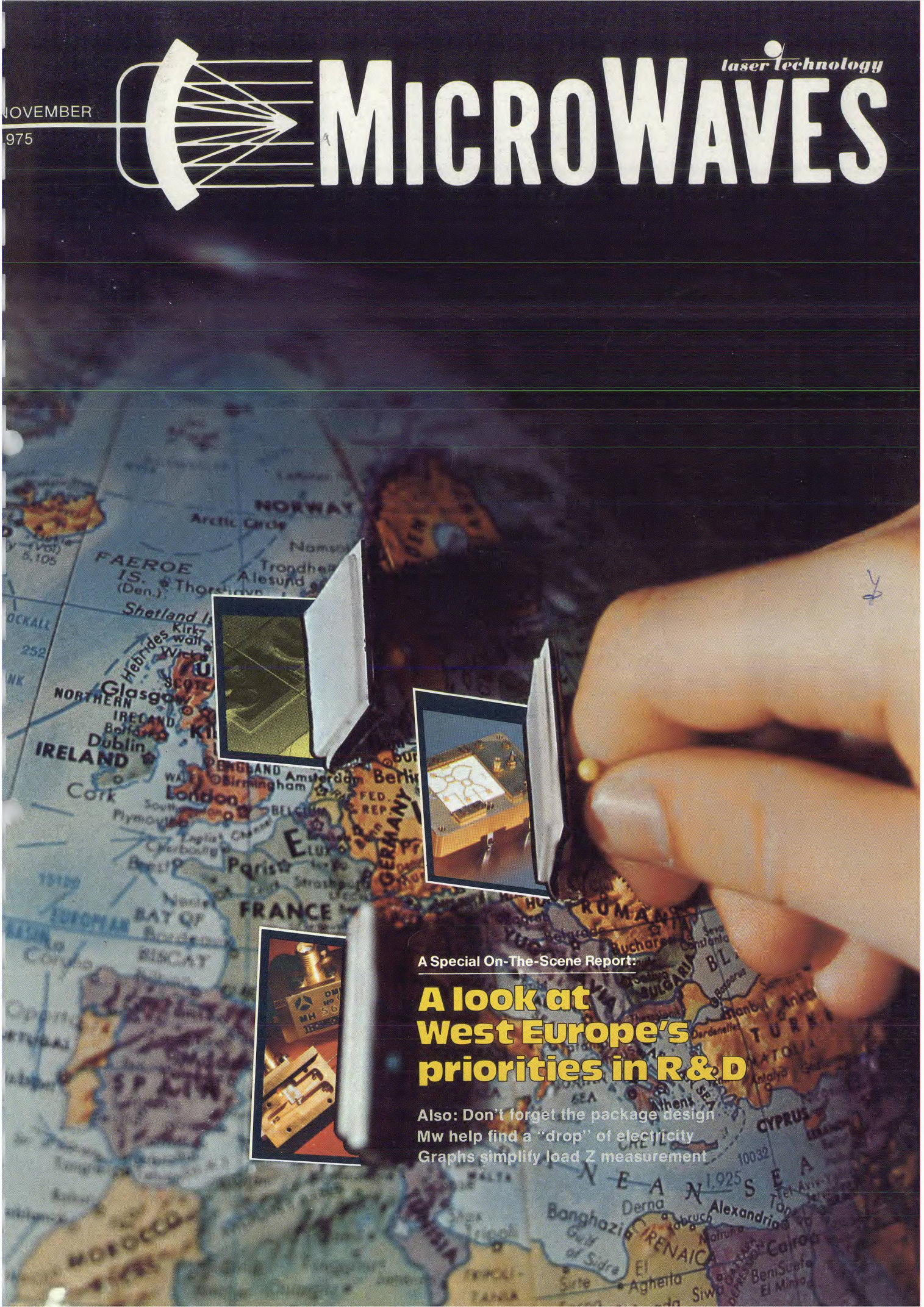

A Special On-The-Scene Report:

A look at West Europe's priorities in R&D

Also: Don't forget the package design
Mw help find a "drop" of electricity
Graphs simplify load Z measurement

MICROWAVES

November 1975
Vol. 14, No. 11

news

editorial

technical section

products and departments

About the cover: A look behind the scenes in Western European R&D reveals Britain's high priority in FET development, France's strength in sources and West Germany's interest in low-cost earth station front-ends for 12 GHz TV telecasting.

coming next month: Test and Measurement

Test Equipment: Weighing The Rent Or Buy Decision. Anthony Schiavo of US Instrument Rentals, Inc., San Carlos, CA, offers a graphical method for determining whether it is more economical to rent or buy a given instrument. The author urges caution, however, since in the long run, it pays to weigh several factors not considered in a simple dollar analysis.

TDM: An Alternate Approach To Microwave Measurements. Dr. Harry Cronson of Sperry Research Center in Sudbury, MA, describes the equipment and techniques used for making time domain measurements of microwave components. Cost, accuracy and speed are major advantages over swept frequency measurements. Details for building a simple impulse generator are included.

Simplify Leakage Probe Calibration. Edward Aslan of Narda, Plainview, NY, details a bench-top method for calibrating radiation hazard meters using slotted waveguide to approximate the field distribution of the hazard. The method is simple and inexpensive, yet yields an accuracy of about ±5%.

Publisher/Editor
Howard Bierman

Managing Editor
Richard T. Davis

Associate Editor
Stacy V. Bearse

Contributing Editor
Harvey J. Hindin

Washington Editor
Paul Harris
Snyder Associates
1050 Potomac St., NW
Washington, DC 20007
(202) 965-3700

Editorial Assistant
Gail Murphy

Production Editor
Sherry Lynne Karpen

Art
Robert Meehan, Dir.

Production
Dollie S. Viebig, Mgr.
Dan Coakley

Circulation
Trish Edelmann, Mgr.
Peggy Long, Reader Service

Promotion Manager
Albert B. Stempel

Directory Coordinator
Janice Tapp

Editorial Office
50 Essex St.,
Rochelle Park, N.J. 07662
Phone (201) 843-0550
TWX 710-990-5071

A Hayden Publication
James S. Mulholland, Jr., President

MICROWAVES is sent free to individuals actively engaged in microwave work at companies located in the U.S., Canada and Western Europe. Subscription price for non-qualified copies is $10.00 for U.S., $15.00 a year elsewhere. Additional single copies $1.50 ea. (U.S.); $2.00 ea. (foreign); except additional Product Data Directory reference issue, $10.00 ea. (U.S.); $18.00 (foreign). POSTMASTER, please send Form 3579 to Fulfillment Manager, MICROWAVES, P.O. Box 13801, Philadelphia, PA 19101.

Back Issues of MicroWaves are available on microfilm, microfiche, 16mm or 35mm roll film. They can be ordered from Xerox University Microfilms, 300 North Zeeb Road, Ann Arbor, MI 48106. For immediate information, call (313) 761-4700.

Hayden Publishing Co., Inc., James S. Mulholland, President, printed at Brown Printing Co., Inc., Waseca, MN.

TED triode performs frequency division

Stacy V. Bearse
Associate Editor

A three-terminal Gunn device has been developed which acts as a frequency divider at ratios as high as 34:1. Major applications appear to be in millimeter wave phase-locked oscillators (Fig. 1) for space and airborne applications, say developers at TRW Systems in Redondo Beach, CA, who note that a TED triode could offer weight and power consumption savings of up to 90%.

The TED triode, shown in Fig. 2, is a simple planar Gunn diode which incorporates an aluminum Schottky barrier gate. Used in a circuit, the TED divider requires both positive and negative bias supplies. Input signals are fed to the gate, which is held at a negative potential ranging from −0.5 to −5 volts. The output is extracted at the anode, which is biased at about +25 volts, just below threshold for diode oscillation. The cathode is grounded.

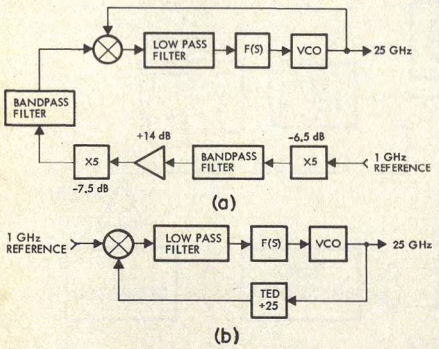

1. Two multipliers, two filters and an amplifier are replaced by a single, solid-state frequency divider in this phased-locked oscillator.

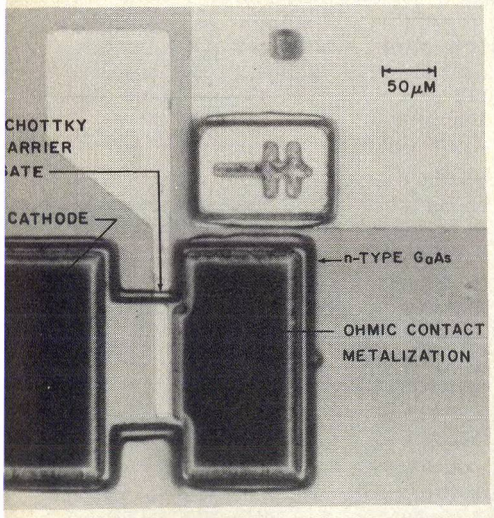

2. No diffusions are required for the fabrication of this planar device.

"Without the gate, the device would act like a diode and oscillate at a frequency determined by cathode-anode spacing when anode bias exceeds threshold level," says Dale Claxton, a member of the technical staff at TRW. "Now consider operating the TED triode with the cathode to anode bias just below the threshold and an additional negative bias applied to the Schottky barrier gate," Claxton explains. "If the gate bias is of sufficient magnitude, the field in the gate region exceeds the threshold level, and dipole domains are launched. The triode oscillates but the transit time frequency, f_t, is now determined by the gate to anode spacing. If an rf input is applied to the gate and the input rf frequency is an integer multiple of f_t and of sufficient magnitude, output oscillations at f_t will again be stimulated."

"Suppose, for example, the input frequency is 10 f_t (Fig. 3). The first time the input voltage goes negative, a domain is launched from the gate region. While the domain is in transit, the field outside of the domain region lowers such that a second domain cannot be initiated. The field under the gate remains low until the first domain clears, then a second domain is launched, starting another output cycle. Thus, with an output of 10 f_t, only every tenth input cycle causes a domain to be launched, and the other nine have no effect on the triode."

According to TRW, frequency division has been demonstrated by every integer up to 34. All devices tested thus far have output frequencies in the 1.1 GHz to 1.6 GHz range. The highest division ratio reported reduced a 38.4 GHz input to 1.13 GHz. Bandwidths of 10% are reported for division ratios of less than 10. Forward and reverse isolations are −35 dB and −40 dB, respectively.

The level of rf power input necessary to initiate frequency division is reported to be as low as −30 dBm, but may be higher for some devices depending on the impedance of the input gate. Dynamic range was measured to be approximately 45 dB (−30 to +15 dBm). The TRW researchers estimate that the minimum energy actually required to trigger a domain in the bulk material is between 13 and 130 femto-joules.

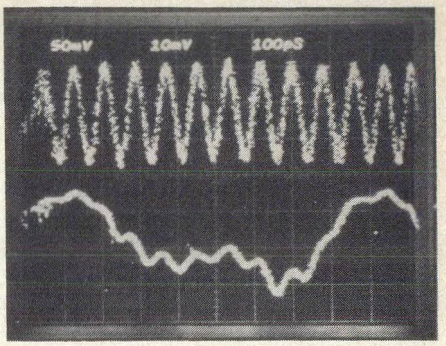

3. A 12 GHz input is converted to a 1.2 GHz output by a divide-by-ten device. Although the output is non-sinsusoidal, it can be improved by circuit matching and harmonic filtering.

Impedance matching circuits have been investigated with an unexpected result. "Matching circuits provided the expected increase in output power, but have a surprisingly small effect on the input. So far as the operation of the triode as a divider, it doesn't seem to make much difference whether or not the input is well matched," Claxton describes.

Claxton feels that the two keys to fabricating a successful TED divider lie in proper substrate surface preparation and ohmic contact annealing. Both liquid and vapor phase processes have been used to grow the epi layer, which has a thickness of 4 to 10 microns, depending on the device. Early devices used Au-Sn-Au ohmic contacts, but TRW researchers are leaning toward AuGe. "Gold-germanium has a little less contact resistance, and appears to adhere better to the gallium arsenide," Claxton observes.

TRW is continuing its investigation of three terminal Gunn devices under an external funding program from an undisclosed source. Other application areas under study include analog to digital conversion and fast Fourier transformation. Details of the TED divider were presented at the 1975 Cornell Conference on Active Semiconductor Devices for Microwaves and Integrated Optics in a paper by Claxton, Tom Mills and Lloyd Yuan. ••

news

Microwaves help find drop of electricity

Harvey J. Hindin
Contributing Editor

Microwave radiation at 25 GHz has been used as a fundamental tool in providing the first photograph of a "drop" of electricity. Recorded as an image from a television screen, the picture clearly shows a mass of electric charges as a single sphere, glowing with infra-red radiation. The existence of the drop, shown in Fig. 1, was predicted based on the results of microwave probing of the interior of an ultrapure, super-cooled, crystal of germanium. Actually the drop is a low-energy plasma or electron-hole drop (EHD) since it contains an equal number of electrons and positively charged "holes" from which the electrons have been dislodged.

1. Photo of a single (1/30 inch diameter) electron-hole drop was obtained by illuminating a Ge crystal with a laser on one side and focusing an infra-red sensitive TV vidicon on the opposite side. The Ge crystal disk in which the drop forms measure 4 mm in diameter and 1.4 mm thick. Laser pump level is 80 mW at about 5000 Å. The outline of the stressing screw is seen on the left.

The making of the photograph required the use of an Argon-Krypton ion laser for stimulating the crystal, cooling to almost absolute zero and an infra-red detector built into a TV camera. The research was performed by Drs. James P. Wolfe and Robert S. Markiewicz and Professors Carons D. Jeffries and Charles Kittel of the University of California at Berkeley Physics Dept. and Drs. William L. Hansen and Eugene E. Haller of the Lawrence Berkeley Laboratory.

The photo-excited charges or plasma produced by the intense laser beam can exist only at very low temperatures. If an external magnetic field is applied, microwaves can propagate through the plasma at its plasma resonance frequency. Thus, when the sample is irradiated by microwaves at this frequency and simultaneously excited by the laser beam, a series of microwave resonances occur whose field strengths depend on the light intensity. Typically, in Ge at T = 2°K, resonances occur at 3 to 20 kilo-oersteds for a 25 GHz microwave signal. These absorptions are called Alfven resonances of the electron hole drop.

The test setup for observing the Alfven resonances, Fig. 2, consists of a disc of polished and etched ultrapure p-type Ge containing only 10^{11} acceptor impurities/cm^3. The crystal is mounted on a rotator in a tunable cylindrical cavity which in turn is immersed in a liquid helium bath in an optical cryostat. Both the ordinary cyclotron resonances of electrons and holes and the new Alfven resonances of the EHD are observed with a sensitive but simple superheterodyne receiver, which has a 12 dB noise figure and a 20 MHz bandwidth. The beam of the variable intensity cw Ar-Kr ion laser is mechanically chopped at 258 Hz and focused by lens system F (Fig. 2.) onto the crystal. The resonances were observed over the frequency range from 24 to 26 GHz.

The Alfven resonances are explained by assuming that the spherical electron-hole drop acts as a microwave resonator. The large dielectric constant within the drop reduces the effective wavelength in order to match the diameter of the drop. The coupling of the plasma to the external field enhances the dielectric constant and lowers the effective

(continued on p. 14)

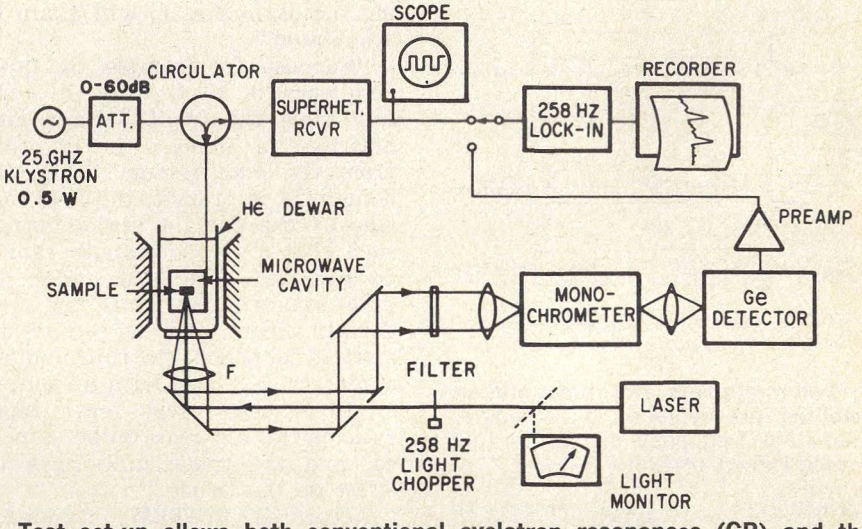

2. Test set-up allows both conventional cyclotron resonances (CR) and the new microwave dimensional resonances (Alfven resonances) to be observed using a laser and microwave source to illuminate a Ge crystal. The home-built superheterodyne receiver uses a lock-in amplifier.

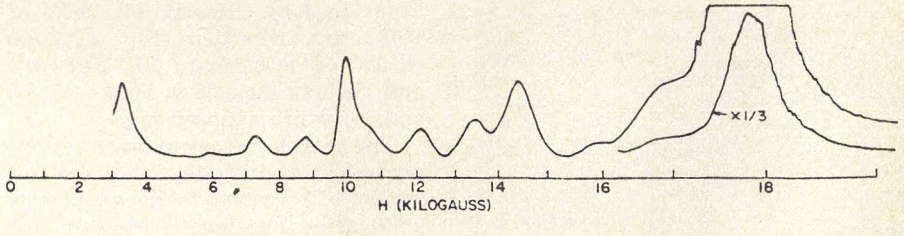

3. Typical microwave absorptions observed due to the standard Alfven waves in the EHD can be seen with about a 100:1 signal-to-noise ratio. The positions of the absorptions shift to higher fields as the drop radius is increased by increasing the laser power.

Satellite offers contoured coverage of Japan

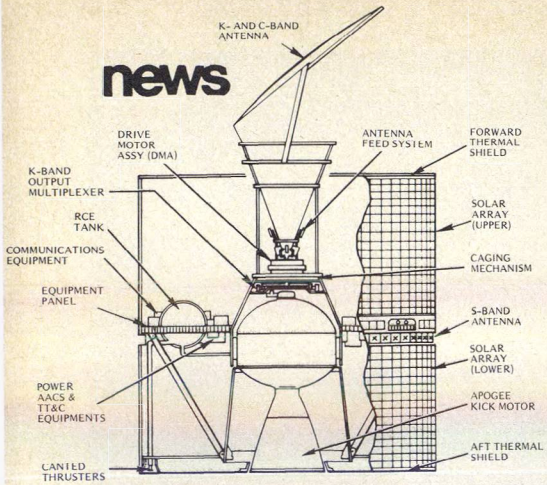

Architects of the next generation of satellite communications systems are anxious to move into K-band, primarily to gain the wide bandwidths necessary to accommodate high bit-rate transmission. But at K-band, antenna designers are discovering a secondary advantage: the ability to tailor the satellite's radiation footprint to cover irregular areas on earth. The benefit: lower transmitter power requirements and closer compliance with strict international laws governing radiation spillover.

A prime example is Japan's CS experimental communications satellite, now under development at Aeronutronic Ford's Western Development Laboratories, in Palo Alto, CA. The spacecraft will spotlight all of the Japanese islands with large, circular radiation patterns at 4 and 6 GHz. But at 20 and 30 GHz, the spacecraft will generate patterns tailored to cover only the major islands of Hokkaido, Honshu, Shikoku and Kyushu.

Signals in all four bands will be handled by the same antenna, a horn-fed reflector. Circularly polarized energy propagates up along the spacecraft's spin axis, through a series of horns and bounces off a specially-designed despun reflector. It is the shape of the graphite-epoxy reflector which creates the far-field radiation pattern that matches the shape of the islands.

According to Adam N. Wickert, manager of the antenna engineering department at WDL, the compound curves forming the surface of the reflector were derived by computer analysis, working backwards from a desired far-field pattern. The computer analysis generated 18,000 sets of (x, y, z) coordinates which define the reflector surface. These, in turn, are used to machine a tool which serves as a form for the graphite-epoxy material. After the composite material is cured on the form, a matching aluminum honeycomb is built on the back, section by section. This is followed by another layer of composite material to form an epoxy-honeycomb-epoxy sandwich. According to Wickert, the final surface accuracy of the 40 x 30 inch reflector is better than 3 mils.

The entire antenna assembly, including feed system and pointing mirrors, weighs about 33 lbs. K-band signals are fed through an orthomode transducer and broadband polarizer. C-band energy enters a branching horn through a series of slots cut into the horn's sidewall. Prior to being fed into the horn, the 4 and 6 GHz signals pass through rat-race hybrids and waffle-iron filters. Resonant "whiskers", mounted in the feed slots, prevent K-band signals from entering the C-band system. All signals are circularly polarized.

Aeronutronic Ford is presently under contract estimated at $30-million to build two of the experimental CS spacecraft, which will be launched from the United States early in 1977. The American firm is working closely with Japan's Mitsubishi Electric Corporation, which is under contract to Japan's National Space Development Agency for the design phase of the country's CS program.

At this point in time, the millimeter-wave CS satellite is strictly an experimental spacecraft. But indications are that this is merely a forerunner to a more ambitious program. Eventually, sources say, the Japanese plan to have a complete communications network of this class of spacecraft. •• *SVB*

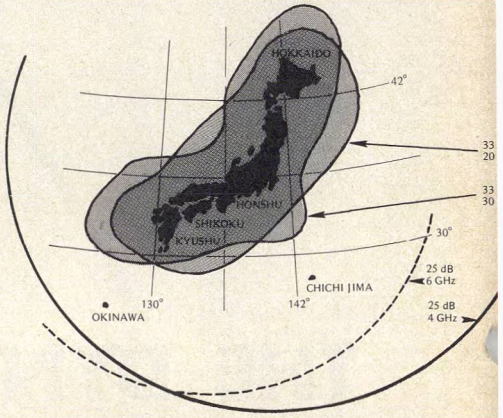

Highest frequency measurement advances to 148,000 GHz

Once again, researchers at the Boulder Laboratories of the National Bureau of Standards have extended the realm of directly measurable frequencies to new heights. Researchers have successfully directly measured a laser frequency of 147.915850 THz (about 148,000 GHz) with a probable error of one part in 10 million. This frequency is only a factor of three below the red end of the visible spectrum, which is the next target of the NBS team of physicists Don Jennings, Russell Peterson and Ken Evenson.

According to NBS, while the wavelength of radiation can be measured at higher frequencies than this, wavelength measurements are inherently much less accurate than direct frequency measurements, which are ultimately traceable to NBS frequency standards.

The measurement technique used by the NBS researchers relies on generating an accurately-known reference frequency which can be compared to unknowns. Using the outputs of lasers and klystrons, the researchers irradiate a metal-on-metal point-contact diode and by a heterodyne effect, produce known frequencies as high as the near infrared region. When the known signal is further mixed with unknown laser radiation on the same diode, a difference frequency is produced which can be measured with conventional instrumentation.

In the 148 THz measurement, two CO_2 lasers and a helium-neon laser were used to synthesize a signal near the frequency of the unknown signal to be measured; that of a xenon laser. No klystron signal was required, since the difference frequency was low enough to be measured directly with a spectrum analyzer.

The measurement was carried out merely to demonstrate the technique. Had stabilized lasers been used the accuracy could have been improved in one part in 10 billion or better, according to NBS. ••

S.V.B.

news

Electro-optical waveguide modulator switches laser light

A GaAs electro-optical switch, consisting of two parallel metal gap optical stripline waveguides, has been developed at Texas Instruments, Dallas, TX. The device, which is essentially a passive coupler with an electro-optic pad at the edge of each waveguide, Fig. 1, has important implications for optical communications and represents a fundamental building block for monolithic integrated optical circuits.

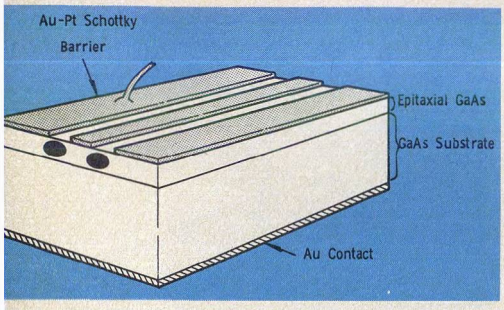

Electro-optic switch controls amount of light coupled between adjacent waveguides by varying bias voltage applied to the pad. The scheme not only permits direct amplitude modulation of the laser light propagating in one channel but allows the light to be switched from one channel to the other.

According to Joe Campbell of TI's Central Research Labs, a distinct advantage of the device is that it can be directly coupled to optical fibers because the guided laser light is well confined in both transverse dimensions. It also requires much less power than bulk modulators. "Such a device has been discussed theoretically for a number of years, but up till now, has never been fabricated using any kind of material."

"It's sort of analogous to a microwave directional coupler," explains Fred Blum, a co-developer and former Program Manager at the Labs. "For dielectric waveguides, such as used in this device, coupling is achieved by the evanescent (decaying) fields which extend beyond the waveguide boundaries."

In the absence of an applied electric field, the propagation constants of the two dielectric waveguides are equal and the power coupled from the input waveguide to the adjacent channel varies sinusoidally with the length of the coupler. When the electric field is applied to one of the waveguide pads, the phase velocity synchronism between the two channels is spoiled, which reduces the coupling and causes all the light to emerge from the input channel.

The measured waveguide losses are about 6 dB/cm, which is close to 4 dB/cm, the lowest measured to date for GaAs waveguide channels. Bandwidths of 100 MHz and power bandwidth ratios of 180 μW/MHz are possible. Only 5% of the laser light which is originally in the coupled guide remains after switching, an extinction ratio of about 13 dB. ••

Court denies challenge to microwave competition

The U. S. Supreme Court last month rejected for the second time this year, a challenge to the 1971 FCC ruling that encourages competition among firms seeking to establish private microwave systems to compete with AT&T. The challenge came from the National Association of Regulatory Utility Commissioners which contended the rule is not in the public interest since intrastate telephone rates could increase as a result.

The high bench, last term, refused to hear AT&T's claims that the FCC followed improper rule-making procedures when it approved the competition rules. The utility commissioners said that the agency forces the FCC to serve unprofitable rural areas and makes up the loss in high-volume areas.

P.H.

Microwaves help find drop of electricity

(continued from p. 10)

wavelength inside the drop. The dielectric constant is inversely proportional to the square of the applied magnetic field. For 10 kilogauss, the dielectric constant is 10^4 and the corresponding wavelength is about 0.1 mm. As the field is swept, a series of resonances occur corresponding to resonator standing waves, Fig. 3. The resonant field values vary linearly with the drop radius.

Finding the drop

Many experiments with these microwave resonances convinced the Berkeley physicists that they knew enough about the properties of the drop to find and photograph it. They concluded that, under certain conditions, a drop measuring about 1/30 of an inch in diameter is produced and could actually be photographed by detecting the infrared radiation it emits. Such a drop was estimated to contain 10^{13} charges. Even though they are imbedded in a solid material lattice, electron-hole drops have many of the properties of a liquid, such as surface tension and thus an ability to move throughout the crystal. In addition to this, Dr. Wolfe notes that "the drop has some of the properties of a metal such as high conductivity. There's nothing quite like it."

In all of the experiments, it was found necessary to apply a mechanical stress to the Ge crystal such that a comparatively large drop was formed rather than several smaller ones. This stress causes a potential well into which the smaller fluid-like droplets flowed and coalesced. Actually, the large drop is formed near the point of maximum crystal stress. More laser power resulted in larger drops. All the drops disappeared in about a millisecond when the laser was turned off.

A number of other research groups throughout the world are presently studying the properties of these drops. Russian scientists first came up with the droplet idea about seven years ago but the Berkeley group is the first to actually photograph it. Program support was provided by the U.S. Energy Research and Development Administration and the National Science Foundation. ••

r&d roundup

Harvey J. Hindin, Contributing Editor

Easy filter picking

In an extensive interview and introduction to microwave filter development of the last 30 years, J. David Rhodes of Leeds University in England has summarized the problems facing the microwave filter design engineer. His paper, "Microwave Filters," which appeared in the Newsletter of the Circuits and Systems Society (Vol. 7, No. 8, pp. 2-8, August, 1975), concentrates on the last 10 years of this now "mature" technology.

Rhodes notes that the present time, most design problems may be solved by a known technique. These problems may include amplitude and/or phase specs or both. It would appear that the major problems now are those of size, environment, tuning and production rather than original design.

"Microwave Filters" may be used as a preliminary design manual by the expert or tyro. The reader is taken from a discussion of the major filter types and how to choose what he needs to closed form design equations which may be solved by means of hand calculators and graphs. Multiplexed channel filters are also briefly discussed.

As an example, the interdigital

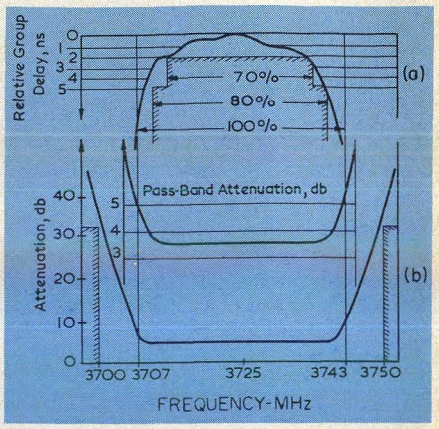

The measured results for a 14th degree interdigital filter are shown in (a) for the relative group delay and (b) for the amplitude response. The interdigital design can also be made broadband (300%) up to 20 GHz.

filter response shown in the figure is ideal for simultaneously realizing amplitude and phase specifications in a TEM structure. It is as inexpensive as the combline filter.

Systems engineers reading the paper will get a good overview of what their vendors can do, since the material is so organized that the design equations can be skipped. The 27 references provide good leads for further reading if desired.

Don't burn up!

Anechoic chambers usually just sit there! Once constructed, they seem to last forever and microwave testing is done with no trouble unless the design is inadequate for the frequencies used.

Unfortunately, M. A. Plonus of Northwestern University has discovered this not to be the case. In "Ignitability of Anechoic Chamber Foam by Electric Currents," (*Proc. IEEE*, Vol. 63, No. 9, pg. 1371, September, 1975), he describes two processes which can and have caused total loss of the chamber by fire.

Plonus's own facility was destroyed, and he made an investigation because the normal causes of fire such as inadequate wiring, bad fusing, soldering irons, etc., were eliminated as the trouble source. A study showed that mysterious chamber fires at other facilities are not uncommon. Fighting these blazes is very difficult because of the toxic gases released.

Simple flammability tests showed that the chamber materials did not burn too readily with matches or hot irons so special mechanisms were suspected. This turned out to be so and two cases were identified. In the first, fire was readily started when two wires carrying 100 volts or more touched the foam. The higher the voltage and sharper the point's, the quicker the fire. Separation between the the contacts was not a factor. Even if discovered early, the smoke is so dense that the fire cannot be controlled.

If the fire does not start readily, due to low voltage or blunt contacts, internal foam heating results. Because of the foam's high conductivity (due to carbon particle impregnation), it acts as a distributed resistor and the heat generated is not conducted to the surface. Again, contact separation is not a factor.

While further work is necessary to fully understand these effects and their characteristics, all users of anechoic chambers should be aware of this major fire hazard and take suitable precautions.

The above mentioned reference is available from: Single Publication Sales, IEEE, 445 Hoes Lane, Piscataway, NJ 08854.

Don't Overlook The Package Design

Here are some manufacturing processes and packaging schemes you'll find useful for MICs. Ways of bonding the carrier to the enclosure and sealing techniques are also covered.

HAVE you ever designed an MIC module that must operate over a −50° to 100°F temperature spec, withstand a salt-laden environment or survive a level of vacuum as found in space applications? If you have, you probably can appreciate the care involved in designing the module's enclosure. The process used in manufacturing the enclosure must be carefully reviewed as well as the type of bond between the substrate and carrier/encosure and the thermal design for limiting temperature excesses of active elements. Obviously, the degree to which these detail designs adhere to design requirements will affect the reliability and unit cost of the microstrip assembly. As such they must be traded off early in the design phase.

Packaging design may be the responsibility of the mechancal designer, but it is important that his electrical counterpart is aware of this tradeoff. For example, the development of a circuit which includes a component such as an exposed semiconductor would be incompatible with a module enclosure design that was not meant to be hermetically sealed, particularly if the module is to be used outside of a controlled environment.

Daniel Olivieri, Senior Member of Engineering Staff, RCA, Government and Commercial Systems, Missile and Surface Radar Division, Moorestown, NJ 08057.

Fabricating the enclosure

A typical enclosure for a microwave integrated circuit consists of a shallow five-sided rectangular can and a cover. Dc and rf connectors are generally mounted to the side walls with the circuitry attached to the bottom inside wall of the enclosure. This arrangement lends itself for interfacing the connectors and the circuits.

A few of the available processes for fabricating this five sided can include:

- drawing of wrought sheet metal
- a welded or brazed fabrication using wrought stock
- casting
- machining of wrought stock

Of the four processes listed, castings could be a poor candidate for an enclosure that will eventually be hermetically sealed. Castings are porous, making a vapor-sealed enclosure difficult, if not impossible to achieve. To circumvent the porous features in castings, vacuum impregnation can be used, but the limitations of such a procedure should be recognized. The casting industry uses either a resin obtained from plants or a material that is chemically synthesized. Both of these impregnants are temperature limited and at temperatures in excess of 500°F break down of the sealing effectiveness occurs. Of the inorganics, industry makes use of a filled sodium silicate due to the ease of handling. It also offers no problem with cleaning after impregnation. However, this form of impregnant is frequently unacceptable since mild temperature cycling can loosen the bond between casting and the sealing material. The possibility of contaminating "exposed" semiconductor chips with use of organic impregnates is also a prime limitation.

In selecting a welded or torch-brazed process (from wrought metal sheets), the designer should be aware of the metallurgical change

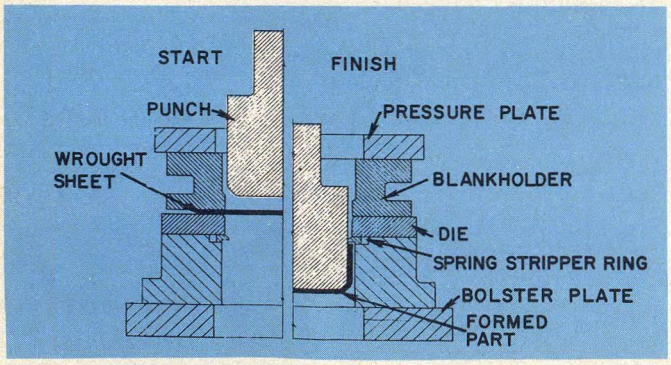

1. **This cross section** shows detailed elements used in the drawing process. This process lends itself to production runs of MIC enclosures.

that can take place in the metal used. This is most apparent when using aluminum. In simple terms, when wrought aluminum is subjected to the high temperatures encountered in most brazing/welding operation, the welded joint, upon cooling takes on the characteristic porous features of the aluminum casting. If this fabrication method is selected, the designer should minimize the total length of seams to be sealed.

One way of achieving minimal seal length is to machine the can from wrought stock or form it by using a drawing process. Drawing is the forming of a sheet of metal into a seamless hollow shape using a punch that causes the metal to flow into a die cavity or opening, Fig. 1. The drawn process does offer dimensional and form factor limitations, however. For example, most MIC enclosures have features such as compartments and surface flatness requirements that are impractical for a drawing process. To obtain a surface flatness of 0.001 inch per inch in a drawn can, requires an additional manufacturing operation which adds to the cost. Flatness of this accuracy is required in most modules when soldering substrates to an inside wall of the enclosure. This is understandable when considering, for example, a substrate size of 2 in. $\times$ 3 in. that is to be soldered down with a solder bond thickness of 0.001 in. to 0.004 in., optimal for a high strength solder joint.

Making the enclosure out of wrought stock has none of the limitations of the welded/brazed process or the drawn and casting methods. Machining technology has advanced to where numerically-controlled machining can be cost competitive with the processes mentioned above. The enclosure shown in Fig. 2 was machined from wrought aluminum using a numerically controlled milling machine. This manufacturing process and the projected unit cost, based on quantities of 5,600 for the package in Fig. 2 proved to be the least costly of all processes considered. For example, a brazed assembly has an approximate unit cost of $21 per can, a casting $18 per can, while a numerically controlled milling process costs only $12 per unit. A drawn can is not included since the form factor was not amenable to this process.

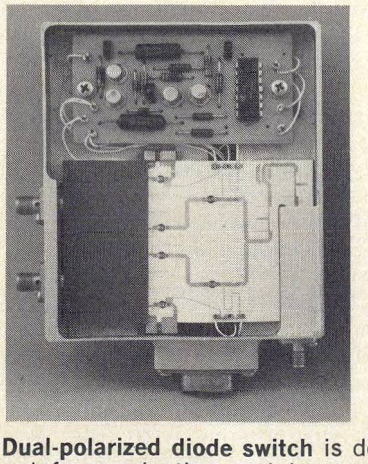

2. **Dual-polarized diode switch** is designed for production and low cost through the use of the up-to-date manufacturing tools, processes and materials.

Bonding substrates to enclosure

Microstrip circuits consist of thin-conductive films on a ceramic substrate with an overplating of a precious metal such as gold. The thin films are generally formed by an evaporated/sputtered/plating system of (but not restricted to) molybdenum and gold on an alumina substrate. Gold is an excellent selection for the rf transmission line. It resists the effects of corrosive contaminants and possesses good bonding properties. The gold metalized ground plane becomes the carrier/enclosure interface. The accepted means by industry of bonding the substrate to the enclosure is by soft soldering. This metallic bond achieves the required electrical grounding and with due consideration to temperature cycling and differential expansion of the bonded materials, a mechanical attachment is obtained.

A properly-designed solder joint between substrate and enclosure/carrier meets most commercial, military and space environmental requirements. For large production quantities, however, care must be taken in the metal selected for electroplating the carrier/enclosure. In addition, the solder selected must be compatible with the metalized surfaces in order to prevent "leaching," i.e. where thin gold dissolves into the predominantly thicker layers of the soldering alley. Intermetallics can then form which leads to voids and poor bond strength. This usually takes place after the repeated heating of a solder joint.

The flow temperature of the solder is also critical when other in-process procedures require heating of the assembly. In large production runs where soldering is done in a temperature profiled oxygen-free conveyor belt oven, relaxation of one control parameter is costly since reclamation of poorly soldered substrates to carrier/enclosure is not economical. Yield factor is a significant item in a belt driven furnace.

Before mounting the substrate to the enclosure, it's critical to first consider the placement of the microwave connection to the outside of the enclosure. Microstrip transmission lines are generally terminated in coaxial connectors mounted to the walls of the enclosure. The metallized ground plane of the substrate and the outer conductor of the connector must join to a common ground in a precise fashion for the microstrip to have minimal rf reflections and losses. This is generally achieved by the proximity of the connector and the edge of the ground plane as well as grounding the edges of the substrate to the enclosure with solder. The bond between substrate and carrier/enclosure is especially important in the vicinity of the rf connector, where a void could detune the circuit. Tracking down this detuning effect is usually quite difficult.

The use of an adhesive for bonding substrates is another method used by industry. The adhesive is generally applied using a stenciling tool, Fig. 3 and is most attractive for both large and small production runs.

The microstrip diode switch in Fig. 2, for example, uses a flexible adhesive bond for holding down the substrate. These adhesives are a room temperature vulcanized silicone rubber which cure to a tough rubbery solid-bond when exposed to moisture in the air.

Adhesives such as loaded RTV (a registered adhesive brand name) and epoxies are not sufficiently (electrically) conductive in most microstrip applications to use as a substitute for soldering. To meet the grounding requirements in the switch design (Fig. 2) where an adhesive was used, a thin ground strap is bonded in the circuit areas where grounding is critical. To make an effective ground connection between the outer conductor

(continued on p. 34)

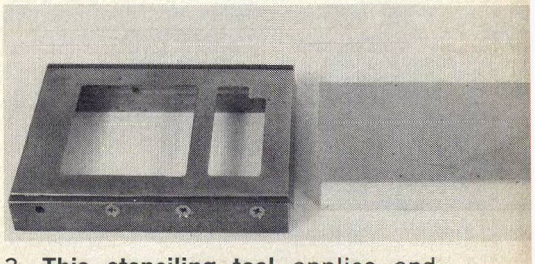

3. **This stenciling tool** applies and controls the thickness of adhesives in bonding substrate to carrier. It can control thickness between 0.004 inch to 0.009 inch.

of the rf connector and the ground plane of the substrate, a one-mil thick metal strap is fusion bonded (parallel gap welded) to the face of the connector directly under the center conductor and then bonded to the ground plane of the substrate. The bonding of the ground strap to substrate ground plane is made after assembling both the connector and substrate into the enclosure. This last bond is made through an aperture in the enclosure as shown in Fig. 4. Sufficient slack is designed into the ground strap to account for thermal expansion of the assembly. A metal (gold ribbon) strap, with slack, is also used in making the rf connection between the center conductor of the connector and printed transmission line.

This grounding technique is a positive connection which soldering techniques may not achieve. Note that the substrate-to-carrier bond can be characterized as a dielectric (adhesive) as opposed to a metallic rigid bond. Loading of this adhesive with metallic particles may be required to improve thermal conductivity. A flexible (silicone base) adhesive can also accommodate thermal differences in expansions of the substrate and carrier/enclosure.

This use of adhesives and grounding with straps are generally associated with non-hermetic solid-state rf modules. For hermetically sealed units outgassing of solvents into the enclosure which may occur and coat exposed semiconductors.

The advantages of ground straps and flexible adhesives must also be reflected in considering yields:

- The design is more reproducible.
- Costly controls are minimal.
- The bond is flexible (using an adhesive like RTV) to accommodate wide temperature cycling.
- The design can accommodate wider dimensional tolerances on component parts.
- The design is less sensitive to aging and deterioration of contact connections such as a bolted-on connector.
- The ground straps eliminate the high rf insertion loss associated with conductive epoxy and silione base adhesive.
- Repair and reclaiming of substrates are easily accomplished by submerging the bonded assembly in solvents.
- The adhesive is easily applied with stenciling tools.

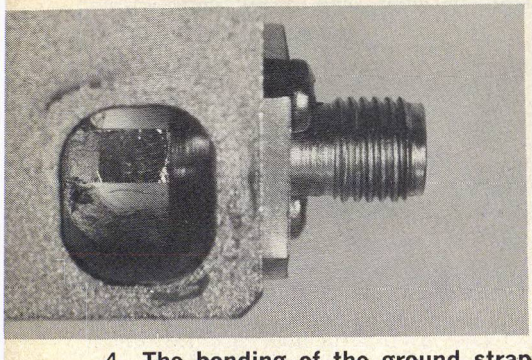

4. **The bonding of the ground strap** to the substrate ground plane is made through a hole using a parallel gap-welding machine.

Mounting the active elements

Generally, the mounting of a shunt diode microstrip requires the drilling of a hole in the substrate for positioning the diode. Grounding is then accomplished by soldering one end of the diode to the carrier. This assembly procedure for diodes may be accomplished at the same time the substrate is soldered to the carrier, Fig. 5. In an assembly that uses a flexible adhesive for bonding substrates, a design similar to a thermally and electrically conductive pad must be fusion bonded to the ground plane of the substrate completely sealing the hole. The diode is also fusion bonded to the pad. The substrate is then assembled to the carrier/enclosure. The switch in Fig. 2, has a screened-on adhesive of RTV loaded with thermally-conductive metal particles. The pad between the diode and carrier provide the required diode ground as well as spreading the dissipated power.

The geometry of the heat spreading pad under the diode is critical to the overall thermal design of the module. A diode in the dual polarization switch has an average power dissipation of 2 W during a normal operating mode, but the specifications require the thermal design to be capable of handling a reflected pulse (for short time durations) having a peak power of 6 W with a pulse width of 1.5 ms. The thermal time constant, τ, is less than 200 μsec which implies the junction temperature of the diode must reach steady state[1] conditions on the first pulse. This dictates the thermal design to be based on the 7 W peak pulsed power and not on the average 2 W dissipation. With the diode having a thermal resistance of 20°C/W, the efficiency of the thermal spreader must be sufficiently high in order to keep the junction temperature below the diode's upper limit of 160°C.

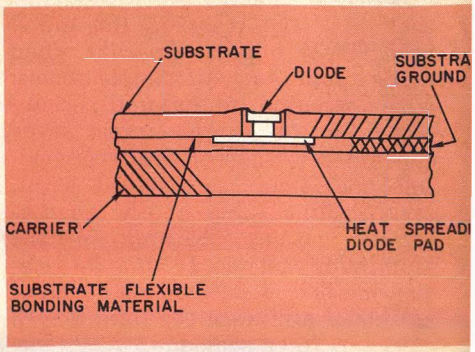

5. **A flexible adhesive or solder** is used to bond this assembled diode and heat spreader to the carrier. The diode pad is fusion bonded to the ground plane of the substrate.

A closed-form solution in designing the geometry of the heat spreader is difficult to obtain if not impractical. A careful (thermal) nodal model must be made using an iterative computer program to obtain the required dimensions. The optimum geometry is one in which an adiabatic boundary is formed between the edge of the spreader and the nodes within the carrier directly below this edge. Of prime importance is the use of a material that has a high thermal conductivity. Further, it is apparent that a spreader has no practical value unless the thermal resistance into the carrier is much greater than the chip carrier and junction.

The selection of other active elements such as a transistor package must also be subjected to a detailed tradeoff study. Flange-type transistors that are used in high-powered microstrip applications generally rely on the torqued screws for low-thermal contact resistance in transferring dissipated power into the circuit carrier/ enclosure. Also, circuit performance is dependent also on intimate contact with substrate edges and the carrier adjacent to both sides of the transistor. Voids between these surfaces will change the impedance match into the transistor.

To avoid these possible voids and minimize parasitics, a thin, soft grounding pad, electrically and thermally conductive material (such as 0.003 thick copper) could be fusion-bonded to the ground plane of the substrate, Fig. 6. This grounding pad is formed to fit under the transistor flange and secured by the clamping action of

(continued on p. 36)

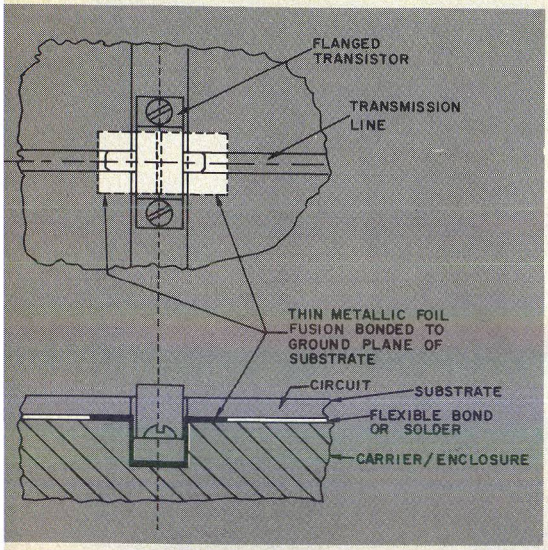

6. **In this typical transistor mounting to a ground pad,** the formed metallic foil is shaped and positioned to eliminate parasitics. It provides a solid connection between the substrate ground plane and transistor.

the screws. This arrangement again permits a non-metallic bond between substrate and carrier and can be used with a stud-mounted transistor package. It should be noted that since the ground pad is fusion bonded to the ground plane of the substrate, a soldering system for bonding substrate to carrier/enclosure could also be used.

Sealing of enclosure

Integrated microwave circuits must be protected to prevent performance degradation or catastrophic failures. Specifically, "exposed" semiconductors are sensitive to sodium ions, temperature extremes and moisture. Available in today's market are hermetically sealed diodes, transistors and moisture-proof (conformal coated) passive components. If the module is used in an environment that is idealized, the choice of hermetic vs. non-hermetic sealing of the enclosure is obvious. For some non-hermetic applications, combinations of exposed components, which are plastic coated, could be used with hermetically-sealed devices.

When the tradeoff calls for hermetic sealing of the enclosure, the designer must then decide on the degree of hermeticity. This is a function of the leak rate of gases out of or into a sealed enclosure. From the gas laws, leak rate is an exponential function of the pressure difference between the inside and outside of the enclosure and inversely related to the "sealed-life" of the module.

The "sealed-life" of the enclosure can be defined as the length of time for the pressure within the enclosure to approximate the external ambient pressure. At this point in time with operational temperature cycling, exchange of internal and external gases will take place. In addition, this normalization of pressure is a factor that must be accounted for in space (partial vaccum) appliations. At enclosure pressures of about a torr, rf voltage breakdown in coaxial transmission lines may occur. Volatilization of solvents in materials at low pressures must also be considered when dealing with modules for use in space.

Since pressurization of most solid-state rf modules is often necessary in harsh environments, the enclosure design is a critical cost item. Primary parameters for determining the material to be used in the design of a pressurized enclosure are weight and deflections of component mounting surfaces within the enclosure. It is also influenced by the process used in the sealing of the module. Processes that are popular for sealing include soldering, TIG (tungsten-inert-gas) welding and parallel seam sealing.

Soldering the cover on is a common, effective and inexpensive means of sealing for small production runs. In selecting this process, consideration must be given to the metallic finish of cover and enclosure body, the reflow temperature of the solder used and the mechanical strength of the soldered joint. The reflow temperature of the solder is critical to temperature sensitive components and joints previously soldered within the enclosure. Typically, the tin lead or indium-tin solders that have liquidous temperatures ranging between 117°C and 238°C could be used for sealing the cover without degrading the performance of most MIC circuits. Metallic finishes that are compatible with these solders are tin plating, copper plating and nickel plating. Those enclosure materials that could be used in an assembly where the cover is sealed with solder including copper base alloys, aluminum, stainless steel and nickel alloys.

When soldering the cover to achieve hermetical seal, the joint should be able to withstand loads from gas pressure differentials or from temperature cycling. This type loading on a soldered joint is subject to fatigue failures when

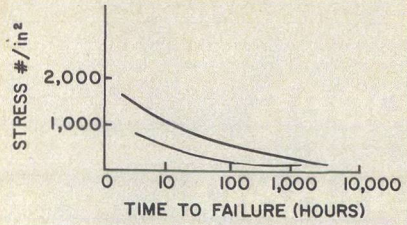

7. **Life expectancy of a soft-soldered joint** decreases as stress increases. Creep failure is also a function of temperature.

improperly designed. The constant loading may be only a small percentage of the load required for ultimate failure when it is suddenly applied to the joint. In other words, these low-level stress failures are time dependent,[2] Fig. 7. The joint configuration should also be one that suffers minimal damage where subject to an accidental blow.

Tungsten-inert-gas welding is a joining process where coalescence is produced by the high temperature generated by an arc between the tungsten electrode and the work piece. The arc is shielded by an atmosphere of argon, helium or a mixture of inert gases which purges the work area of oxygen-nitrogen atmopshere. TIG welding requires a high frequency, high voltage, low-current source to produce a spark across the gap, thereby forming a gaseous particle ionization. The positively charged gaseous atoms are attracted to the electrode (cathode) giving up kinetic energy and generating heat. Emitted electrons are attracted by the positively charged work piece (anode). The plasma zone formed (at a temperature greater than 5000°F) is quite small which localizes the heat in the parts to be joined. Proper heat sinking of the work piece prevents damaging temperature sensitive areas within the MIC modules.

Materials which are suitable for TIG welding include most stainless steels, copper, cupro-nickel, Kovar, aluminum and brass. A joint between the cover and enclosure body is characterized by a good fit, equal cross section of parts to be joined and sharp welding edges, Fig. 8.

Parts that are formed for TIG welding are generally more costly, for example, than parts that are shaped for soldering. The advantages of this joining process are:

- no flux is used which can contaminate the enclosed circuit
- joints are less porous
- fillers are not required.

(continued on p. 72)

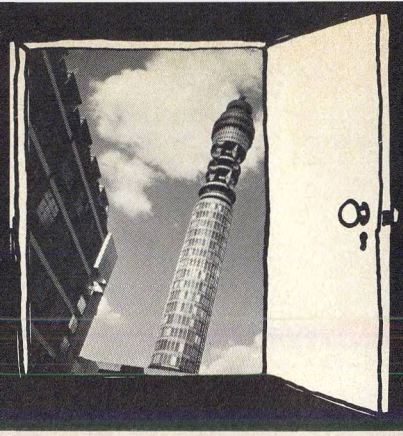

A Look At West Europe's Priorities In R&D

Richard T. Davis
Managing Editor

HOW does microwave technology in Europe stack up against that in the United States? If you think that there's no comparison, that the U. S. is ahead on all counts, perhaps you're not aware that:

- Britain has a lead of about five years on the United States in indium-phosphide technology. InP offers better efficiencies—15% vs. 6 or 7% for GaAs Gunns at Ku-band. A 17-GHz battlefield radar, initially designed for a 3W peak output with a GaAs Gunn device, will soon deliver 10 W. Why? An InP Gunn diode will be substituted without any additional battery drain.
- Plessey in Towcester England, is selling surface-acoustic-wave (SAW) oscillators, with custom designs available within six to eight weeks. In the United States, Teledyne MEC, the only American concern that appears serious about getting into the market at present, is still studying the sales outlook for such devices.
- Interest in the direct telecasting programs from satellites to homes is spurring the design of high-power European TWTs and simple, inexpensive monolithic and hybrid front-ends. Plessey is shooting for a 6 dB noise figure at 12 GHz in a FET monolithic front-end. Valvo (Philips) also has developed a 12 GHz MIC mixer for TV down-converting with a conversion loss of 3 dB.
- Impressive results are being achieved by European manufacturers in field-effect transistor technology. While top honors still go to Japan, improvements in both low-noise and high-power FETs are being made by such companies as Plessey, Siemens AG in Munich, Thomson CSF in France and the Philips Laboratory d'Electronique et de Physique Appliquee, also in France. Plessey is producing its own GaAs material. Most American FET manufacturers are dependent on outside materials sources, and most of the devices are being developed for in-house use only.
- A good deal of European R&D is still going into the improvement of microwave tubes. "We don't have any obsession with replacing every tube in a system with solid-state components," notes Tony Cooper, marketing manager of EMI-Varian in Hayes, England.

Better efficiency with InP

Plessey started investigating InP for transferred electron devices back in 1970 and more recently, for FET work. In the United States, InP is only starting to be investigated at such laboratories as RCA, Hewlett-Packard, Varian, Westinghouse in Pittsburgh and Cornell University.

InP offers improved efficiencies and higher powers in GaAs for transferred-electron devices. This is particularly important at frequencies above 12 GHz.

InP FETs allow working with larger geometries for a given frequency. A GaAs FET at 12 GHz needs a submicron gate length, while with InP the gate length can be greater than 1 μ. Obtaining submicron geometries on semiconductors usually means more costly electron-beam photolithography. InP FETS also offer improved gains above 10 GHz.

The best reported efficiency for InP Gunn diode is 21%, obtained by the Royal Radar Establishment in Malverne, England, while the best with GaAs is about 10 to 12%—and that's not too repeatable.

Plessey plans to market an InP TEA in about a year. The reflection amplifier, already developed in the laboratory, has an 8 dB noise figure at 15 GHz with an output of 10 mW. Gain is 10 dB over a 1 GHz bandwidth.

"We're looking at Ku-band initially," explains George Gibbons, manager of microwaves and optoelectronics research at Plessey's Allen Clark Research Centre, "X band is already pretty well established by GaAs FETs. We think the noise figure will also be less than FETs at these frequencies."

Plessey has also developed a lab model of a InP FET with a 4-μ gate length and a noise figure of 2.5 to 3 dB.

"We're planning to concentrate in the 1-μ gate length area and make improvements in the device technology," explains Gibbons. "We find the techniques involved with building InP devices, such as the etching, more difficult than with GaAs. But we have made some 1-μ gate length FETs using InP."

"For InP Gunn diode oscillators, we're replacing the ohmic contacts with a high-field contact or a hot-electron injecting cathode contact that overcomes the 'dead space' that exists."

SAWs for simple, stable sources

Surface-acoustic-wave oscillators, another area where Europeans appear to have a clear lead, were invented at the Royal Radar Establishment. In their simplest form, the oscillators are amplifiers with a SAW delay line connected as a feedback loop (Fig. 1).

SAW oscillators offer several important improvements over the lower-frequency bulk quartz reasonator. For one thing, they can be operated up to 1 GHz and even 1.5 GHz, thereby reducing by a factor of up to 10 the order of multiplication common to crystal-controlled oscillators. They also have the advantage of a degree of linear fm. This fm tuning capability can be traded off against the fixed frequency stability. Short-term stability of 1 in 10^9 is currently available—close to the performance of conventional quartz oscillators.

Another main advantage of SAW oscillators is that most of the ingenuity of the design is built into the mask, which can be printed

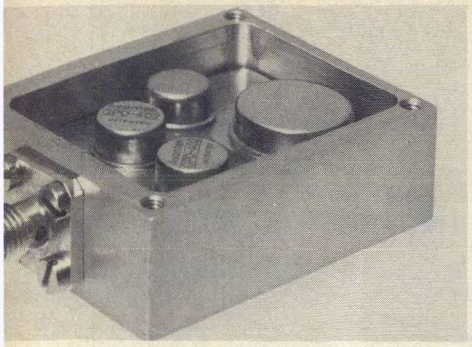

1. Experimental SAW stable oscillator developed by MESL operates at 490 MHz It consists of an AT-cut quartz substrate (the large can to the right) which forms the feedback loop across the three modular rf amplifiers.

onto substrates very accurately and in volume. The potential for inexpensive, stable oscillators is there. In fact, Plessey recently announced the availability of a commercial SAW oscillator, the SWO 170, which sells for about $600 (see p. 67). A library of marks is available, and the frequency can be tailored over a range of 10 MHz to 1 GHz.

"An fm capability to 700 MHz is also available, depending on the mask used," says Jim Heighway, manager of Plessey's SAW unit in Towcester. "Finger spacing for a typical unit is 1.5 μm, with each finger about 0.4 μm wide. We can go to about 0.25 μm, but that's about the limit."

The Plessey SAW substrate is being packaged in a TO-8 can with a separate amplifier, but plans are to mount the SAW device and a GaAs FET amplifier on a single substrate.

GEC/Marconi Research Laboratories in Great Baddow, England, is also producing SAW oscillators with fundamental operating frequencies to 1 GHz (see p. 67). According to Vince Wilkinson, manager of the Material Applications Group, Marconi is using a photolithographic technique to get approximately 1-μm finger spacing for 1-GHz operation. Wilkinson says that operation to 1.5 GHz is barely feasible at present, but he predicts ultimate operation to 2 GHz.

These SAW oscillators are not presently available off the shelf, but they can be built quickly on special order. As an example, a 400 MHz SAW oscillator built by Marconi uses a three-stage loop amplifier that delivers 5 W. The loop itself runs at a 10 mW level. The output power is achieved through additional stages of gain, and efficiency is 60%.

Frequency tuning of 1% of the center frequency is possible, and stability over 0 to 70° C variation is typically 50 ppm. Noise levels of −150 dB/Hz at 25 kHz have been obtained at 20 MHz.

Prominent in surface-acoustic wave technology development is MESL (Microwave and Electronics Systems Ltd.) of Scotland. It recently built an experimental SAW oscillator, Fig 1, at 490 MHz that has an fm deviation of up to 0.5% of center frequency.

Thomson-CSF is also very active in a wide variety of SAW devices, SAW oscillators included. For example, it recently developed a 500 MHz oscillator with a 10 dBm output and short-term stability of 5×10^{-9}/sec. Long-term stability is 5×10^{-5}/year.

Long-term stability is one area where SAW oscillators are inferior to AT-cut crystal oscillators. The surface-aging effects seem to get worse as frequency increases, and this is one aspect being improved on in laboratories throughout Europe.

Satellite telecasting TWT power

Interest in a 12 GHz TV broadcasting satellite, particularly in West Germany, is leading to the development of high-power, space-qualified TWTs and inexpensive, microwave front-end designs. Compromises in quality are not acceptable here—as with, say, educational TV broadcasts to remote areas. Satellite transmitter power of 700 to 800 W cw is essential to keep the cost of the 12 GHz/uhf down-converter commensurate with the $600 to $800 price of the TV receiver in Europe today.

According to Rudiger Teupser in Siemens' Satellite Communications Dept., Munich, feasibility studies by German industry show that TWTs can be developed with sufficient power (EIRP) for the direct transmission of TV signals. The European Satellite Research Organization (ESRO) has contracted with Siemens and Telefunken for the development of a tube with 700W output, efficiency of not less than 50% and weight of less than 3 kg. At Siemens, TWTs with multi-stage collectors are being designed to provide this power—a tenfold increase over what's available today. It now seems certain that within two to three years, tubes to meet this specification will be in production.

The biggest expense in telecasting by satellite is the need for inexpensive receivers. According to J. Siebeneck of Valvo in Hamburg, Germany, which is part of the Philips group, the use of existing TV sets requires a weighted video signal/noise ratio of about 55 dB for good picture quality. An 80 cm or 120 cm parabolic antenna would provide 37 to 41 dB gain, respectively. Siebeneck suggests a double-down conversion technique with a first i-f of about 900 MHz and a second i-f of about 120 MHz.

"This allows the reception of up to five channels in a 400 MHz band," he says. 'It also allows 'AFC'ing only the second converter and thus minimizing the frequency stability requirements for the first LO.

A simple, free running Gunn oscillator can then be used, Siebeneck points out.

In the proposed Valvo design, the first i-f down-converter is part of the antenna and is placed at the end of a TE_{11} feed guide, which also serves as a high-pass filter. As shown in Fig. 2, this converter consists of a microstrip-balanced mixer and integrated Gunn LO with a flat, round TM_{010} cavity. LO power is coupled to one port of the 3 dB hybrid coupler by means of slot/strip coupling. The conversion loss is about 3 dB for LO power of 9 dBm at 11 GHz. A thin-film i-f amp in this phototype is used with a noise figure of 5 dB, resulting in a receiver noise figure of 8 dB.

"This amplifier will be replaced by a monolithic integrated version, preceded by a low-noise stage in order to improve the receiver noise figure," says Siebeneck.

Plessey is looking at its FET capability for 12 GHz TV receivers and plans to come up eventually with a monolithic design. A prototype model consisting of a separate

(continued on p. 40)

2. Valvo's MIC front end for 12-GHz telecasting consists of a sum-enhanced-balanced mixer and Gunn LO. The LO is temperature-compensated to provide a total frequency drift of about ±1 MHz over −30° to +70°C.

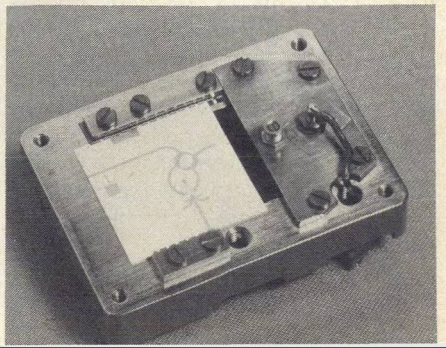

FET mixer, oscillator and preamp is planned.

"A FET mixer has the major advantage of conversion gain," says Gibbons of Plessey. "An overall noise figure of 4 to 5 dB could be achieved over a 500 MHz bandwidth at 12 GHz."

In addition, the cross-modulation between multi-TV signals is better with GaAs FETs than with Si bipolar devices.

FET oscillators also look particularly good for LOs in an integration receiver design because of their low-power consumption. Also, because the FET is a high-impedance device, it does not lower the Q of the oscillator resonant circuit, and good spectral purity signals can be obtained.

According to Jim Turner, FET group leader at Plessey, a microstrip FET oscillator has been developed at 11 GHz on a 0.025-in. thick alumina substrate.

He reports in a paper: "We're using a GAT-3 FET, operated in the common-source configuration, with the source connected to the microstrip ground plane via a 0.450-in.-length wrap-around metalization. When the gate is terminated by a short-circuit, stable oscillation is readily obtained."

"It is a wrap-around structure that gives this oscillator the high stability and low-noise performance that is more characteristic of coaxial than microstrip circuits. With a drain voltage of 7.6 V, the drain current is 13 mA, and the output power is 10 mW at 11.225 GHz, representing an efficiency of 10%. Varying the drain voltage from 2.5 to 7.6 V produced a remarkably smooth variation in output power of about 23 dB."

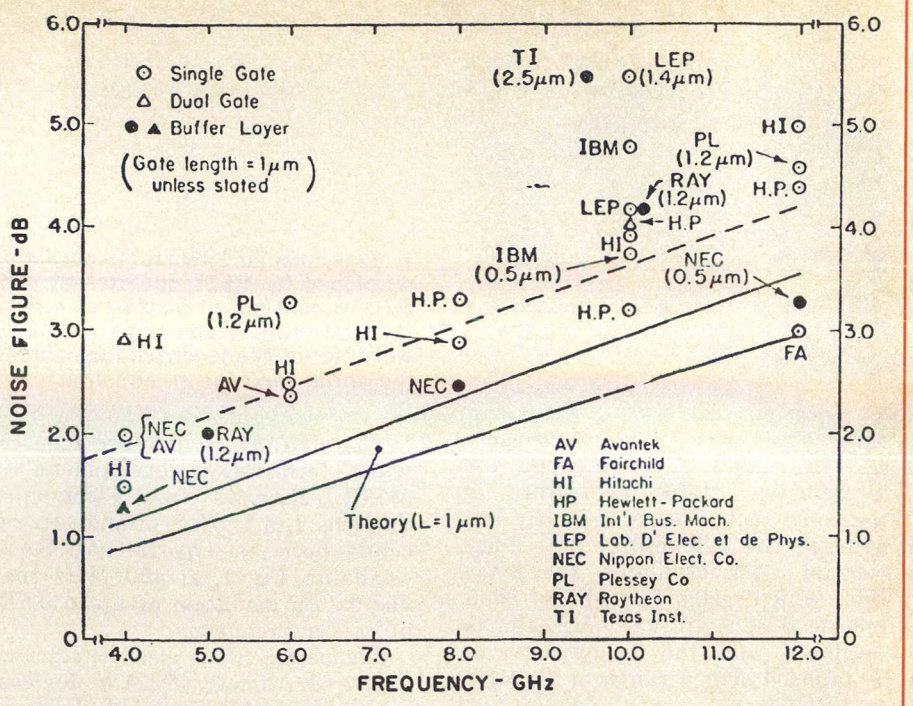

3. **The best noise figures** being achieved in laboratories with GaAs FETs use a high-resistivity buffered layer.

Main action in FETs

Field-effect transistor technology is the most dynamic field in microwaves today, and improvements in both low-noise and high-power FETs are being made constantly by European companies. They aren't necessarily the leaders—both the Americans and Japanese are pouring in tremendous R&D effort, and the results show it. The current leader in high-frequency, low-noise GaAs FETs appears to be the NE 38806 made by Nippon Electric Co. in Japan. This device, with a 0.5 μ gate length, has a typical noise figure of 2.5 dB at 8 GHz. Watkins-Johnson in Palo Alto, CA, is the leading producer of FET amplifiers, and is reported to have 80% of the market. It uses NEC's devices almost exclusively.

Nonetheless it's a wide-open race, and several European manufacturers, who tend to concentrate on higher-power devices, rather than lower-noise figures, have achieved some fairly impressive results.

The major European firms and institutions in FET work are in Britain, France and Germany. Siemens AG in Munich and the University of Aachen in West Germany are quite active, along with Thomson CSF and LEP (Laboratory d'Electronique et de Physique Appliquee) in France and SERL (Service Research Laboratories) in England.

Plessey in Towcester developed the first GaAs FET about 10 years ago. Today it is very heavily committed to both R&D and the selling of a variety of FETs, Fairchild Microwave is presently the only U. S. manufacturer of GaAs FET devices and presently sells 2 μ devices. Hewlett-Packard plans to introduce a 1-μ-gate device, competitive with NEC's beginning next year.

The field-effect transistor has almost overnight established itself as a signal amplifier up to 15 GHz, with a noise figure that is better than all other front-ends except the parametric amplifier. The key to this success has been not only the 1-μm gate length, which can be achieved with conventional photolithographic techniques, but also the extreme simplicity of the device structure. Companies aiming at GaAs FETs with a gate length of 0.5 μm will probably have to go to electron-beam photolithography.

The state-of-the-art for FETs in the 4-to-12 GHz range (Fig. 3) shows that noise figures increase correspondingly from 2 dB to 4 dB. The best devices all use a high-resistivity buffered layer to separate the critical epitaxial layer from the highly doped substrate.

While the graph shows NEC leading the FET noise-figure race, the best European performance is registered by Plessey in England and LEP in Paris. But both Plessey and LEP show a noise figure that is about 0.5 dB more than those obtained in Japanese and American laboratories. Plessey is producing a submicron-gate FET, with a noise figure of 5 dB and 8 dB gain at 9.5 GHz.

The power FET, which is in an early stage of development, does not compete as a device of proved reliability at present. Part of the reason is that the planar simplicity of the small-signal FET is lost; it's necessary to use double-layer epitaxy or an interdigitated mesa structure to achieve desired power levels.

Once more, a Japanese firm, Fijutsu, has the lead in this area with a 1.6 W MESFET at 8 GHz and 45% efficiency. Engineers at Fujitsu predict that with improved techniques to reduce common-source lead inductance—the main limitation with power FETs—5 to 10 W at X band will be achieved, surpassing the best performance of bipolar transistors.

How do the devices of European manufacturers compare with these results? At Thomson-CSF, Dept.

(continued on p. 42)

Power FET results at Plessey

Device gate length	Frequency	Output power ~ mW	Associated gain	Power added efficiency	Low-level gain	1 dB compression point
3.5 μm	2 GHz	1300 mW	6.2 dB	32%	8.3 dB	1.2 W
2.0 μm	5 GHz	370 mW	4.0 dB	19%	7.2 dB	200 mW
2.0 μm	8 GHz	210 mW	4.0 dB	12%	5.3 dB	190 mW

Microelectronique Hyperfrequence in Paris, 1 W at 6 GHz has been achieved with 6 dB gain. Some of Plessey's latest results are 1.3 W at 2 GHz; 370 mW at 5 GHz, and 210 mW at 8 GHz (see table).

According to Gibbons at Plessey, European engineers tend to use FETs at frequencies as low as 1 GHz, while Americans rely more on bipolar devices in this area.

"European firms did not develop their bipolar transistor capability as early as the U. S. did, and, as a result, we tend to rely more on our existing FET capabilities," Gibbons says.

Gallium-arsenide FETs with gate lengths of 1 μm or less are being produced by IBM in Zurich, LEP, and Plessey, in laboratories. These devices are providing power gains of 10 dB at X band with a 6 dB noise figure. Commercially available from Plessey are 1, 2 and 4 μm gate-length devices for operation at X, C and L-band frequencies, respectively. Plessey's GAT 2010, for example, a 2 μm gate-length FET, gives 8 to 10 dB of gain with a 3 dB noise figure at 3 GHz.

Buffer layer lowers noise figure

Material quality is of the utmost importance in fabricating FETs. "For this reason," says Jim Turner, FET group leader at Plessey, "many European laboratories are using epitaxial GaAs containing an intermediate high-resistivity buffer layer grown between the semi-insulating substrate material and the thin active epi layer."

This reduces the diffusion of unwanted impurities from the substrate to the active layer. The buffer material, however, does offer improved NF performance (Fig. 3). "We use high-resistivity buffer layers that are either chromium-doped or grown from a pure GaAs ingot source," Turner observes.

There are other approaches, however. At Siemens in Munich, ion implantation of sulfur into the semi-insulating substrate is being used to implant the impurity. Typical results for a 1.8 μm gate device are 8 dB gain at 10 GHz.

At a semiconductor conference at Cornell University, Ithaca, NY, last summer, Turner described other fabrication procedures. The small-signal FETs at Plessey, for example, are fabricated by the now conventional "float-off" metalization process, and both photolithographic and electron-beam resist exposures are used to define the short-gate devices for X-band operation. Both Plessey and the Technical University of Aachen in West Germany use a "notched" gate technology, where, rather than define the channel thickness by the thickness of the n-type epitaxial layer, a thicker layer is grown and the channel region under the gate is defined by etching. This removes the high tolerance in thickness required for the epitaxial layer when the channel region is not etched. Plessey uses a preferential etch that gives a very flat-bottom hole.

According to Prof. Heinz Benneking of the Technical University, in the laboratory they are using a two-stage etch process—first a wet etch and then a slow desputter etch that removes about 170 Å of GaAs a minute. The university has developed a V-shaped device that gives microwave performance similar to that of a one μ device (Fig. 4). The V-shaped channel is defined by a preferential etch. It provides about 14 dB of gain at 10 GHz.

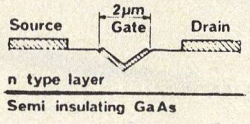

4. V-shaped channel of FET developed at Aachen measures 2μ across top of V, but it gives performance similar to a 1μ device.

Up to now, most research in microwave FETs has been directed toward small-signal, low-noise devices. Recently, however, 1-W power FETs have made their debut in Europe, challenging TWTs in various medium-power applications, particularly at S and X band, where satellite communications and phased-array radar applications are being considered.

Thomson-CSF which is concentrating on power FETs, has developed one that delivers about 1 W at 6 GHz with 6 dB gain. The device is made on a p-type substrate that acts as the control gate. Sputter etching defines the channel thickness. The total gate width determined by the drain-to-source spacing is 3060 μm. It is composed of 37 source and drain fingers 1.5 μm apart.

At the university in Aachen, four small-signal devices have been paralleled for use in high-speed (50 ps) switching applications—such as in optical communications. High-power FETs are necessary here for switching the high currents that exist in an injection laser.

The Technical University is also experimenting with a two-layer power FET. The channel consists of two sections: a low-doped layer under the Schottky gate and a high-doped layer next to the semi-insulating substrate.

"By etching source and drain, contacts next to the heavily-doped layer are made to the heavily-doped layer, giving high values of transconductance," says Professor Benneking in Aachen. "The low-doped layer under the gate electrode enables high voltages to be applied between source and drain."

Power FETs soon?

According to Gibbons, Plessey in Towcester is going to market GaAs power MESFETs (metal epitaxial semiconductor) in 1976. Plessey has already developed two power FETs in S-band. They provide 1 dB compression powers in excess of 1 W and over 8 dB gain. And Gerard Vigne of Thomson-CSF, Div. Micro Electronique Hyperfrequence in Orsay, France, says his company will be putting on the market next year a 0.25 W FET that operates at 6 GHz.

Figure 5 shows a Plessey MEGFET with a planar meander gate geometry, so-called because the gate fingers "meander" across the GaAs

(continued on p. 44)

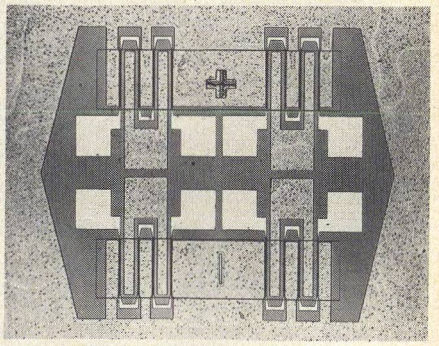

5. Plessey's meander gate GaAs MEGFET has source fingers that surround the chip, resulting in a low-impedance common connection and thermal path.

substrate several times to create a four-stripe gate over each of the four cells. The four cells are connected by bonding wires.

"It is fabricated in a sulfur-doped, n-type epitaxial layer, grown on a buffer layer of high-resistivity material upon a semi-insulating substrate," explains Turner of Plessey. The large metal source contact helps to remove heat from the surface of the device while also providing a low-source impedance contact. Source and drain contacts are indium/germanium/gold, and the Schottky barrier gate metal is aluminum. Total gate width is 2500 μ, and the gate length is 3.5 μ.

"At 2 GHz, this device produces a low-level gain of 6.3 dB with a 1-W output power," continues Turner. "Power out at 1 dB gain compression is 650 mW with 22% added efficiency."

A 2 μ gate length version of this MEGFET has also been developed. At 3 GHz, it produces 700 mW output power with 6 dB gain and 25% power-added efficiency. At the 1 dB compression point, the output is 530 mW.

"Saturated output power for this 2 μ MEGFET is over 500 mW at 4 GHz and 400 mW at 5 GHz, but the low-level of gain was less than expected," says Turner.

A second design that Plessey recently developed is the diamond-shaped gate power GaAs FET, or DIGFET (Fig. 7). Its total gate width is 2800 μ, and the gate length is 3.5 μ. Output power at 2 GHz is 1.3 W with 6.2 dB gain and 32% power-added efficiency.

A four-cell DIGFET has also been developed. It provides 800 mW cw with 6 dB gain at 2.5 GHz and 4 dB gain at 3.5 GHz. Two-tone intermodulation tests performed at 2 GHz produced −24 dB IMP at 500 mW output power. This device has also operated under pulsed conditions providing 1.3 W with 5.7 dB gain at 2.5 GHz.

The highest reported power-added efficiencies for power MESFETs have been reported by RCA at the David Sarnoff Research Center outside of Princeton, NJ, where Class B amplifiers are reported to have achieved 68% at 4 GHz and 41% at 8 GHz. At 4 GHz, the power output was 260 mW with 11 dB gain, and at 8 GHz, 280 mW at 8 dB gain.

At Plessey, Turner predicts that "operation from 8 to 12 GHz is even within reach." However, he adds, MESFETs are unlikely to challenge TWTs in the region beyond X band."

At these higher bands, Thomson-CSF engineers say that with Schottky gate technology, 20 mW at 13 GHz and 10 mW at 18 GHz are possible.

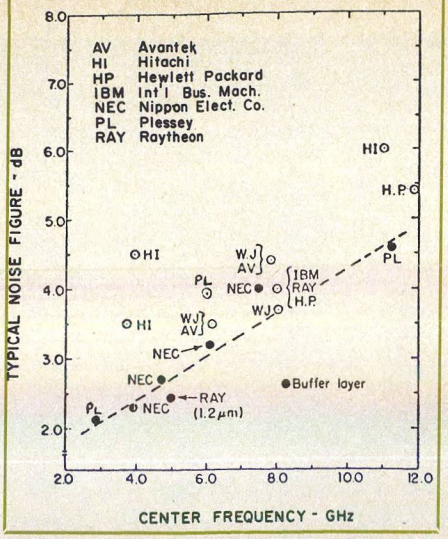

6. Noise figures of FETs become slightly degraded when devices are designed into narrow-band amplifiers. This is due to input matching.

Matching high FET impedance

In the design of FET amplifiers, one of the most difficult matching problems is how to handle the high output impedance of several hundred ohms. Although FETs are inherently broad-band devices, their bandwidth is limited by the matching of its high input and output impedances to 50 ohms. This is important in wideband amplifier designs, where up to 3 dB in noise figure can be incurred through matching at the input. Even in narrow-band designs, as shown in Fig. 6, at least a 0.5 dB increase in noise figure is introduced in matching the FET input/output impedance to 50 ohms. On conventional 0.025 in. thick alumina, high impedance lines are not easy to produce because they're so narrow. Plessey solved this problem by milling a 0.010 in. slot to the alumina substrate and laying a bond wire along the length of the slot. Result: a 300-ohm transmission line.

Another approach at Plessey is to use variable output impedance matching elements. These consist of additional metalized areas, or or "islands," that can be bonded into the circuit.

"This enables the performance of the module to be tweaked, to take account of spreads in a FET's rf characteristics," Turner explains. "It can also be used to vary the center frequency and to vary gain and noise figure."

This technique has been applied to a Plessey GAT-3 FET, in a microstrip design, which offers typical maximum gain of 8.5 to 6.9 dB from 8 to 10 GHz. The transistor chip is mounted on a 1-mm-diameter post that protrudes through a hole drilled in the 0.635-mm thick alumina. The flange of the post is soldered or bonded to the microstrip ground plane, thereby providing a low-inductance dc return for the source contact of the transistor.

To achieve high gain over an extended bandwidth, a broadband input matching circuit was found to be essential. The output impedance is varied through the bonding of adjoining pads. This provides a center frequency match and allows the amplifier gain to be tuned over 2 GHz.

Typical gain of 7 dB can be obtained from 8 to 10 GHz. A noise figure of 4.7 dB with an amplifier gain of 5.8 dB was obtained by Plessey at 9.5 GHz.

"The noise figure at any tuned frequency can be reduced," Turner explains, "at the expense of gain and input match, without affecting bandwidth, by applying negative voltage to the gate of the transistor."

"A minimum noise figure of 4.4 dB with gain of 3.1 dB was obtained at 9.5 GHz. By cascading two of these modules, Plessey researchers got over-all gain of 12.5 dB and a noise figure of 6 dB at 9 GHz.

For narrow-band designs at X band, where it's difficult to measure a FET's S parameters accurately and design matching networks on alumina, Plessey has developed a disk-tuning technique (Fig. 7). The FETS are mounted along a 50-ohm transmission line, and metal disks are slid along the line between the FETs until the desired response is obtained. The disks are then rigidly fixed in position with epoxy or solder. The three-stage amplifier provides over 20 dB gain at 11.2 GHz.

6-12 GHz lumped element design

One technique that looks par-

(continued on p. 46)

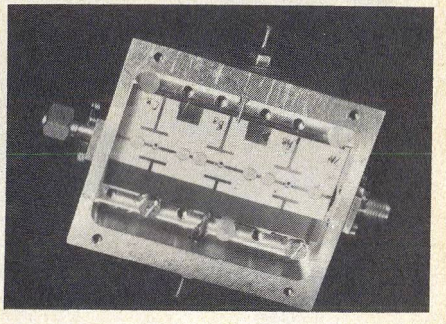

7. Narrow-band FET amplifier is tuned when metal disks are moved on a 50-ohm microstripline. The dc bias is applied via bond wires from the microstrip bias tees. A resistive film is attached to the gate bias network to introduce loss and thus prevent low-frequency oscillations.

ticularly promising for wideband FET amps at X band is the use of lumped-element techniques. Ray Pengelly, senior microwave engineer at Plessey, Roke Manor, Hampshire, England, reports that a three-stage amplifier has been developed through use of GAT-3 FETs in chip form. A two-stage lumped element design provided power gain of 9.5 ±1 dB over 6.5 to 12 GHz, with a noise figure of about 7 dB. A three-stage design provided over 16 dB over the same range.

To characterize the intrinsic transistor, an automatic network analyzer, together with a computer program, is used to correct the measured S parameters for jig parasitics, wire-bond inductances and end-effect capacitances. At the first stage, the input matching network is optimized for input VSWR and noise admittance match, while the output coupling network provides a frequency-dependent attenuation that compensates the FET gain slope at less than 12 GHz. The input/output matching networks for the remaining stages are designed similar to the first, except they're optimized for gain and output VSWR.

These techniques for achieving broad bandwidths have also been applied at Plessey to a monolithic amplifier chip designed and fabricated on GaAs (Fig. 8). A single stage is capable of producing 3 dB gain from 7.7 to 11.7 GHz, and chips can easily be cascaded. Each lumped inductor and capacitor on GaAs is about one-quarter the size of those used in a hybrid design.

"To retain resolution in fabricating the lumped networks, we found it necessary to use a 1 μ metalization thickness," explains Pengelly. "This results in Q's of 15 to 60. By increasing the thickness to aproximately 3 μ, a 25% improvement can be expected along with improved gain."

The "on-chip" matched FET was fabricated on GaAs with a normal photolithographic process, but the 1 μ long gate was fabricated with electron-beam exposure techniques.

Another monolithic design at Plessey has also been developed to cover 6 to 12.4 GHz with 5 dB gain. "These monolithic designs hold great promise as low-noise, front-end preamps," Turner contends. "They will come close to matching the performance of even the lowest noise-figure paramps."

Their potential low cost and the intrinsic reliability of a monolithic design also makes them candidates for phased-array radar systems, he adds.

Cooled GaAs FETs reduce NF

Cryogenic cooling of FET amplifiers makes it possible to achieve even lower noise figures, allowing the amps to compete with parametric amplifiers at frequencies up to 12 GHz. A few years ago at the National Center for Telecommunications Study in Lannion, France, a 5.9 to 6.4 GHz FET amplifier was cooled to −60°C. Its noise figure was reduced to a little over 2 dB at 6.15 GHz. At −20°C, noise figures of less than 4 dB were achieved in the laboratory.

Speaking at the European Microwave Conference in Hamburg, Germany, in September, Charles Liechti, section head in Hewlett-Packard's Solid-State Laboratory, Palo Alto, CA, announced a three-stage GaAs MESFET amplifier operating in the 11.7 to 12.2 GHz band. When the amplifier was cooled to 40°K, he reported, a noise figure of 1.6 dB (T_e = 130°K) with 31 dB gain. The same amplifier at room temperature had a 5.3 dB T_e = 700°K) noise figure and 18 dB gain.

As a comparison, Peltier-cooled parametric amplifiers operating in this range are capable of about 100°K noise temperatures, and cryogenic parametric amplifiers can offer 50°K noise temperatures.

According to B. S. Lee, sales executive of Ferranti's Solid-State Microwave Group, Cheshire, England, paramps are being used in radio astronomy, radar, tropospheric-scatter and satellite communications. Since astronomy requires the ultimate in low-noise performance, the most vulnerable markets for intrusions by FETs appear to be radar, tropo and satcom.

Lee admits that Americans are

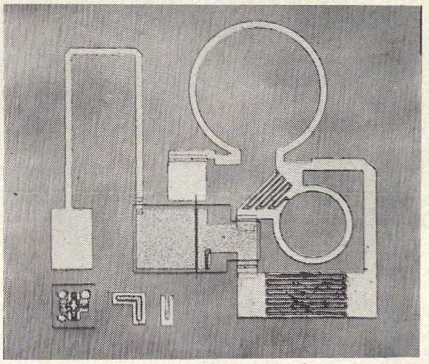

8. Single-state monolithic FET amplifier, developed at Plessey, covers 7.7 to 11.7 GHz. It measures 6.35 mm × 6.35 mm and is on 0.635-mm alumina substrate. Careful layout of the elements and good common grounding are important to minimize unwanted rf leakage.

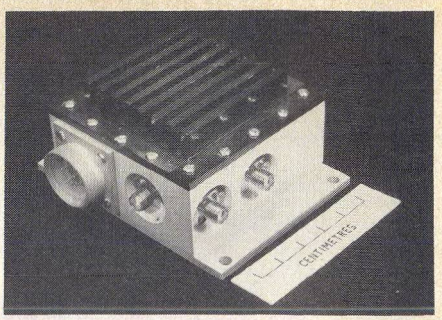

9. MIC paramp developed by Marconi provides a 200°K noise temperature at 7 GHz.

ahead in paramps in the 3.7-to-4.2 GHz range, which are available with 45°K noise temperatures. "This is an area we have not put much money into developing," he explains. "Instead we are going into the low-cost, moderate-performance and small-sized paramp."

For example, Ferranti is pinning its hopes on a small and relatively inexpensive, uncooled parametric amplifier. This X-band paramp, weighs about 1.33 lb and measures 2.36 × 3 × 2.5 in. It provides a 500-MHz bandwidth in the 8.5-to-10.5 GHz range. Other frequencies are also available. The paramp has a typical noise figure of 2.3 dB and 15 dB gain at 9.5 GHz. According to Lee, it would sell for about $4500 in quantities of 100.

"We feel this is a great candidate for airborne radar front end," he observes. "We're very interested in this paramp for the radar intended for the new F-16, which Hughes and Westinghouse are presently competing for. But it's unlikely the Americans will select a foreign paramp vendor. Our prospects for the European version of the F-16, however, are much brighter."

The Ferranti paramp can be made small because it uses a patented, double-diode circuit in which two GaAs varactor diodes are mounted back-to-back in phase opposition. The idler circuit for this double-diode paramp series uses an idler frequency at 31 GHz or 43 GHz, depending on the signal frequency of the paramp. Since this idler circuit is balanced, it doesn't require any external filter circuits. The pump frequency is about 31 to 34 GHz, and Varian Gunn-diode pump sources are commonly used.

Mullard, Ltd., in London has also developed an inexpensive, uncooled paramp (Fig. 9) for a satellite communications terminal. It was built under contract from the British Directorate of Components, Valves and Devices.

According to Stuart Longley, product engineer at Mullard's Communications Electronics Div., the 7.2-to-7.76 GHz, computer-de-

signed paramp is built on microstrip and offers a 1-dB instantaneous bandwidth of 50 MHz with 15-dB gain. It uses a 34-GHz Gunn pump and a single unencapsulated GaAs varactor chip that is etched to resonate in the circuit. Noise temperature is less than 200°C at 50°C, held constant at that temperature by a heater.

Longley sees the unit, built-in quantities, selling for $2,000, or about one-fifth the usual cost of a paramp at that frequency.

"A major factor in the cost of the paramp is the price of the pumps used, and while millimeter pump prices have been coming down, a 34-GHz pump still costs about $1400," notes Lee of Farranti. On the other hand, a 17 GHz Gunn pump costs only $200. As a result, where low-cost is essential and size and weight aren't that critical—such as in the tropo market—we'll use a 17 GHz pump and an idler circuit with a single varactor diode."

For the 2.5 GHz tropo link from Scotland to British Petroleum's North Sea oil fields, for example, Ferranti paramps are used with a 16 to 17 GHz pump. The tropo system was built by GEC/Marconi, Ltd., Great Baddow, England.

Impatts used in paramp pumps

An interesting aspect of European parametric amplifier designs is the wide use of avalanche diode oscillators in paramp pumps. In the U.S. a few years ago, a controversy raged over the suitability of Impatts as a pump source[1]. Some designers contended that Impatts could degrade a paramps's noise figure. For example, when a composite signal is large enough to cause the slightest degree of nonlinearity in a paramp, the noise present on an Impatt source is cross-modulated into the signal band. Now a much better understanding of the basic device mechanisms has shown that Impatts can be improved up to 10 dB if operated typically 10 dB below their maximum power output.

Cyril Brown, head of the Microwave Div. at the GEC/Hirst Research Centre, Wembley, England, believes that Americans were premature in their dismissal of Impatt pumps in favor of Gunn sources. "Many of the paramp systems in the U. K. use Impatts," he notes.

J. R. Lehan, microwave marketing manager at AEI Semiconductor, Ltd., Lincoln, England, says: "The application of Impatts as pump sources is increasing rapidly, now that the noise problem has been overcome."

He contends that output level control and stability with Impatts is even better than in other solid-state sources. For example, AEI markets a high stability Impatt pump source, the DA1116 series, which provides 100 to 200 mW output power in the 30 to 41 GHz band. Typical stability is 100 kHz/°C.

Plessey in Towcester is developing both Impatts and Gunns as paramp pumps. "We have more or less abandoned GaAs in favor of silicon for our millimeter wave Impatt work," says Gibbons. "We're presently selling Impatt waveguide source designs that provide klystron performance in terms of spurious noise far from the carrier. In the lab we've developed double-drift Impatt sources that deliver 850 mW with 12% efficiency, 350 mW at 70 GHz with 10% efficiency and 100 mW at 90 GHz 5% efficiency. Most of the pump work is in the 40 to 75 GHz range, and we've supplied pump sources at 50 and 75 GHz to Comsat."

Thomson-CSF in Paris is also very active in Impatt-diode oscillators for paramp pumps, local oscillators and transmitters for millimeter-wave communications. The TH 5104 for example is a 40-GHz source that delivers 200 mW and can be tuned ±250 MHz anywhere in the preset frequency range of 32 to 40 GHz. Electrical efficiency is 4%, and stability is 3 MHz/°C.

At lower frequencies. Impatt diodes are being widely used in power-amplifier applications.

At X band, Plessey has recently developed in the lab a GaAs Impatt diode that delivers 2.5 W cw with an efficiency of 15 to 16%. "This device was developed for the Ministry of Defense," explains Gibbons, "for use as an amplifier." The bias voltage requirements are 50 V. Commercially available from Plessey are 1.5 W cw GaAs Impatts that offer 12% efficiencies at X-band.

At Siemens AG, a double-drift Impatt has been developed that delivers over 3 W cw at 7 GHz with 11% efficiency. According to Guenther Kesel, head of microwave device development in Munich, Siemens plans to go after the low-power TWT market (less than 10 W) with a lower-power version of this device.

Pulsed avalanche diodes are also being developed by Mullard, Stand-

(continued on p. 48)

ard Telecommunications Laboratories and Plessey for use as Trapatt sources in high-power pulsed applications, such as radar and navigation systems.

"Trapatts, in the past, have been reported to be unreliable," notes Longley of Mullard, "but that's not true. We usually find a malfunction in the modulator is the cause."

The interface between the circuit design and the device is very critical. Mullard recently developed an MIC version of a pulsed Trapatt oscillator that provides 100 W peak at 2.5 GHz in the fundamental mode, with 30% efficiency, using a 0.5 μsec pulse at a 2 kHz rep rate. In the second harmonic mode, 30 W at 5 GHz is obtained with 10% efficiency. The circuit (Fig. 10) uses an unencapsulated Trapatt chip mounted on a copper header at the substrate edge.

"The chip is connected to the triggering line, using a 25 μ diameter gold wire," Longley reports. "However, computer modeling for a Trapatt is difficult. Therefore to optimize power output at the fundamental and to provide a suitable match for extracting the second harmonic power, a tunable matching filter was initially used, consisting of five-movable, gold-plated steel plates held in position by magnets under the substrate. A final microstrip design for fundamental extraction was obtained by direct translation into photo-mask form of the movable plate configuration.

"We're presently concentrating on obtaining high peak power levels with longish pulses—that is, where the burst—several microseconds followed by a coded cycle—is long compared to the thermal time constant of the diode. To do this, we use a double-sided heat-sinking technique. Also, a Trapatt diode with a mesa profile is being used to prevent edge breakdown and premature failure. This is being accomplished with a plasma-etching process."

Plessey in Towcester is working on X-band Trapatt diodes in a phased-array program for the British Ministry of Defense.

"They're presently achieving 15 W peak at 30 to 35% efficiency at 8.5 GHz, with 25 μsec pulse lengths," Gibbons reports. To obtain a properly shaped pulse, it's important to tune out the higher-order harmonics—at least the third and preferably the seventh."

A smaller package with a cutoff well into the millimeter range and a 3 mm, 50-ohm coaxial line have been used to optimize efficiency and operating frequency.

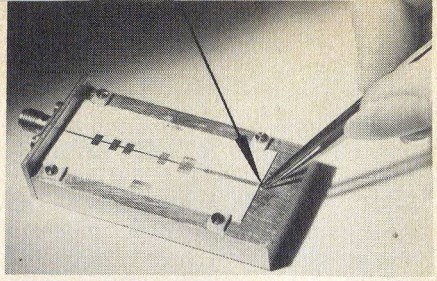

10. Pulsed Trapatt source uses sliding gold-plated steel plates for matching the fundamental output and extracting the second-harmonic power.

Gunn sources in widespread use

The GaAs Gunn diode is finding its way into numerous applications with a wide range of specifications and costs. Its low operating voltage—6 to 12 V at X-band—has made it the most popular low-power source. In a cheap ($20) and unsophisticated role, the Gunn source has found its widest use in the intruder alarm market at 10 GHz. The efficiency of a Gunn diode is a low 1 or 2% but what's important here is not efficiency but the device's ability of dc into 5 to 10 mW of relatively clean X-band power.

Thousands of these alarm devices have been sold commercially in the European security market.

AEI Semiconductors, Ltd., in Lincoln, England, has a line of Gunn oscillators with reduced second and third-harmonic radiation to meet the requirements of the American market.

Gunn oscillators are also being used to replace the klystron LO in the marine radar business, which Decca continues to lead. As with most civil applications, the crucial question is cost, and many small-boat radars are still operating with klystron LOs.

Gunn sources are also well-suited for wideband military applications, such as ECM, and in frequency-agile radars and automatic test equipment. MESL of Newbridge, Scotland has developed a series of Gunn VCOs capable of ultra-fast tuning over the 5 to 16 GHz range in four overlapping units. The sources include isolator, switches, linearizing and stabilizing circuitry and thermoelectric heating and cooling.

Gunn oscillators are also being used in Europe in radar altimeters. MESL has a 4.3 GHz Gunn source in the STR 40J radio altimeter used in the automatic landing system of the British Airways Trident fleet. Plessey has also developed a 16 GHz Gunn source for altimeter use. The 7 ns pulses turn

(continued on p. 51)

on within 3 ns, and output is 5 W peak min.

AEI Semiconductor has developed Gunn diodes that deliver 50 mW over the range of 3.7 to 9.5 GHz in a Yig-tuned cavity.

"We can also obtain 45 mW over the 8 GHz to 12 GHz band, and material is now being prepared to achieve 30 mW over the 12 to 18 GHz band," says J. H. Lohoar, marketing manager. The diodes have been developed for microwave instrumentation, such as broadband sweepers.

At Marconi Instruments, Ltd., in Stevenage, England, Paul Beaujeux, commercial manager, reports: "We find that the economics of making microwave test equipment, such as sweepers, requires an in-house capability of the discrete components. Unlike low-frequency circuits, which are abundant and can be purchased from outside suppliers, the market for microwave devices is small and specialized. We found them expensive on the outside, and figured we could develop Yig-tuned Gunn oscillators cheaper ourselves."

As a result, Marconi has developed a range of Yig-tuned oscillators that cover 4 to 18 GHz and have power outputs to 80 mW.

"Some of the Yig-tuned oscillators are also being offered separately as components," Beaujeaux continues. "We've also developed an 8 to 18 GHz source which delivers 10 mW, and, in addition to our standard line, an 8 to 16 GHz source, which puts out 30 mW."

Other multi-octave bands covered are 6 to 14 GHz, and Marconi is also working on a 3.7 to 9.5 GHz, Yig-tuned sources. The Yig spheres used in these designs are being purchased from Litton and Watkins-Johnson. The oscillators all have a high-frequency tuning coil or fm coil that has narrowband tuning capability for use in frequency locking or fine tuning.

Philips Research Laboratories in Hamburg, Germany, also has a Yig-tuned Gunn oscillator (Fig. 11). The source delivers 50 mW from 4 to 8 GHz and was developed in cooperation with LEP in France. A small, thick-film, printed-circuit fm coil allows fine tuning over a 20 to 30 MHz range at a 3 to 4 MHz rate for modulating or phase locking. These Yig-tuned sources are sold commercially through Philips' Sivers Laboratories in Stockholm.

Tube R & D still going strong

One difference between microwave R&D in Europe and that in the United States is that Europe is still spending a good deal to develop tubes. One London research house believes that the U. S. has let "exaggerated hopes for solid state" cause "dangerous neglect" of microwave tubes, despite their importance in defense work. In fact, funding support for tube R&D in the U. S. declined from over $20-million a year in the early 1960s to about $5-million by the early '70s[2].

In Britain, the development of tubes, as well as many other microwave components is coordinated and funded through the Government's Directorate of Components, Valves and Devices.

"When a new requirement comes up which can't be met with existing tube technology, CVD will consider funding the development," EMI-Varian's marketing manager, Tony Cooper notes. "We don't have a flyoff, such as in the U. S., between two companies competing for a single contract. A single company is funded, based on the merits of its proposal. It's just too expensive to fund more than one company for a single device.

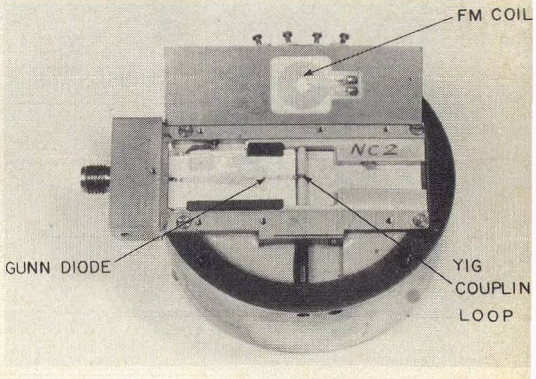

11. Yig-tuned Gunn oscillaltor covers 4 to 8 GHz and delivers 50 mW. Thick-film fm coil allows rapid tuning over a 30 to 40 MHz range.

"Also, because production quantities are seldom significant, a British firm would seldom 'buy into' a contract in the hopes of recouping its R&D expenditure in a follow-on production contract." ■■

References

1. Richard T. Davis, "Front End Designs—Assaulting the Old Noise Barriers," *MicroWaves*, Vol. 10, No. 4, pp. 32-36, (April, 1971).
2. Nathan Butler, "The Climate Is Changing in M/W Tube R&D—Can We Survive?" *Microwave Journal*, Vol. 18, No. 8, pp. 12-16, (August, 1975).

Graphs Simplify Load Impedance Measurements

Here are some handy curves for converting measured phase and amplitude data to complex impedance values.

CLASSICALLY, transmission line loads of unknown impedance have been measured using a slotted line and plotting VSWR and position of first null on a Smith Chart. This method is time consuming since it can only be done at spot frequencies. Usually a network analyzer is employed instead, which compares the amplitude and phase at a test port with a reference channel and displays the values on a meter.

This article provides graphs (Fig. 1) for converting reflection coefficient and phases to impedance values; namely, R/Z_o and X/Z_o. The charts are derived from computer data, applicable to any kind of load and frequency.

Converting amplitude and phase data

To make a complex impedance measurement on a load with only a basic network analyzer, one must convert the measured phases and amplitudes to complex impedance values. A typical measurement setup used for spot frequency or swept frequency measurement is shown in Fig. 2. Here the load is a log-periodic antenna which terminates a 50-ohm coaxial cable. After a short is used correctly for calibration, (a short gives a voltage-reflected wave phase of 180 degrees) the network analyzer displays the voltage reflection coefficient amplitude, $|\rho|$, and phase angle, ϕ, directly in dB and degrees.

There are two ways to convert to normalized load impedance values. The first is to use the relationships

$$\frac{R}{Z_o} = \frac{1 - |\rho|^2}{1 + |\rho|^2 - 2|\rho|\cos\phi} \quad (1)$$

$$\frac{X}{Z_o} = \frac{2|\rho|\sin\phi}{1 + |\rho|^2 - 2|\rho|\cos\phi} \quad (2)$$

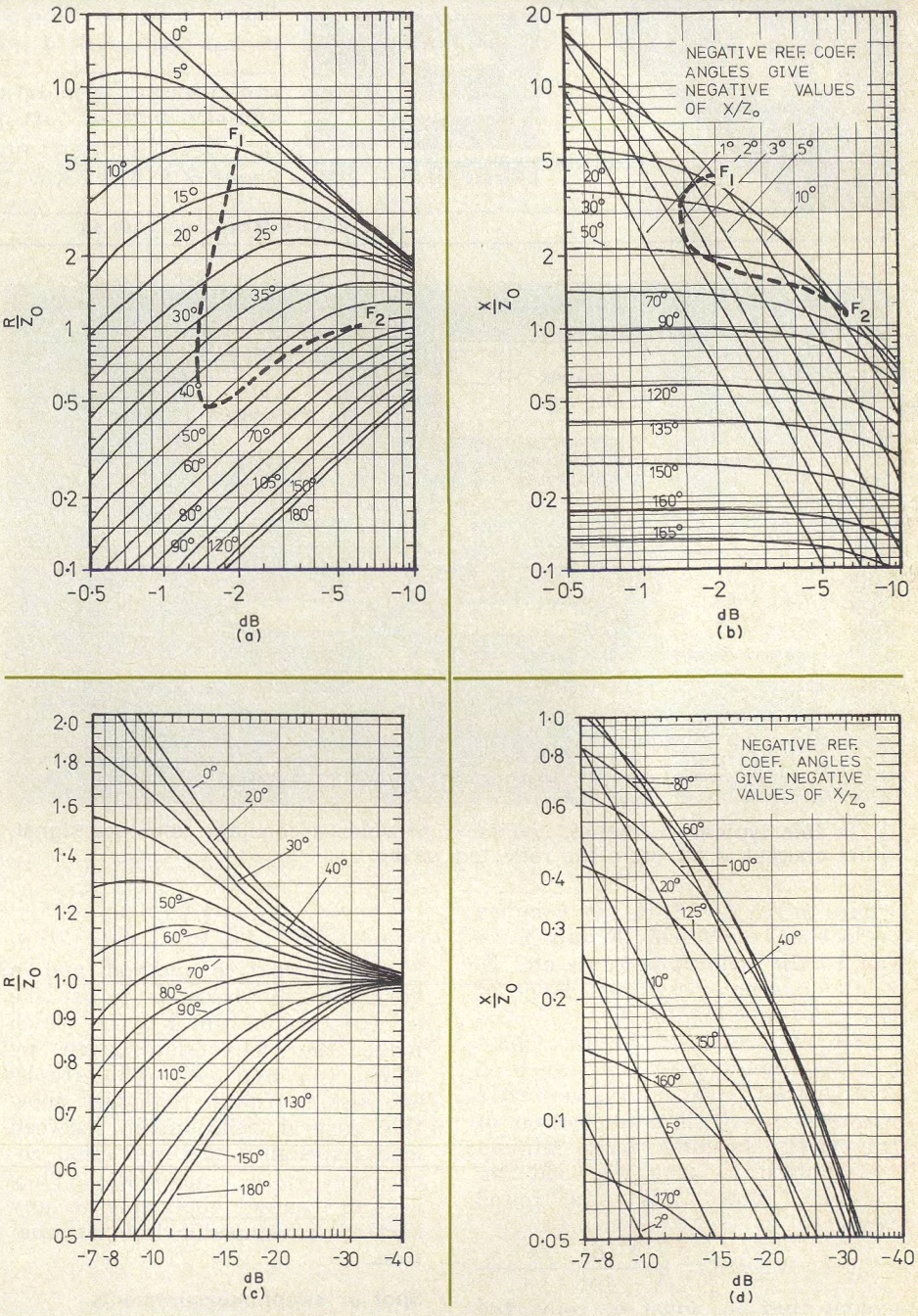

1. **Curves of normalized resistance and reactance** versus reflection coefficient for relatively large reflected wave amplitudes, (a) and (b), and for relatively small reflected wave amplitudes, (c) and (d), are plotted for constant phase angles. Reflection coefficient amplitudes are expressed in dB.

Keith M Keen, European Space Research Organization, European Space Research and Technology Center, Domeinweg-Noordwijk-Netherlands.

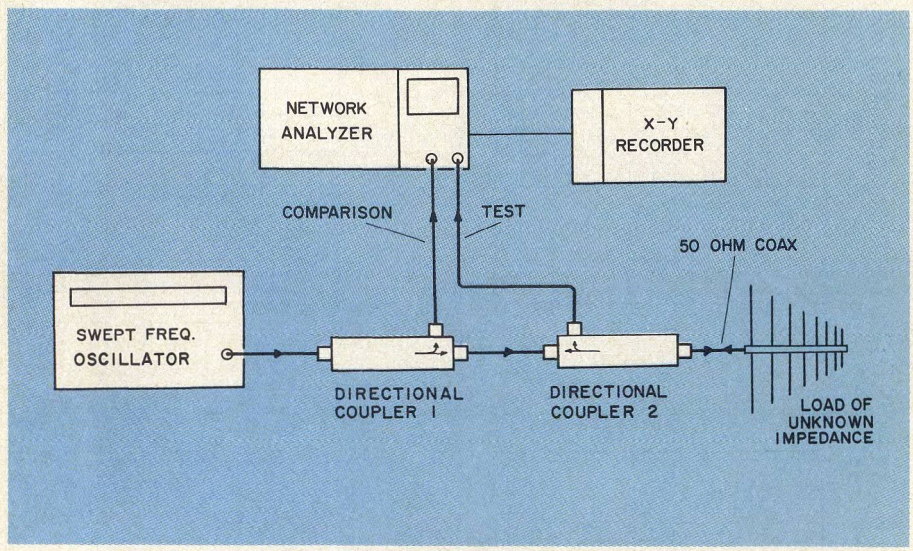

2. **In this typical test setup,** coupler 1 provides a constant reference signal, while coupler 2 monitors the reflected wave.

where $\rho = |\rho|e^{j\phi}$ is the complex reflection coefficient, R and X refer to the load impedance and Z_0 is the characteristic impedance of the transmission line.

Alternatively, a Smith Chart can be employed in the way used for slotted-line measurements where the VSWR and position of the first standing wave minima are plotted to give the load impedance. The VSWR is found from:

$$\text{VSWR} = \frac{1 + |\rho|}{1 - |\rho|}$$

except that $|\rho|$ must be converted from decibel units. Most Smith Charts are already calibrated in degrees of reflection coefficient phase, but if not the phase must be converted to the corresponding first minima position, χ_{min}, using

$$\chi_{min} = \frac{\lambda}{4}\left(1 - \frac{\phi}{\pi}\right)$$

An alternative method and a very convenient one is to use the set of graphs in Fig. 1 which make the conversion given by Eqns. (1) and (2). The graphs are also useful in that they show the general relationship between load impedance and reflection coefficient in a simple way. They are, of course, applicable to any sort of transmission line termination.

Spot or swept measurements

Consider the test setup in Fig. 2 in which the log-periodic antenna used as a load is found to have a reflection coefficient of −12.5 dB amplitude and −65 degrees phase at some frequency F_{cw}.

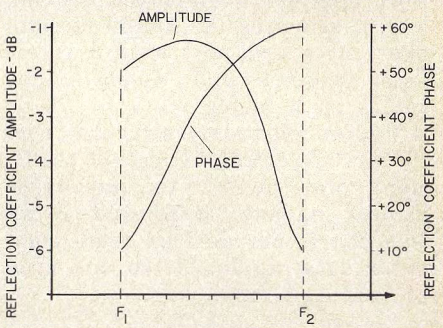

3. **Swept frequency measurement** records amplitude and phase of the reflection coefficient.

From 1(c) and 1(d), the normalized impedances are:

$$R/Z_0 = 1.11,\ X/Z_0 = -0.48$$

As the transmission line has a characteristic impedance, Z_0, of 50-ohm the impedance values of the log-periodic antenna at F_{cw} are

$R = 55.5$ ohms $\quad X = -24$ ohms

The curves are also suited for swept measurements. Suppose, for example, that the input impedance of a stripline device with one coaxial input port is required over the band between frequencies F_1 and F_2. The amplitude and phase of the reflection coefficient is plotted by the X-Y recorder as shown in Fig. 3. To find the corresponding impedance values, the data from the X-Y recorder is plotted in Figs. 1(a) and 1(b) as shown by the boldfaced dotted lines. From these, the normalized impedance values can be read off for any frequency within the band. For $Z_0 = 50$ ohms, the input impedance of the device varies between $Z = 275$ ohms, $X = -210$ ohms at F_1 to $Z = 50$ ohms, $X = 58$ ohms at F_2. ••

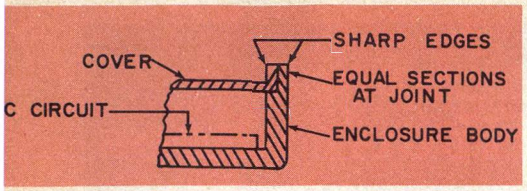

8. **A typical joint for the TIG welding** of a cover to an enclosure requires the point to have equal sections and sharp edges.

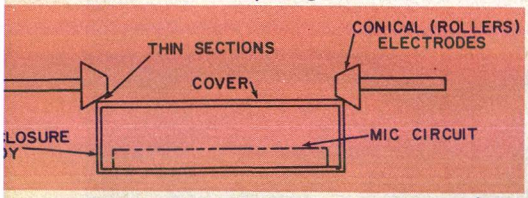

9. **For parallel-seam sealing** of a cover to the enclosure, the cover must be thin in the vicinity of the joint.

(text continued from p. 37)

Parallel seam sealing is accomplished by passing high-frequency current pulses between two electrodes that roll along the edge of the cover. The pulsating energy fuses the metal with overlapping welds, Fig. 9. The time duration and frequency of the pulse are such that just enough heat is generated at the joint interface for melting the metal locally without overheating the body of the module. Typically 40°C rise of temperature surfaces is all the circuit will be subjected to.

Materials that are compatible with this sealing process include Kovar, stainless steels, cupronickel and other nickel alloys. Metals that are characterized by being electrically conductive are also sealed effectively by finishing with an appropriate electroplate and placing a brazing or soldering preform between the cover and body of the enclosure.

Parallel seam sealing of covers to enclosures has all the advantages of TIG welding plus repeated passes over the joint, can be made without disfiguring the joint.

Aside from cost factors and availability, there are no hard and ready made rules for the selection of an appropriate sealing process or in selecting enclosure material.

The material should be capable of transferring dissipated heat, possess anti-corrosive properties, have a low vapor permeability and be amenable to not only a sealing process, but also lend itself to an inexpensive manufacturing process.

References

1. Gene K. Baxter, "Thermal Response of Microwave Transistors Under Pulse Power Operation," IEEE Transactions On Parts, Hybrids and Packaging, Vol. PHP-9, No. 3, (September, 1973).
2. W. A. Baker, "The Creep Properties Of Soft Solder and Soft Solder Joints," Journal Inst. Metals, Vol. 65-1939, pp. 277-297.

application notes

Here's how to s-t-r-e-t-c-h spdt switch bandwidth

Single-pole, double-throw PIN diode switches are constructed with the devices in series, shunt or series/shunt combination. Each design approach has distinct advantages and disadvantages. The series switch is capable of multi-octave bandwidth, but provides poor isolation. Isolation is the major asset of the typical shunt configuration, but the two quarter-wavelength transmission lines required by the design lead to increasingly serious mismatch problems as the input frequency deviates from f_0. A series/shunt hybrid design boasts good isolation and broad bandwidth, but at the expense of twice as many devices, and twice the power consumption.

Application Note 957-1 from Hewlett-Packard, "Broadbanding The Shunt PIN Diode SPDT Switch," suggests a modified shunt switch, designed with a third length of tuned transmission line to broaden the frequency capability. The note also advises that the characteristic impedance of the quarter-wave lines be set at some value below 50 ohms for the broadest bandwidth (see figure). An analysis shows that by introducing the third transmission line, and carefully choosing a proper impedance level, the 1.43:1 VSWR bandwidth of a typical shunt switch can be improved by a factor of 2.5.

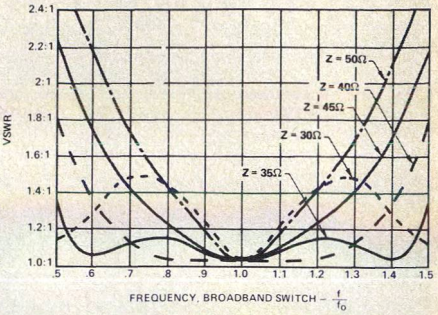

Note that the bandwidth exceeds 100% when 35-ohm lines are used.

The two-page note is available at no charge from: **Inquiries Manager, Hewlett-Packard Company, 1501 Page Mill Road, Palo Alto, CA 94304 (415) 493-1501.**

CIRCLE NO. 100

Block out power supply interference

In switched-mode power supplies, RFI may be produced by direct radiation or by the conduction of interfering currents through the input and output terminals. Direct radiation can be adequately suppressed by enclosing the power supply in a shielded box, and by paying careful attention to the layout of internal wiring. Interference conducted through the supply and output terminals, however, is more difficult to suppress.

"Radio Frequency Interference Suppression in Switched-Mode Power Supplies," application note F-601 from Ferroxcube, investigates a variety of techniques which reduce interference eminating from various power supply sections. Transistors mounted on a heatsink with mica washers are one major source of interference, due to capacitance created by the mica dielectric. The solution: operate the heatsink at a positive potential to insure that the current in the collector-to-heatsink capacitance remains in the primary circuit and is prevented from flowing into the line via ground.

RFI can also be generated by power supply diodes. Interference due to diode snap-off can easily couple into all parts of the power supply circuit and develop appreciable voltages across ground connections and across the metal case enclosing the supply. One remedy is to use "soft" recovery capacitors. **Ferroxcube Corporation, Saugerties, NY 12477 (914) 246-2811.**

CIRCLE NO. 101

How much improvement does 10 dB buy?

It's common knowledge that the directivity of a coupler in a swept-frequency measurement system introduces some degree of error. But how much can measurement accuracy be improved by using a component with a higher directivity?

A new technical note from Com Dev, Ltd. of Montreal, Canada, will help you to answer that question. "Coupler Directivity vs. Measurement Error" introduces a new series of 50 dB directional couplers, and compares their theoretical error limits with those of 40 dB couplers. It is shown that the added 10 dB of directivity can reduce maximum error limits by a factor of about three, for return loss measurements up to 34 dB. The six-page note includes a chart which derives maximum error limits from measured return loss and coupler directivity. **Com Dev, Ltd., 6 Ronald Drive, Montreal, Canada H4X, IM8 (514) 487-9010.**

CIRCLE NO. 102

laser technology

MICROWAVES

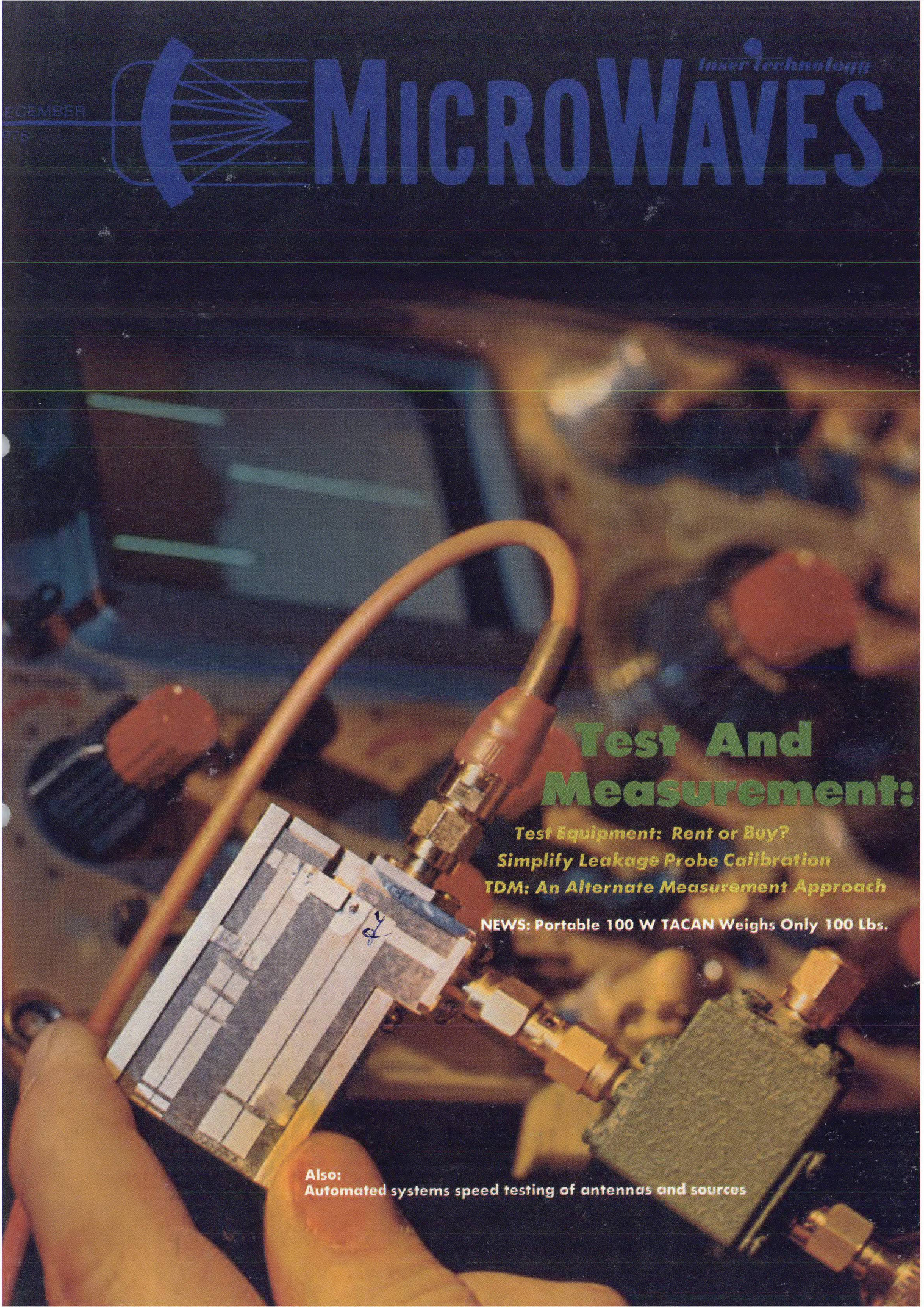

Test And Measurement:

Test Equipment: Rent or Buy?

Simplify Leakage Probe Calibration

TDM: An Alternate Measurement Approach

NEWS: Portable 100 W TACAN Weighs Only 100 Lbs.

Also:
Automated systems speed testing of antennas and sources

MICROWAVES

December 1975
Vol. 14, No. 12

news

editorial

technical section

products and departments

About the cover: A Trapatt under test is captured in this photograph by Tom Cook, courtesy of RCA Laboratories, Princeton, NJ.

coming next month: Front Ends

What's New With Receiver Protectors? Harry Goldie of Westinghouse, Baltimore, MD, discusses the advantages of receiver protectors using tritium ignitors and diode limiters. Unlike the TR tube, a dc keepalive is not required for a plasma diode receiver protector.

How Noisy Is That Load? Matts Viggh of Transmission Lines, Inc., Ipswich, MA, describes how noise temperature measurements of microwave radiometers and other low-noise receivers can have a significant error if the noise power emitted by a temperature controlled termination is assumed proportional to temperature and independent of frequency.

Try Fused Silica Substrates For J-Band Mixer Design. E. James Crescenzi, Ferenc Marki and W. Keith Kennedy of the Watkins-Johnson Company, Palo Alto, CA, abandon traditional alumina substrate in favor of a more promising material: fused silica.

Publisher/Editor
Howard Bierman

Managing Editor
Richard T. Davis

Associate Editor
Stacy V. Bearse

Contributing Editor
Harvey J. Hindin

Washington Editor
Paul Harris
Snyder Associates
1050 Potomac St., NW
Washington, DC 20007
(202) 965-3700

Editorial Assistant
Gail Murphy

Production Editor
Sherry Lynne Karpen

Art
Robert Meehan, Dir.

Production
Dollie S. Viebig, Mgr.
Dan Coakley

Circulation
Trish Edelmann, Mgr.
Peggy Long, Reader Service

Promotion Manager
Albert B. Stempel

Directory Coordinator
Janice Tapp

Editorial Office
50 Essex St.,
Rochelle Park, N.J. 07662
Phone (201) 843-0550
TWX 710-990-5071

A Hayden Publication
James S. Mulholland, Jr., President

MICROWAVES is sent free to individuals actively engaged in microwave work at companies located in the U.S., Canada and Western Europe. Subscription price for non-qualified copies is $10.00 for U.S., $15.00 a year elsewhere. Additional single copies $1.50 ea. (U.S.); $2.00 ea. (foreign); except additional Product Data Directory reference issue, $10.00 ea. (U.S.); $18.00 (foreign). POSTMASTER, please send Form 3579 to Fulfillment Manager, MICROWAVES, P.O. Box 13801, Philadelphia, PA 19101.

Back Issues of MicroWaves are available on microfilm, microfiche, 16mm or 35mm roll film. They can be ordered from Xerox University Microfilms, 300 North Zeeb Road, Ann Arbor, MI 48106. For immediate information, call (313) 761-4700.

Hayden Publishing Co., Inc., James S. Mulholland, President, printed at Brown Printing Co., Inc., Waseca, MN.

Portable 100 W TACAN weighs only 100 pounds

Stacy V. Bearse
Associate Editor

A new class of TACAN, specifically designed to be parachuted into forward combat zones and provide azimuth and range information to aircraft within 75 miles, is currently being developed by the U. S. Air Force. The 100-watt system weighs only 100 pounds, and is the first all solid state USAF TACAN. Early, tube-type TACAN units weighed in the neighborhood of 15,000 lbs.

"The new TACAN was specially designed for simple operation," notes Fred Ausseresses, Director of Requirements at the Montek Division of E-Systems in Salt Lake City, UT. "Take its frequency synthesizer, for example. This unit will operate on any of the 252 channels that are authorized for TACAN, just by turning (thumbwheel) selector switches." The indirect frequency synthesizer, as well as the YIG-tuned receiver preselector, can be tuned to any of the 1 MHz channel slots in the 962-1213 MHz band. Frequency stability is 0.002%.

Simple operation is the key to this design, for the TACAN station must be assembled by nontechnical personnel under battlefield conditions (see figure). The new TACAN system, designated by the Air Force as AN/TRN-41, breaks down into three packages: the antenna assembly, transmitter/receiver and tripod and battery. Each member of a three-man combat control team, a spearhead force that sets up drop zones and tactical landing strips, carries one package in a drop bag attached to their parachute harness. When the soldiers are about 200 feet above the ground, they release the bags on tether ropes, allowing the jumpers to touch down with less weight. On the ground, the three TACAN packages are removed from their shock-absorbing landing bags and attached to harnesses to form 35-pound backpacks.

Once assembled and activated, the battery-powered TRN-41 will reportedly operate continuously for more than four hours without recharging. A demand-only mode, which may be selected by a front-panel switch, extends this time by disabling the transmitter and antenna drive until interrogated by an aircraft. A built-in test system monitors 10 critical parameters, including peak output power, VSWR and pulse rate, and shuts the station down if any fall out of specification.

Discriminator cuts interference

The new TACAN receiver uses a dual-mode Ferris disciminator in conjunction with a broadband i-f detector to improve adjacent channel rejection. A Ferris discriminator inverts the polarity of unwanted signals, which are subsequently eliminated when the signal passes through a diode or amplifier, Ausseresses explains.

The output of a 63 MHz i-f strip is split in two, feeding the parallel combination of a narrowband Ferris discriminator and a wide-band i-f detector. The discriminator acts as a gating amplifier, merely to identify a qualified TACAN pulse. When properly gated, the broadband detector passes the main signal, and thus preserves the spectrum of the TACAN pulse, Ausseresses notes.

As a result, adjacent channel receiver selectivity exceeds 70 dB, while i-f selectivity is greater than 80 dB. Overall receiver sensitivity is about −90 dBm, and dynamic range is specified as 80 dB.

The receiver has been designed to be considerably more immune to cw jamming than earlier TACAN designs. According to Ausseresses, cw jamming merely reduces receiver sensitivity, as opposed to fully blocking the receiver. "As long as the interrogation signal from the aircraft is at least an order of magnitude higher than the interfering signal, it will be processed," he notes.

Mechanical scanning selected

Antenna design was a major difference among the competing designs initially considered by the Air Force. "It's been vogue in the last three to five years to go to electronically-scanned antennas," Ausseresses comments, "but we

(continued on p. 14)

news
Microwave market to grow 6% per year

Richard T. Davis
Managing Editor

The U. S. microwave components market, estimated at $426-million in 1974, can be expected to grow to $586-million by 1980 and to $828-million by 1985. According to a recent market report by Frost and Sullivan, market researchers in New York City, gross shipments of microwave devices are estimated to have been $476.5-million in 1975. Of this, microwave tubes represent 37% of the market or $175-million; passive components about 23% or $107-million; solid-state components, 13% or $64-million and solid-state devices, such as transistors and diodes, 8.5% or $40-million.

It's predicted that the microwave tube market will be relatively flat over the next five to ten years with solid-state components and devices in stripline MIC assemblies capturing a greater percentage of the total market.

Impatt diodes, for example, can be expected to show a 40% annual growth rate between 1974 and 1980, with GaAs FET registering a 37% increase; Impatt amplifiers and Gunn oscillators 20%; bipolar transistors, 17%; Yig components, 16% and Gunn diodes and low-noise, solid-state amplifiers, a 15% increase (see Table).

Some of the markets that will show negative growth include tunnel diodes and multiplier diodes. The manufacturers of passive components, such as waveguide and coax couplers and filters will also be vulnerable as more and more MICs and stripline are manufactured by the systems' manufacturers. Certain specialized passive components, however, will be exempt from this decline such as matched attenuators, Yig-filters, double-balanced mixers and millimeter-wave components.

As in the past, the major market for microwave components (defined in this report as operating above 1 GHz) is the military; specifically ECM, airborne, ground and shipborne radar, military communications and more recently, military and non-military satellite communications.

"Because of this, the microwave components industry has not seen the severe declines in business that have been witnessed in other U. S. industries in the late 1974 to mid-'75 period," says Henry Burler, Vice President of Research.

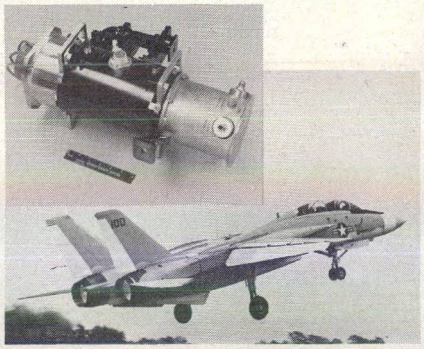

Mircowave tubes, which command 37% of the microwave component market, will maintain their dominant market share, despite solid-state inroads. New high-power designs and increased interest in the higher frequency bands particularly by the military will provide a 1% market growth per year.

TWT market still the biggest

One trend pointed out in the report was the continuing dominant market position for traveling-wave tubes, presently about $80-million a year. Growth will be about 1% per year. "This market position will be maintained despite the incursions by solid-state at the low-power end of the TWT market," notes Burler. "Part of the reason for this is increased ECM funding particularly for TWTs operating in the 18-40 GHz frequency range where new systems are being developed."

The leading manufacturer of TWTs is Hughes Aircraft, Fullerton, CA, followed by Varian, Raytheon, Teledyne/MEC, Litton and Watkins-Johnson. Those R&D areas reported being worked on include low-cost printed circuit TWTs, higher efficiencies (goals: 60% at 12 GHz and 50% for frequencies to 40 GHz), dual-mode TWTs with 10 dB gain for ECM jamming systems, and improved helix structures to achieve higher power with lower input voltages.

Growth for solid-state and m-m

Selected areas of the microwave industry that will grow in excess of 10% per year are given in the table. The Impatt diode shows good growth potential because it will be used to replace low and medium power tubes operating above 5 GHz. Bipolar power transistors, on the other hand, are expected to be replacing tubes under 4 GHz.

According to Frost and Sullivan, the leading manufacturer of microwave bipolar transistors (i.e., above 1 GHz) ls MSC, of Somerset, NJ, who had sales of $5.5-million in 1974 (this includes sales other than transistors). The $12-million bipolar transistor market is predicted to grow to $30-million by 1980 and $45-million by 1985. Additional areas of growth for transistors will be in terrestrial communications, electronic ware, avionics and radar, particularly phased arrays.

"The available market for the GaAs FET was around $600,000 in 1974," says Burler. "This might

(continued on p. 13)

Selected growth areas of the microwave market

Component or device	Value of shipments ($ million) 1974	75	76	77	78	79	80	Average annual growth rate '74-80	'80-85
Gunn diodes	2.0	2.3	2.6	3.0	3.5	4.0	9.0	15%	15%
Impatt diodes	0.7	1.0	1.4	2.0	2.5	3.0	10.0	40%	23%
GaAs FETS	0.6	1.0	1.4	1.8	2.2	2.0	4.0	37%	15%
Bipolar transistors	12	15	18	21	24	27	30	17%	8%
Millimeter passive components	2.0	2.2	2.4	2.6	2.9	3.4	3.7	11%	6%
Yig components	10	12	14	16	18	21	24	16%	11%
Transistor amplifiers									
Low-noise	24	27	32	36	42	48	56	15%	10%
High-power	4	4.5	5.0	5.6	6.3	7.0	8.0	12%	12%
Impatt amplifiers	0.5	0.8	1.2	1.6	2.0	2.5	3.0	35%	22%
Oscillators									
Gunn	2.0	2.3	2.8	3.5	4.0	5.0	6.0	20%	20%
VCOs	4.5	5.0	5.6	6.3	7.1	7.9	8.8	12%	10%
Yig-tuned	6.5	7.5	8.7	10.1	11.8	13.6	15.8	16%	11%

news
European weather satellite to improve forecasts

The European Space Agency plans to send into orbit a new meteorological satellite capable of photographing cloud movements and atmospheric phenomena from an altitude of 36,000 km. The weather satellite, called Meteosat, is due to start operating in mid-1977 and will survey an area extending from Northern Europe to the South Atlantic and from the Mid-Atlantic to the Indian Ocean.

The main ground station located near Michelstadt in West Germany, operates at S-band and uses a 15-meter reflector antenna. One ordinary and one infrared picture will be transmitted to the ground station at half-hour intervals where a computing center will compare the newly-received pictures with previous ones. This will allow wind directions and speeds to be determined quickly and accurately.

Siemens in Munich developed the ground-station antenna which has a tracking accuracy of 0.016 degrees. It also has a phase cancellor capability to protect it from the numerous post office radio links in the area. •• *RTD*

Microwave market *(con't from p. 10)*

seem to be a small value compared to the amount of publicity the device has received over the last couple of years, but that's because the device is still in development and not readily available to the marketplace. Also, those companies manufacturing FETs are using them for their own use. It's still largely a captive market." (The figures and projection for this report are based on the non-captive portion of the market). The one company that appears to have the edge in supplying GaAs FETS is Nippon Electric Co. Ltd., of Japan. The other major U. S. supplier is Fairchild. Other U. S. companies known to manufacture GaAs FETS include Avantek, Hewlett-Packard, Hughes Aircraft Company, Raytheon, TRW and Varian.

The only passive component market that will show any significant growth (i.e. in excess of 10%), is in millimeter-waves such as circulators, switches, hybrid, couplers, filters, mixers and detectors operating above 26.5 GHz. According to the report, TRG/Alpha of Woburn, MA, is the leading U. S. manufacturer followed by Baytron and Hughes. Hitachi is the major Japanese manufacturer. This $2-million market is expected to grow slowly but steadily to five million by 1985.

Many specialty mw companies

The report states that over 500 U. S. companies are actively involved in the microwave components market. It predicts the most successful companies in this field will be those that continue to develop state-of-the-art products, or produce real breakthroughs in terms of the performance over existing available components. Solid-state, low-noise amplifiers and Yig-tuned oscillators were two examples called out in the report where significant improvements have been made over older existing designs.

Some of the technological trends noted in the report (besides the more obvious ones of miniaturization, replacing tubes by solid state and use of higher frequencies), is the trend towards vertical integration, whereby component houses expand manufacturing capability to include subsystems and even small systems designs. Conversely, system houses are also expanding their capabilities to manufacture certain components and sub-systems. The report did note, however, that those systems houses that are selling to the military market will tend to be much slower in this vertical integration process than those serving the commercial communications area. "The reason for this," explains Burler, "is that certain system manufacturers, such as Raytheon, Westinghouse and Hughes, cannot develop all of the state-of-the-art advances, demanded by new military equipments." Thus, the systems houses must still depend on smaller and more flexible companies to develop expertise in certain technological areas. In fact, this situation tends to support the existence of the smaller company and explains why there are so many companies that make up the industry." ••

Reactance compensation improves oscillator tunability

Reactance compensation—a technique originally used to improve the gain-bandwidth product of paramps—can double the tuning bandwidth of varactor-tuned Gunn oscillators, says a researcher from Great Britain's Chelsea College. According to C. S. Aitchison, reader in electronics at the University of London college, the object of the technique is to minimize changes in the oscillator's susceptance with frequency.

"The common feature of parametric amplifier circuits and varactor-tuned Gunn oscillators is that the operating frequency is determined by the frequency at which the sum of the reactances (or susceptances) is zero. The principle (of reactance compensation) is that a shunt resonant circuit is provided between the series resonant signal circuit and its load. The shunt circuit slope is adjusted to give a zero $\delta X/\delta\omega$ over the required frequency range," explains Aitchison.

In laboratory models of a coaxial X-band oscillator, the reactance compensation is provided by two distributed lines, placed a quarter wavelength from the Gunn device and terminated in sliding short circuits (see Fig. 1). "A particular feature of this arrangement is that the short circuits and inner conductors of the compensatory coaxial lines can be removed, while the oscillator remains switched on, to simplify the direct comparison of varactor tuning ranges," the researcher notes.

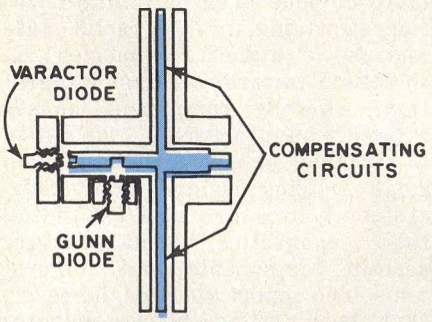

1. Two shunt circuits are used to increase the oscillator's tuning range.

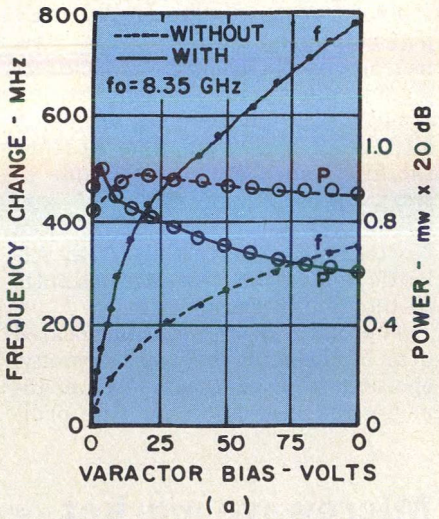

2. Tuning range is nearly doubled in these two experimental cases. More improvement could be expected if lumped-element networks were used instead of transmission lines.

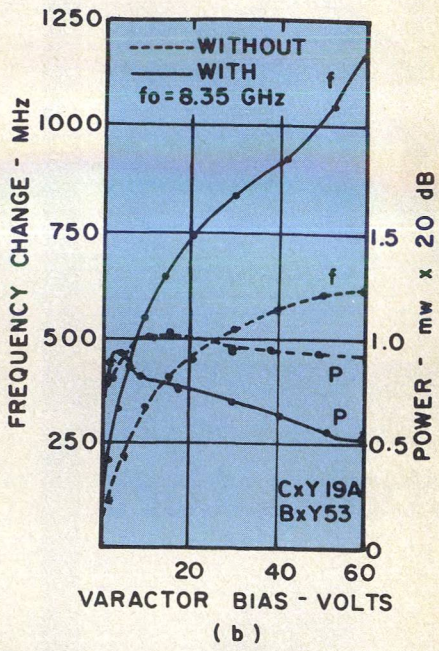

Early laboratory results are impressive (Fig. 2). In one oscillator that used a Mullard Gunn device, model CXY19A operating at about 12 V and 0.5 A, and a Mullard varactor, model BXY90, which has a zero bias capacitance of 2 pF and breakdown voltage of 100 V, tuning bandwidth increased from 350 MHz to 775 MHz with the addition of reactance compensation—an improvement of over 120%. The maximum output power for compensated and uncompensated versions is approximately 100 mW, Aitchison reports, but the compensated design suffers a maximum power loss of about 1.7 dB over the band.

The same uncompensated circuit designed with a varactor rated at a lower breakdown voltage (Mullard BXY 53: $C_o = 2$ pF; $V_{bd} = -60$V) exhibits a 625 MHz tuning range. "The application of the reactance compensation circuit again increases this figure by a factor of approximately two, to a value of 1180 MHz. The maximum loss in power on adding the compensatory circuit was 2.4 dB. The maximum power output is little changed at about 100 mW," Aitchison reports. •• *SVB*

PORTABLE 100 W TACAN (continued from p. 9)

had mixed emotions whether it was a viable approach for the TRN-41." E-Systems finalized on a mechanically-scanned antenna, which, Ausseresses claims, offers better performance and higher reliability than competing electronically-scanned designs. The antenna consists of a disk containing parasitic arrays which revolves at 900 rpm around a central radiating array.

Performance data includes ±0.5 degree azimuth accuracy and 3 dB peak gain. Vertical polarization is used, and horizontal components are reported to be suppressed by more than 30 dB. The radiation pattern is essentially a multi-lobe cardioid which rotates in space.

"The most exciting thing about this antenna is that it does not consume any more power than a competing electronically-scanned antenna," Ausseresses emphasizes. The antenna consumes about 25 watts, and may be driven by 18 to 30 Vdc.

The Montek Division of E-Systems was selected to build the TRN-41 in a competitive procurement program. Under a $756,-898 contract from the Electronic Systems Division of the Air Force Systems Command at Hanscom Field, E-Systems will provide two pre-production units for operational testing in late 1976. A follow-on production option for 60 units by early 1977 could bring the total contract value to more than $2.5-million. ••

r&d roundup

Harvey J. Hindin, Contributing Editor

That's quite a cavity!

Determining accurately the driving point impedance of a coaxial cavity with a gap in its center conductor is not an easy task. In wideband oscillator designs, (2-22 GHz for example), certain deficiencies in calculating the impedance at the gap terminals occur when the transmission-line-equivalent circuit technique is used.

In "Wideband Characteristics of a Coaxial-Cavity Solid-State Device Mount" (*IEEE Trans. on MTT*, Vol. 23, No. 10, pp. 831-832, October, 1975), authors Philip H. Alexander and Peter J. Khan show that for wideband characterization, radial wave modal field analysis can considerably improve the situation. Previously, only the lowest order resonant modes were considered, resulting in a poor impedance characterization.

The theoretical analysis can not be directly studied by the reader without a knowledge of the references in the literature, for only the results are presented. The radiation impedance at the gap for both propagating and non-propagating modes is expressed in terms of Bessel functions.

A comparison between prediction and experiment was made for cavities in the 2-22 GHz range using both transmission line and radial wave analysis. It was found that the latter technique successfully predicted several resonances not forecast by the transmission line model. This happens when the cavity diameter is of the same magnitude as its length. It was also found that the driving point impedance characteristics can be somewhat modified by varying the position of the gap in the cavity center conductor.

Take a deep breath

In "Noninvasive Microwave Measurement of Respiration," (*Proc. IEEE*, Vol. 63, No. 10, pg. 1530, October, 1975), by James C. Lin, preliminary results are reported in measuring the respiration rate of humans and animals using a noncontacting cw microwave system, (see Fig.). The reflections from the animal's moving chest cavity are received, detected and compared with the transmitted wave. The output of the ratio meter is a voltage whose frequency corresponds to the breathing rate. The reflected wave was modulated both in amplitude and phase.

The oscillator used had a 10 mW output at 10 GHz. Incident power density on the subject was estimated to be in the range of $\mu W/cm^2$.

Lin notes several advantages for his system including the facts that the method is noncontacting, and the subject does not have to be anesthetized or unclothed. In addition, the older methods sometimes cause skin irritation, electrode problems and breathing restriction. Straightforward and conventional technology is used for the apparatus and the use of the ratio meter enables the researcher to ignore the stability of the oscillator.

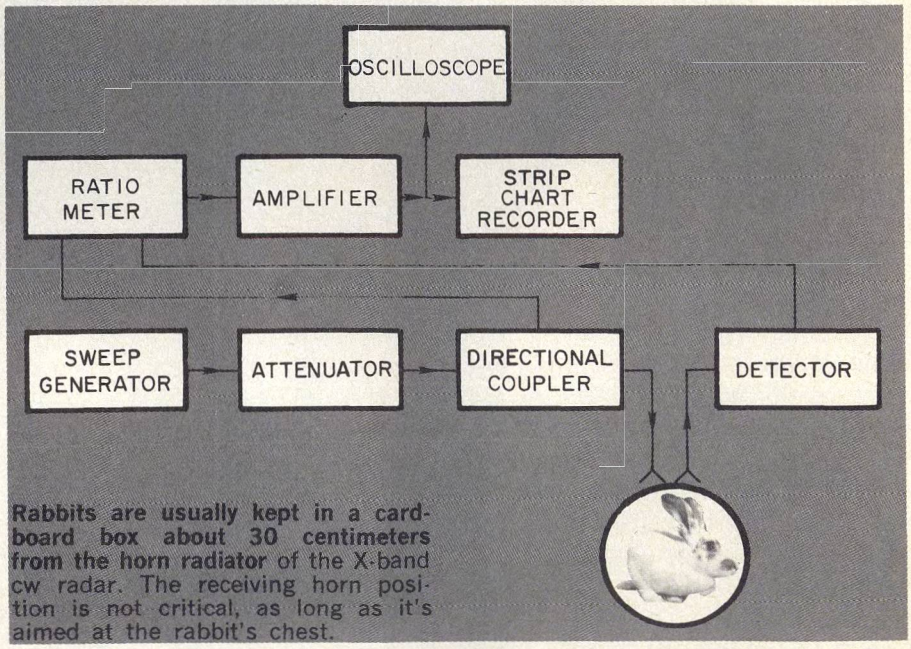

Rabbits are usually kept in a cardboard box about 30 centimeters from the horn radiator of the X-band cw radar. The receiving horn position is not critical, as long as it's aimed at the rabbit's chest.

Test Equipment: Weighing The Rent Or Buy Decision

You can apply a formula to determine whether it is more economical to rent or buy a given instrument, but in the long run, it pays to weigh several factors not considered in a simple dollar analysis.

THE advent of test equipment rental on a national level has brought a welcome degree of flexibility to equipment acquisition practices in the microwave industry. With rental, the old all-or-nothing formula—buy all your test equipment or do without—has gone the way of the cash-only sale, and the microwave industry has been quick to capitalize on that development.

There is one problem, though, in having more than one road to choose: making the right decision. Frequently, it seems, the rental decision must be made in a hurry, when rental is expedient, without careful consideration of the overall costs of that decision. The purchase decision, on the other hand, is commonly made through habit—equipment is bought just because it has always been acquired that way. In either case, the selection process is usually a nonobjective, passive one.

That needn't be the case. There are a number of methods of reducing the guess work involved in the rent or buy decision, methods that can be quantified and graphically represented over a standard set of acquisition conditions. While short of foolproof, these analytical methods deserve every engineer's—and purchasing manager's—careful inspection. They could prove to be one of the most effective means of competing for critical business.

That, at least, seems to be the consensus among a growing number of microwave instrumentation users who have come to regard rental as essential to the full conduct of their business. Happy to have a practical rental alternative in emergency situations (breakdown, sudden overloads, etc.), test equipment users have begun to discover new, business-broadening applications made possible by rental that were inconceivable under purchase-only conditions.

Consider, for example, the case of the medium-sized systems house that wants to bid on a government package requiring EMI/RFI testing to a particular MIL-SPEC. The company may have a good handle on the systems technology, but the $40,000 purchase price of EMI/RFI test equipment is impractical for six weeks of testing. By renting the gear at about 10% of the purchase price per month, the small firm can compete more effectively against much larger outfits.

Anthony M. Schiavo, Director of Marketing, US Instrumental Rentals, Inc., 951 Industrial Road, San Carlos, CA 94070.

Similarly, a manufacturer of YIG oscillators that needs sweepers for production line checkout may be able to benefit through rental. While the frequency band he has to test varies for different lots, the range within any one lot is usually only 2 or 3 GHz, making the purchase of a full broadband system unnecessary. The manufacturer may be able to save money by buying the mainframe and commonly-used plug-ins, and renting less frequently used plug-ins on an as-needed basis.

These and many other operational applications within the rapidly developing microwave industry are being satisfied in increasing amounts by rental. But there are other reasons of a non-operational nature that more strongly suggest instrument rental.

The objective choice

What factors should be considered in making an objective buy-rental choice and how are they worked into a formula? Utilization is one, probably the most important. Most simply put, equipment that is going to be needed day in and day out for a long period of time should probably be purchased, provided the heavy front-end cost doesn't disrupt a company's normal operations. Similarly, an item that is going to spend much of its useful life on the shelf should be rented, because it is paid for only when it is needed.

The utilization factor is normally expressed as a rate based on the percentage of time a given instrument is expected to be in use. Thus, an instrument with a high-expected utilization will have a utilization rate of around 70% or more, while an infrequently used item will have a rate of 30% or less.

These, of course, are the extremes. The decision must usually be made in the gray area in between. Furthermore, care must be taken in determining the average utilization rate of an instrument over its useful life. An item may have a high usage rate in its first few months, then find its way to the shelf for the next few months. If utilization is expected to be seasonal or sporadic in any way, rental is the ideal solution.

Another complicating factor must be thrown into the utilization equation: the threat of obsolescence. Many instruments are purchased with the intent of putting them into heavy use, only to find that shortly thereafter new technology has rendered them relatively less efficient, if not obsolete.

Technical obsolescence is especially prevalent in the microwave industry. Recent state-of-the-art in-

(Continued on p. 36)

strumentation advances now allow operation at higher frequencies and increased sensitivities and dynamic ranges. Furthermore, semiconductor technology continues to produce more and more compact components, which permit more efficient racking and space utilization. When this happens, the buyer must decide to replace his expensive new equipment with newer equipment or try to get by with what he has—an extremely difficult decision the month-to-month renter does not have to make.

There is another form of obsolescence, however, that can be even more crippling to the equipment owner. Project obsolescence occurs when instrumentation requirements within a given application change, as they frequently do. A systems house that specializes in building radars, for example, may purchase test equipment for C-band, then suddenly decide to shift applications indefinitely to Ku-band. By renting, the firm can accommodate such frequency changes without taking a big loss on displaced test equipment.

Because many microwave companies are frequently on a project or program basis with their contractors, large equipment-need swings are quite common. This is another situation in which the outright purchase of instrumentation may be inappropriate. Rental makes it possible to adjust equipment needs as contractors adjust programming, without the worry of having a lot of leftover equipment to dispose of. And rental makes it easy to allocate testing expenses directly to the contractors involved on an equitable basis.

Deriving ownership and rental costs

Utilization and all the factors that affect it, including technical and project obsolescence, contribute a major part to any objective analysis of the buy-rent decision. But there are other considerations that must be balanced against the utilization rate to develop an accurate overall picture of the acquisition decision. Two of the most important—the only two quantifiable factors besides utilization used in the derivation of the following buy-rent formula—are ownership and rental costs.

Just as in the ownership of any major productive asset, purchase price is not an accurate measure of true ownership costs because it is only part of the total expense. Instrument maintenance and calibration, depreciation, property taxes, cost of capital, storage and insurance are all part of the hidden expenses that have a significant bearing on true ownership costs.

All of these costs vary from company to company and from instrument to instrument, of course. Learning to make reliable estimates of each can be a valuable tool in a company's long-term financial strategy. But for most companies, estimates of these costs fall within a fairly standard range that can be expressed as a set of percentages of original equipment cost.

Annual maintenance and calibration expenses, for example, will usually range between 10 and 22% of equipment cost. Depreciation, depending on the instrument and the depreciation method, will normally be between 12 and 25%. Cost of capital (the cost of financing equipment) is typically from 8 to 16% and property taxes, storage, insurance and the like add another 1 to 7% to annual ownership costs. Based on this range of percentages, then, an equipment owner can expect true annual ownership costs to fall between 30 and 70% of original equipment cost.

(continued on p. 39)

To rent or not to rent: Consider the numbers

For any given situation, the cost of renting test equipment equals the cost of owning the equipment when the following equality is satisfied:
12 x monthly rental rate (%) x acquisition cost x utilization (%) = ownership cost factor (%) x acquisition cost.
or,
when 12 x R x A x U = O x A.

Any equipment user who knows his ownership costs and the rental rate for a given instrument can, by this formula, determine the break-even utilization rate for which buying and renting costs are the same: U = O/12 R. Assuming fixed ownership costs and various rental rates, then, a series of utilization indifference curves can be developed (see graph).

For any two points on the rental rate and ownership costs axes, an instrument user will be indifferent to renting and buying if his utilization rate falls on the curve through those two points. If his utilization rate is expected to be above and to the right of the curve, buying is probably the desired method of acquisition. If it's below and to the left of the curve, renting is favored.

If, for example, an equipment user expects his annual ownership costs to be 50% and knows the monthly rental rate to be 8.3% of the equipment list price, the indifference utilization rate is 50%. If he intends to use the equipment more often than half the year, he should probably buy it; if less, he should rent it.

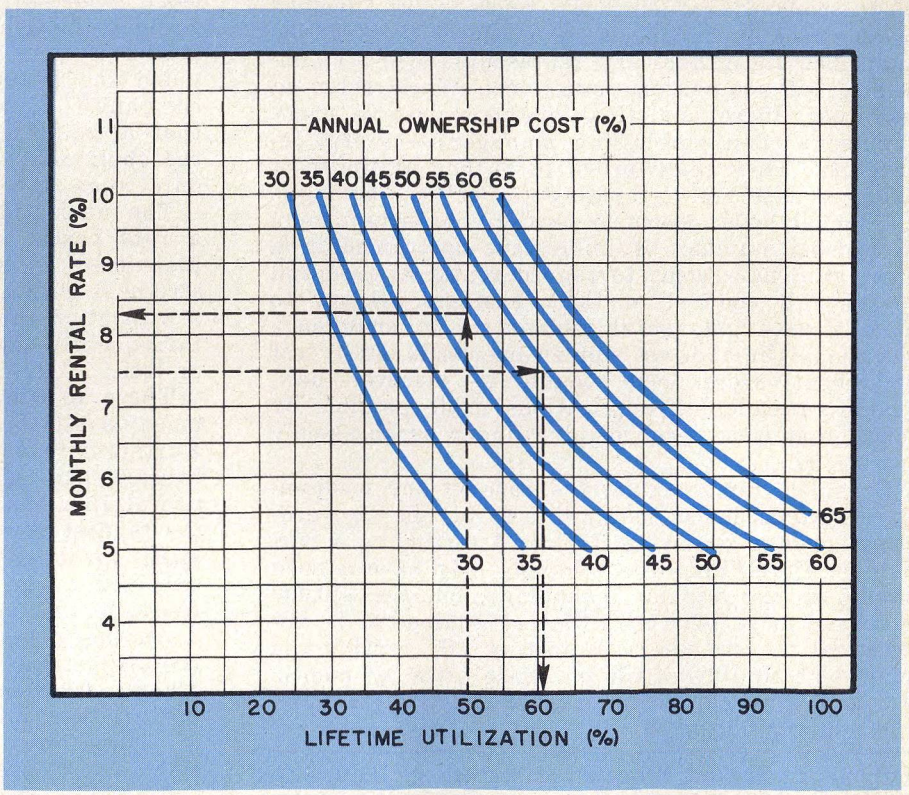

TEST EQUIPMENT: RENT OR BUY?

Rental costs are normally paid on a month-to-month basis in level payments equivalent to a set percentage of original equipment cost. However, unlike ownership costs (which are incurred continuously), rental costs are only incurred when the equipment is in use. An instrument that is needed only six months of the year, accordingly, has an annual rental cost of six times its monthly rental rate.

Given these relationships, a simple expression for the break-even cost relationship between buying and renting can be defined as follows:

rental rate (%) x no. of months = ownership costs (%).

If, for a particular instrument, the left side of the expression is less than the right, rental is the preferred method of acquisition. If the right is smaller, buying may be appropriate.

Since the formula involves only three variables, one of which (rental rate) is easily determined, it can be used to solve for break-even utilization rate or break-even ownership costs, if estimates of either prove particularly troublesome (see box).

Beyond dollar-for-dollar comparisons

For some instrument users, considerations other than absolute costs often affect the acquisition decision. Rental's flexibility is a natural defense against obsolescence, especially when, as noted earlier, project requirements tend to change rapidly or new technologies are frequently introduced. Furthermore, renters aren't burdened with maintenance and calibration responsibilities. The rental company handles them as part of the rental agreement.

There are, additionally, several important tactical considerations that should be weighed in any buy versus rent comparison. Tight budgets, for instance, can be stretched through rental. When the proper performance of necessary tasks requires more equipment than a company's budget can handle, rental is a practical economic solution. This is particularly true in the microwave industry, where entrepreneurial ideas are plentiful but cash for expensive equipment is limited, especially before a prototype can be produced.

Tax advantages may also generate a timely benefit to renting. Since rental payments are fully tax deductible, a company in the 50% tax bracket effectively pays half the rental rate for instrument use. Purchased equipment, of course, can be depreciated for tax purposes, but the depreciation period as defined by the Internal Revenue Service is usually about seven years. The kind of direct and immediate subsidy which accrues to renters, therefore, is not possible with a purchase.

Rental is a good way to overcome credit constraints, too. The large chunk of money needed for a purchase may require replenishing through borrowing, thus putting an additional strain on credit lines. Rental preserves a company's borrowing capacity and keeps credit lines intact.

Try before you buy

The considerable complexity of microwave instrumentation points up a further use of rental—as a kind of protection against buying improper equipment. An instrument user, for example, may feel certain he needs a multi-instrument hookup for a long enough period to justify buying it, but he may not be sure of its applicability until he's tried it. By renting the hookup for a short time, he can gain hands-on experience with the equipment to assure himself that his purchase is a proper one. A single month's rental, many buyers have found, is inexpensive insurance against the possibility of a five-figure purchasing error.

Finally, some segments of the microwave industry have regulations requiring periodic tolerance checks. The FCC often requires frequency tolerance and fm deviation checks to be made on microwave transmission links. If such checks must be made every six months or so, renting the necessary equipment may be the most efficient way to handle them.

These are just some of the more prominent uses to which instrument rental has been put. As an expedient, of course, rental continues to serve a necessary function. But a host of new applications within the microwave industry seems to have surfaced with the increased availability of rental equipment across the country. And while a planned approach employing both rental and buying is the best solution, it seems clear that instrument rental has passed from the emergencies-only phase into an active phase—one characterized by the aggressive use of rental as an important competitive tool. ••

Test your retention

1. Name five factors which are critical in evaluating the rent or buy decision.
2. What tax advantage does renting provide?
3. Generally, if an instrument is used frequently, should it be purchased or rented?
4. In a rental agreement, which party bears the burden of instrument calibration?

TDM: An Alternate Approac To Microwave Measuremen

Time Domain Metrology techniques team up with processing oscilloscopes to provide a valuable alternative to traditional cw measurements. Cost, accuracy and speed are major advantages.

THE observation of transient responses to pulses with risetimes of less than 100 picoseconds is an important alternative technique to wideband cw measurements. Most engineers are aware of the advantages of the direct physical interpretation available in traditional time-domain reflectometry, where each line discontinuity can be associated with an observed signal pertubation. Within the last few years, however, the use of computer-controlled waveform scanning procedures have extended the potential of time-domain measurements to the point where microwave component measurements can be made to an accuracy of a few tenths of a dB over the frequency range of 0.4 to 16 GHz.

The unique advantages of TDM methods are that multi-octave frequency information can be obtained with a simple and inexpensive pulse generator, and that errors due to imperfect loads are eliminated. In many cases wideband TDM measurements can be made more directly, and with less error, than with conventional cw methods.

A good grasp of TDM techniques can best be obtained by studying a simple example, as shown in Fig. 1. The basic configuration consists of a baseband* pulse generator, two sections of delay line, the component-under-test and a sampling oscilloscope.

The generator produces a 60 ps impulse and a synchronized trigger pulse for the processing oscilloscope. This transmitted signal, $v_{tr}(t)$, travels through the delay lines and component-under-test into the sampling head, where it is subsequently digitally converted and stored. To complete the measurement procedure, the component-under-test is removed and the incident impulse passing through the two delay lines, $v_i(t)$, is acquired. These two time-domain waveforms may then be translated into the frequency domain using the fast Fourier transform (FFT). Their ratio, $F\{v_{tr}(t)\}/F\{v_i(t)\}$, represents the insertion loss of the component being tested, where $F\{v(t)\}$ represents the FFT of $v(t)$. The net result is that using a simple pulse generator and relatively inexpensive equipment, the insertion loss of a component can be determined within a few tenths of a dB over a typical bandwidth of 0.4 to 8 GHz.

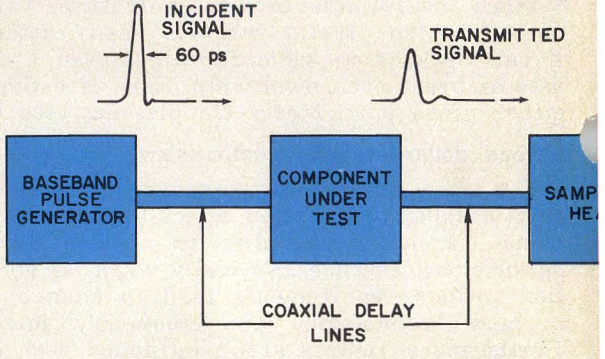

1. A basic TDM system analyzes how a component passes an impulse containing a broad spectrum of energy.

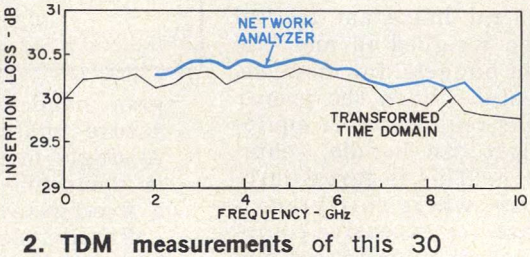

2. TDM measurements of this 30 dB attenuator compare favorably with network analyzer results.

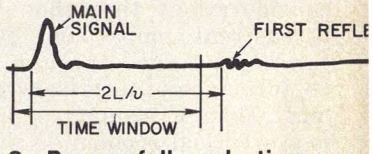

3. By carefully selecting a su time window, the sampling he prevented from "seeing" reflec in the measurement system. L length of coaxial delay lines in

As an example, consider the data shown in Fig. 2, representing TDM measurements on a 30 dB attenuator. Note the excellent agreement with data taken on a computer-controlled network analyzer. Both sets of data were taken at 0.4 GHz frequency intervals.

One of the principal advantages of TDM is the ability to "window out" extraneous system reflections. By acquiring only a selected time window of the entire signal incident on the sampling head, as shown in Fig. 3, unwanted reflections from the generator and sampling head cannot distort the desired data. The window width

Harry M. Cronson, Ph. D., Member of the Technical Staff, Sperry Research Center, 100 North Road, Sudbury, MA 01776.

*Here, baseband signifies a unipolar pulse. Note that the pulse is a video pulse and should not be confused with the envelope of an rf carrier.

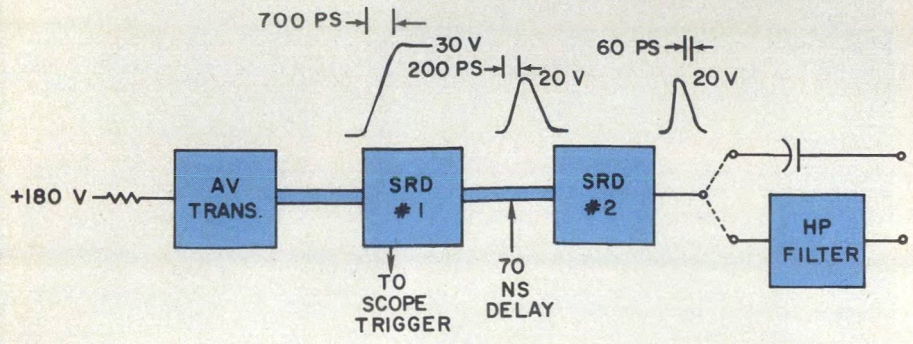

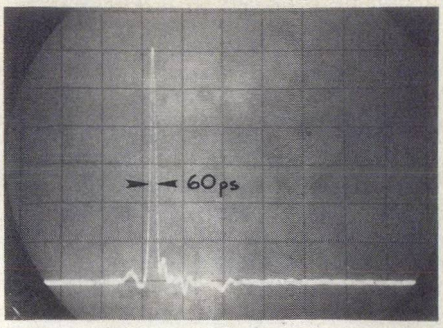

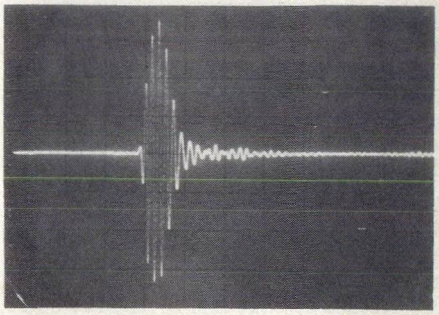

4. A 60 ps impulse generator (a) is much simpler to build than its cw counterpart. The impulse (b) contains energy up to about 8 GHz. By using a waveguide filter on the output, an rf pulse (c) can be generated for tests to 18 GHz.

must be chosen to be less than the two-way transit time in the individual delay lines.

It should be mentioned that for some applications, the time-domain waveforms themselves may be used directly without frequency translation. For example, certain flaws in passive components can cause decreased risetime, undershoot and ringing in the transmitted pulse. These component problems could be easily detected on a sampling oscilloscope display by semi-skilled production line personnel and rejected. There has also been considerable time-domain studies done in transient scattering work and antenna characterization.[1]

Generator features simple circuit

As mentioned previously, the simplicity of the picosecond pulse generator is one of the main advantages of TDM method. A typical rf generator consists of an avalanche transistor and two step-recovery diodes, as shown in Fig. 4(a). In this circuit, the avalanche transistor produces a 30 V step waveform (actually a long, square pulse) which has a risetime of approximately 700 ps. This step is then sharpened to a 200 ps risetime by a step-recovery diode (SRD) stage. A coupler incorporated into the SRD fixture can be used to extract a trigger signal for the sampling oscilloscope. The main signal is delayed approximately 70 ns after the initial SRD stage to allow for the delay in the oscilloscope trigger circuits, then sharpened to a risetime of about 60 ps by a second SRD stage and differentiated by a series capacitor to form the impulse shown in Fig. 4(b).

This type of generator can be used to obtain 1% measurements of components up to about 8 GHz. A photograph of the interior of a typical pulse generator of this sort is shown in Fig. 6. Note the microstrip construction techniques and coaxial delay lines. Besides the main rf output, an impulse reference waveform is also supplied for use in the closed-loop scanning procedure described in the accompanying box.

The spectral amplitude at higher frequencies can be increased by resorting to other excitation waveforms. For measurements to about 18 GHz, the differentiating capaci-

(continued on p. 42)

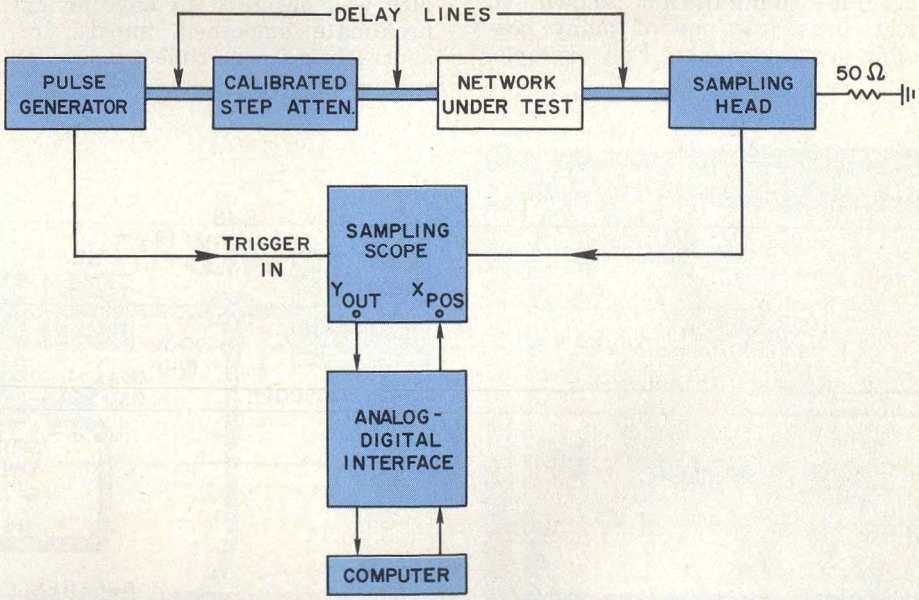

5. A practical system uses a computer and A/D interface. Once the computer acquires the sampled time-domain waveforms, it can perform FFTs and other calculations to extract the desired frequency information. Present scanning time is about one minute for a 256-point waveform.

tor can be replaced by a waveguide filter to produce the rf pulse waveform shown in Fig. 4(c).

Practical systems computer aided

A practical insertion-loss measurement system would incorporate a calibrated step attenuator and a computer interface for closed-loop control and calculation, as shown in the block diagram of Fig. 5.

It is often desirable to include a calibrated step attenuator between the pulse generator and the device-under-test, so that similar deflection waveforms can be compared. In this way, errors due to vertical non-linearities and different mV/cm settings are eliminated. For example, in determining the insertion loss of a nominal 10 dB attenuator, the step attenuator is set to 0 dB with the test attenuator in place and the test waveform acquired. Then the step attenuator is set to 10 dB, the test attenuator removed and a second waveform acquired. These two waveforms are then processed to give the unknown insertion loss. It should be mentioned that the step attenuator is calibrated by using a set of standard attenuators at the network-under-test position.

The delay lines and connectors on both sides of the network-under-test must be of the highest quality. Even a small mismatch in the lines or improper mating of the connectors can cause errors. For measurements below 9 GHz, the General Radio 900 Series of lines and connectors proves very satisfactory.

It should be noted that the delay-line configuration shown in Fig. 5 is just one of many possible arrangements. For example, to measure S_{11} as well as S_{21}, the system illustrated in Fig. 7 has been used. With the switches in the T position, insertion loss of the component-under-test is measured, while for return loss measurements, the R position is used. For this application, a directional coupler was designed to have an approximate smoothed impulse response in a 2.5 ns time window for both the transmitted and coupled pulse. This was accomplished by extending the length of the uniform coupling region so that the two-way travel time between the inevitable coupler discontinuities was greater than 2.5 ns.

The insertion loss of a 30 dB attenuator has already been presented in Fig. 2. Figure 8 illustrates S_{21} and S_{11} measurement for a 40

Adaptive scanning improves accuracy

Computer-controlled sampling and subsequent processing of time-domain waveforms are accomplished with the sampling oscilloscope, computer and necessary analog-digital interfacing. The sampling head and oscilloscope act as a sample and hold circuit with a very narrow sample gate.

Early work in acquiring sampling oscilloscope waveforms showed that simple averaging was only partially successful in reducing noise errors. The main reason is that simple averaging assumes a zero mean, whereas longer term vertical amplifier drift and timing shifts are present at the sampling scope output.

In 1969, Nicolson[6] devised an adaptive scanning procedure to stabilize the time window. With this method, the waveform is scanned nonsequentially using the three points above in Fig. A-1. Preliminary to scanning, point P_1 is manually placed on a flat portion of the trace outside the time window of interest. A reference pulse with a fast risetime region, derived from the excitation pulse, is introduced with P_2 positioned on its high-slope region. The original voltage V_{21} is stored in the computer. The point P_3, during which the acquisition steps along the waveform of interest, is initially set at the beginning of the time window.

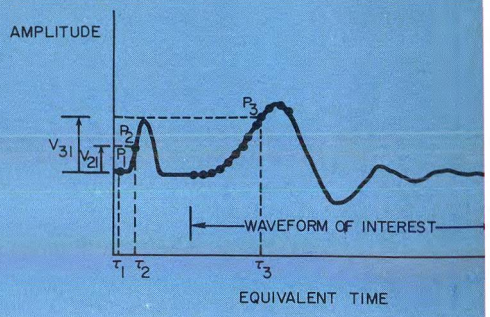

A-1. Adaptive scanning corrected waveform drift and jitter.

Note that any vertical amplifier drift will move P_1 and P_3 in the same direction. Therefore, to remove the drift, the voltage difference, V_{31}, between P_3 and P_1 is averaged and stored. During scanning the voltage difference V_{21} is continually monitored. Any change from its original value is interpreted as a timing shift and the entire waveform is shifted to restore the original value of V_{21} before acquiring the P_3 point. The adoption of this closed loop scanning procedure greatly improves the accuracy of time-domain metrology.

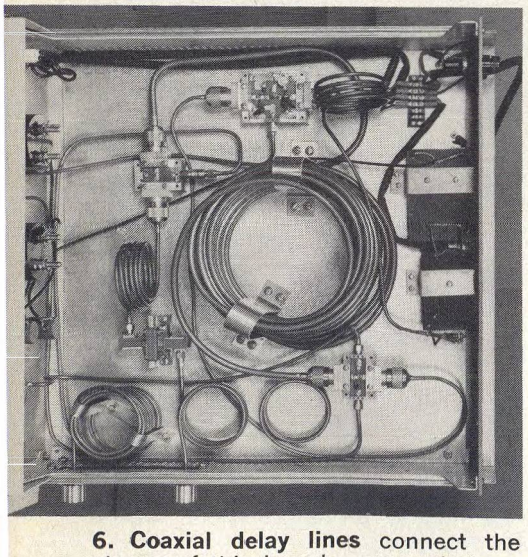

6. Coaxial delay lines connect the stages of this impulse generator.

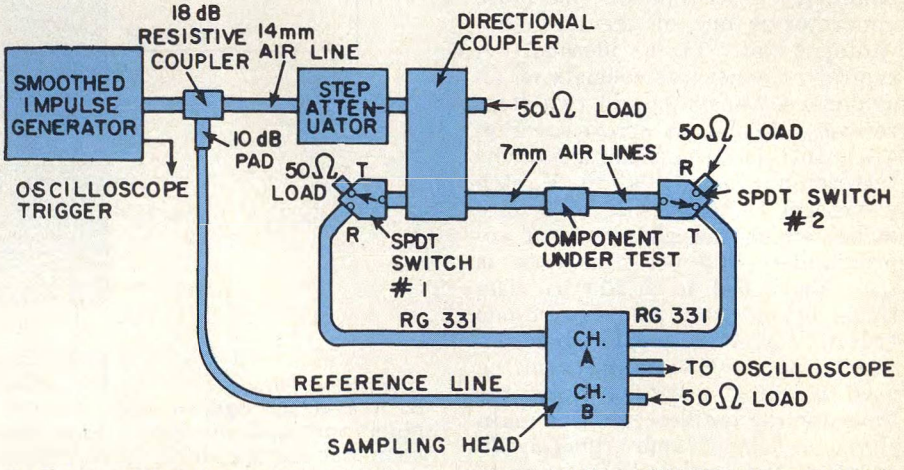

7. S-parameter measurements can be made quickly with this arrangement.

dB attenautor. Each graph shows three sets of data points: Two time-domain measurements to assess repeatability, and a network analyzer result to serve as an accurate, independent reference. The divergences in the S_{21} transformed time domain above about 6 GHz are the result of a poorer signal-to-noise ratio because of the limited available spectral amplitude. Although there is a reasonable agreement between the transformed S_{11} time domain runs and network analyzer values, the spreads are much larger than the S_{21} results. This is thought to be caused by residual ripples in the directional coupler.

Fortunately, accurate measurements of S_{11} are usually not required. One only needs to show that S_{11} is below some minimum value and for this situation, present time-domain techniques should be satisfactory.

Insertion loss measurements can also be taken using an rf pulse waveform to overcome the high-frequency deficiencies of the impulse waveform. Some of these results are illustrated in Fig. 9, for a 30 dB attenuator. Note, in general, the good agreement between

(continued on p. 44)

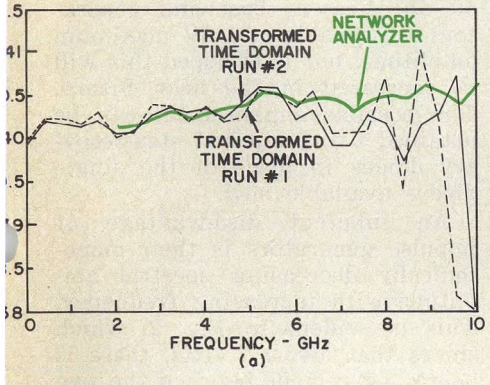

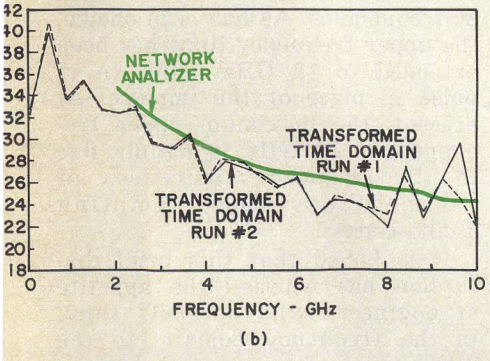

8. TDM s-parameter data for this 40 dB attenuator diverges from analyzer data above 6 GHz due to the limited spectral amplitude of the impulse at the higher frequencies.

the three sets of data. The divergences seen below 10 GHz and above 16 GHz are due to the decreased spectral amplitude of the pulse in this range.

Narrowband tests are tough

Like most measurement methods, TDM has limitations. Some are basic to the technique and others are due to the state of present technology. One fundamental limitation is that incorrect frequency information is obtained for non-linear elements, such as large-signal amplifiers. The reason is that time-to-frequency translation is no longer valid when non-linearities occur.

A second restriction limits the accuracy of narrow-band measurements. Since the excitation waveforms used have a very wide instantaneous spectrum, the spectral energy contained in a narrow band, say 10 MHz wide, is necessarily very small, and therefore, the signal-to-noise ratio (SNR) can be very low. Thus, considering this intrinsic limitation, it is more natural to determine very wideband characteristics with short pulses and to use cw generators for narrow-band measurements.

Due to the state of present technology, the dynamic range of TDM measurements is limited to about 50 dB. Present baseband generators are capable of a 6V maximum amplitude, but it is hoped this will be increased in the near future. One possible enhancement can be obtained using stacked step-recovery diodes in place of the single diodes available now.

An inherent disadvantage of impulse generators is their monotonically decreasing spectral amplitude with increasing frequency. This is evident in Fig. 2, which shows that above 7 GHz, there is poorer agreement between the two curves because of the lower SNR of the baseband generator at higher frequencies. As has been shown, the upper frequency limit has been extended to 18 GHz using an rf pulse in place of the impulse. At present, the maximum upper frequency of 18 GHz is mainly due to the frequency limitations of commercially-available sampling oscilloscopes.

It is hoped that this brief discussion has whetted the appetite of engineers who normally think in the frequency domain, to the possibilities of time-domain, to the niques for wideband measurements. Although the pulse generators described here are not currently commercially available, and the spe-

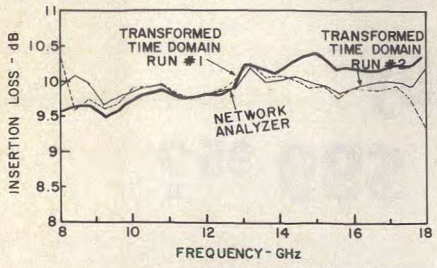

9. An rf pulse was used for this 8 to 18 GHz measurement.

cial scanning algorithms are not widely known, satisfactory time-domain systems can be assembled from off-the-shelf tunnel-diode generators and digital processing sampling oscilloscopes.[5] It is anticipated that as engineers become more aware of time-domain techniques, the more these methods will complement the conventional cw approach. ••

Acknowledgement

The author gratefully acknowledges the many pioneering contributions of his colleagues, Dr. G. F. Ross, Dr. A. M. Nicolson and Mr. P. G. Mitchell of the Sperry Research Center and the continued interest and support of Mr. F. Seeley of the Army Metrology and Calibration Center, Redstone Arnsenal, AL.

A large part of the work reported in this article was supported by the U.S. Army Metrology and Calibration Center, Army Missile Command, Redstone Arsenal, AL, under contract DAAHO1-71-C-1414.

References

1. A. M. Nicolson, C. L. Bennett, Jr., D. Lamensdorf and L. Susman, "Applications of Time-Domain Metrology to the Automation of Broadband Microwave Measurements," *IEEE Trans. Microwave Theory Tech.*, Vol. MTT-20, pp. 3-9, (January, 1972).
2. A. M. Nicolson and G. F. Ross, "Measurement of the Intrinsic Properties of Materials by Time Domain Techniques," *IEEE Trans. Instrum. Meas.*, Vol. IM-19, pp. 377-382, (November, 1970).
3. H. M. Cronson and G. F. Ross, "Current Status of Time-Domain Metrology in Material and Distributed Network Research," *IEEE Trans. Instrum. Meas.*, Vol. IM-21, pp. 495-500, (November, 1972).
4. H. M. Cronson, A. M. Nicolson and P. G. Mitchell, "Extension of Time Domain Metrology Above 10 GHz to Materials Measurments," *IEEE Trans. Instrum. Meas.*, Vol. IM-23, pp. 463-468, (December, 1974).
5. D. Hannaford, "The Application of Picosecond Pulses in Time Domain Metrology," Joint Measurement Conference, Gaithersburg, MD, (November, 1974).
6. A. M. Nicolson, "Wideband System Function Analyzer Employing Time to Frequency Domain Translation," presented at WESCON Convention, San Francisco, CA, Sess. 22, (August, 1969).

Test your retention

1. Why use TDM?
2. How is time domain data translated into the frequency domain?
3. In what way can a computer be used to improve measurement accuracy?
4. What are some fundamental limitations of time-domain metrology?
5. Describe a simple picosecond pulse generator.

Digital Processing Adds Accuracy To TDR

Digital processing enhances traditional time domain reflectometry by improving the overall signal-to-noise ratio and adding the ability to make accurate difference measurements.

TIME-domain reflectometry has gained widespread acceptance as a precise means to measure cables, connectors and devices. Traditional TDR techniques simply call for a tunnel-diode step generator with a source impedance of 50 ohms and a "feed-through" sampler. But data acquisition can be greatly enhanced by using a minicomputer (Fig. 1) with user interactive software to "massage" the data output.

Perhaps the most important offspring of the marriage of data processing and TDR techniques is the ability to perform highly accurate, automated difference measurements. The differencing technique relies on precision standards for initial calibration of the measurement system. Precision standards are first tested by the system, and their characteristics are stored in a minicomputer. Once the system is so calibrated, the reflection characteristics of other components can be compared to the stored values for the standard to an accuracy of ±0.025 ohms.

But the minicomputer can do much more than merely store data points in a TDR system. One of the major drawbacks of a non-assisted TDR system is a limited signal-to-noise ratio (SNR), typically about 42 dB for a sampler with a bandwidth from dc to 14 GHz. With digital processing techniques, however, the limiting SNR can be improved to approximately 66 dB for more exacting, repeatable measurements.

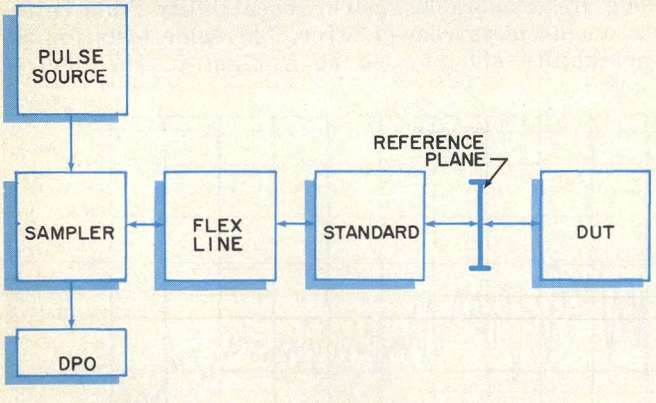

1. A digital processing oscilloscope (DPO) containing a minicomputer can greatly enhance traditional TDR.

A carefully designed sampling system is the first step towards improving the overall SNR capability. In fact, noise reduction in the sampler, or "smoothing" as it is commonly called, can improve the signal-to-noise ratio by as much as 12 dB, thus enabling system SNRs as low as 54 dB.

Smoothing is a process which reduces the error signal between the high-speed sampling gate at the input of the sampler and the low-speed sample and hold circuit at the sampler's output. In practice, smoothing is achieved by introducing a variable series resistance (R), shunt capacitance (C) integration circuit (Fig. 2).

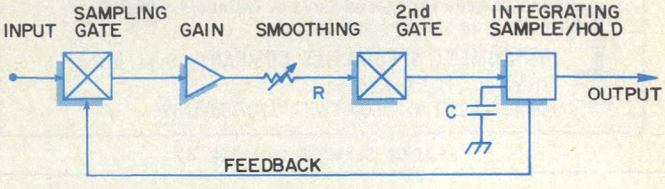

2. Smoothing in the sampler requires an R-C circuit.

It should be noted that smoothing requires a higher sampling density to maintain display accuracy. This is accomplished by slowing the display rate at a constant displayed time per division. The number of samples required to achieve the correct signal level is defined by:

$$n = \log (1 - E_o/E_{in})/\log (1 - A)$$

or

$$E_o = E_{in} (1 - (1-A)^n)$$

where A is equal to the loop gain from the sampler input to the output of the sample and hold circuit ($A \leq 1$) and n is the number of samples taken between two levels of E_{in}.

For example, if A has a value of 0.1, then n must be 28 for E_o to achieve a value of 95% of E_{in}. Alternately, it is necessary for the display rate to be reduced by a factor of 28 in order for the data accuracy to be within 5% of the true value. Yet another method of viewing this process is to consider what would happen to a single noise spike. Clearly, such a spike would require 28 samples to reduce its amplitude by 95%.

The computer-aided system is also used to average data from the sampler, thus providing additional "smoothing" of data points. Applying computerized averaging together with the sampler circuit design described above can further improve overall signal-to-noise ratio to better than 66 dB.

Averaging with the computer in the system is simply equivalent to summing n sets of data, then dividing by n. The number of sets, n, is increased by a power of two, and another set of data summed with the first set. The ideal improvement is 3 dB

(continued on p. 48)

Gene Cowan, Tektronix, Inc., P.O. Box 500, Beaverton, OR 97005.

for each power of two used in summing data sets. The total number of data sets to be summed is determined by the final signal-to-noise ratio desired.

Since most raw data is not ideal, auto-correlation should be used on final, averaged data to check the averaging process and noise characteristics.

Auto-correlation reduces noise

Auto-correlation is one waveform compared to itself once. The mathematical correlation process determines whether or not a characteristic in the data is repeating. Line frequencies are a major problem in the time domain and can be classed as "correlated" noise. Correlated noise is usually enhanced by the triggering process of the sampling system phase locking onto the line frequency.

The environment around the TDR system may also be a source of noise, other than 60 Hz, onto which the system can phase lock. Sampling display rates slower than one second—giving high-dot densities—are required to force random cyclic phase changes of the lowest frequency noise components. By averaging many displays, these random phase changes will reduce noise magnitudes to low mean values at each horizontal data location.

By increasing the overall signal-to-noise ratio, computer smoothing, averaging and auto-correlation checks improve the ability of a TDR system to make accurate measurements on precision standards. And it's by taking a series of measurements on standard components that a measure of system repeatability and random error can be obtained.

A measure of the repeatability and random errors of the system is checked by performing several measurements on precision standards. The repeatability of the TDR system is first determined by taking the difference between two sets of averaged data without disconnecting the precision standards. The precision standards are then disconnected and reconnected to give new sets of data which are again differenced. The second set of differenced data should have significant local differences not in the first set, ideally by a factor of five times. Then, it can be assumed that the system repeatability will have a minimum effect on the measurement and that the second set represents true measurement of the precision standards repeatability.

If, however, the relative magnitudes of the two sets are comparable, system repeatability could be introducing measurement error. The same tests for repeatability should also be applied to the device-

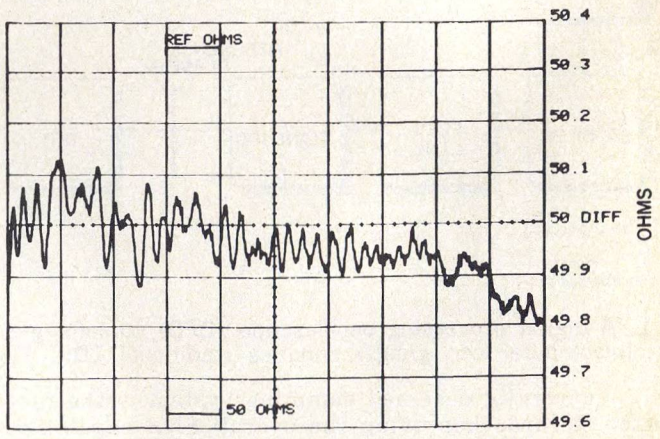

3. Data for reference of precision 14 mm air lines shows a slope due to losses in the measurement system.

under-test. Clearly the repeatability of the system together with the precision standards should also satisfy the criterion of being five times better than the repeatability of the system together with the device-under-test.

Once the repeatability is demonstrated, the TDR system is calibrated by measuring the step reflected from a standard short circuit connected at the measurement plane. From Fig. 1, it can be seen that the measurement plane is located at the input of the device-under-test. The step will thus have traversed the flex line twice, once as the incident step towards the measurement plane and then, after 100% reflection at the short circuit, as the reflected pulse passes back through the sampler where the waveform is recorded as data. The flex line provides delay or time displacement between reflections that occur in the vicinity of the sampler and those that occur at or near the measurement plane. The cable's characteristic impedance (Z_o) and variations from Z_o will also introduce reflections in the measurement system (cable Z_o changes with flexure must also be checked). Most measurements will be made through a standard at the measurement plane.

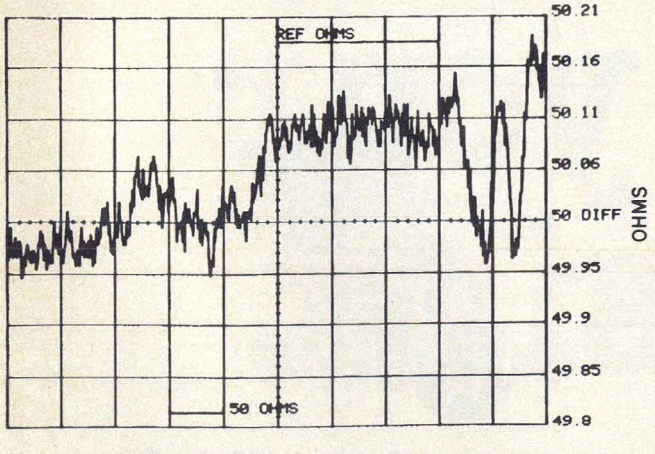

4. When differenced with the 14 mm reference line, the 7 mm line shows an impedance of about 50.09 ohms. The 7 mm line begins at 4.6 on the horizontal axis.

Typical repeatability measurements

Once the computer-aided TDR system has been checked for repeatability and properly calibrated, it's all set for difference measurements. A typical difference measurement might involve the comparison of a secondary standard to a precision standard. This measurement requires a reference and/or a precision standard for a benchmark.

The reference standard chosen for this example is the 14 mm GR 900-LZ15, a 15 cm air line, while the precision standard is the 14 mm GR 900-L30, a 30 cm air line. Figure 3 shows data obtained on the reference standard cascaded with the precision standard. The precision standard starts at 4.6 on the horizontal scale. Note that most of the slope is caused by measurement system losses.

To check a 7 mm Amphenol air line against the 14 mm precision standard, a GR 900 QAP7 adapter must be used. Figure 4 shows the 7 mm air line differenced with the data obtained for the 14 mm precision standard, when the 7 mm line is terminated with a Type 909A load from Hewlett-Packard. Taking the accuracy of the 14 mm lines shown in Fig. 3 as absolute, it can be seen that the final

(continued on p. 51)

value of the 7 mm line is 50.09 ohms, well within its stated range.

The additive noise in the vicinity of the measurement can now be mathematically averaged for a final estimate of impedance. Note that the system slope of Fig. 3 is now removed from the display. The reflections that were part of the system in both sets of data are now removed as seen in Fig. 4. Also, the impedance scale is now 0.05 ohms per division.

A final example of repeatability measurements is checking the integrity of adapters. Data on 10 plug-to-plug adapters for the BNC connector series is shown in Fig. 5. The plug-to-plug section goes from

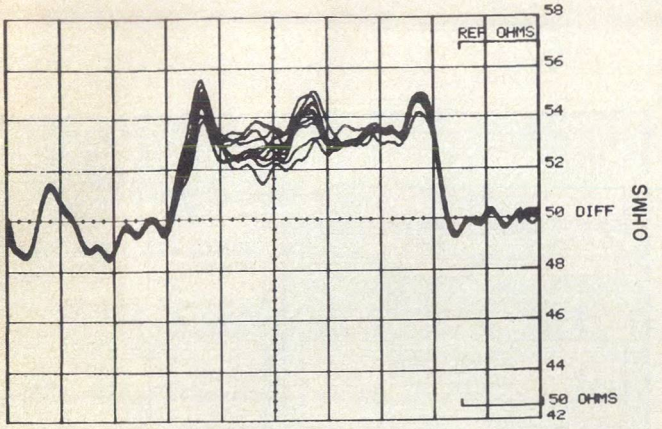

5. Ten plug-to-plug BNC adapters show nominal impedances of about 53 ohms.

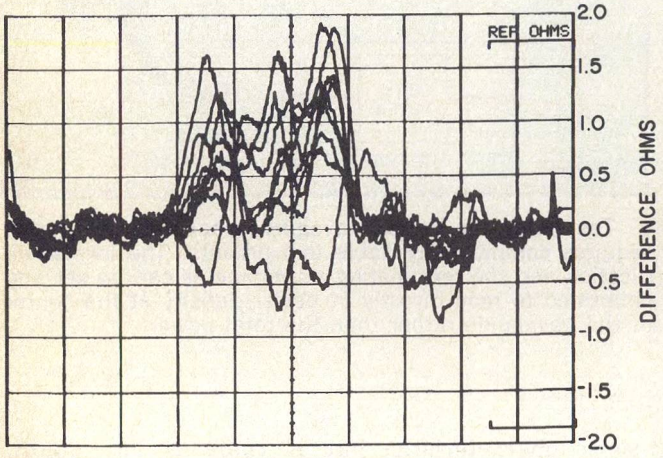

6. Using one plug-to-plug adapter as a reference and differencing the other nine sets of data shows a good deal of impedance variation between connectors.

the division 3 to 5.7 and the jack-to-jack BNC adapter to the BNC 50-ohm termination extends from 5.7 to 8. Note that this early connector design is nominally 53 ohms. Five of the plug-to-plug adapters measured had received at least 10 years' use and the rest less than three years' use. Figure 6 shows nine sets of data differenced from a selected data run. The fluted connector design of this series is responsible for much of the impedance variation. Although most transmission systems, active or passive, can be differenced with computer aided TDR, this waveform photograph does not lend itself to averaging, differencing or auto correlation. ••

Simplify Leakage Probe Calibration

This method for calibrating radiation hazard meters uses a slotted waveguide that approximates the field distribution near a faulty oven door. It's simple and inexpensive to set up. Accuracy is ±5%.

ALTHOUGH there is presently no standard or accepted procedure for the near field calibration of radiation monitoring equipment,[1,2] the accurate calibration of radiation probes is vital for personnel safety. Standard near-field methods are being generated by ANSI and the IEEE, but in the interim, users of radiation hazard meters must rely on the manufacturers of probes, who frequently provide a calibration service, or do it themselves. Some firms, such as manufacturers of microwave ovens, are required by law to maintain an in-plant means to periodically calibrate their radiation in density probes. It is the responsibility of the oven manufacturers to devise a system which is acceptable to the Bureau of Radiological Health, which could be as simple as a comparison with a probe that is set aside as a standard.

This article describes a near field method that is safe, more accurate and probably less expensive than any other secondary standard calibration means. It provides an accuracy of approximately ±5% for calibrating small probes using equipments commonly found in a microwave lab. This bench-top technique uses a guided rather than a free space propagated wave such as in the standardized far-field method.[3,4] As a result, it doesn't need a standard gain horn to generate a field of known strength nor does it require the real estate associated with an anechoic chamber or antenna range. This near-field technique, while not the most accepted method for a standard calibration, is not totally new*, but it does fill a current need and is quite precise.

The technique is based on propagating the fundamental TE_{01} mode in a side wall slotted section of waveguide.

One restriction is it requires the probes to have a uniform E-field response over at least an 180-degree arc and couple lightly into the field. The former property is essential because the radiation emitted from a faulty microwave oven door, for example, is largely concentrated at the sides of the probe and not directly in front of it.

This waveguide technique, therefore, only measures the E-field on the probe in one axis, the other axis is assumed equal in response. Most probes for leakage monitoring do have this symmetrical response characteristic, but if there is any doubt, check with the manufacturer of the probe before using this test procedure.

*The use of waveguide for the calibration of radiation monitors at lower frequency using oversized waveguide has previously been demonstrated.[5]

Edward Aslan, Principal Research Engineer, Narda Microwave Corporation, 75 Commercial Street, Plainview, NY 11803.

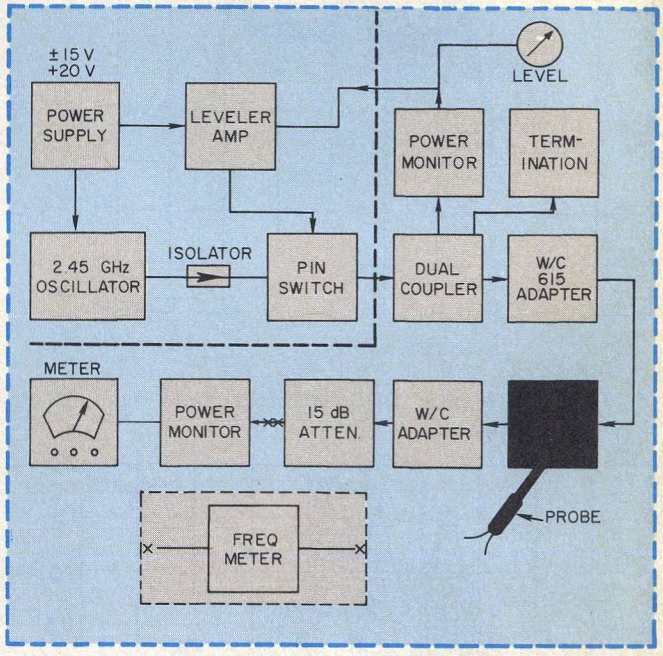

1. **Test setup for slotted waveguide near-field calibration** requires commonly-available instruments. The leveler indication and the terminating power meter can be set and calibrated to read directly in power density at the center of the waveguide rather than the total power.

Modified waveguide uses shimstock

Figure 1 shows the bench setup suitable for calibrating small probes, such as used in leakage monitors for measuring the radiation from microwave ovens and diathermy machines. This equipment operates in narrow bands, generally at the assigned ISM frequencies in the 2450 MHz band. The signal source can therefore be a narrow band cavity oscillator, but should be capable of delivering at least 50 mW.

A dual-directional coupler is used to monitor both incident and reflected power. This coupler is followed by a waveguide-to-coax adapter for matching to the waveguide slotted line. This waveguide section is standard rectangular WR430 guide which has a slot milled into it and slide fitted to the side wall.

(continued on p. 54)

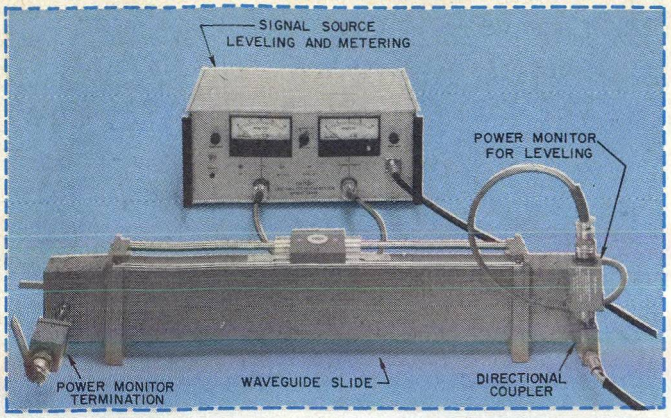

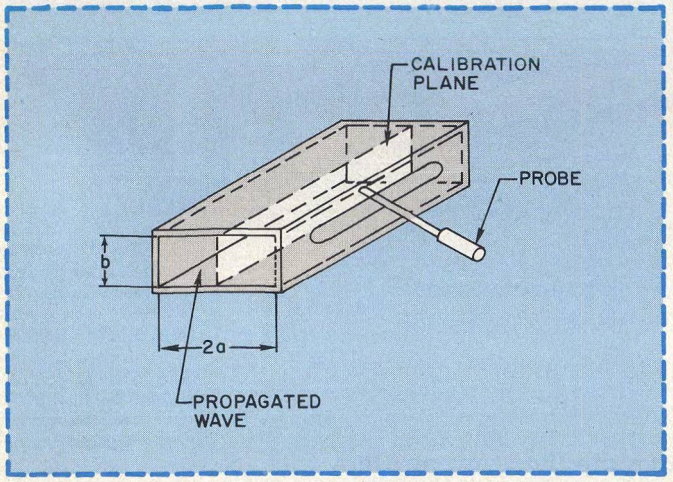

2. **Slotted waveguide section (a)** has a calibration plane as shown in (b). The probe handle and coupling leads are essentially invisible because they're normal to the E-field.

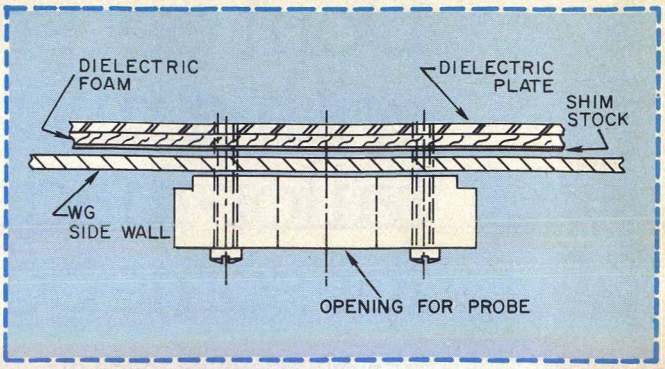

3. **The dielectric plate and foam pressure plate which cover the slot minimize** E-field perturbations. The 0.075 shim-stock minimizes energy leakage from the guide.

The slot provides access of the probe elements to the guide center where a maximum and calculable power density field is obtained. The side holds the probe with its antenna elements in a plane that is normal to the broadwall of the guide. The side also permits the antenna elements to be moved along the center axis of this calibrating plane, Fig. 2. The modified waveguide can be easily fabricated, as shown in Fig. 3. A strip of 0.75 mm brass shimstock, which covers the slot, bears on the inside surface of the guide and moves as the slide is moved. This shimstock is held in contact to the side wall with a dielectric plate, the pressure to the shimstock being transmitted through a sheet of 0.3 cm dielectric foam, as shown in Fig. 3. The shim, foam and pressure plate move with the slide. This shim arrangement is necessary to reduce any perturbation of the field as would be caused by an uncovered slot.[6]

A hole, slightly larger than the probe diameter in this strip, allows for entrance of the probe to the guide. With this strip, no measurable energy will leak from the guide through the slot, either with or without the probe inserted in the guide.

Operation and test principles

The system is calibrated at the point of maximum field strength in the plane normal to the propagation vector. The power density at this plane is calculated assuming a sinusoidal distribution of the E field across the guide with a maximum near the center and zero at the side, which is the normal TE_{01} mode E-field distribution, Fig. 4. The calibration plane is slightly off center due to the presence of the dielectric pressure plate, but the field is uniform in the orthogonal direction.

For standard guide, WR(430), and with the foam and the polystyrene pressure plate ($\epsilon_r = 2.5$) both 0.3 cm thick, Fig. 3, a power density at the center of the guide is 1 mW/cm^2, for an input power, P_T of 30.15 mW. The presence of the dielectric materials introduce approximately a 1-1/2% perturbation of the total transmitted power.

Distortion of the field caused by scattering from the probe is evaluated with the slide. The slide is traversed through one-half wavelength and the minimum and maximum indications are noted, the true calibration being the average of these readings. Some scattered energy from the probe antenna cannot be evaluated by movement of the probe with the slide. This energy is that which is returned to the probe antenna due to reflection from the guide sidewalls, the phase of which does not vary as the probe is moved. It represents that portion of the scattered field that is normal to the sidewalls and for the small dipoles generally used, it contributes an almost immeasurable error.

Standing waves within the guide will be caused by reflections from the terminating load as well as the scattering from the probe under test. If the probe has been well designed for its application and couples lightly to the field, the standing waves will be essentially a function only of the reflection coefficient of the terminating load. The associated uncertainty at any random distance along the calibrating plane is:

$$\epsilon_1 = [(1 + |\Gamma|)^{-2} - 1] \times 100\%$$

The voltage reflection coefficient, Γ for a well made waveguide termination is 0.005, which would contribute a 1% uncertainty. This uncertainty is completely eliminated by averaging the minimum and maximum readings as the probe is traversed along the calibrating plane.

Locating the probe antenna in the center axis of the guide is found by positioning the probe for a maximum indication as the probe is inserted into the guide. The slope of the slide and error in maintaining this center axis contributes very small error. The relative deviation of power density as a function of distance from the center is:

$$\epsilon_1 = [1 - |\Gamma|)^{-2} - 1] \times 100\% \qquad (4)$$

(continued on p. 57)

4. **Electric field distribution** across the waveguide is basically that of a TE_{01} mode, the asymmetrical distribution is caused by the dielectric at the sidewall.

If Δa, the variation in wave-guide width, is assumed to be 0.25 cm, which is a liberal tolerance, $\epsilon_2 = 0.005$ which means a 0.5% error.

Error due to the ability to average the probe scattering error is estimated at less than 1/2%. This is based upon typical maximum to minimum deviations as the slide is traversed approximately ±5%. If the incident power is maintained constant during the movement of the slide and probe, the variation caused by scattering from the probe is substantially reduced. This can be accomplished by a leveling loop with the monitor or reference point at the power meter at the incident arm of the directional coupler, Fig. 1. With a high gain leveling loop, this variation could be reduced close to zero. The residual variation will be caused by reflections from the termination. With a high gain leveling loop and a precision termination, a reasonably good calibration could be obtained without the special sidewall slotted section of waveguide. Attenuation in the section of guide is negligible, being approximately 0.004 dB per foot.

Insertion loss of the coax-to-waveguide adapter may be accounted for using the two-adapter measurement method and attributing the loss equally to the two adapters, the insertion loss being one half of the total measured. The coupling factor of the directional coupler used to monitor incident power should be determined from the side arm to the output port of the main line as opposed to the usual calibration which is from the side arm to the incident port of the main line.

Comparison of results with far field tests

In a far-field calibration, such as the NBS standard that exists today, the field strength over the length of the probe would be quite uniform and the handle of the probe might have perturbation effects on the calibration. In the near field, the reactive fields as well as the radiation fields would be rapidly changing over the length of the probe with the resultant lesser perturbing effects of the handle. The field distribution in the waveguide more closely resembles the rapidly-changing leakage fields near an imperfect device with the resultant calibration that relates to the actual use of the probe.

Six probes calibrated using a standard gain horn and anechoic slide in a 1 mW/cm² field, indicated, respectively, 1.00, 1.01, 0.98, 1.00, 0.95, 1.01. In this guided wave calibration they indicated, respectively, 0.97, 1.01, 1.01, 0.98, 0.92, 1.05, mW/cm². The maxima to minima variation as the slide was traversed was 4%.

In these comparison tests, the reflected power as indicated by the directional coupler at the coax-to-waveguide adapter varied as the probe was moved in its slide from 16 to 20 dB below incident power, which was maintained constant by a leveling loop. The variation is due to scattering from the probe. The return loss without the probe inserted was 27 dB. The incident power was corrected for this power. The transmitted power as read by the incident directional coupler was 30.15 mW for 1 mW/cm². Three probes calibrated by the Bureau of Radiological Health read exactly 3% higher in this system. The maximum possible accumulative error of the BRH calibration is ±.7 dB.

An estimate of the accuracy of this system is as follows:

Incident power measurement	±2.0%
ϵ_2, Position and slope error	±0.5%
Coupler coupling factor	±1.0%
Insertion loss estimate	±0.5%
Averaging of scattering effect	±1.0%
Waveguide tolerance	0.3%
Total	5.3%

The calibration as described is for probes which have antenna elements in a single plane. Isotropic probes using multiple plane construction would require a calculation of average power density over the entire surface being monitored. If three elements in mutually perpendicular planes are used, calibration is possible without more involved calculation, provided two of the elements are oriented in the center plane[7]. This may not be practical to accomplish while maintaining the entrance port in the sidewall of the guide. ••

References

1. Edward Aslan, "Electromagnetic Leakage Survey Meter," *Journal of Microwave Power*, Vol. 6, No. 2, pp. 169-177, (July, 1971).
2. A. W. Rudge, "An Electromagnetic Radiation Probe For Near-Field Measurements At Microwave Frequencies," *Journal of Microwave Power*, Vol. 5, No. 3, pp. 155-174, (November, 1970).
3. "Measuring Field Strength In Radio Wave Propagation," *IEEE Standards, Report* #291, (May, 1969).
4. R. R. Bowman, "Near Zone Calibrations For Antennas and Field Intensity Meters," *Rome Air Development Center Report*, RADC-TR-69-415, (January, 1970).
5. D. Woods, "Standard Intensity Electromagnetic Field Installation for Calibration of Radiation Hazard Monitors from 400 MHz to 40 RHz," *Non-ionizing Radiation*, Vol. 1, No. 1, pp. 9-17, (June, 1969).
6. S. Silver, *Microwave Antenna Theory and Design*, p. 287, (1949).
7. R. R. Bowman, "An Isotropic Electric Energy-Density Probe For High Level Fields," *URSI*, Spring Meeting, (April, 1971).

Test your retention

1. What are the advantages of a waveguide calibration system over one using a free space propagated wave?
2. What two characteristics should a probe have in order to be used with this system?
3. Why are probe handle and coupling leads essentially invisible when the probe is inserted into the waveguide?

Matching: When Is A Single Line Sufficient?

Here's a simple, graphical method to quickly predict whether a single, constant impedance transmission line is capable of matching a real source impedance to a complex load.

IMPEDANCE matching is an essential element of microwave design. Perhaps the simplest impedance matching network is the low-loss, series transmission line. Given a source and load impedance, the electrical characteristics of a series matching section are easily calculated[1,2]. But to save time, before attempting to design the matching section, check to see if the two impedances can be matched with a single section of line.

The technique outlined here can be used to quickly determine whether a single, series transmission line of constant impedance can be used to match a load and source. Once the equations are mastered, the method reduces to a simple Smith Chart construction.

A source and load, connected by a series transmission line, are shown in Fig. 1, where Z_L is the load impedance, Z_o and Θ are the characteristic impedance and electrical length of the series transmission line and Z_{in} is the input impedance of the circuit consisting of the transmission line and load combination. In order for a matched condition to exist, Z_{in} must be equal to the real source impedance being considered.

The transmission line equation relates the parameters shown in Fig. 1:

$$Z_{in} = Z_o \left[\frac{Z_L + jZ_o \tan\Theta}{Z_o + jZ_L \tan\Theta} \right] \quad (1)$$

Two equations, which completely describe the characteristic impedance and electrical length of the matching section, can be derived from Eqn. (1) by segregating real and imaginary parts:

$$Z_o = \sqrt{(Z_{in} R)\left(1 - \frac{x^2}{R(Z_{in} - R)}\right)} \quad (2)$$

$$\Theta = \mathrm{Tan}^{-1}\left(\frac{Z_{in} Z_o - Z_o R}{x\, Z_{in}}\right) \quad (3)$$

Inspection of Eqns. (2) and (3) reveal several familiar properties of series transmission lines. For example, if $x = 0$, the argument of Eqn. (3) approaches infinity, indicating that $\Theta = \pm 90°$. In addition, under these conditions, Eqn. (2) reduces to:

$$Z_o = \sqrt{Z_{in} R} \quad (4)$$

Thus, it's apparent that a resistive source is matched to a resistive load with our familiar friend: the quarter-wave transformer.

Kurt P. Schwan, Senior Engineer, Northrop Corporation, Defense Systems Department, 600 Hicks Road, Rolling Meadows, IL 60008.

1. A section of constant impedance transmission line can be used to match a real source impedance to a complex load.

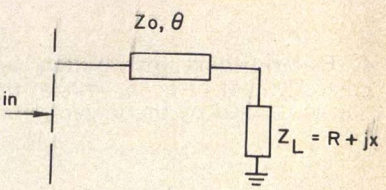

Referring back to Eqn. (2), note that Z_o, the characteristic impedance of the matching section, must be real. Thus, the arguments of Eqn. (2) must be positive:

$$\left(1 - \frac{x^2}{R(Z_{in} - R)}\right) > 0 \quad (5)$$

Depending on whether Z_{in} is larger or smaller than R, Eqn. (5) can be manipulated to yield the following inequalities, which are plotted in Fig. 2:

$$\left(R - \frac{Z_{in}}{2}\right)^2 + x^2 < \frac{Z^2_{in}}{4} \quad \text{for: } Z_{in} > R \quad (6a)$$

$$\left(R - \frac{Z_{in}}{2}\right)^2 + x^2 > \frac{Z^2_{in}}{4} \quad \text{for: } Z_{in} < R \quad (6b)$$

Using a single section of transmission line, a source impedance, Z_{in}, can be matched to a load impedance, Z_L, only if either Eqn. (6a) or (6b) is fulfilled.

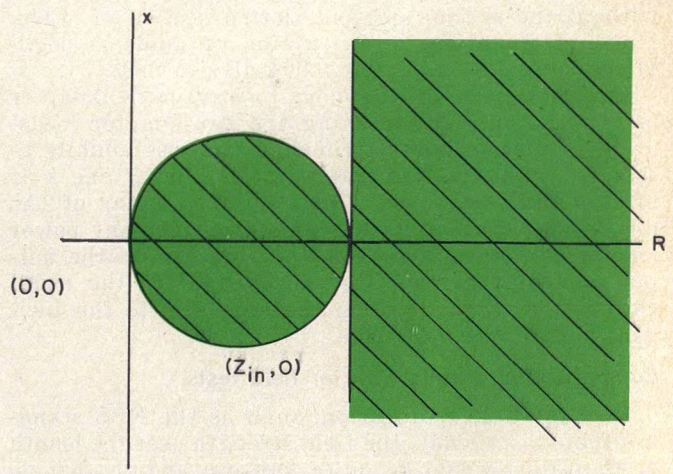

2. Shaded areas correspond to loads ($Z_L = R + jx$) which can be matched to a real source impedance (Z_{in}) with a single section of line.

Graphically, this means that given a source impedance, the load impedance must fall within the shaded areas shown in the complex Z_L plane of Fig. 2. Relation (6a) determines the area inside the circle,

(continued on p. 60)

whose diameter is Z_{in} and relation (6b) represents the semi-infinite plane to the right of $R = Z_{in}$.

It is sometimes easier to visualize impedances on the Smith Chart. The transformation used to transform from the Z_L plane to the reflection coefficient, or Γ, plane is

$$\Gamma = \frac{Z_L - Z'_o}{Z_L + Z'_o} \qquad (7)$$

where Z'_o is the arbitrary normalizing impedance. Performing the transformation, equations (6a) and (6b) become:

$$\left(\Gamma_R + \frac{Z'_o}{Z_{in} + Z'_o}\right)^2 + \Gamma_I^2 < \left(\frac{Z_{in}}{Z_{in} + Z'_o}\right)^2 \qquad (8a)$$

$$\left(\Gamma_R - \frac{Z_{in}}{Z_{in} + Z'_o}\right)^2 + \Gamma_I^2 < \left(\frac{Z'_o}{Z_{in} + Z'_o}\right)^2 \qquad (8b)$$

where Γ_R and Γ_I are the real and imaginary parts of Γ.

Often, the given source impedance is 50 ohms. Thus, with $Z_{in} = 50$, and normalizing to 50 ohms, or $Z'_o = 50$, Eqn. (8) becomes:

$$(\Gamma_R \pm 1/2)^2 + \Gamma_I^2 < 1/4 \qquad (9)$$

This equation, when plotted on a Smith Chart (Fig. 3), takes the form of two circles. Thus, in order to match a load to 50 ohms by means of a single series transmission line, the normalized load impedance, $Z_L/50$, must fall within one of the two circles.

In practical situations, the range of characteristic impedances for the matching transmission line is often limited. In microstrip, the high impedance limit may be set by the fine line resolution of the fabrication technique used, while the minimum impedance restriction might be approached when the width of the line nears a quarter wavelength, thus permitting transverse resonance. Low-impedance coax may be limited by power handling requirements. Mathematically, these limitations can be expressed as:

$$Z_{min} \leqq Z_o = \sqrt{(Z_{in}R)\left[1 - \frac{x^2}{R(Z_{in} - R)}\right]} \leqq Z_{max} \qquad (10)$$

Here, Z_{min} and Z_{max} represent the minimum and maximum impedances which are practical.

Rearranging Eqn. (10), it's possible to incorporate these restrictions:

For $R < Z_{in}$

$$\left(R - \frac{Z^2_{in} + Z^2_{min}}{2Z_{in}}\right)^2 + x^2 \leqq \left(\frac{Z^2_{in} - Z^2_{min}}{2Z_{in}}\right)^2 \qquad (11a)$$

$$\left(R - \frac{Z^2_{in} + Z^2_{max}}{2Z_{in}}\right)^2 + x^2 \geqq \left(\frac{Z^2_{in} - Z^2_{max}}{2Z_{in}}\right)^2 \qquad (11b)$$

and for $R > Z_{in}$

$$\left(R - \frac{Z^2_{in} + Z^2_{min}}{2Z_{in}}\right)^2 + x^2 \geqq \left(\frac{Z^2_{in} - Z^2_{min}}{2Z_{in}}\right)^2 \qquad (11c)$$

$$\left(R - \frac{Z^2_{in} + Z^2_{max}}{2Z_{in}}\right)^2 + x^2 \leqq \left(\frac{Z^2_{in} - Z^2_{max}}{2Z_{in}}\right)^2 \qquad (11d)$$

Once again, given Z_{in}, Z_{min} and Z_{max}, and depending on whether R is larger or smaller than Z_{in}, the load impedance must satisfy both Eqns. (11a) and (11b) or both Eqns. (11c) and (11d) if it is to be matched by a single, series transmission line.

General plots of the relationships in Eqn. (11) depend on the relative values of Z_{in}, Z_{min} and Z_{max}. When their relationship is:

$$Z_{min} \leqq Z_{in} \leqq Z_{max}$$

the plot will be similar to Fig. 4a. If the relationship is:

$$Z_{min} \leqq Z_{max} \leqq Z_{in}$$

the plot will resemble Fig. 4b. In general, the circles will be tangent to the point $(Z_{in}, 0)$, degenerating to

(continued on p. 63)

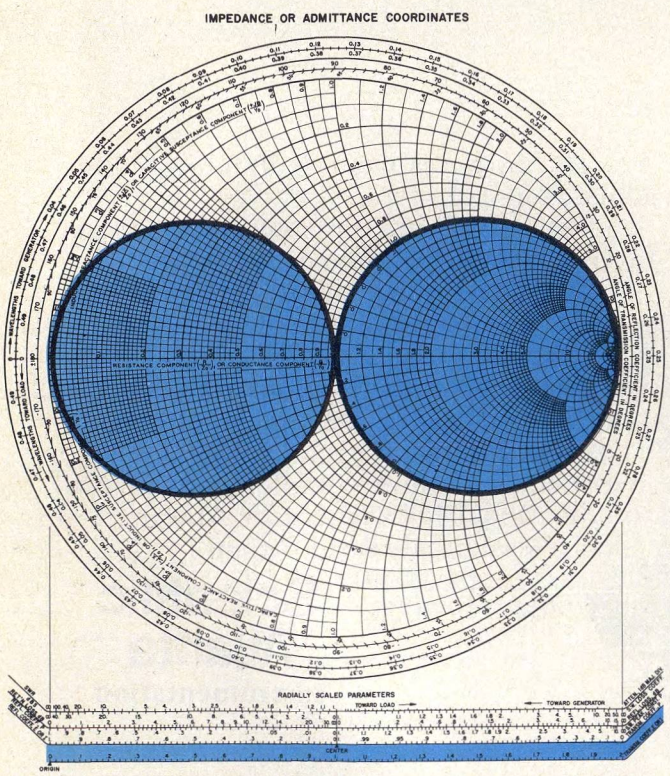

3. Assuming a source impedance of 50 ohms, the shaded areas of Fig. 2 are transformed to this Smith Chart, normalized to 50 ohms.

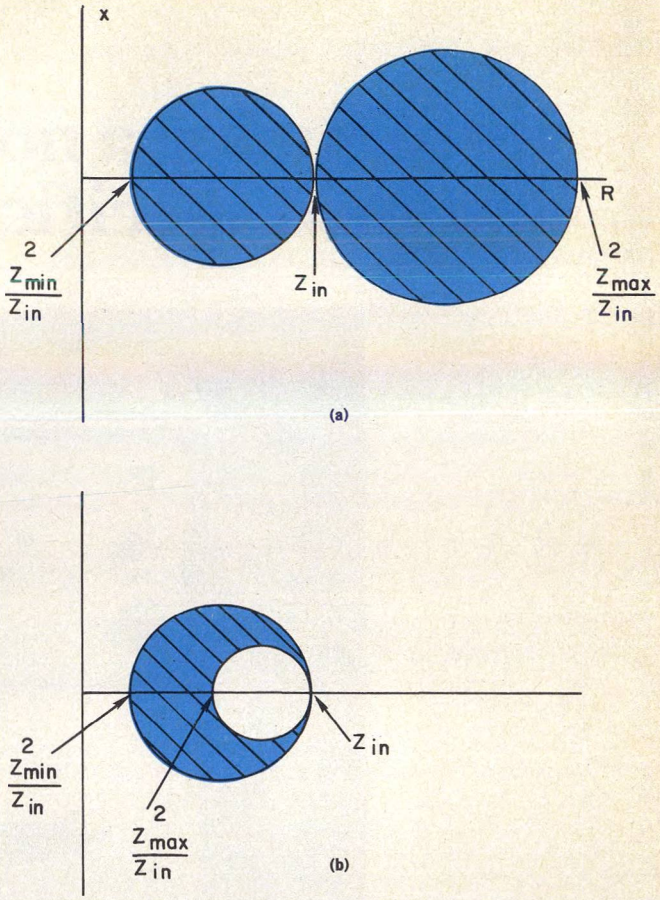

4. Practical cases often dictate maximum and minimum impedances. A load falling in shaded area can be matched to a real source with a single section of line.

Plotting the curves

All working equations in this article are arranged in the general form for a circle to facilitate plotting in a rectangular coordinate system. Reviewing basic algebra, the equation for a circle in an orthagonal x-y coordinate system is:

$$(x - a)^2 + (y - b)^2 = r^2$$

where (a, b) are the coordinates of the circle's center and r is the radius of the circle.

Plotting Eqns. (6) or (11) in the (R, x) complex plane is straightforward. Merely choose the proper equation, or pair of equations, based on the value of R relative to Z_{in}, and compute the "a" and "r" terms. Place the center of each circle "a" units to the right of the origin and draw a circle of radius "r".

A Smith Chart construction of Eqns. (8) and (12) in the Γ, or reflection coefficient plane, calls for a little imagination. Picture a rectangular (Γ_R, Γ_I) coordinate system, centered on the Smith Chart at (1 +j0), with the Γ_R axis coinciding with the j0 line. Compute the "a" and "r" terms in Eqns. (6) or (8). Now, using the radially-scaled parameter transmission coefficient scale at the bottom of the chart, measure off a distance equal to the magnitude of the "a" terms either to the right (−a) or left (+a) of the origin. Using these points as centers, draw circles with radii equal to the corresponding "r" terms.

that point as Z_{min} or Z_{max} approaches Z_{in}. As either of the limits approach 0 ohms, the radius of the associated circle approaches $Z_{in}/2$, corresponding to the circle in Fig. 2. Conversely, as either limit becomes large, the radius also becomes large, approaching infinity, corresponding to the semi-infinite plane in Fig. 2.

Equation (11) can also be transformed to the Γ plane, and plotted on the Smith Chart. For $R < Z_{in}$:

$$\left[\Gamma_R - \frac{Z_{in}(Z^2_{min} - Z'^2_o)}{(Z_{in}+Z'_o)(Z^2_{min}+Z'_oZ_{in})}\right]^2 + \Gamma_I^2 \leq \left[\frac{Z'_o(Z^2_{min} - Z^2_{in})}{(Z_{in}+Z'_o)(Z^2_{min}+Z'_oZ_{in})}\right]^2 \quad (12a)$$

$$\left[\Gamma_R - \frac{Z_{in}(Z^2_{max} - Z'^2_o)}{(Z_{in}+Z'_o)(Z^2_{max}+Z'_oZ_{in})}\right]^2 + \Gamma_I^2 \geq \left[\frac{Z'_o(Z^2_{max} - Z^2_{in})}{(Z_{in}+Z'_o)(Z^2_{max}+Z'_oZ_{in})}\right]^2 \quad (12b)$$

For $R > Z_{in}$:

$$\left[\Gamma_R - \frac{Z_{in}(Z^2_{min} - Z'^2_o)}{(Z_{in}+Z'_o)(Z^2_{min}+Z'_oZ_{in})}\right]^2 + \Gamma_I^2 \geq \left[\frac{Z'_o(Z^2_{min} - Z^2_{in})}{(Z_{in}+Z'_o)(Z^2_{min}+Z'_oZ_{in})}\right]^2 \quad (12c)$$

$$\left[\Gamma_R - \frac{Z_{in}(Z^2_{max} - Z'^2_o)}{(Z_{in}+Z'_o)(Z^2_{max}+Z'_oZ_{in})}\right]^2 + \Gamma_I^2 \leq \left[\frac{Z'_o(Z^2_{max} - Z^2_{in})}{(Z_{in}+Z'_o)(Z^2_{max}+Z'_oZ_{in})}\right]^2 \quad (12d)$$

The areas shown in Fig 4 transform to the Γ plane as shown in Fig. 5.

These equations and plots can easily be used by the circuit designer to quickly determine whether it is possible to match with only one transmission line. If it is not possible, the plots can provide target areas for multiple element matching networks, using the series transmission line as the matching element nearest the load. The purpose of the other elements, then is to move the load into one of the circles. Aids of this type are especially useful since multiple element, narrow-band matching networks are not unique. It was shown that the single element network resulted in two equations and two unknowns. The multiple element network results in more unknowns than equations. ••

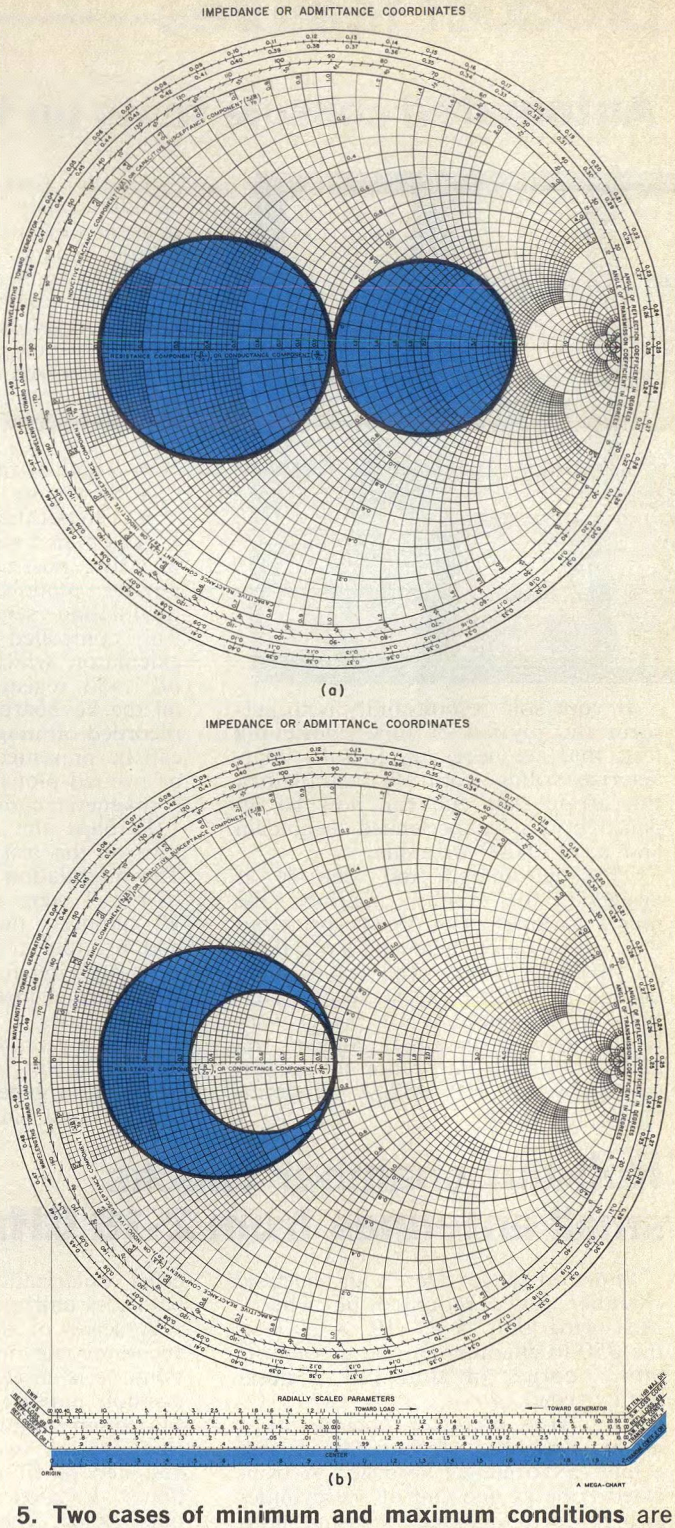

5. Two cases of minimum and maximum conditions are illustrated here. Figure (a) illustrates the case of $Z_{min} \leq Z_{in} \leq Z_{max}$ under the conditions: $Z_{in} = Z'_o = 50\Omega$, $Z_{min} = 16\Omega$ and $Z_{max} = 104\Omega$. Figure (b) shows the case of $Z_{min} \leq Z_{max} \leq Z_{in}$ for the specific conditions: $Z_{in} = Z'_o = 50\Omega$, $Z_{min} = 16\Omega$ and $Z_{max} = 29\Omega$. Note that loads falling within the area common to both circles cannot be matched to a real source impedance with a constant-impedance line.

References

1. M. A. Hamid and M. M. Yunik, "On The Design Of Stepped Transmission Line Transformers," *IEEE Trans. MTT (Correspondence)*, Vol. MTT-15, pp. 528-529, (September, 1967).

. R. M. Arnold, "Transmission Line Impedance Matching Using The Smith Chart," *IEE Trans. MTT (Letters)* Vol. MTT-22 pp. 977-978, (November, 1974).

Automated console tests up to four VCOs in just minutes

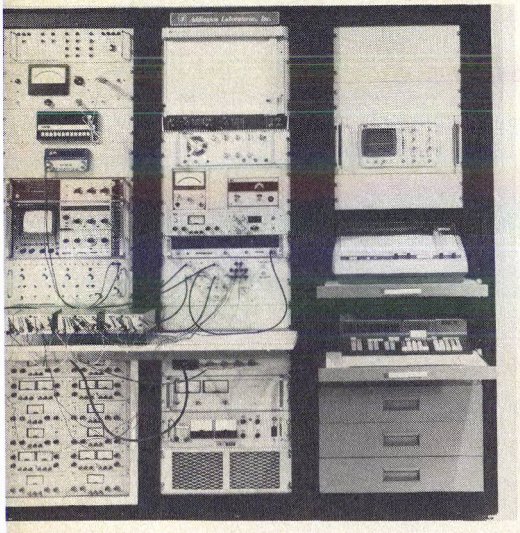

If your sole responsibility is to perform the myriad of time consuming tests that are necessary to fully characterize voltage-controlled oscillators, I'm afraid that you can now be repaced by an inexperienced technician and a $150,000 machine.

This automated test console is designed to rapidly measure the major parameters of VCOs, print out data points, plot them and store them on magnetic cards. The test system, housed in a three-bay enclosure, consists of a symphony of power supplies, thermal chambers and rf, dc and analog instrumentation all orchestrated by an HP 9820A programmable calculator.

Up to four oscillators may be simultaneously tested by the VCO console. Typical measurement capabilities include:

- Tuning linearity
- Modulation sensitivity
- Modulation sensitivity variation
- Post-tuning drift
- Rf power output
- Modulation bandwidth
- Harmonic/spurious rejection
- Frequency pulling and pushing
- Residual fm
- Slew time
- Temperature stability

Automated measurements of tuning linearity, post-tuning drift, rf output power, modulation sensitivity and modulation sensitivity variation are fully controlled by the programmable calculator, which has a memory size of 1,453 registers. Programs entered on the keyboard may be permanently recorded on magnetic cards. Test data can be presented in print-out, display or printed plot form and recorded on a magnetic card.

Perhaps the most significant feature of the test console is its speed. The modulation characteristics shown in Fig. 1 were generated in less than 10 minutes, including programming and printout times.

In addition to a complement of dc and thermal instrumentation, the system includes a preselector and spectrum analyzer, function generator, rf power meter, frequency counter, modulation generator, 15 MHz oscilloscope and analog and digital x-y plotters. Most of the rf equipment is manufactured by Hewlett-Packard. Custom power supplies, generators and distribution panels are designed and manufactured by Addington.

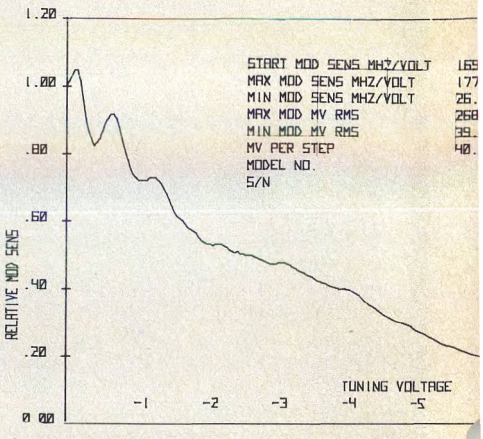

1. Modulation data is measured at a constant deviation, under the same conditions the source experiences in the field.

VCO test console, part number 291-01-03120, is specifically designed for measuring sources used in ECM systems, but according to the manufacturer, any type of VCO could be accommodated with little or no modification. P&A: $150,000 (depending on options); 120-180 days. **Addington Laboratories, Inc., 680 West Maude Avenue, Sunnyvale, CA 94086 (408) 245-6810.** CIRCLE NO. 100

Roll-out chamber checks small antennas from 2-18 GHz

Short on space? Here's an anechoic chamber that's mounted on wheels. Measuring only 5 × 10 × 7 feet, the 350 lb chamber can be pushed off into a corner or stored in a closet until needed.

The basic chamber consists of a metal, barrel-like structure lined with a high-performance absorber. A truncated cone at one end of the cylinder swings open to mount transmit horn antennas. A hinged door, lined with absorber, caps the opposite end of the chamber. Primary access to the interior is through a spring-loaded door cut into the side of the cylinder, which also activates an internal lighting system.

Orientation of the cone containing the transmit antenna is remotely controllable by motor drive. Continuous rotation allows any polarization from vertical to horizontal. Rf is piped in through a rotary joint.

Electrical specifications of the basic chamber include 2 to 18 GHz frequency coverage, −25 dB minimum cross polarization level and ±0.30 path loss uniformity.

A series of options are offered to accommodate individual needs. Option one is an azimuth positioner with position indicator and speed control. Maximum rotational rate is about 1 rpm. Option two, a model tower, is designed to fit on the azimuth positioner. Located in the center of the quiet zone, the tower accepts test antennas up to 10 lbs and six inches in diameter. Option three, an elevation positioner with indicator and speed control, can be attached directly to the model tower.

Five transmit horn assemblies, options four through eight, cover 2.60-3.95 GHz, 3.95-5.85 GHz, 5.85-8.20 GHz, 8.20-12.4 GHz and 12.4-18.0 GHz. A complete set of five horns covering 2.6-18 GHz is offered as option nine, while a single transmit horn covering 2-18 GHz is planned for the future. P&A: Basic chamber: $14,605; option 1: $2,431; option 2: $1,598; option 3: $3,948; option 4: $1,624; option 5: $1,531; option 6: $1,398; option 7: $1,263; option 8: $1,520: option 9: $7,336; 5-6 mos. **Transco Products, Inc., 4241 Glencoe Avenue, Venice, CA 90291 (213) 821-7911.** CIRCLE NO. 101

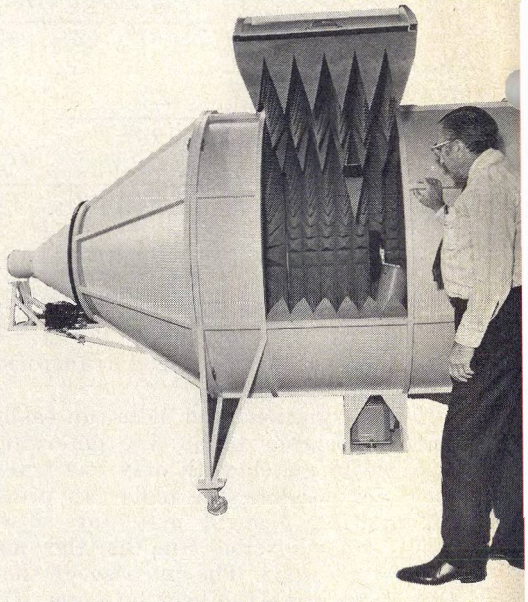

Octave band phase-shifters available with 7-bit inputs

This series of digital ferrite phase-shifters covers 2 to 18 GHz with just four models. Accepting as many as seven control bits, the components offer three degree maximum phase resolution and repeatability, and are intended for applications in automated test systems.

Models MpSM-1, MpCM-12, MpXM-8 and MpKuM-1 operate in octave bandwidths with a switching rate of 100 kHz, for 15 milliseconds at 10%. Common specifications include a typical VSWR of 2.0:1 and standard SMA connectors; individual specs are listed in the table.

Model	Frequency	Peak Power	Mid-band Loss
MpSM-1	2-4 GHz	1 kW	1.5 dB
MpCM-12	4-8 GHz	400 W	1.74 dB
MpXM-8	8-12 GHz	150 W	2.50 dB
MpKuM-1	12-18 GHz	1 kW	2.00 dB

Drivers of these phase shifters can be located as far as ten feet from the components without distorting phase accuracy. Either serial or parallel-fed TTL data can be used to control the driver. Supply voltages are +12 V for switching and +5 for logic, and LED phase-shift monitors are provided on each driver board.

Operating temperature is specified as 10 to 40°C.

Length ranges from 11 inches for the S-band model, to 5.5 inches for the Ku-band version. P&A: Under $3000; 150 days. **Raytheon Company, Special Microwave Devices Operation, 130 Second Avenue, Watham, MA 02154 (617) 890-8080.**

CIRCLE NO. 103

Software-based system automates antenna range pattern measurements

A fully-automated measurement system recently introduced by Scientific-Atlanta, Inc., is the first commercial product designed specifically for automated antenna pattern measurements. The Series 2020 Antennalyzer is a software-based measurement system which automatically measures and processes the extensive data required to fully characterize complex pattern geometries.

The basic system features 1-18 GHz rf measurement capability of single or dual-port amplitude and phase information, in conjunction with positioner control of up to six axes. The collected data may be displayed in contour, single scan or three-dimensional representation or may be processed to provide listings or plots of such quantities as gain, beamwidth, sidelobe levels, polarization properties, directivity, percent coverage and other information.

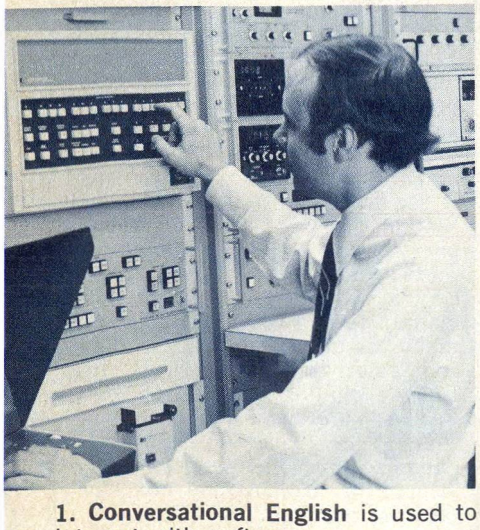

1. Conversational English is used to interact with software.

The product includes all the conventional range instrumentation except the positioning system and may be operated manually if desired.

Antenna range criteria generally requires a minimum separation of $\frac{2D^2}{\lambda}$ (where D is the test antenna diameter and λ the wavelength) between the source and test antennas. To accommodate this basic requirement, the 2020 system is designed to permit remoting the signal source YIG-tuned rf oscillator up to 2,500 feet from the operator control console. The rf input to the receiving subsystem may be remoted up to 200 feet from the console, and the positioning system may be controlled up to 2,500 feet from the console. A block diagram of the system is shown in Fig. 2.

Automation is accomplished by means of a digital processing subsystem with 32K(16 bit) memory and 2.5 megaword dual disc storage system. System software is designed to enable the operator to develop specific test programs from general measurement programs by simply adding appropriate test frequencies, scan angles and data point spacing, in English, through the crt graphics terminal. User program additions may be easily added with conventional programming language. Test programs may be stored and executed upon command to gather, process and display data without further operator intervention. Disc stored data may be processed at a later date, if desired.

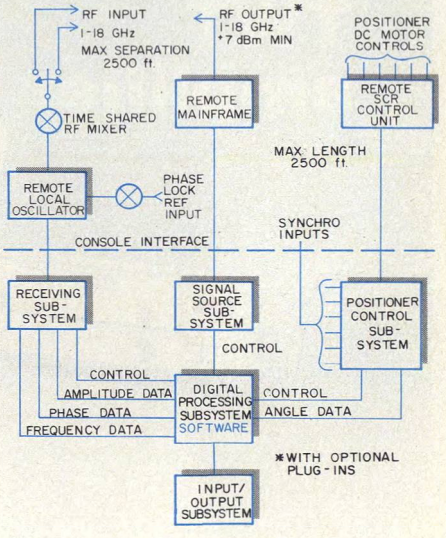

2. Model 2020 is designed to be a complete instrumentation system for antenna test ranges.

The data handling, control and processing capabilities of model 2020 enable multiple frequency or multiple beam data to be collected during a single positioner scan significantly increasing the volume of data obtained within a given test time. P&A: $230,000, 9 months. **Scientific-Atlanta, Inc., 3845 Pleasantdale Road, Atlanta, GA 30340 (404) 449-2000.**

CIRCLE NO. 102

new products

ISOLATOR/CIRCULATOR

12 GHz isolator is rated at 158 W

Isolator, model 410-9, is capable of 12 GHz operation at 158 W cw into a VSWR of 1.75:1 under vacuum conditions. In-band insertion loss is 0.15 dB max (0.08 dB typ.) while isolation is 26 dB. Input VSWR is 1.07:1 max and weight is about 4.26 oz. **Electromagnetic Sciences, Inc., P. O. Box 80508, Atlanta, GA 30341 (404) 448-5770.** CIRCLE NO. 104

AMPLIFIERS

Amp has guaranteed 3.5 dB noise figure

Transistor amp, model MHT-251, covers 5-500 MHz with a max noise figure of 3.5 dB. In the band, gain is 14 dB min, output is −2 dBm min and input and output VSWRs are 2.0:1. Power requirements are +15 Vdc @ 10 mA max. Package is a four-pin TO-8. P&A: $70; stock to 2 wks. **Aydin Vector Division, P.O. Box 328, Newton, PA 18940 (215) 968-4271.** CIRCLE NO. 105

Hybrid klystron— TWT delivers 9 MW peak

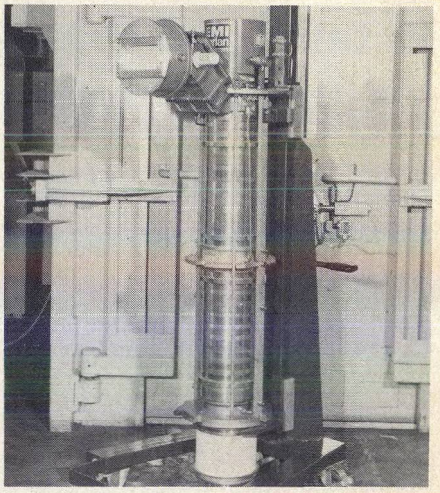

Hybrid pulsed amplifiers, models PT1141, 1142 and 1143, deliver peak outputs up to 9 mega-watts and consist of a broadband klystron driver section and an extended interaction traveling wave tube output section. The tubes can be factory tuned from 1.22 to 1.38 GHz for a wide variety of specific operating conditions. Under broadcast tuning conditions, the PT1141 provides an 1.5 dB electronic bandwidth of 150 MHz dB. For max power output, peak output levels of 3 to 9 MW can be obtained. The power output variation over 150 MHz is less than 1.5 dB. The min efficiency is 30% at max bandwidth while gain under broadband conditions, is at least 30 dB. Random noise and peak spurious outputs are at least 60 dB below carrier level. The tubes are free from pulse edge and rf drive induced oscillations. Beam voltage is 160 kV peak while beam current is 130 A peak. Load VSWR is 1.2:1. **EMI-Varian, Ltd., 248, Blyth Road, Hayes, Middlesex, UB 3 1HR, England 01-573 5555.**

CIRCLE NO. 107

Correction

In last month's issue on page 40, it was stated, "Watkins-Johnson in Palo Alto, CA, is the leading producer of FET amplifiers and is reported to have 80% of the market." The statement is not a fact; industry figures for this market are not available to MicroWaves. It can be stated that Avantek and Watkins-Johnson are leading suppliers of GaAs FET amplifiers.

Also, on page 40, it was reported that Fairchild is the only U.S. manufacturer of GaAs FETs. Actually, as shown in Fig. 3, other companies are manufacturing FETs, including Avantek, Hewlett-Packard, Raytheon and TI.

Also, on page 46, the MIC paramp shown in figure 9 was developed by Mullard and not Marconi as indicated.